UNIVERSITAT DE BARCELONA

Development and optimization of inkjet printing based technologies for hybrid printed circuit boards

Javier Arrese Carrasquer

ADVERTIMENT. La consulta d'aquesta tesi queda condicionada a l'acceptació de les següents condicions d'ús: La difusió d'aquesta tesi per mitjà del servei TDX (**www.tdx.cat**) i a través del Dipòsit Digital de la UB (**diposit.ub.edu**) ha estat autoritzada pels titulars dels drets de propietat intel·lectual únicament per a usos privats emmarcats en activitats d'investigació i docència. No s'autoritza la seva reproducció amb finalitats de lucre ni la seva difusió i posada a disposició des d'un lloc aliè al servei TDX ni al Dipòsit Digital de la UB. No s'autoritza la presentació del seu contingut en una finestra o marc aliè a TDX o al Dipòsit Digital de la UB (framing). Aquesta reserva de drets afecta tant al resum de presentació de la tesi com als seus continguts. En la utilització o cita de parts de la tesi és obligat indicar el nom de la persona autora.

ADVERTENCIA. La consulta de esta tesis queda condicionada a la aceptación de las siguientes condiciones de uso: La difusión de esta tesis por medio del servicio TDR (**www.tdx.cat**) y a través del Repositorio Digital de la UB (**diposit.ub.edu**) ha sido autorizada por los titulares de los derechos de propiedad intelectual únicamente para usos privados enmarcados en actividades de investigación y docencia. No se autoriza su reproducción con finalidades de lucro ni su difusión y puesta a disposición desde un sitio ajeno al servicio TDR o al Repositorio Digital de la UB. No se autoriza la presentación de su contenido en una ventana o marco ajeno a TDR o al Repositorio Digital de la UB (framing). Esta reserva de derechos afecta tanto al resumen de presentación de la tesis como a sus contenidos. En la utilización o cita de partes de la tesis es obligado indicar el nombre de la persona autora.

WARNING. On having consulted this thesis you're accepting the following use conditions: Spreading this thesis by the TDX (**www.tdx.cat**) service and by the UB Digital Repository (**diposit.ub.edu**) has been authorized by the titular of the intellectual property rights only for private uses placed in investigation and teaching activities. Reproduction with lucrative aims is not authorized nor its spreading and availability from a site foreign to the TDX service or to the UB Digital Repository. Introducing its content in a window or frame foreign to the TDX service or to the UB Digital Repository is not authorized (framing). Those rights affect to the presentation summary of the thesis as well as to its contents. In the using or citation of parts of the thesis it's obliged to indicate the name of the author.

Development and optimization of inkjet printing based technologies for hybrid printed circuit boards

Javier Arrese Carrasquer

Supervisors

Dr. Albert Cirera Hernández

Dra. Elena Xuriguera

Department of Electronics and Biomedical Engineering

2019

UNIVERSITAT DE BARCELONA

Development and optimization of inkjet printing based technologies for hybrid printed circuit boards

A dissertation submitted in partial fulfilment of the requirements for the degree of

Doctor of Philosophy in Nanoscience

by the University of Barcelona

Author

Javier Arrese Carrasquer

Supervisor

Dr. Albert Cirera Hernández

Dra. Elena Xuriguera Martin

Tutor

Dr. Albert Cirera Hernández

Barcelona, June 2019

Nanoscience Program

Micro and Nanotechnology and Nanoscopies for Electronic Devices (MIND)

Institute of Nanoscience and Nanotechnology (IN^2UB)

Department of Electronics and Biomedical Engineering, Physics Faculty, University of Barcelona

A la meva familia,
aquest és el fruit del vostre esforç

Acknowledgements

En primer lloc, voldria agrair als meus directors de tesi, el Dr. Albert Cirera Hernández i la Dra. Elena Xuriguera Martin, gràcies per la formació, la dedicació i la guia rebuda durant aquest temps. Voldria també agrair al professor Albert Cornet Calveras i al Dr. Albert Cirera Hernández per haver-me donat l'oportunitat de col·laborar i treballar en el Departament d'Enginyeria Electrònica i Biomèdica de la Universitat de Barcelona, que finalment ha portat a la redacció d'aquesta tesi doctoral.

Querría también agradecer la estrecha colaboración llevada a cabo con el Dr. Sergio Llorente Gil, Julio Rivera Peman y Arturo Peitivi Asensio de la empresa BSH electrodomésticos España S.A. Fruto de esta colaboración se ha desarrollo gran parte de la tesis doctoral que aquí se presenta, bajo los proyectos: Themprint (2013-2016) y Printedcooking (2016-2017).

Agradecer la estrecha colaboración realizada con la empresa Torrecid S.A. por el arduo trabajo realizado en el desarrollo de tintas funcionales en el marco de un proyecto CDTI de desarrollo con el nombre de Digielect (2012-2013).

Querría también agradecer la colaboración llevada a cabo con el Dr. Carlos Sánchez Somolinos, Jorge Alamán Aguilar y María López Valdeolivas del Laboratorio de Manufacturación Avanzada del Instituto de Ciencias de Materiales (ICMA) en el desarrollo de una parte importante de esta tesi doctoral.

Voldria també agraïr la col·laboració duta a terme amb en Dr. Sergi Claramunt Ruiz i l'Ana Ruiz Flores del grup Reliability of Electronic Devices and Circuits (REDEC), del Departament d'Enginyeria Electrònica de la Universitat Autonoma de Barcelona (UAB). Part del treball resultant de la colaboració duta a terme amb ells està reflexat en aquesta tesis doctoral.

Resum

Durant els últims anys, l'electrònica flexible i adaptable s'està integrant en una àmplia varietat d'objectes i productes d'ús quotidià per l'esser humà, incorporant valor afegit i generant noves necessitats. De fet, hi ha prediccions, que vaticinen que l'electrònica es trobarà integrada en pràcticament qualsevol objecte en el futur pròxim.[1] Per fer-ho possible, els costos de fabricació s'han de reduir dràsticament, ja que en molts casos l'augment del preu del producte final actua com a barrera envers la incorporació d'electrònica.

Per resoldre aquest repte, s'estan fent grans esforços en substituir i/o combinar la fabricació de la microelectrònica tradicional basada en silici per les tècniques de fabricació basades únicament en mètodes additius. Aquestes tècniques de fabricació additives es troben agrupades en el concepte d'electrònica impresa (Printed Electronics, PE), un paradigma de la fabricació d'electrònica.[2] Mitjançant aquestes tècniques es pot dur a terme la fabricació d'electrònica sobre grans superfícies, d'electrònica lleugera, d'electrònica amb propietats elàstiques, flexibles i conformables que alhora compleixen els requisits de les noves àrees d'aplicació i a un cost assumible.

El camp de la PE està format per un conjunt de tècniques antigues d'impressió gràfica, que en lloc de ser utilitzades per dipositar els pigments convencionals, s'utilitzen per dipositar materials funcionals (conductors, semiconductors i aïllants) imprescindibles per fabricar components i circuits electrònics. El concepte de PE inclou no només les tècniques d'impressió, sinó també les tintes, les pastes i els substrats.

Entre les tècniques d'impressió disponibles, la tècnica d'impressió per ejecció de tinta (Inkjet Printing, IJP) és un mètode de fabricació d'electrònica prometedor. La tècnica d'injecció de tinta gota a gota permet transferir un patró digital a un substrat sense necessitat de màscares, pantalles, motllos gravats, ni condicions de baixa pressió. Això redueix significativament el procés de validació del disseny i els costos associats, per tant, ofereix una gran flexibilitat en la fabricació de prototips. A més, el fet que el dipòsit es dugui a terme sense la necessitat de contacte entre la font de tinta i el substrat receptor, fa que la tècnica IJP sigui compatible amb substrats que es deformen amb l'esforç o amb superfícies irregulars i inclinades, que no són compatibles amb altres tècniques d'impressió. Pel que fa a la resolució, la impressora d'injecció de tinta permet dipositar patrons amb

resolucions màximes que van dels micròmetres als sub-micròmetres.[22,23] A més, entre les tècniques d'impressió existents, la IJP és una de les més respectuoses amb el medi ambient degut al principi de funcionament de gota per demanda i del contenidor de tinta, que permet l'emmagatzematge d'aquesta i evita la seva degradació prematura. Al final, la IJP és compatible amb processos de fabricació tipus rotllo a rotllo (Roll to Roll, R2R), que és un sistema de fabricació de producció a gran escala. Entre els camps de recerca on aquesta tècnica d'impressió està sent implementada, trobem: pantalles LCD/OLED, en fotovoltaica, en fabricació de sensors, en fabricació de components i circuits electrònics, en enginyeria de teixits, entre d'altres. Pels aspectes esmentats anteriorment, es va decidir triar la IJP com a tècnica de fabricació per dur a terme aquesta tesi doctoral.

Com s'ha esmentat, l'electrònica s'està integrant a un gran nombre d'objectes de la vida quotidiana, el que es coneix també amb el nom del internet de les coses (Internet of Things, IoT). De fet, entre els objectes del dia a dia, s'estan fent grans esforços per a la integració d'aquests circuits electrònics en roba, envasos, material d'esport/entreteniment, mobles, interiors de vehicles, pegats mèdics/cosmètics, entre d'altres. Tot i que algunes de les aplicacions poden ser fabricades completament mitjançant tècniques de PE, les aplicacions actual i les que estan per arribar estan creixent en complexitat i requeriments de computació. Això implica la necessitat de implementar circuits integrats (Integrated Circuits, IC) cada cop més sofisticats/densificats que es trobem més enllà de les capacitats tecnològiques de les tècniques de PE. A més, tot i que s'estan realitzant grans esforços en la fabricació impresa de ICs i els seus components electrònics bàsics, com són els transistors, actualment els ICs impresos estan poc densificats i els seus components bàsics encara han de superar diversos punts febles. Entre aquestes mancances, trobem que els ICs impresos tenen unes prestacions limitades i una durabilitat baixa, això es degut a capacitats paràsites existents, a problemes d'aïllament elèctric i a la limitada resolució de les tècniques de PE envers la tecnologia tradicional del silici.

Per tal d'aconseguir l'alt nivell de fiabilitat i qualitat de les aplicacions electròniques actuals i futures, s'ha proposat una electrònica híbrida. Aquesta tecnologia consisteix en la combinació dels avantatges de la tècnica de impressió IJP amb els components electrònics de la tecnologia de muntatge superficial (Surface Mount Technology, SMT). És dins d'aquest context que s'ha desenvolupat aquesta tesi doctoral. Així, per aprofundir i contribuir en aquest camp, en aquesta tesi doctoral s'ha realitzat l'estudi, la caracterització i l'optimització d'un mètode per connectar components electrònics de muntatge superficial (Surface Mount Device, SMD) mitjançant la tècnica IJP. A continuació, s'ha posat a prova la incorporació i connexió d'un circuit integrat sobre un circuit imprès (Printed Circuit Board, PCB) mitjançant IJP i una tècnica de connexió mitjançant plans inclinats. Finalment, s'ha treballat la impressió d'estructures multicapa per caracteritzar diferents materials aïllants que puguin ser útils per fabricar circuits híbrids multicapa.

En resum, inicialment s'han estudiat diferents tintes per caracteritzar les seves propietats en ejectabilitat i mullabilitat. També s'han caracteritzat les propietats funcionals dels dipòsits un cop sinteritzats i finalment s'han escollit les tintes més adequades per realitzar la resta de la tesi. Aquestes tintes són: una tinta amb càrrega de nanopartícules de plata (DGP 40LT-15C), una tinta amb càrrega de nanopartícules de Al_2O_3 (23-VA12-1), una tinta amb càrrega de nanopartícules de SiO_2 (24-VA12-2) i una tinta amb càrrega polimèrica de 4-Poly(4-vinyl phenol) (xdi-cds). A més, aquest estudi ha servit per aprofundir en el coneixement de les diferents etapes que intervenen en el procés de fabricació additiva IJP.

A continuació, s'ha dut a terme l'objectiu principal d'aquesta tesi, que ha estat la caracterització del novedós mètode de connexió elèctrica de SMDs mitjançant el dipòsit de tinta amb càrrega de nanopartícules de plata. La tinta es diposita en la zona de contacte entre l'elèctrode i la pista conductora, i aprofitant el fenomen de la capil·laritat, la tinta difon per la interfície entre el SMD i la pista impresa. El mètode de soldadura proposat junt amb altres de convencionals (soldadura d'estany i adhesiu conductor) s'han provat sobre diferents substrats, paper fotogràfic, poliimida i vidre. Les soldadures s'han caracteritzat mitjançant mesures elèctriques de resistència elèctrica de contacte, i mesures mecàniques de resistència a esforç de cisalla. Finalment, s'han comparat les prestacions entre les diferents tècniques estudiades. Dels resultats obtinguts, es pot concloure que el mètode de soldadura inkjet presenta un valor de resistència elèctrica de contacte comparable a els materials convencionals, que és al voltant de 0,3 Ω en tots tres tipus de substrats utilitzats. A més, la quantitat de material utilitzat per fer la soldadura de inkjet és molt menor que l'utilitzat en les soldadures convencionals. Això fa que la tècnica de inkjet sigui més respectuosa amb el medi ambient que les altres tècniques convencionals caracteritzades. Amb la tècnica de inkjet s'obté una soldadura que compleix els requeriments elèctrics per la fabricació de circuits electrònics a una temperatura de procés, entorn els 150 °C, que és compatible amb el substrat tèrmicament més limitant dels utilitzats en aquesta tesi, el paper fotogràfic. En quant als resultats obtinguts de la prova a esforç de cisalla, la soldadura mitjançant inkjet té menys resistència que l'adhesiu conductor en els substrats de paper i vidre. En canvi, en el cas del substrat Kapton®, la soldadura de inkjet i la d'adhesiu conductor posseeixen una resistència similar. Per altra banda, les soldadures de inkjet i d'estany tenen valors de resistència a l'esforç de cisalla comparables en tots els substrats utilitzats.

Posteriorment, en col·laboració amb el Laboratorio de Manufactura Avanzada del Instituto de Ciencia de Materiales de Aragón (ICMA), s'ha realitzat un estudi per reforçar mecànicament les soldadures. En aquest punt, quan els SMDs ja estan soldats amb la tinta de plata sinteritzada, s'ha imprès sobre les soldadures una tinta de material aïllant, 3glicocidoxipropiltrimetoxisilà (GPTMS). Aquesta tinta s'ha utilitzat com a reforç per a millorar la resistència mecànica de la soldadura de inkjet i s'han caracteritzat les prestacions obtingudes mitjançant proves d'esforç a cisalla. Alhora,

s'han realitzat mesures elèctriques de la soldadura, quan les mostres estan sotmeses a esforços de flexió. En aquest estudi s'han comparat els resultats obtinguts degut al reforç mecànic incorporat a la soldadura amb els resultats obtinguts prèviament amb els materials de soldadura convencionals i amb la soldadura feta amb inkjet. Dels resultats obtinguts, es pot concloure que la impressió del reforç en la zona de soldadura afavoreix significativament la resistència mecànica d'aquesta. Fins el punt que la soldadura de inkjet amb el reforç imprès mostra una resistència a cisalla 4 vegades superior en el cas del substrat de vidre i 1.5 vegades superior en el cas del plàstic i el paper, si ho comparem amb el valor de la soldadura inkjet sense reforç. A més, els valors obtinguts de resistència mecànica amb la tècnica de inkjet amb el reforç imprès, són comparables als obtinguts amb l'adhesiu conductor en tots els substrats.

Per una altra banda, s'han estudiat les prestacions elèctriques de les soldadures fetes amb dos subconjunts de SMDs i tinta de nanopartícules de plata, un dels subconjunts de SMDs té elèctrodes amb forma quadrada i l'altre els té amb forma de pla inclinat. Aquest estudi s'ha dut a terme amb la intenció de millorar la resistència elèctrica de contacte i reduir la quantitat de soldadures de inkjet fallides. Dels resultats obtinguts es pot concloure que els elèctrodes amb forma de pla inclinat aconsegueixen retenir la tinta que es diposita sobre d'ells envers els elèctrodes que tenen la paret de l'elèctrode en paral·lel a la direcció de caiguda de les gotes. Tot i així, les mesures elèctriques no han estat concloents ja que el mètode de fabricació dels elèctrodes dels SMDs no han permès la reproductibilitat necessària.

En col·laboració amb el grup de recerca Reliability of Electronic Devices and Circuits (REDEC) del departament d'enginyeria electrònica de la Universitat Autònoma de Barcelona (UAB) s'ha fabricat un circuit en el qual s'ha connectat directament, mitjançant plans inclinats, una mostra de silici amb transistors de grafé sobre una PCB. Aquest desenvolupament s'ha realitzat per demostrar la potencialitat de les connexions mitjançant plans inclinats que permeten connectar IC directament sobre PCBs sense la necessitat de fabricar els SMDs chips convencionals. A més, aquest tipus de connexió directe redueix el gruix dels circuits impresos i per tant els fa més flexibles. El circuit imprès s'ha connectat a un microscopi de forces atòmiques (AFM) i a una unitat de font i mesura (SMU), que ha permès estudiar la degradació del material 2D immediatament després de ser sotmès a un corrent elèctric. Aquest material 2D, en aquest cas grafé, és utilitzat en el transistor d'efecte de camp (Graphene Field Effect Transistor, GFET) com el semiconductor del canal.

Finalment, com les PCBs convencionals són majoritàriament circuits multicapa, s'han estudiat diferents materials dielèctrics, SiO_2, Al_2O_3, i 4-Poly(4-vinyl phenol) (PVP) amb la finalitat de trobar l'aïllant més adient per a imprimir circuits híbrids multicapa sobre paper. En aquest estudi els materials aïllant s'han estudiat mitjançant la fabricació d'estructures tipus metall-aïllant-metall i les propietats estudiades han estat la fiabilitat en la fabricació, la permitivitat dielèctrica, la tangent

de pèrdues i la resistència dielèctrica. Dels resultats obtinguts es pot concloure que el PVP és el material que dona més fiabilitat i que els dipòsits de SiO_2 i Al_2O_3 presenten esquerdes degut a la falta de sinterització i també degut a les dilatacions i contraccions que pateix el substrat de paper en els tractaments tèrmics utilitzats per curar les tintes. Degut a aquestes esquerdes es produeixen curtcircuits entre els dos elèctrodes de la estructura multicapa. Aquests curtcircuits es poden evitar imprimint una capa final de PVP abans de imprimir l'elèctrode superior, mitjançant aquest mètode la fiabilitat dels components augmenta considerablement. Els dipòsits de SiO_2 i Al_2O_3 donen valors de permitivitat dielèctrica significativament menors als corresponents del material bulk, això es degut a que aquest materials no sinteritzen a les temperatures de curat de les tintes i l'espai que queda entre les partícules dona com a resultat una capa composta de nanopartícules i aire. Degut a això s'ha aconseguit una capa de SiO_2 + PVP que presenta una permitivitat dielèctrica entorn 4.2 amb una fiabilitat del 100%, aquesta permitivitat dielèctrica és la mateixa que presenten els materials dielèctrics utilitzats en la fabricació de PCBs convencionals.

Organització de la tesi

El capítol 1 és una introducció a l'estat de l'art de les diferents tècniques de impressió i dels diferents treballs relacionats amb la integració de components electrònics sobre PCB fabricades mitjançant tècniques additives.

El capítol 2 és una caracterització detallada de la tècnica de fabricació additiva de inkjet. En aquest es tracten les característiques principals d'aquesta tècnica i les variables de les qual depèn el correcte dipòsit dels materials funcionals. En aquest capítol també es presenten els resultats de la caracterització de diverses tintes de inkjet i l'elecció de les més adients per realitzar la resta de la tesi.

El capítol 3 presenta el mètode de soldadura mitjançant tinta amb càrrega de nanopartícules de plata dipositada amb inkjet. En aquest capítol s'estudien les propietats elèctriques i mecàniques de la soldadura proposada i es compara amb els resultats obtinguts amb altres materials. Finalment, es fabrica un circuit demostrador.

El capítol 4 presenta la col·laboració duta a terme amb el Instituto de Ciencia de Materiales de Aragón (ICMA). En aquest cas s'utilitza una tinta de inkjet desenvolupada per ICMA per a donar-li una altra funcionalitat. La funcionalitat inicial d'aquesta tinta es per fer dispositius optoelectrònics i guies d'ona. La tinta no conté solvents, així el material funcional després de polimeritzar es pràcticament del 100% del patró depositat. S'estudia aquesta tinta com a reforç mecànic per millorar les prestacions obtingudes al capítol 3. En aquest capítol s'estudien les propietats mecàniques de la soldadura reforçada i també s'estudia la resistència elèctrica de contacte sota esforços de flexió. Els resultats obtinguts es comparen amb els resultats obtinguts al capítol 3.

Al capítol 5 es presenta l'estudi de la resistència elèctrica de contacte de dues poblacions de SMDs connectats amb tinta de nanopartícules de plata, un dels subconjunts d'elèctrodes amb forma quadrada i l'altre amb forma de pla inclinat. Es comparen els valors de la resistència elèctrica de contacte obtinguts en aquest treball amb els obtinguts en el capítol 3.

Per altra banda, en aquest capítol també es presenta la fabricació de l'equip de mesura per a caracteritzar materials 2D integrats en transistors, concretament el grafé. Aquest equipament es desenvolupa gràcies a integrar una mostra de silici sobre un circuit imprès sense la necessitat d'utilitzar "wire bonding". Mitjançant la incorporació d'unes rampes, per suavitzar l'esglaó entre la superfície de la PCB i la superfície de la mostra de silici, es van connectar els transistors amb contactes 2D impresos amb inkjet.

El capítol 6 presenta un estudi de les propietats aïllants de diversos materials dielèctrics mitjançant estructures multicapa metall-aïllant-metall impreses sobre substrat de paper. En aquest estudi es caracteritza la fiabilitat en la fabricació, la permitivitat dielèctrica, la tangent de pèrdues i la resistència dielèctrica dels diferents materials provats.

El capítol 7 conté les conclusions generals de la tesi i les conclusions específiques.

Contents

CHAPTER 1. INTRODUCTION 1

1.1 Motivation 2

1.2 State of the art on Printing Techniques 5

1.2.1 Offset printing 6

1.2.2 Gravure printing 6

1.2.3 Flexographic printing 7

1.2.4 Screen-printing 8

1.2.5 Micro-contact printing 9

1.2.6 Nanoscale transfer printing 10

1.2.7 Aerosol jet printing 10

1.2.8 Laser-induced forward transfer printing 11

1.2.9 Inkjet printing. 11

1.3 State of the art of the additive manufactured printed circuit boards PCBs. 12

1.3.1 Drawbacks of the current strategies for inkjet-printed hybrid PCBs. 24

1.4 Objectives 25

1.5 Outline 25

1.6 References 27

CHAPTER 2. FUNCTIONAL ASPECTS OF INKJET PRINTING TECHNOLOGY. 39

2.1 Introduction 40

2.2 Generation of droplets with PIJ printers. 42

2.3 Jettable fluids 46

2.3.1 Particle size 46
2.3.2 Volatility 46
2.3.3 Viscosity 47
2.3.4 Surface energy 48
2.3.5 Z dimensionless number 48
2.3.6 Jettability characterization of tested inks. 50

2.4 Drop-substrate interaction 53
2.4.1 Drop impact and spreading 53
2.4.2 Drop-substrate interaction of tested inks. 58

2.5 Drop spacing, drop coalescence and fluid bead stability 60
2.5.1 Fluid beads characterization of tested inks 63
2.5.2 Fluid beads profile depending on the printer constrains. 65

2.6 Liquid/solid phase change of the functional deposit. 68
2.6.1 Profile of the tested inks 71

2.7 Functionality 76
2.7.1 Functional material characterization 78

2.8 Adhesion 83
2.8.1 Wettability 83
2.8.2 Surface roughness and diffusive effect. 83
2.8.3 Chemical bonds 85
2.8.4 Adhesion promoters. 86
2.8.5 Adhesion test 86

2.9 Insulation and encapsulation of printed electronics 87

2.10 Conclusions 88

2.11 References 90

CHAPTER 3. DEVELOPMENT OF A NOVEL SMD ASSEMBLING METHOD CAPILLARITY-ASSISTED 97

3.1 Motivation 98

3.2 Novel procedure for hybrid circuit manufacturing by inkjet printer 99

3.2.1 Materials 99
3.2.2 Procedure 100
3.2.3 Characterization 104
3.3 Results and discussion. 104
3.3.1 Electrical contact resistance 105
3.3.2 Shear strength 109
3.3.3 Morphology characterization 114
3.4 Application: a multi-sensor circuit on paper 117
3.5 Conclusions 118
3.6 References 120

CHAPTER 4. MECHANICAL IMPROVEMENT OF THE SMD INKJET ASSEMBLING METHOD 125
4.1 Motivation 126
4.2 Inkjet-printed mechanical reinforcement for SMD assembling 127
4.2.1 Materials 127
4.2.2 Procedure 128
4.2.3 Characterization 129
4.3 Results and discussion 130
4.3.1 Shear strength performance 130
4.3.2 Electrical resistance measurements in bending stress mode 133
4.4 Morphological FESEM inspection 135
4.5 Conclusions 136
4.6 References 138

CHAPTER 5. PRINT-ON-SLOPE TECHNIQUE FOR ELECTRONIC COMPONENTS INKJET-ASSEMBLING 141
5.1 Motivation 142
5.2 Ramp-shaped SMD electrodes 142

5.2.1 Ramp-shape SMD electrode: materials, procedure and characterization..... 144
5.2.2 Results and discussion 146
5.2.3 Conclusions 149

5.3 Inkjet strategies for integrated circuits assembling 149
5.3.1 System on package (SoP): materials, procedure and characterization 153
5.3.2 Results and discussion 154
5.3.2.1 Setup design and manufacturing.. 154
5.3.2.2 Material characterization 158
5.3.3 Conclusions 159

5.4 References 161

CHAPTER 6. DIELECTRIC MATERIALS FOR MULTILAYER PRINTED CIRCUIT BOARDS 163

6.1 Motivation 164

6.2 Metal-Insulator-Metal structures 166
6.2.1 Materials 166
6.2.2 Procedure 168
6.2.3 Characterization 169

6.3 Results and discussion 170
6.3.1 Feasibility 170
6.3.2 Relative permittivity and loss tangent 175
6.3.3 Dielectric strength 182

6.4 Conclusions 184

6.5 References 185

CHAPTER 7. GENERAL CONCLUSIONS AND FUTURE WORK 189

GLOSSARY

PE	Printed Electronics
IP	Inkjet Printing
EHD	Electrohydrodynamic
LIFT	Laser Induced Forward Transfer
R2R	Roll to Roll
µCP	Micro-Contact Printing
nTP	Nanoscale Transfer Printing
AJP	Aerosol Jet Printing
IoT	Internet of things
SMT	Surface Mount Technology
SMD	Surface Mount Device
PCB	Printed Circuit Boards
IC	Integrated Circuit
ICA	Isotropically Conductive Adhesive
CTE	Coefficient of Thermal Expansion
TFTs	Thin Film Transistors
SoP	System on Package
SiP	System in Package
FHE	Flexible Hybrid Electronics
CIJ	Continuous Inkjet technology
DOD	Drop-on-Demand
PIJ	Piezoelectric Inkjet
TIJ	Thermal Inkjet
Re	Reynols Number
We	Weber Number
Oh	Ohnesorge Number
η	Viscosity
ρ	Density and Conductivity
γ	Surface Tension
d_{con}	Contact diameter or footprint
θ_{eqm}	Static contact angle
θ_{adv}	Advancing contact angle
θ_{rec}	Reciding contact angle
Ds	Drop spacing
GPTMS	3Glycocidoxypropyltrimethoxysilane
LTCC	Low Temperature Curing Ceramics
AgNP ink	Silver Nanoparticle-based ink
SEM	Scanning Electron Microscope

NCA	Non Conductive Adhesive
ECA	Electrical Conductive Adhesive
FR4	Glass-reinforced epoxy laminate substrate
AFM	Atomic Force Microscope
CAFM	Conductive Atomic Force Microscopy
BTI	Bias Temperature Instability
GFET	Graphene-based Field Effect Transistor
SMU	Source Meter Unit
MIM	Metal Insulator Metal structure
PVP	4-Poly(4-vinyl phenol)
C	Electrical capacity
ε_r	Relative Permittivity
ε_0	Dielectric permittivity of vacuum
tanδ	Loss tangent
FIB	Focused Ion Beam
E	Dielectric Strength

INTRODUCTION

CHAPTER 1

1.1 Motivation

Nowadays, small-smart-transparent-flexible electronics are being integrated in a wide variety of common objects in the human surrounding environment, incorporating an added value to daily life objects and generating new necessities. In fact, there are predictions, which expect that electronics will be part of anything in next future.[1] Therefore, to make it conceivable, the manufacturing costs must be dramatically reduced. To solve this challenge, huge efforts are being done on substituting and/or combining the traditional silicon-based microelectronics fabrication by/with the novel and already existing electronics manufacturing techniques, which are clustered in the printed electronics (PE) concept, a paradigm of electronic manufacturing.[2] By means PE, it can be provided the indispensable large area, low weight, flexible, stretchable and conformable electronics that fulfil the requirements of the new application areas, and thus, doing them available for the consuming market.

PE is a set of age-old graphic printing techniques,[3,4,5] which are being used to deposit functional materials (conducting, semiconducting and insulating), instead of the conventional pigments, to develop monolayer and multilayer electronic components and circuits. PE concept encompasses printing techniques as well functional materials-based inks, pastes and substrates.[5]

The highlights of PE manufacturing techniques, which make them so competitive are that provide routes for processing materials in conditions that are compatible with low physico-chemical resistance substrates, as polymer-based substrates.[6–10] In addition, these techniques have also opened new chances on large area fabrication with rigid and flexible substrates, as well on irregular surfaces,[11–13] which is expensive and noprofitable with the conventional silicon-based fabrication techniques. Furthermore, PE techniques provide a set of economic benefits in comparison with traditional manufacturing processes due to simplified processing steps and reduced materials wastage.[10,14] All the above-mentioned cost-effective advantages make the PE techniques very attractive for their integration in the manufacturing lines, and hence allow the increasing and expanding of their presence in the goods market. In fact, as shown in *Figure 1.1*, the forecast for printed electronics is increased from 100 M$ at 2018 to 600 M$ at 2028 only regarding conductive inks and pastes in emerging sectors according to market research company IDTechEx estimation.[15] Moreover, according to IDTechEx

the global market of printed electronics will reach $73 billion by 2027.[2] This is an evidence of the enormous and dynamic PE market.

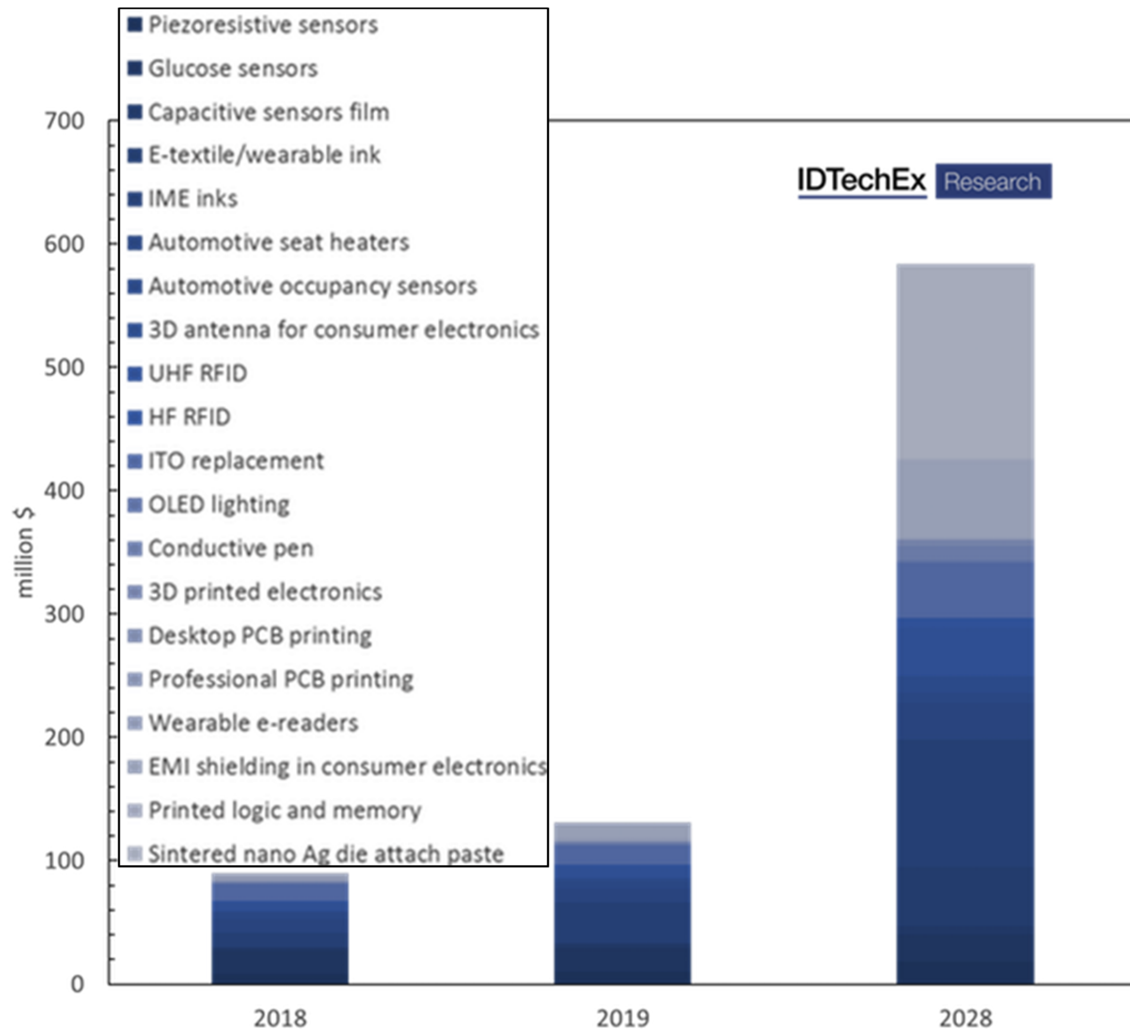

Figure 1.1 Market growth opportunity for conductive inks and pastes in emerging sectors. Here, volume applications like touch screen edge electrodes, automotive (exterior), membrane switch and photovoltaic are excluded. Image from [15]

PE market encloses several printing techniques, which can be classified into two blocks: contact printing and non-contact printing techniques as it can be seen in the block diagram of *Figure 1.2*.[3] Regarding the contact printing techniques, the substrate has direct contact with printing stencils where the ink is located before its transfer, which generates risks of substrate damages and contamination. The contact printing techniques are: screen,[16,17] gravure,[18] Offset,[19] flexography,[17] micro-contact and nanoscale

transfer[16], from which screen, gravure, offset and flexography are usually catalogued as high processing speed and low-cost due to the possibility to implement them on a roll to roll (R2R) manufacturing process, which is an indicator of mass production. Further, these kind of manufacturing techniques require the development of specific stencils to perform each printing process, ensured by a time consuming pre-processing before they can be implemented in a fast, high-scaled production. In fact, some printing processes such as gravure or flexography have a very high start-up cost and they are economically viable only for very large batches.[20]

Regarding the non-contact printing methods that eject the ink from a controlled distance of the substrate, such us inkjet (IP),[21] Electrohydrodynamic inkjet (EHD),[21–23] laser-induced forward transfer (LIFT),[20,24,25,26] and aerosol-jet[27], are typically based on the digital direct-writing approach. Therefore, any little pattern modification is solved without associated costs, which makes these manufacturing processes attractive for rapid prototyping, as well for highly individualized products and products with short run length. Although the printing velocity at non-contact printing techniques is usually slower than contact printing techniques, the non-contact printing techniques can be implemented on Roll to Roll (R2R) manufacturing process, and hence mass production is also performed.[13] In the *Figure 1.3* the printing techniques are represented in a graph where printing velocity and resolution are the axis parameters.

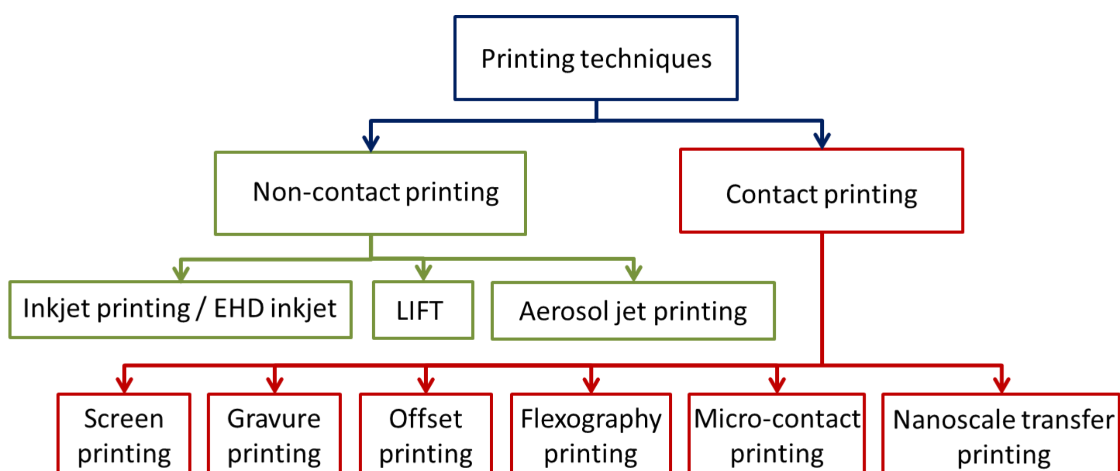

Figure 1.2 The classification of common electronic printing technologies.

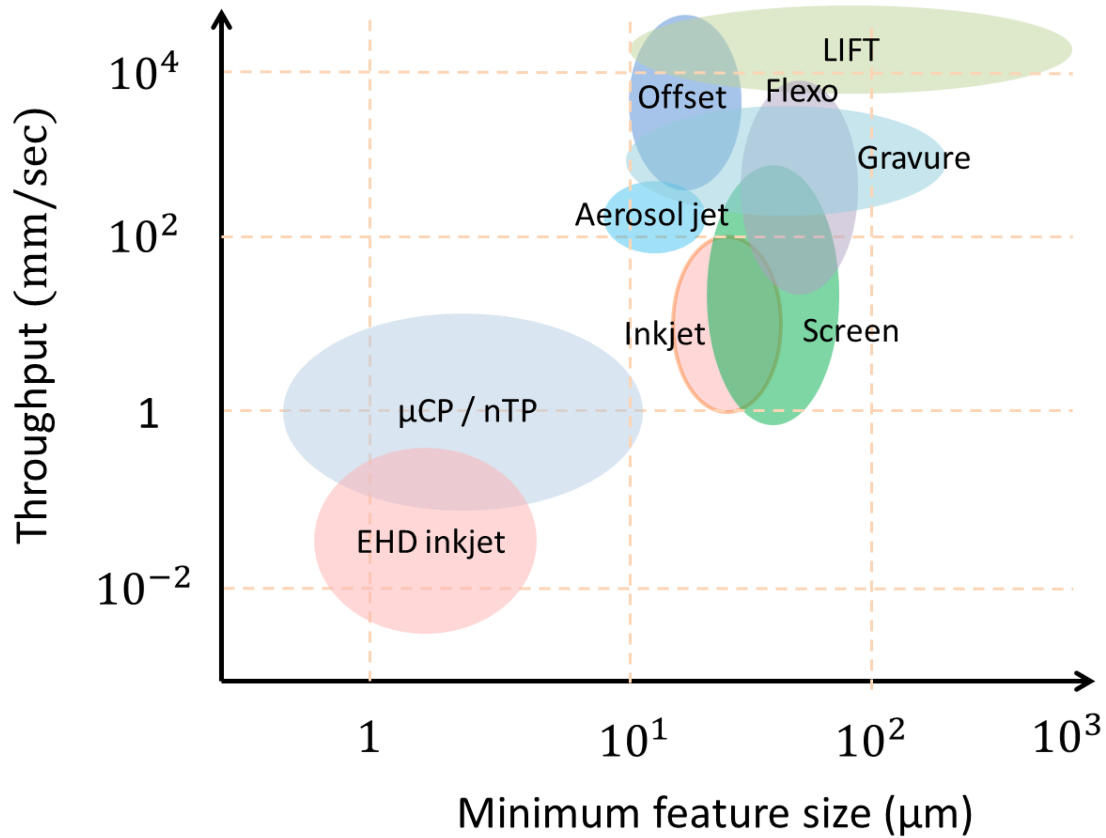

Figure 1.3 Comparison of printing velocity and resolution of printing technologies actually used for electronics manufacturing. Image adapted from [3,16–18]

1.2 State of the art on Printing Techniques

Printing electronics is based on different printing techniques that operate in a different manner depending on the many interface relations concerning the designed pattern structure (thickness and resolution requirements), the physical and chemical properties of the deposited functional material, and the selected substrate characteristics. In addition, as commented above, according to the substrate proximity of the deposition process, it is possible to define two main printing methods: printing techniques that require an exclusive mask or special framework for a contact process (offset, gravure, flexographic, screen, micro-contact and nanoscale transfer printing) and the mask-less non-contact method (inkjet, LIFT and aerosol jet printing).

1.2.1 Offset printing

Offset printing is a printing method which is based on the difference of surface energy between the plate cylinder that transfers the hydrophobic ink (water-repellent) from a printing plate and the substrate (*Figure 1.4*).[28] The localized surface energy gradient on the substrate defines the patterned areas (hydrophobic region) from the empty areas (hydrophilic region). Although the required high viscosity (30-100 Pa·s) and high pressure system (~1 MPa, impracticable for pre-patterned substrates with soft materials), offset printing ensures thin layers of thickness ranging from 0.5 to1.5 µm.[29] Up to date, few electronic applications have been achieved with this technique due to starting expensive costs and the water presence into the system.[30]

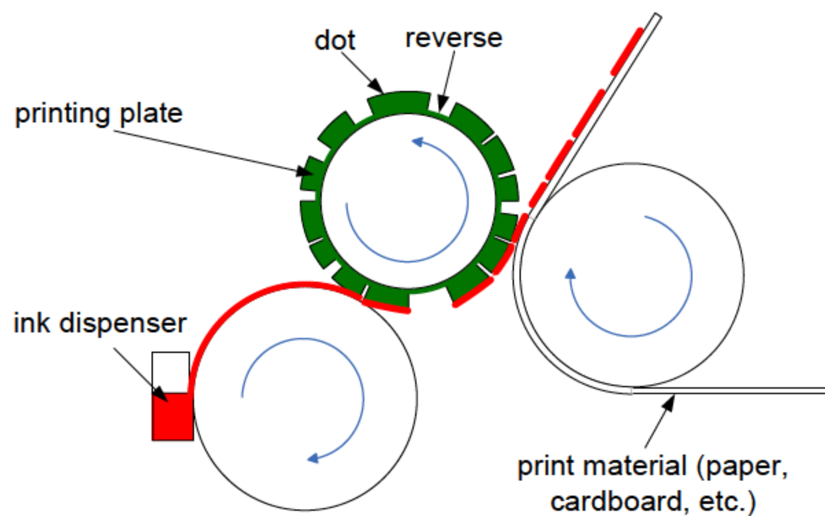

Figure 1.4 Offset printing process. Image from [28]

1.2.2 Gravure printing

Gravure printing[31,32] relies on an engraved pattern into a ceramic or metallic cylindrical plate surface (with resolution around 20 µm), whereas the unpatterned regions remain at the original level of the plate (*Figure 1.5*).[33,34] First of all, the engraved printing cylinder is dipped into a selected ink reservoir, and then a *Figure 1.5* doctor blade is used to remove the unwanted excess of ink. Finally the gravure-plate transfers the ink onto the moving substrate under high-pressure (~3 MPa, impracticable for pre-patterned substrates with soft materials) with thickness resolution ranging from 0.8 to 8 µm. In spite of the very expensive engraved cylindrical plate and the waste material, gravure

printing offers high printing resolution (~10-20 μm), high print velocity and requires low viscosity ink (50-200 mPa·s). These features have been exploited for the fabrication of fully-printed electronic devices, such as antennas, organic solar cells and OLEDs.[35]

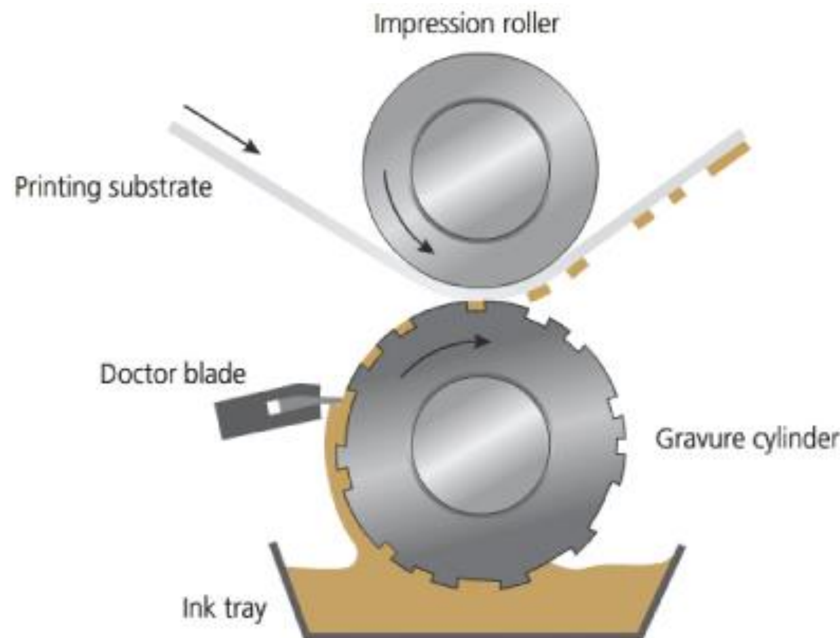

Figure 1.5 Gravure printing process. Image from [35]

1.2.3 Flexographic printing

In flexographic printing, there are at least three cylindrical plates: the anilox roller, the raised imaged-patterned plate and the substrate plate.[36] First of all, the anilox cylinder, a polymeric plate with well-distributed and uniform-volume cells, is dipped into a reservoir ink and, as in gravure printing, the excess of ink is removed by a doctor blade. Afterwards, the ink, filled into the anilox cells, is transferred with controlled thickness (ranging from 0.8 to 1 μm) onto the raised patterned-plate. Finally, using a soft pressure (~0.3 MPa, practicable for pre-patterned substrates with soft materials) the direct contact transfers the ink from the raised image plate to the substrate (*Figure 1.6*).[37] Printing resolution (20-75 μm) and desired ink viscosity (50-500 mPa·s) are comparable to gravure printing. Electronics applications,[38] such as RFID antennas[39] and transistors,[40] have been demonstrated by flexographic printing.

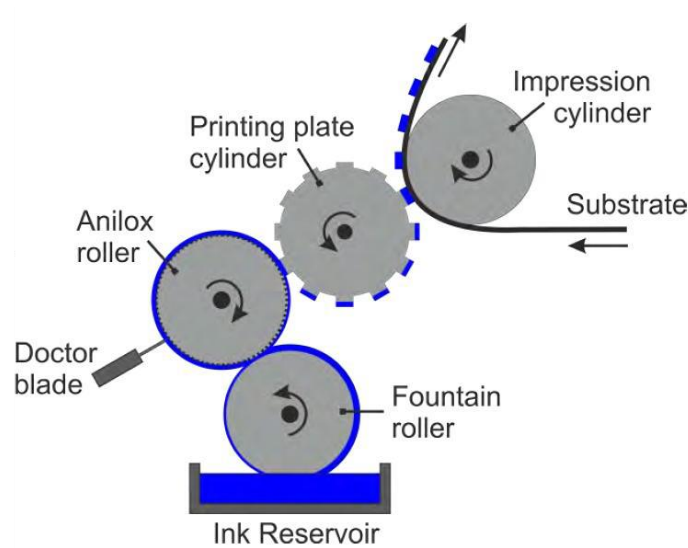

Figure 1.6 Schematic illustration of flexographic printing process. Image from [41]

1.2.4 Screen-printing

Screen-printing is characterized by using screens, which are made of a mesh support, generally from materials like stainless steel or polyester. The mesh support is pre-coated with an emulsion that fills the unwanted pores in order to define the desired pattern. Thus, once the screen is placed on top of the substrate, the ink is dragged across the screen surface using a squeegee, which squeezes the ink through the open pores (*Figure 1.7*). A trade-off between ink properties, such as the viscosity (0.5 – 50 Pa·s) and mesh density (depending on the fineness of the screen) demarcate the best printing resolution (~30-80 µm) and an expected layer thickness ranging from 3 to 100 µm. Electronic applications such as antennas, photovoltaic cells,[42] transistors and even fully-printed circuits[43] have been demonstrated by screen-printing.

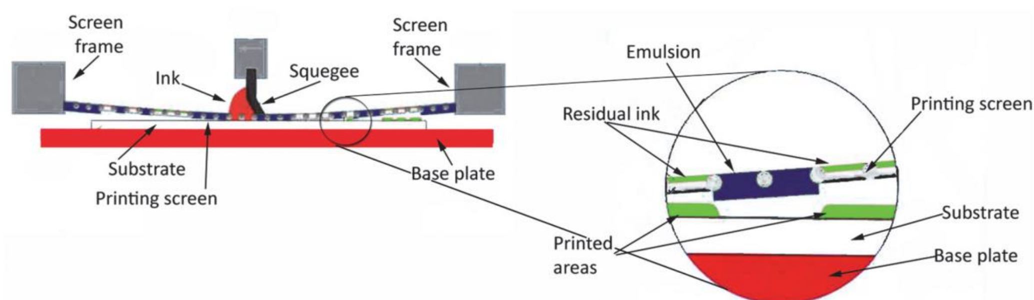

Figure 1.7 Schematic illustration of screen-printing process. Image from [44]

1.2.5 Micro-contact printing

In micro-contact printing (µCP), the ink is applied to an elastomeric stamp with a pattern of surface relief. The stamps are typically fabricated by curing elastomer, commonly poly(dimethylsiloxane) (PDMS), on a silicon master fabricated through traditional optical lithography and etching techniques (*Figure 1.8*).[45] Sufficiently low adhesion of the elastomer to the master allows the stamps to be peeled from the master. Under ideal conditions, the peeled elastomer stamp is an exact negative replica of the master. The stamp deformation during stamp removal from the template and during the contacting of the substrate limits the resolution of the patterning.[46] The mechanical properties of the elastomeric PDMS stamps provide sufficient mechanical stability for the printing down to 500 nm.[47] Micro-contact printing is relatively simpler and inexpensive than photolithography. In addition, at µCP the material transfer could be promoted by means self-assembled mono layers coatings, which are used as glues taking advantage of the chemical bounds to assure the substrate transfer. This technique is used to manufacture electronics applications, such as a photodetectors,[48] as well for precision patterning of metals, bio-molecules and colloidal nanocrystals.[48]

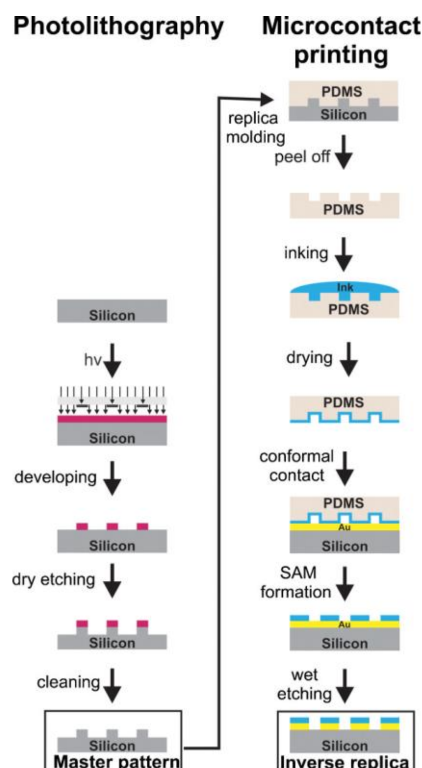

Figure 1.8 Schematic comparison of photolithography versus µCP. The crucial step in both techniques consists of the accurate transfer of the patterned etch-resist layer. Image from [45]

1.2.6 Nanoscale transfer printing

Nanoscale transfer printing (nTP) is the process of transferring a thin, solid film from a stamp with nanoscale-patterned features to a substrate.[49] The stamp can be either a soft or a hard material, such as PDMS or silicon. As in (μCP), the material transfer could be promoted by means self-assembled mono layers coatings, which are used as glues taking advantage of the chemical bounds to assure the substrate transfer (*Figure 1.9*).[50] This technique is used for precision patterning and for applications where harsh conditions should be avoided as organic electronics.[51,50]

Figure 1.9 Schematic of SAM assisted nanoscale transfer printing (nTP) process. Image from [50]

1.2.7 Aerosol jet printing

Aerosol jet printing (AJP) has emerged as a promising method for microscale digital additive manufacturing using functional nanomaterial inks.[52] In AJP, a functional ink is aerosolized and delivered to the substrate by a carrier gas, achieving resolution as fine as 10 μm (*Figure 1.10*). Due to its non-contact, line-of-sight, and digital nature, AJP offers advantages complementary to many traditional methods. Some of the first examples of use include transistors and more complex circuits, and it continues to be widely used in this field today.[53,54]

Figure 1.10 Schematic of Aerosol jet printing process. Image from [55]

1.2.8 Laser-induced forward transfer printing

Laser-induced forward transfer (LIFT) is a printing technique based on the action of a laser pulse that is focused on a thin film of a precursor ink for getting the transfer of a droplet onto a substrate. The laser beam is scanned along the donor film at a certain scan speed and repetition rate. Each laser pulse results in the formation of a long jet of ink, which contact with the receiving substrate leads to the printing of a droplet (*Figure 1.11*).[25,26] This technique is being tested on photovoltaic research,[56,57] and humidity sensors manufacturing.[25,26]

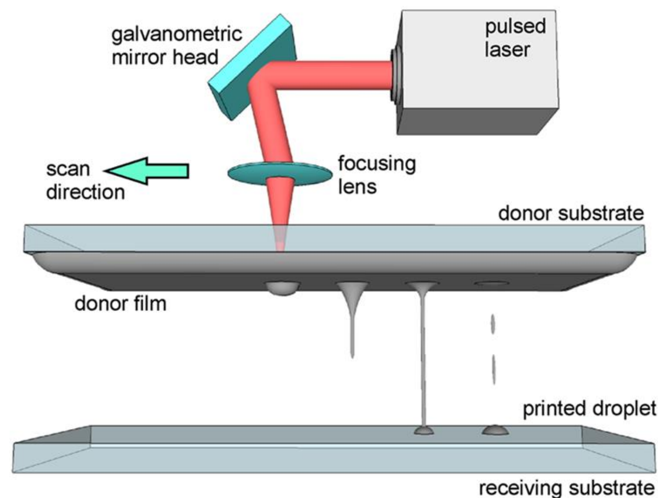

Figure 1.11 Sketch of the setup and principle of operation of pulsed LIFT. The laser beam is scanned along the donor film at a certain scan speed and repetition rate. Each laser pulse results in the formation of a long jet of ink, which contact with the receiving substrate leads to the printing of a droplet. Image from [25]

1.2.9 Inkjet printing.

Among the printing techniques available, inkjet printing (IP) technique is a promising electronic manufacturing method.[10] The drop-on-demand inkjet printer allows transfer digital design to substrate without mask or screen, which reduces significantly the design-validation time-process and the costs associated, thereby offers the flexibility required to fast circuit prototyping. Moreover, the non-contact process makes IP technique compatible with irregular surfaces, as well non-planar substrates, which are forbidden for other printing techniques. Concerning on substrates compatibility, several inks can be sintered at very low temperatures and performing properties close to the bulk materials[10,58], thus IP allows work with low temperature resistance substrates, as

polymeric-based ones.[10] Regarding the resolution, the inkjet printer allows drops ejection from 1 to 100 pl,[59] which corresponds to printed patterns with a maximum resolution about tends of microns, even micrometer and sub-micrometer resolution could be accomplished by means electrohydrodynamic inkjet (EHD), which allows drops ejection of femtoliter volume.[21,22,23] Among the printing techniques, IP is one of the most eco-friendly due to the drop on demand operating principle and the ink reservoir container, which allows ink storage and avoid premature ink degradation. At the end, IP is compatible with Roll to Roll (R2R) manufacturing process, which is a mass production manufacturing system. The highlights above presented, are the ones that make us to choose IP as the manufacturing technique to conduct the presented work. Nowadays, this technique is being used on several areas of technology, including displays,[60] paper and plastic electronics,[61] solder dispensing,[62] surface mount devices connecting,[10] rapid prototyping,[63] electronic components manufacturing,[64] enzyme-based sensors,[65] and tissue engineering.[66,67] In the following chapter, the IP technique is widely described.

1.3 State of the art of the additive manufactured printed circuit boards PCBs.

As above-mentioned, the electronic circuits are being integrated to everywhere (IoT). In fact, among the human daily life objects, huge efforts are being done onto the integration of electronic applications on cloths (or directly manufactured on fabric substrates), packaging, entertainment, furniture, vehicles interior, medical/cosmetic/entertainment smart-wearable patches and so on (*Figure 1.12*).

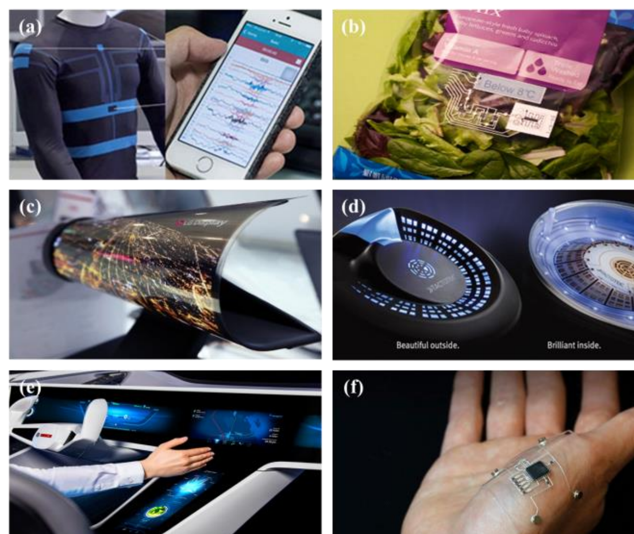

Figure 1.12 (a) Sensors integrated on cloths.[68] (b) Datalogger for tracking food.[69] (c) Flexible displays.[70] (d) Conformable electronics.[70] (e) Vehicle interior displays.[71] (f) Smart-wearable patche.[70]

This kind of applications make mandatory that electronic circuits possesses properties as flexibility,[72,3] stretchability[73,74] and conformability[75] among others. Therefore, in order to make it possible, the current functional materials, manufacturing techniques and substrates have being changed, adapted or modified, where PE techniques have positioned as successful manufacturing alternative. However, although some of the emerging applications can be fully manufactured by means PE techniques,[76,77] the present and incoming applications are growing on complexity i.e computational requirements, which force the integration of sophisticated/densified integrated circuits IC (microelectronic technology) beyond the capability of present-day PE technology. Due to this, although huge efforts have being done in the fully-printed IC and electronic circuits components such as transistors,[78–80] MIMs,[14] diodes,[43] resistances[81] and conductive strips,[82] at present, the printed IC are low densified and its basic components are under research to overcome several flaws: poor performances[83,84] and self-life[85,86] due to parasitic capacities, poor isolation and resolution. Therefore, in order to accomplish the high degree of reliability and quality of the incoming electronic applications, it is proposed a hybrid electronics which is fulfilled by combining the advantages of the printing technologies with the surface-mount technology (SMT).[87–91] The main issue related to this procedure is the attachment of the regular SMDs and standard silicon SMD packages onto the printed substrate. The current material employed for SMT is reflow paste,[92] a sticky mixture of flux and solder particles which shows high incompatibility with inkjet-printed pads. Solder particles on reflow process provokes a leaching effect by removing and damaging printed pads and generating undesired functional errors,[87] as well the elevated processing-temperature are not compatible with some of the substrates used in the incoming applications. In order to solve this gap between printed electronics and SMT some research groups have worked on alternatives to current assembling materials and processes. Among the related works on this field, the most prominent works are the follow:

A1. Niittynen *et al.* (2012)[87] assembled SMDs on inkjet-printed substrates by using an screen-printed isotropically conductive adhesive (ICA) (*Figure 1.13*). This study evaluated the reliability of ICA connections on inkjet-printed substrates by means temperature cycling test.[87]

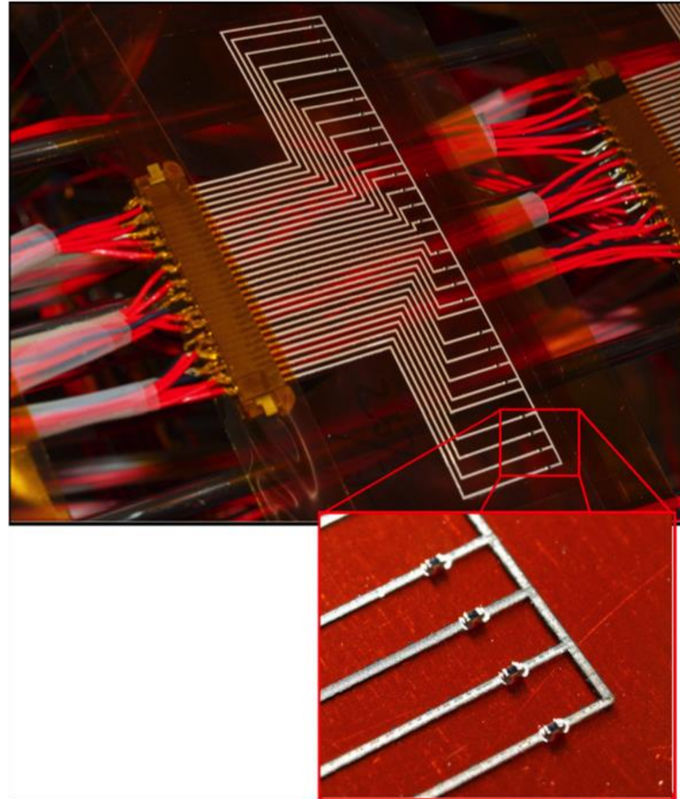

Figure 1.13 Setup for temperature cycling reliability test. Image from [87]

A2. Jussy Putaala *et al.* (2014)[89] assembled SMDs ceramic resistors on inkjet-printed flexible substrates by using different screen-printed isotropically conductive adhesives (ICA). The main research focus of their study was to investigate the reliability, by means temperature cycling test, of the interconnections between discrete, low-CTE ceramic passive components and high-CTE, flexible, thin plastic substrates with inkjet-printed lines and connecting pads (*Figure 1.14*).[89]

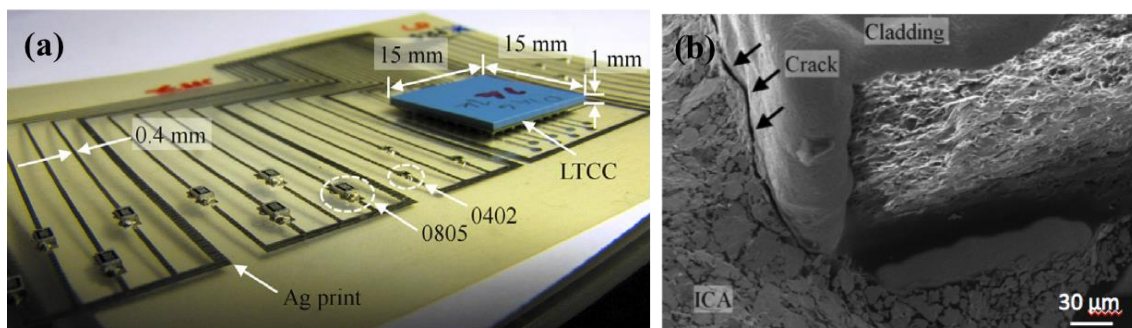

Figure 1.14 (a) Image of a fabricated test structure to conduct the reliability test. (b) SEM image of crack between the ICA and the component pad's solder cladding. Image from [89]

A3. Andersson *et al.* (2014)[88] assembled regular SMDs onto ink-jet printed photographic paper by means isotropic conductive adhesive (ICA), solder (iron-applied) and conductive adhesive tapes. In addition, the bonding strength was characterized by means a pull of test.[46] At other work, Andersson *et al.* (2016)[91] connected regular and silicon SMDs packages by means low melting temperature (138 °C) solder paste screen-printed on inkjet-printed photographic paper. Near field communications (NFT) tag on photographic paper was fabricated as demonstrator, which show cracks on paper coating due to elevated temperature on soldering process (*Figure 1.15*).[91]

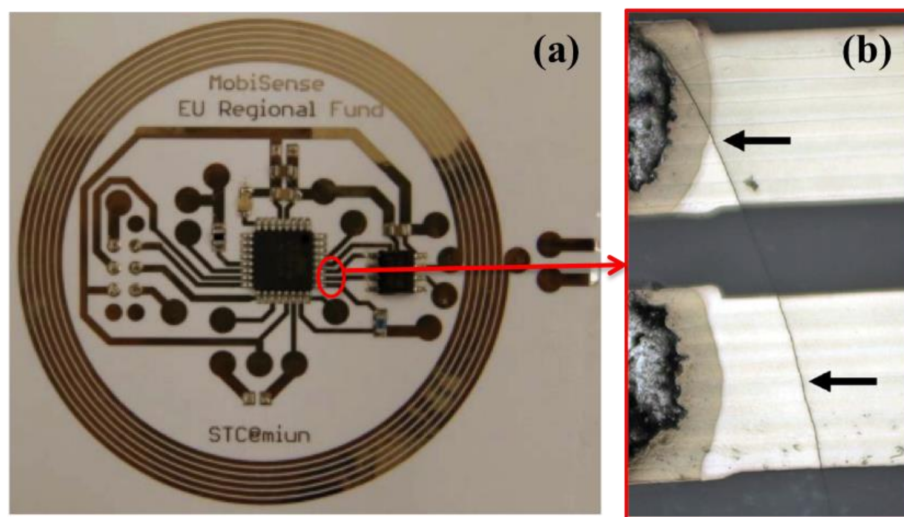

Figure 1.15 (a) NFC tags with quad flat package (QFP) and two-port packages soldered. (b) Magnification image of cracks on the paper coating and hence on the conductive strips, as indicated by arrows. Image from [91].

A4. GL Whiting *et al.* (2014)[93] combined a mixture of printed electronic components as photodiodes (blade-coated), temperature sensor (screen-printed), multiplexor organic thin-film transistors (TFTs) (inkjet-printed and spin-coated), resistors (inkjet-printed), capacitor (inkjet-printed and spin-coated), RF antenna and conductive wires (extruded) with complex microelectronic components. The silicon SMDs packages were mounted to the substrate (*Figure 1.16*) using a non-conductive two-part epoxy adhesive, and electrically connected to the system by means the extrusion of a viscous silver particle ink (DuPont5028).[93]

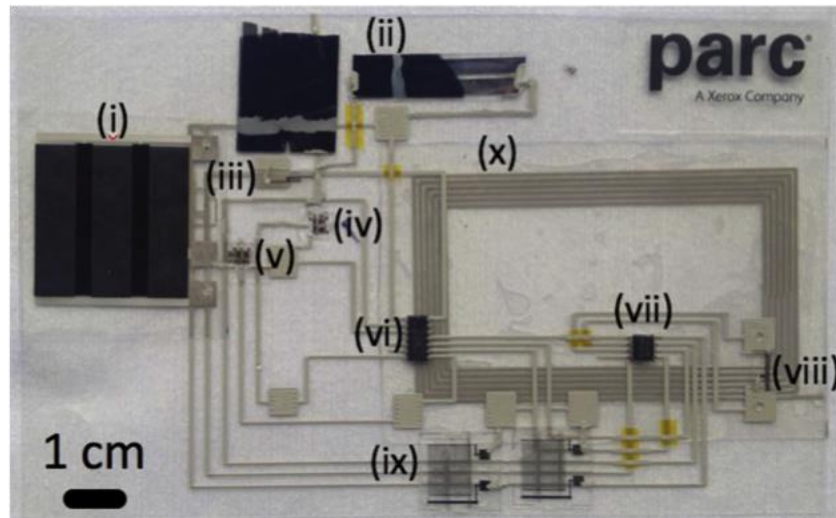

Figure 1.17 Optical image of device with the follow electronic components: (i) thermistor and static resistor for temperature sensor bridge (ii) photodiode (iii) static resistor for photodiode bridge (iv) photodiode multiplexing TFT (v) thermistor multiplexing TFT (vi) Microchip PIC (vii) Radio Frequency IC (viii) antenna capacitor (ix) pull-up resistors, (x) antenna. Image from [93]

A5. Xiaotian Li *et al.* (2018)[90] investigated the possibilities of using Sn42/Bi57.6/Ag0.4 low-temperature solder paste together with a reflow solder oven and hot air solder iron to mount regular surface mount device (SMD) components and standard Si SMD packages on screen-printed silver tracks on paper substrate. The solder paste was screen-printed and the bonding strength was characterized by means bending test and international standards.[90] NFC humidity sensing tag was fabricated as demonstrator (*Figure 1.18*).

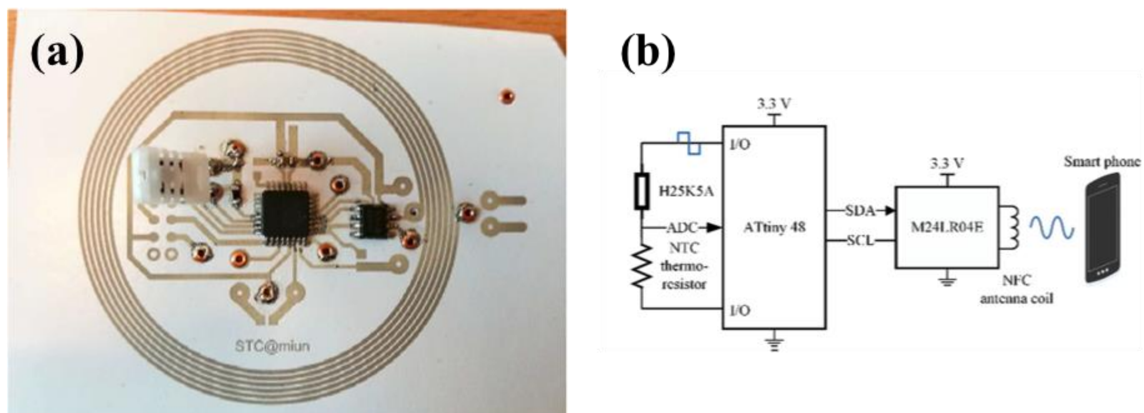

Figure 1.18 (a) An assembled NFC tag circuit board with RH sensing functionality. (b) Circuit diagram for the NFC tag. Image from [90]

Following, at the hybrid surface mount technology SMT, huge efforts are being performed to develop new connecting strategies for assemble silicon integrated circuits ICs on PCBs.[94–98] Concerning the ICs components currently encapsulated in standard Si SMD packages, its present manufacturing process is shown at *Figure 1.19*, where complex steps (die cutting, mounting, wire bonding) and a packaging are indispensable, this technology is also known as system on package (SoP). The current technologies, as wire bonding and flip-chip, used to connect the silicon die with the packaging terminations have some drawbacks. The wire bonding has high parasitic inductance and often requires of passive components for compensation at mm-wave frequencies. The flip-chip technique reduces interconnection length and parasitic yet suffer from high sensitivity to coefficient of thermal expansion (CTE) mismatch.[54] In addition, the standard Si SMD packages size difficult the bending and flexibility of the hybrid printed circuits.[99]

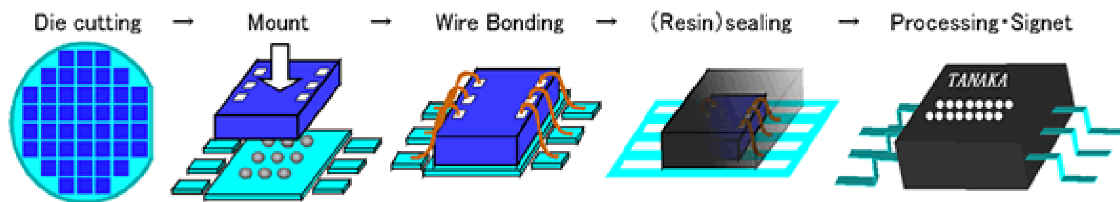

Figure 1.19 Schematic of SoP manufacturing process. Image from [60]

As above mentioned, in the last decade, some authors have proposed innovative ideas to assemble the silicon dies ICs on the PCB avoiding the current packaging. At some cases this assembling strategies reduce manufacturing steps, manufacturing wastage and promotes rapid prototyping, low cost electronics and flexible hybrid electronics (FHE). Among the related works on this field:

B1. Matti Mäntysalo *et al.* presented (2007)[101] a highly-integrated RF module where IC and discrete components are integrated together by means conventional printed wiring board technology and partly by inkjet printer avoiding standard IC packaging (*Figure 1.20*).[101] This is known as system in package SiP.

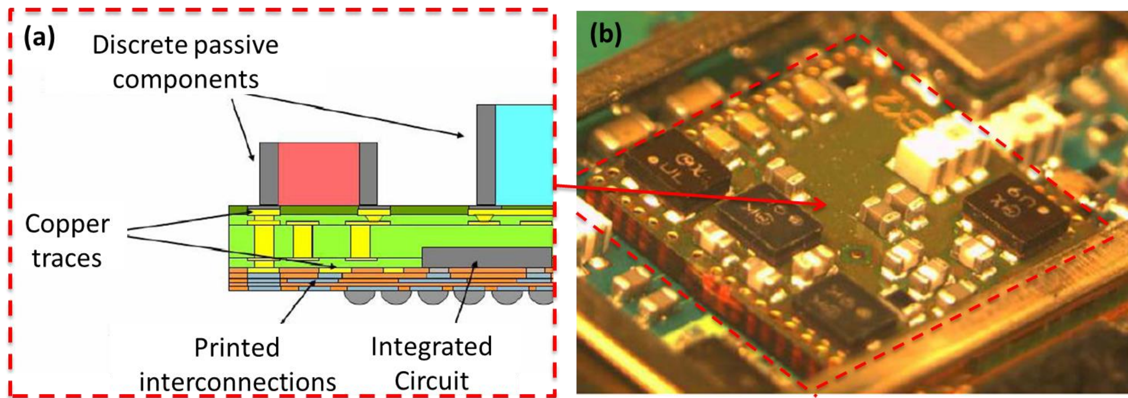

Figure 1.20 Schematic of the highly-integrated RF module architecture, where IC and discrete passive components integrated are connected by means conventional printed wiring board technology and partly by inkjet printer. (b) The finalized SiP attached on the main board. Image from [101]

B2. Jani Miettinen *et al.* presented (2008)[97] an electronic module where the IC and the discrete components are embedded inside a molding material that works as a substrate for inkjet printing. A multilayer circuit of six conductive layers with the respective insulating layers between them is inkjet-printed on the substrate, and hence connecting the electronic module (*Figure 1.21*).[97]

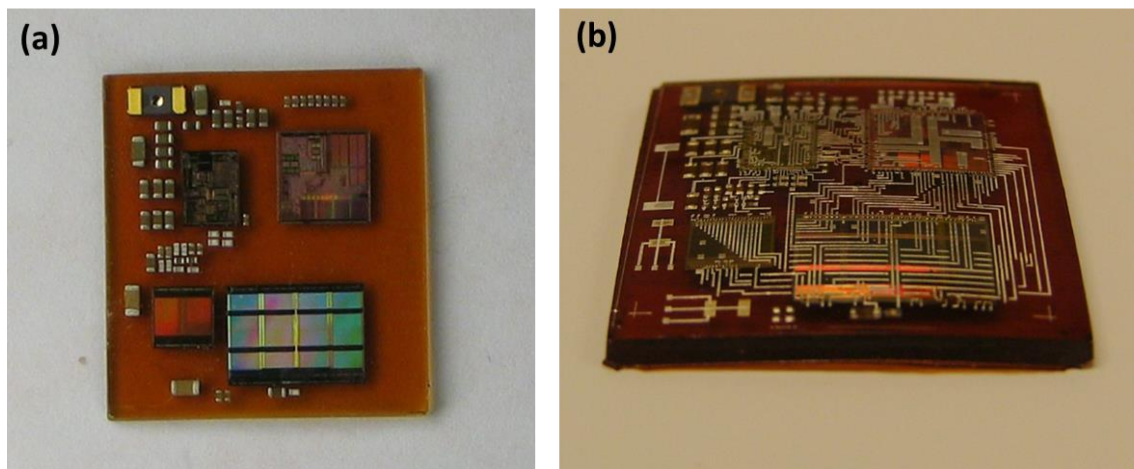

Figure 1.21 (a) Picture of the ICs and the discrete passive components embedded inside molding material. (b) After 1st inkjet-printed conductive layer. Image from [97]

B3. Ville Pekkanen *et al.* presented (2010)[98] a similar ICs and regular electronic components integration as Jani Miettinen[97] where the electronic components are embedded inside a molding material that works as a substrate for inkjet printing. The *Figure 1.22* shows a scheme of the corresponding manufacturing process and a first layer of conductive silicon die interconnections.[98]

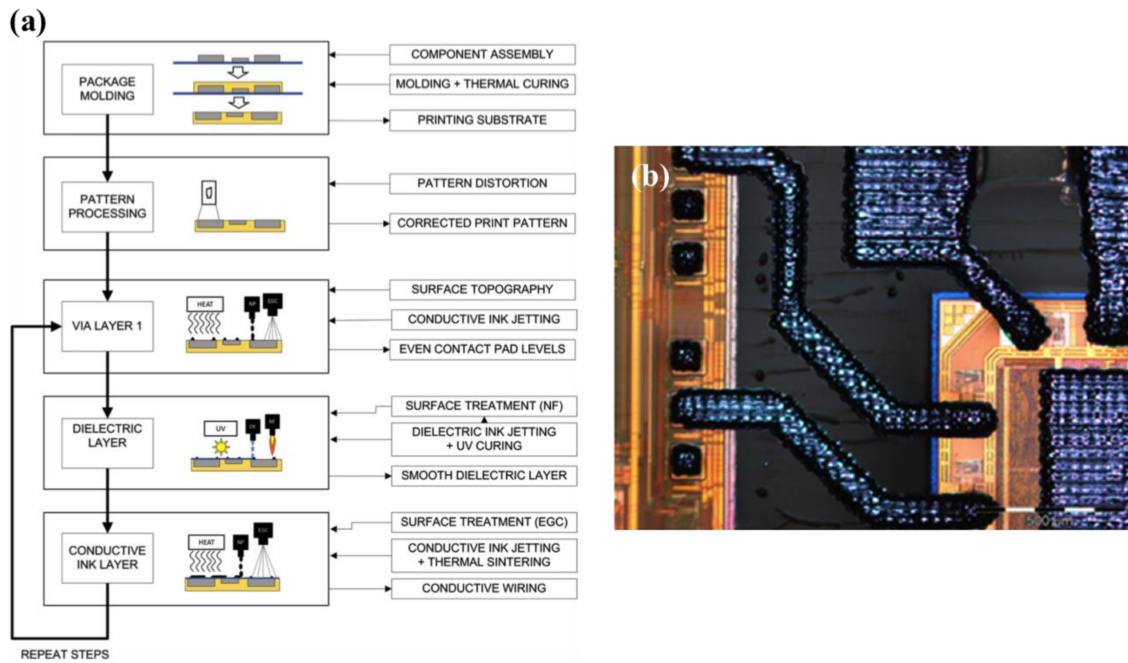

Figure 1.22 (a) SiP device interconnection manufacturing process flow. (b) Successful silicon chip interconnections in the first layer and interface between first dielectric layer and conductive wiring. Image adapted from [98]

B4. Bijan K. Tehrani *et al*. presented (2016)[94] an mm-wave antenna where the silicon IC die is attached and connected to glass substrate by means a SU8-based ramp and the print-on-slope technique, respectively. The coplanar waveguide (CPW) transmission lines are silver-based and all device is inkjet-printed (*Figure 1.23*).[94]

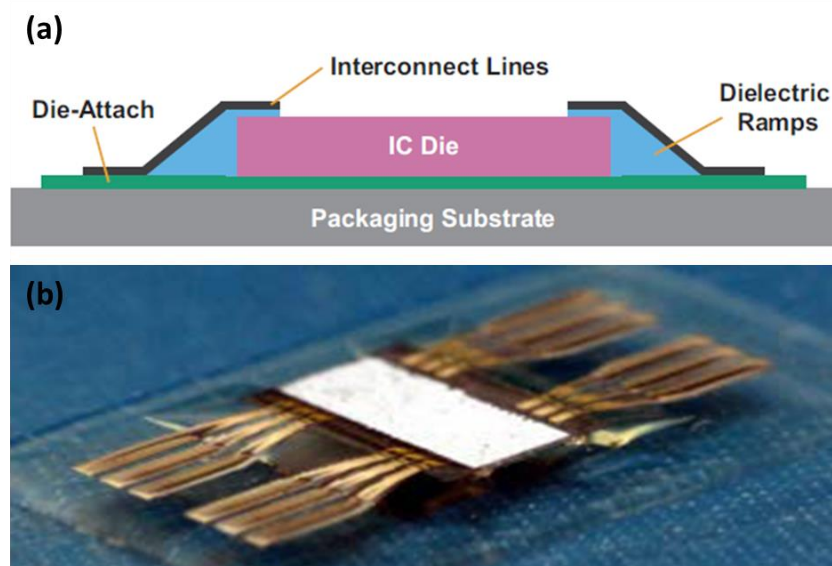

Figure 1.23 (a) Schematic of the print-on-slope technique for direct substrate IC die integration and connection. (b) mm-wave antenna on glass substrate with IC die connected by means a SU8-based ramp using the print-on-slope technique. Image adapted from [94]

B5. Jussi Putaala *et al.* presented (2017)[95] radio-frequency identification (RFID), where IC die is adhesive attached to flexible substrate, and the connections are performed by means inkjet print-on-slope technique (*Figure 5.5*).[95]

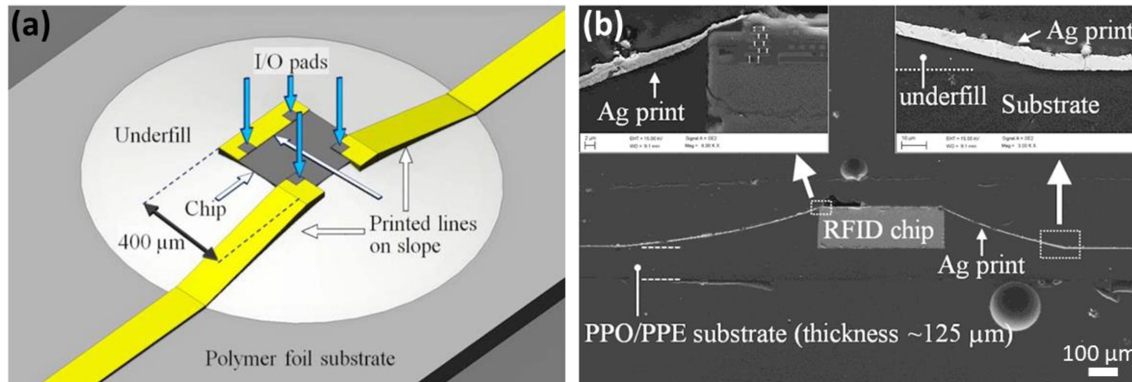

Figure 1.24 (a) Scheme of the print-on-slope technique for direct substrate IC die integration and connection. (b) Flexible radio-frequency identification (RFID), where IC die is connected by means inkjet print-on-slope technique. Image adapted from [95]

B6. Val R. Marinov presented (2017)[102] a semi-empirical test method, which allows for the estimation of the flexural strength of the highly compliant ultra-thin dies. At this work, the limiting Radius of Curvature (RoC) is tested, which is an important parameter for the flexible hybrid electronic FHE device since it accounts for the bending characteristics of the entire FHE device, not only the IC bending.[102] *Figure 1.25* depicts a photograph[102] to illustrate the imperativeness of thin dies, specifically of 25µm and 250µm thick dies attached onto a flexible substrate bent to a radius of approximately 1.2cm.

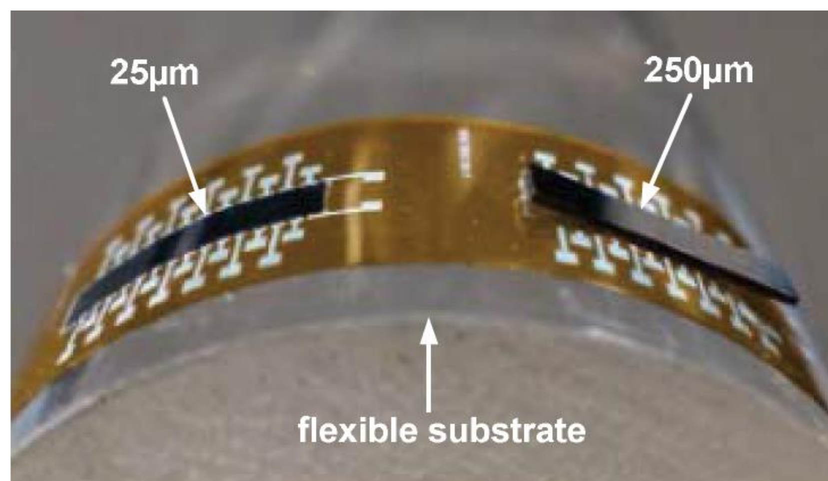

Figure 1.25 Photograph of a 25 µm thick silicon die (left) and a 250 µm thick die (right) on a flexible substrate. Image from 102

B7. Uniqarta Inc. developed (2017)[103] their innovative FlexChip Technology to handle ultra-thin silicon ICs. This technology can be used to assemble silicon ICs with <50 µm thickness onto flexible substrate without damaging the IC (*Figure 1.26*).[103]

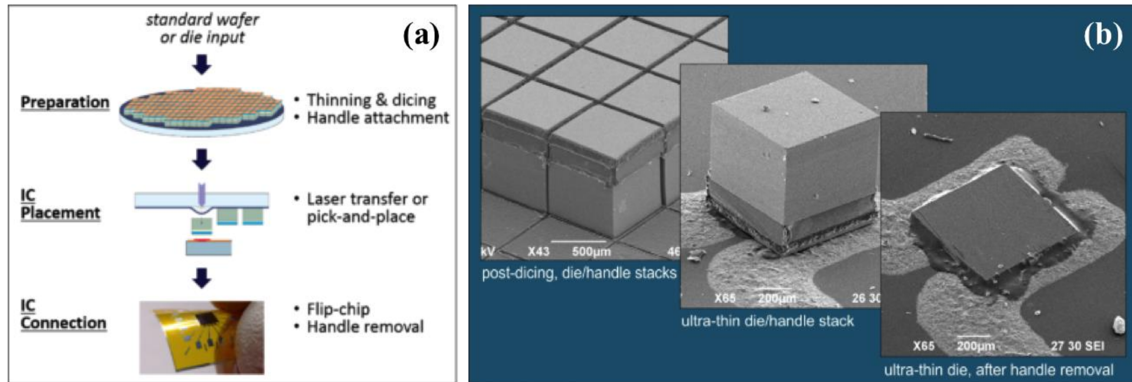

Figure 1.26 (a) Schematic of the Uniqarta ultra-thin silicon ICs assembling process proposed for fhe. (b) SEM images of ultra-thin die assembled by means a handle stack. Image from [103]

In addition to silicon die and regular SMDs assembling, research on inkjet multilayer manufacturing must be conducted in order to approach as much as possible the performance of the hybrid circuits inkjet-printed to the current PCB. In addition, additive manufacturing/rapid prototyping of multilayer PCB avoid wastage and tedious manufacturing steps of traditional PCB technology such as etching, stacking and laminating. Aiming to go ahead with hybrid PCBs inkjet-printed, more research on the dielectric materials is needed, which are currently used as insulators between strips and strips-ground on PCBs or into integrated circuits,[104,105,106,107,108] as well as electrical insulator on embedded devices.[109] Regarding the hybrid PCBs inkjet-printed, some companies presented pioneering solutions,[110] as Nano Dimension, which manufacture 3D PCBs by means a developed inkjet printer, which integrate layer by layer photo-sintering (Dragonfly) and specific inks (Figure 1.27).

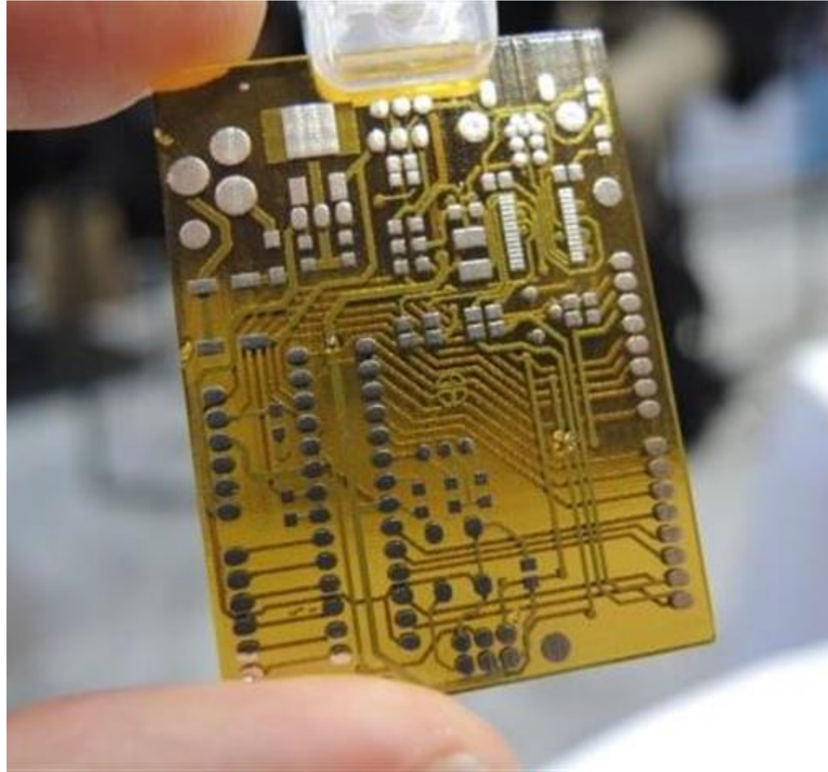

Figure 1.27 Multilayer inkjet-printed circuit board of Nano Dimension. Image from [111]

Among the platforms available for incoming hybrid PCBs, paper substrate has attracted considerable attention due to the properties shown as environmentally friendly, wearable, lightweight and low cost technology promoter. Several works presented the use of dielectric inks on paper substrate employing additive techniques. However, to the best of our knowledge, there are not works where the electrical properties performance of dielectric layers inkjet-printed on paper substrate is studied for insulating purposes. Among the related works on this field:

C1. Verónica Sánchez-Romaguera *et al.* presented (2008)[106] metal-insulator-metal crossovers study with SU-8 polymer insulator inkjet-printed onto glass substrate. They investigated and discussed the complex interrelation between surface treatment, print strategy, and materials processing on functionality, but not the properties of the insulating material.[106] On that study, they describe the optimization of a simple 3D all inkjet-printed feature. *Figure 1.28* shows the scheme of the pattern used to perform the study.

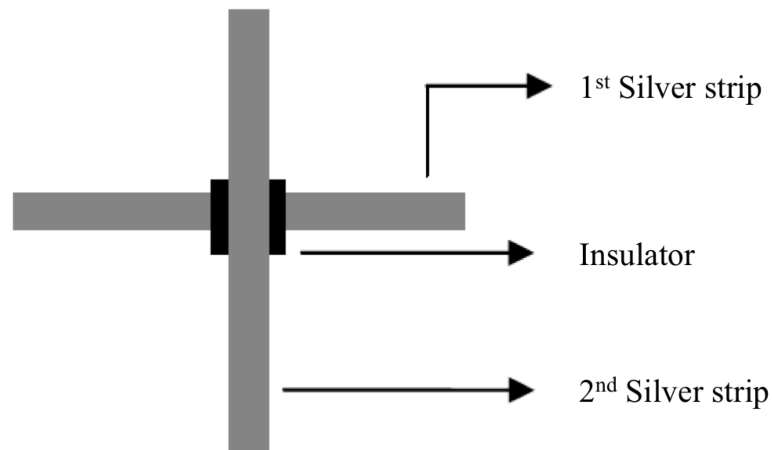

Figure 1.28 Schematic representation of the metal/insulator/metal (MIM) crossover used to perform the investigation at Verónica Sánchez-Romaguera *et al* work. Image adapted from [106]

C2. Myung-sung Hwang *et al.* presented (2010)[112] the dielectric properties performance of inkjet-printed alumina-resin hybrid films within copper plates. The dielectric properties of the hybrid films such as dielectric constant and Q-value are measured in order to evaluate if they are applicable to the package substrates. Several theoretical models are applied to the experimental data to understand the relative permittivity of alumina-resin hybrid material system.[112]

C3. Induja I. Jayapalan Nair *et al.* characterized (2016)[113] dielectric properties of alumina films screen-printed on photographic paper and biaxially-oriented polyethylene terephthalate (BoPET) substrates. In their work, they report for the first time, the microwave dielectric properties of the micron sized alumina ink. The rheological, structural, low frequency and microwave dielectric properties of the developed Al_2O_3 ink are also investigated.[113]

1.3.1 Drawbacks of the current strategies for inkjet-printed hybrid PCBs.

Nowadays, despite of the huge efforts that are being done on the manufacturing of inkjet-printed hybrid PCBs, the only automated method available to connect the regular SMDs and the standard silicon SMD packages is the screen-printing of reflow paste or ICA.[87–89,91] However, this method require specific stencil (screen) and produce considerable material wastage, which is the opposite of rapid prototyping and eco-friendly process, respectively. In addition, the assembling method does mandatory the combination of two different PE techniques (inkjet and screen-printing), which corresponds to expensive and large manufacturing line. Regarding the reflow process, currently used at PCB manufacturing, it is incompatible with some of the substrates used at incoming IoT low cost electronics.[10,87] Concerning the ICA connecting material, the electrical resistivity is 2 orders of magnitude higher than the current solder material employed at PCB manufacturing, and hence is not well-desired for the very low consuming applications.[10] Taking into account the evolution towards more densified circuits, the screen-printing technique could limits the gap reduction between terminations at silicon standard packaging due to their maximum resolution at factories, which is about 150 μm.

Concerning the ICs components currently assembled on hybrid PCBs, their manufacturing process contains complex steps, such as ICs manufacturing, die cutting, mounting, wire bonding and packaging, which suppose costs that couldn't be assumed by some low costs IoT applications. In addition, the current technologies, as wire bonding and flip-chip, used to connect the silicon die with the packaging terminations have some drawbacks. The wire bonding has high parasitic inductance at mm-wave frequencies and the flip-chip technique suffers from high sensitivity to coefficient of thermal expansion (CTE) mismatch. [54] At the end, the standard Si SMD packages size difficult the bending and flexibility of the hybrid printed circuits.[74]

Concerning the inkjet-printed multilayer circuits, further research on insulating materials deposit on paper substrate and the electrical properties characterization should be performed. In addition, at multilayer structures, each printed layer should be sintered previous to new material addition, which supposes considerable damage for weak substrates and the materials on it deposited.

1.4 Objectives

The aim of this thesis is to contribute on the development of the incoming low cost electronics by means of inkjet printing technology. Regarding that, a novel solution for assembling regular SMDs and standard silicon SMD packages by inkjet printing is explored. The novel connecting method should allow the assembling at very low temperatures, and thus assure the compatibility with the incoming substrates. The novel assembling method reliability and its electrical and mechanical performance should be at least comparable to current benchmarking materials. In addition, the improvement of the mechanical and electrical performance of the proposed novel assembling method is investigated.

Another objective of the work is to apply and adapt the print-on-slope technique to assemble directly the silicon dies on PCB, proposing a novel strategy to overcome the drawbacks of the wire bonding in the Conductive AFM measurements.

In the field of multilayer hybrid PCB manufacturing, the goal is to prove the potentiality of different metal-insulator-metal structures inkjet-printed and evaluate their reliability and the electrical performance for low cost multilayer circuit based on paper substrate.

1.5 Outline

The presented doctoral thesis is the outcome of a research done on inkjet-printed hybrid PCBs. The structure of this thesis dissertation can be divided in three specific blocks. The first block consists on chapters 2, on which the IP technique and several material-adding steps are explained in detail. In addition, several inks are tested aiming to choose the most appropriated for conducting the following chapters. The second block clusters the chapters 3, 4 and 5, which are focused on SMDs and silicon die assembling on printed circuit substrates by means IP. At the end, the third block consists on chapter 6, in which the properties of dielectric materials have been studied in order to develop multilayer paper PCB.

The chapter 1, gives a briefly overview of the printed electronics, as well a state of the art deeply overview of the specific hybrid-PCBs inkjet-printed field. In addition, the aims of this doctoral thesis are proposed.

In chapter 2, the main topic is the analysis of the inkjet printing technique by means testing a sample of inks and substrates. This chapter follows the attainment of different objectives as: establishing the guideline to characterise inkjet inks, discus different surface treatments for wettability control and show electrical and mechanical characterization methods of the deposited functional materials At the end, from the inks characterization performed, the best situated inks are selected for the following thesis research.

In chapter 3, 4 and 5, the main topic is related with the SMD and silicon die assembling to inkjet printed circuit boards by means IP. Aiming to manufacture a hybrid circuit fully inkjet-printed, at chapter 3, a novel method for SMD assembling by means inkjet is proposed. The mechanical and electrical performance accomplished is compared to benchmark materials and current assembling processes. Following, on chapter 4 the mechanical properties of the SMDs inkjet-assembled are improved by means the application of a mechanical reinforcement, which is characterized. Concerning the chapter 5, SMDs modified with slope-end are tested and properly characterized, as well compared to with the performance shown by the current SMDs with squared-end. Furthermore, taking advantage of the slope-end strategy and deepen on the potentiality of hybrid PCB, inkjet printer is used for direct integration of silicon die on printed substrate avoiding the use of the current wire bonding used at present system of package (SoP) manufacturing.

At the end, on chapter 6, aiming to contribute on the development of multilayer hybrid printed electronics, a research on different dielectric materials is presented and hence dielectric properties as relative permittivity, loss tangent and dielectric strength are characterized. At the end, a multilayer temperature sensor is fabricated as example of multilayer device inkjet-printed.

1.6 References

(1) Correia, V.; Mitra, K. Y.; Castro, H.; Rocha, J. G.; Sowade, E.; Baumann, R. R.; Lanceros-Mendez, S. Design and Fabrication of Multilayer Inkjet-Printed Passive Components for Printed Electronics Circuit Development. *J. Manuf. Process.* **2018**, *31*, 364–371.

(2) Wade, J.; Hollis, J. R.; Wood, S. Printed Electronics. **2018**, 0–17.

(3) Kessler, F. B.; Kessler, F. B.; Khan, S.; Lorenzelli, L.; Dahiya, R.; Member, S. Technologies for Printing Sensors and Electronics Over Large Flexible Substrates : A Review Technologies for Printing Sensors and Electronics over Large Flexible Substrates : A Review. *IEEE Sens. J.* **2015**, *15* (June), 3164–3185.

(4) Choi, H. W.; Zhou, T.; Singh, M.; Jabbour, G. E. Recent Developments and Directions in Printed Nanomaterials. *Nanoscale* **2015**, *7* (8), 3338–3355.

(5) Das, R. N.; Lin, H. T.; Lauffer, J. M.; Markovich, V. R. Printable Electronics: Towards Materials Development and Device Fabrication. *Circuit World* **2011**, *37* (1), 38–45.

(6) Hummelgård, M.; Zhang, R.; Nilsson, H. E.; Olin, H. Electrical Sintering of Silver Nanoparticle Ink Studied by In-Situ TEM Probing. *PLoS One* **2011**, *6* (2), 1–6.

(7) Grouchko, M.; Kamyshny, A.; Mihailescu, C. F.; Anghel, D. F.; Magdassi, S. Conductive Inks with a “Built-in” Mechanism That Enables Sintering at Room Temperature. *ACS Nano* **2011**, *5* (4), 3354–3359.

(8) Kang, J. S.; Ryu, J.; Kim, H. S.; Hahn, H. T. Sintering of Inkjet-Printed Silver Nanoparticles at Room Temperature Using Intense Pulsed Light. *J. Electron. Mater.* **2011**, *40* (11), 2268–2277.

(9) Moon, Y. J.; Lee, S. H.; Kang, H.; Kang, K.; Kim, K. Y.; Hwang, J. Y.; Cho, Y. J. Electrical Sintering of Inkjet-Printed Silver Electrode for c-Si Solar Cells. *Conf. Rec. IEEE Photovolt. Spec. Conf.* **2011**, 001061–001065.

(10) Arrese, J.; Vescio, G.; Xuriguera, E.; Medina-Rodriguez, B.; Cornet, A.; Cirera, A. Flexible Hybrid Circuit Fully Inkjet-Printed: Surface Mount Devices

Assembled by Silver Nanoparticles-Based Inkjet Ink. *J. Appl. Phys.* **2017**, *121* (10).

(11) Kiriya, D.; Javey, A.; Cho, G.; Chen, K.; Yeom, C.; Yu, Z. Large-Area Compliant Tactile Sensors Using Printed Carbon Nanotube Active-Matrix Backplanes. *Adv. Mater.* **2015**, *27* (9), 1561–1566.

(12) Arias, A. C.; MacKenzie, J. D.; McCulloch, I.; Rivnay, J.; Salleo, A. Materials and Applications for Large Area Electronics: Solution-Based Approaches. *Chem. Rev.* **2010**, *110* (1), 3–24.

(13) Søndergaard, R. R.; Hösel, M.; Krebs, F. C. Roll-to-Roll Fabrication of Large Area Functional Organic Materials. *J. Polym. Sci. Part B Polym. Phys.* **2013**, *51* (1), 16–34.

(14) Vescio, G.; López-Vidrier, J.; Leghrib, R.; Cornet, A.; Cirera, A. Flexible Inkjet Printed High-k HfO 2 -Based MIM Capacitors. *J. Mater. Chem. C* **2016**, *4* (9), 1804–1812.

(15) Ghaffarzadeh, K.; Yamamoto, Y. Conductive Ink Markets 2018-2028: Forecasts, Technologies, Players: IDTechEx https://www.idtechex.com/research/reports/conductive-ink-markets-2018-2028-forecasts-technologies-players-000580.asp (accessed Jul 20, 2018).

(16) Wu, W. Inorganic Nanomaterials for Printed Electronics: A Review. *Nanoscale* **2017**, *9* (22), 7342–7372.

(17) Kim, S.; Sojoudi, H.; Zhao, H.; Mariappan, D.; McKinley, G. H.; Gleason, K. K.; Hart, A. J. Ultrathin High-Resolution Flexographic Printing Using Nanoporous Stamps. *Sci. Adv.* **2016**, *2* (12).

(18) Grau, G.; Cen, J.; Kang, H.; Kitsomboonloha, R.; Scheideler, W. J.; Subramanian, V. Gravure-Printed Electronics: Recent Progress in Tooling Development, Understanding of Printing Physics, and Realization of Printed Devices. *Flex. Print. Electron.* **2016**, *1* (2).

(19) Harrey, P. M.; Ramsey, B. J.; Evans, P. S. A.; Harrison, D. J. Capacitive-Type Humidity Sensors Fabricated Using the Offset Lithographic Printing Process.

Sensors Actuators, B Chem. **2002**, *87* (2), 226–232.

(20) Hennig, G. Lasersonic® LIFT Process for Large Area Digital Printing. *J. Laser Micro/Nanoengineering* **2012**, *7* (3), 299–305.

(21) Mashayekhi, M.; Winchester, L.; Evans, L.; Pease, T.; Laurila, M. M.; Mantysalo, M.; Ogier, S.; Teres, L.; Carrabina, J. Evaluation of Aerosol, Superfine Inkjet, and Photolithography Printing Techniques for Metallization of Application Specific Printed Electronic Circuits. *IEEE Trans. Electron Devices* **2016**, *63* (3), 1246–1253.

(22) Kirbus, B.; Brachmann, E.; Hengst, C.; Menzel, S. B. Additive Manufacturing of 96 MHz Surface Acoustic Wave Devices by Means of Superfine Inkjet Printing. *Smart Mater. Struct.* **2018**.

(23) Laurila, M. M.; Khorramdel, B.; Mantysalo, M. Combination of E-Jet and Inkjet Printing for Additive Fabrication of Multilayer High-Density RDL of Silicon Interposer. *IEEE Trans. Electron Devices* **2017**, *64* (3), 1217–1224.

(24) Mathews, S. A.; Auyeung, R. C. Y.; Kim, H.; Charipar, N. A.; Piqué, A. High-Speed Video Study of Laser-Induced Forward Transfer of Silver Nano-Suspensions. *J. Appl. Phys.* **2013**, *114* (6).

(25) Sopeña, P.; Arrese, J.; González-Torres, S.; Fernández-Pradas, J. M.; Cirera, A.; Serra, P. Low-Cost Fabrication of Printed Electronics Devices through Continuous Wave Laser-Induced Forward Transfer. *ACS Appl. Mater. Interfaces* **2017**, *9* (35), 29412–29417.

(26) Fernández-Pradas, J. M.; Sopeña, P.; González-Torres, S.; Arrese, J.; Cirera, A.; Serra, P. Laser-Induced Forward Transfer for Printed Electronics Applications. *Appl. Phys. A* **2018**, *124* (2), 214.

(27) Mahajan, A.; Frisbie, C. D.; Francis, L. F. Optimization of Aerosol Jet Printing for High-Resolution, High-Aspect Ratio Silver Lines. *ACS Appl. Mater. Interfaces* **2013**, *5* (11), 4856–4864.

(28) Joost, R.; Salomon, R. High Quality Offset Printing. In *Proceedings of the 9th annual conference on Genetic and evolutionary computation - GECCO '07*;

ACM Press: New York, New York, USA, 2007; p 2053.

(29) Nomura, K. I.; Ushijima, H.; Mitsui, R.; Takahashi, S.; Nakajima, S. I. Screen-Offset Printing for Fine Conductive Patterns. *Microelectron. Eng.* **2014**, *123*, 58–61.

(30) Choi, Y.-M.; Lee, S.; Lee, E.; Lee, T.-M.; Kwon, S.; Kang, D.; Jo, J.; Kim, H. Development of a Precision Reverse Offset Printing System. *Rev. Sci. Instrum.* **2016**, *87* (1), 015102.

(31) Pudas, M.; Halonen, N.; Granat, P.; Vähäkangas, J. Gravure Printing of Conductive Particulate Polymer Inks on Flexible Substrates. *Prog. Org. Coatings* **2005**, *54* (4), 310–316.

(32) Secor, E. B.; Lim, S.; Zhang, H.; Frisbie, C. D.; Francis, L. F.; Hersam, M. C. Gravure Printing of Graphene for Large-Area Flexible Electronics. *Adv. Mater.* **2014**, *26* (26), 4533–4538.

(33) Jung, M.; Kim, J.; Noh, J.; Lim, N.; Lim, C.; Lee, G.; Kim, J.; Kang, H.; Jung, K.; Leonard, A. D.; et al. All-Printed and Roll-to-Roll-Printable 13.56-MHz-Operated 1-Bit RF Tag on Plastic Foils. *IEEE Trans. Electron Devices* **2010**, *57* (3), 571–580.

(34) Ding, J. M.; de la Fuente Vornbrock, A.; Ting, C.; Subramanian, V. Patternable Polymer Bulk Heterojunction Photovoltaic Cells on Plastic by Rotogravure Printing. *Sol. Energy Mater. Sol. Cells* **2009**, *93* (4), 459–464.

(35) Kopola, P.; Tuomikoski, M.; Suhonen, R.; Maaninen, A. Gravure Printed Organic Light Emitting Diodes for Lighting Applications. *Thin Solid Films* **2009**, *517* (19), 5757–5762.

(36) Izdebska, J. Flexographic Printing. In *Printing on Polymers*; Elsevier, 2016; pp 179–197.

(37) Liu, X.; Guthrie, J. T. A Review of Flexographic Printing Plate Development. *Surf. Coatings Int. Part B Coatings Trans.* **2003**, *86* (2), 91–99.

(38) Deganello, D.; Cherry, J. A.; Gethin, D. T.; Claypole, T. C. Patterning of Micro-Scale Conductive Networks Using Reel-to-Reel Flexographic Printing. *Thin*

Solid Films **2010**, *518* (21), 6113–6116.

(39) Boutant, Y.; Tedjini, S.; Delattre, A.; Vena, A.; Perret, E.; Garet, F.; Eymin Petot Tourtollet, G. Design of Chipless RFID Tags Printed on Paper by Flexography. *IEEE Trans. Antennas Propag.* **2013**, *61* (12), 5868–5877.

(40) Yan, H.; Chen, Z.; Zheng, Y.; Newman, C.; Quinn, J. R.; Dötz, F.; Kastler, M.; Facchetti, A. A High-Mobility Electron-Transporting Polymer for Printed Transistors. *Nature* **2009**, *457* (7230), 679–686.

(41) Lo, C. Y.; Huttunen, O. H.; Hiitola-Keinanen, J.; Petaja, J.; Fujita, H.; Toshiyoshi, H. MEMS-Controlled Paper-like Transmissive Flexible Display. *J. Microelectromechanical Syst.* **2010**, *19* (2), 410–418.

(42) Krebs, F. C.; Jørgensen, M.; Norrman, K.; Hagemann, O.; Alstrup, J.; Nielsen, T. D.; Fyenbo, J.; Larsen, K.; Kristensen, J. A Complete Process for Production of Flexible Large Area Polymer Solar Cells Entirely Using Screen Printing—First Public Demonstration. *Sol. Energy Mater. Sol. Cells* **2009**, *93* (4), 422–441.

(43) Krebs, F. C. Fabrication and Processing of Polymer Solar Cells: A Review of Printing and Coating Techniques. *Sol. Energy Mater. Sol. Cells* **2009**, *93* (4), 394–412.

(44) *Handbook of Print Media*; Kipphan, H., Ed.; Springer Berlin Heidelberg: Berlin, Heidelberg, 2001.

(45) Perl, A.; Reinhoudt, D. N.; Huskens, J. Microcontact Printing: Limitations and Achievements. *Adv. Mater.* **2009**, *21* (22), 2257–2268.

(46) Bietsch, A.; Michel, B. Conformal Contact and Pattern Stability of Stamps Used for Soft Lithography. *J. Appl. Phys.* **2000**, *88* (7), 4310.

(47) Sotomayor Torres, C. M. Alternative Lithography; 2003; pp 1–14.

(48) Zhou, X.; Xu, H.; Cheng, J.; Zhao, N.; Chen, S.-C. Flexure-Based Roll-to-Roll Platform: A Practical Solution for Realizing Large-Area Microcontact Printing. *Sci. Rep.* **2015**, *5* (1), 10402.

(49) Gates, B. D.; Xu, Q.; Stewart, M.; Ryan, D.; Willson, C. G.; Whitesides, G. M.

New Approaches to Nanofabrication: Molding, Printing, and Other Techniques. *Chem. Rev.* **2005**, *105* (4), 1171–1196.

(50) Loo, Y.-L.; Willett, R. L.; Baldwin, K. W.; Rogers, J. A. Interfacial Chemistries for Nanoscale Transfer Printing. *J. Am. Chem. Soc.* **2002**, *124* (26), 7654–7655.

(51) Nagel, R. D.; Haeberle, T.; Schmidt, M.; Lugli, P.; Scarpa, G. Large Area Nano-Transfer Printing of Sub-50-Nm Metal Nanostructures Using Low-Cost Semi-Flexible Hybrid Templates. *Nanoscale Res. Lett.* **2016**, *11* (1).

(52) Secor, E. B. Principles of Aerosol Jet Printing. *Flex. Print. Electron.* **2018**, *3* (3), 035002.

(53) Kim, B. J.; Lee, S.-K.; Kang, M. S.; Ahn, J.-H.; Cho, J. H. Coplanar-Gate Transparent Graphene Transistors and Inverters on Plastic. *ACS Nano* **2012**, *6* (10), 8646–8651.

(54) Cao, C.; Andrews, J. B.; Kumar, A.; Franklin, A. D. Improving Contact Interfaces in Fully Printed Carbon Nanotube Thin-Film Transistors. *ACS Nano* **2016**, *10* (5), 5221–5229.

(55) Agarwala, S.; Goh, G. L.; Yeong, W. Y. Optimizing Aerosol Jet Printing Process of Silver Ink for Printed Electronics. *IOP Conf. Ser. Mater. Sci. Eng.* **2017**, *191* (1), 012027.

(56) Sanchez-Aniorte, M. I.; Mouhamadou, B.; Alloncle, A. P.; Sarnet, T.; Delaporte, P. Laser-Induced Forward Transfer for Improving Fine-Line Metallization in Photovoltaic Applications. *Appl. Phys. A Mater. Sci. Process.* **2016**, *122* (6), 1–5.

(57) Andree, S.; Heidmann, B.; Ringleb, F.; Eylers, K.; Bonse, J.; Boeck, T.; Schmid, M.; Krüger, J. Production of Precursors for Micro-Concentrator Solar Cells by Femtosecond Laser-Induced Forward Transfer. *Appl. Phys. A Mater. Sci. Process.* **2017**, *123* (10), 1–8.

(58) Wong, W. S.; Salleo, A. *Flexible Electronics : Materials and Applications*; Springer, 2009.

(59) Derby, B. Inkjet Printing of Functional and Structural Materials: Fluid Property Requirements, Feature Stability, and Resolution. *Annu. Rev. Mater. Res.* **2010**, *40*

(1), 395–414.

(60) Mizukami, M.; Cho, S. Il; Watanabe, K.; Abiko, M.; Suzuri, Y.; Tokito, S.; Kido, J. Flexible Organic Light-Emitting Diode Displays Driven by Inkjet-Printed High-Mobility Organic Thin-Film Transistors. *IEEE Electron Device Lett.* **2018**, *39* (1), 39–42.

(61) Wang, Y.; Guo, H.; Chen, J. J.; Sowade, E.; Wang, Y.; Liang, K.; Marcus, K.; Baumann, R. R.; Feng, Z. S. Paper-Based Inkjet-Printed Flexible Electronic Circuits. *ACS Appl. Mater. Interfaces* **2016**, *8* (39), 26112–26118.

(62) Hayes, D. J.; Wallace, D. B.; Royall Cox, W. MicroJet Printing of Solder and Polymers for Multi-Chip Modules and Chip-Scale Packages. *Proceedings-SPIE Int. Soc. Opt. Eng.* **1999**, 242–247.

(63) Schnitker, J.; Adly, N.; Seyock, S.; Bachmann, B.; Yakushenko, A.; Wolfrum, B.; Offenhäusser, A. Rapid Prototyping of Ultralow-Cost, Inkjet-Printed Carbon Microelectrodes for Flexible Bioelectronic Devices. *Adv. Biosyst.* **2018**, *1700136*, 1700136.

(64) Fang, Y.; Wu, X.; Lan, S.; Zhong, J.; Sun, D.; Chen, H.; Guo, T. Inkjet-Printed Vertical Organic Field-Effect Transistor Arrays and Their Image Sensors. *ACS Appl. Mater. Interfaces* **2018**, *10*, acsami.8b06625.

(65) Li, Y.; Dahhan, O.; Filipe, C. D. M.; Brennan, J. D.; Pelton, R. H. Optimizing Piezoelectric Inkjet Printing of Silica Sols for Biosensor Production. *J. Sol-Gel Sci. Technol.* **2018**, *87* (3), 657–664.

(66) Bittner, S. M.; Guo, J. L.; Melchiorri, A.; Mikos, A. G. Three-Dimensional Printing of Multilayered Tissue Engineering Scaffolds. *Mater. Today* **2018**, *xxx* (xx).

(67) Williams, C. Ink-Jet Printers Go beyond Paper. *Phys. World* **2006**, *19* (1), 24–29.

(68) Insulectro printed Electronics. Printed electronics division. Apparel http://www.insulectro-pe.com/apparel.html (accessed Mar 5, 2019).

(69) Kari Embree. Breakthrough in printed electronics | Packaging Digest https://www.packagingdigest.com/smart-packaging/breakthrough-printed-

electronics (accessed Mar 5, 2019).

(70) Design HMI. Flexible Hybrid Electronics http://www.designhmi.com/2016/07/26/flexible-hybrid-electronics/ (accessed Mar 5, 2019).

(71) Ertico. Bosch turns the connected car into a personal assistant - ERTICO Newsroom https://erticonetwork.com/bosch-turns-connected-car-personal-assistant/ (accessed Mar 6, 2019).

(72) Eshkeiti, A.; Reddy, A. S. G.; Emamian, S.; Narakathu, B. B.; Joyce, M.; Joyce, M.; Fleming, P. D.; Bazuin, B. J.; Atashbar, M. Z. Screen Printing of Multilayered Hybrid Printed Circuit Boards on Different Substrates. *IEEE Trans. Components, Packag. Manuf. Technol.* **2015**, *5* (3), 415–421.

(73) Vanfleteren, J.; Gonzalez, M.; Bossuyt, F.; Hsu, Y. Y.; Vervust, T.; De Wolf, I.; Jablonski, M. Printed Circuit Board Technology Inspired Stretchable Circuits. *MRS Bull.* **2012**, *37* (3), 254–260.

(74) Tong, G.; Jia, Z.; Chang, J. Flexible Hybrid Electronics: Review and Challenges. *Proc. - IEEE Int. Symp. Circuits Syst.* **2018**, *2018–May*, 1–5.

(75) Plovie, B.; Yang, Y.; Guillaume, J.; Dunphy, S.; Dhaenens, K.; Van Put, S.; Vandecasteele, B.; Vervust, T.; Bossuyt, F.; Vanfleteren, J. Arbitrarily Shaped 2.5D Circuits Using Stretchable Interconnects Embedded in Thermoplastic Polymers. *Adv. Eng. Mater.* **2017**, *19* (8), 1–8.

(76) Lee, G.; Cho, G.; Lim, N.; Jung, M.; Kim, J.; Kim, J.; Kang, H.; Tour, J. M.; Lim, C.; Noh, J.; et al. All-Printed and Roll-to-Roll-Printable 13.56-MHz-Operated 1-Bit RF Tag on Plastic Foils. *IEEE Trans. Electron Devices* **2010**, *57* (3), 571–580.

(77) Kang, H.; Cho, G.; Jung, M.; Park, H.; Park, Y.; Kim, B. C.; Wallace, G. Fully Roll-to-Roll Gravure Printable Wireless (13.56 MHz) Sensor-Signage Tags for Smart Packaging. *Sci. Rep.* **2014**, *4* (1), 2–8.

(78) Huang, L.; Huang, Y.; Liang, J.; Wan, X.; Chen, Y. Graphene-Based Conducting Inks for Direct Inkjet Printing of Flexible Conductive Patterns and Their

Applications in Electric Circuits and Chemical Sensors. *Nano Res.* **2011**, *4* (7), 675–684.

(79) Torrisi, F.; Hasan, T.; Wu, W.; Sun, Z.; Lombardo, A.; Kulmala, T. S.; Hsieh, G.-W.; Jung, S.; Bonaccorso, F.; Paul, P. J.; et al. Inkjet-Printed Graphene Electronics. *ACS Nano* **2012**, *6* (4), 2992–3006.

(80) Ko, S. H.; Pan, H.; Grigoropoulos, C. P.; Luscombe, C. K.; Fréchet, J. M. J.; Poulikakos, D. All-Inkjet-Printed Flexible Electronics Fabrication on a Polymer Substrate by Low-Temperature High-Resolution Selective Laser Sintering of Metal Nanoparticles. *Nanotechnology* **2007**, *18* (34).

(81) Materials, A. Inkjet Printed Via-Hole Interconnections and Resistors for All-Polymer Transistor Circuits . Adv Mater 13 : 1601. **2016**, No. April, 1601–1605.

(82) Jang, S.; Seo, Y.; Choi, J.; Kim, T.; Cho, J.; Kim, S.; Kim, D. Sintering of Inkjet Printed Copper Nanoparticles for Flexible Electronics. *Scr. Mater.* **2010**, *62* (5), 258–261.

(83) Li, J.; Zhao, Y.; Tan, H. S.; Guo, Y.; Di, C. A.; Yu, G.; Liu, Y.; Lin, M.; Lim, S. H.; Zhou, Y.; et al. A Stable Solution-Processed Polymer Semiconductor with Record High-Mobility for Printed Transistors. *Sci. Rep.* **2012**, *2*, 1–9.

(84) Tseng, H. Y.; Subramanian, V. All Inkjet-Printed, Fully Self-Aligned Transistors for Low-Cost Circuit Applications. *Org. Electron. physics, Mater. Appl.* **2011**, *12* (2), 249–256.

(85) Faber, H.; Burkhardt, M.; Jedaa, A.; Kälblein, D.; Klauk, H.; Halik, M. Low-Temperature Solution-Processed Memory Transistors Based on Zinc Oxide Nanoparticles. *Adv. Mater.* **2009**, *21* (30), 3099–3104.

(86) Chung, S.; Kim, S. O.; Kwon, S. K.; Lee, C.; Hong, Y. All-Inkjet-Printed Organic Thin-Film Transistor Inverter on Flexible Plastic Substrate. *IEEE Electron Device Lett.* **2011**, *32* (8), 1134–1136.

(87) Niittynen, J.; Kiilunen, J.; Putaala, J.; Pekkanen, V.; Mäntysalo, M.; Jantunen, H.; Lupo, D. Reliability of ICA Attachment of SMDs on Inkjet-Printed Substrates. *Microelectron. Reliab.* **2012**, *52* (11), 2709–2715.

(88) Andersson, H. a; Manuilskiy, A.; Haller, S.; Hummelgård, M.; Sidén, J.; Hummelgård, C.; Olin, H.; Nilsson, H.-E. Assembling Surface Mounted Components on Ink-Jet Printed Double Sided Paper Circuit Board. *Nanotechnology* **2014**, *25* (9), 094002.

(89) Putaala, J.; Hannu, J.; Kunnari, E.; Mäntysalo, M.; Nousiainen, O.; Jantunen, H. Reliability of SMD Interconnections on Flexible Low-Temperature Substrates with Inkjet-Printed Conductors. *Microelectron. Reliab.* **2014**, *54* (1), 272–280.

(90) Li, X.; Andersson, H.; Sidén, J.; Schön, T. Soldering Surface Mount Components on Screen-Printed Ag Patterns on Paper and Polyimide Substrates for Hybrid Printed Electronics. *Flex. Print. Electron.* **2018**, *3* (1), 015003.

(91) Andersson, H.; Siden, J.; Skerved, V.; Li, X.; Gyllner, L. Soldering Surface Mount Components onto Inkjet Printed Conductors on Paper Substrate Using Industrial Processes. *IEEE Trans. Components, Packag. Manuf. Technol.* **2016**, *6* (3), 478–485.

(92) Xu, S.; Habib, A. H.; Pickel, A. D.; McHenry, M. E. Magnetic Nanoparticle-Based Solder Composites for Electronic Packaging Applications. *Prog. Mater. Sci.* **2015**, *67*, 95–160.

(93) Whiting, G. L.; Schwartz, D. E.; Ng, T. N.; Krusor, B. S.; Krivacic, R.; Pierre, A.; Arias, A. C.; Härting, M.; van Buren, D.; Short, K. L. Digitally Fabricated Multi-Modal Wireless Sensing Using a Combination of Printed Sensors and Transistors with Silicon Components. *Flex. Print. Electron.* **2017**, *2* (3), 034002.

(94) Tehrani, B. K.; Cook, B. S.; Tentzeris, M. M. Inkjet-Printed 3D Interconnects for Millimeter-Wave System-on-Package Solutions. *IEEE MTT-S Int. Microw. Symp. Dig.* **2016**, *2016–Augus*.

(95) Putaala, J.; Niittynen, J.; Hannu, J.; Myllymäki, S.; Kunnari, E.; Mäntysalo, M.; Hagberg, J.; Jantunen, H. Capability Assessment of Inkjet Printing for Reliable RFID Applications. *IEEE Trans. Device Mater. Reliab.* **2017**, *17* (2), 281–290.

(96) Mäntysalo, M.; Mansikkamäki, P.; Miettinen, J.; Kaija, K. Evaluation of Inkjet Technology for Electronic Packaging and System Integration. In *Electronic components and technology conference*; 2007; Vol. c, pp 89–94.

(97) Miettinen, J.; Pekkanen, V.; Kaija, K.; Mansikkamäki, P.; Mäntysalo, J.; Mäntysalo, M.; Niittynen, J.; Pekkanen, J.; Saviauk, T.; Rönkkä, R. Inkjet Printed System-in-Package Design and Manufacturing. *Microelectronics J.* **2008**, *39* (12), 1740–1750.

(98) Pekkanen, V.; Mäntysalo, M.; Kaija, K.; Mansikkamäki, P.; Kunnari, E.; Laine, K.; Niittynen, J.; Koskinen, S.; Halonen, E.; Caglar, U. Utilizing Inkjet Printing to Fabricate Electrical Interconnections in a System-in-Package. *Microelectron. Eng.* **2010**, *87* (11), 2382–2390.

(99) Tong, G.; Jia, Z.; Chang, J. Flexible Hybrid Electronics : Review and Challenges.

(100) TANAKA HOLDINGS Co. Bonding Lab Process of gold bonding wire https://pro.tanaka.co.jp/en/solution/technology/technology09/ (accessed Feb 14, 2019).

(101) Mantysalo, M.; Mansikkamaki, P.; Miettinen, J.; Kaija, K.; Pienimaa, S.; Ronkka, R.; Hashizume, K.; Kamigori, A.; Matsuba, Y.; Oyama, K.; et al. Evaluation of Inkjet Technology for Electronic Packaging and System Integration. In *2007 Proceedings 57th Electronic Components and Technology Conference*; IEEE, 2007; Vol. c, pp 89–94.

(102) Marinov, V. R. The IC in the Flexible Hybrid Electronics Technology: Flexibility and Bend Testing. *Int. Symp. Microelectron.* **2017**, *2017* (1), 000103–000108.

(103) Uniqarta, I. FlexChip Ultra-Thin Die Assembly https://uniqarta.com/?page_id=347 (accessed Feb 25, 2019).

(104) McKerricher, G.; Gonzalez, J.; Shamim, A. All Inkjet Printed 3D Microwave Capacitors and Inductors with Vias. *IEEE MTT-S Int. Microw. Symp. Dig.* **2013**, 9–11.

(105) Jiang, J.; Bao, B.; Li, M.; Sun, J.; Zhang, C.; Li, Y.; Li, F.; Yao, X.; Song, Y. Fabrication of Transparent Multilayer Circuits by Inkjet Printing. *Adv. Mater.* **2016**, *28* (7), 1420–1426.

(106) Sanchez-Romaguera, V.; Madec, M. B.; Yeates, S. G. Inkjet Printing of 3D Metal-Insulator-Metal Crossovers. *React. Funct. Polym.* **2008**, *68* (6), 1052–

1058.

(107) Laurila, M. M.; Khorramdel, B.; Mantysalo, M. Combination of E-Jet and Inkjet Printing for Additive Fabrication of Multilayer High-Density RDL of Silicon Interposer. *IEEE Trans. Electron Devices* **2017**, *64* (3), 1217–1224.

(108) Baklanov, M. R.; Adelmann, C.; Zhao, L.; De Gendt, S. Advanced Interconnects: Materials, Processing, and Reliability. *ECS J. Solid State Sci. Technol.* **2014**, *4* (1), Y1–Y4.

(109) Boettcher, L.; Manessis, D.; Ostmann, A.; Karaszkiewicz, S.; Reichl, H. Embedding of Chips for System in Package Realization - Technology and Applications. In *2008 3rd International Microsystems, Packaging, Assembly & Circuits Technology Conference*; IEEE, 2008; pp 383–386.

(110) Muthu, V.; Chatterjee, P.; Jet, T. K. Review on Application of Additive Manufacturing for Electrical Power Converters. *Ieee Tencon* **2016**, 2327–2333.

(111) 3ders.org. Nano Dimension has completed its “Switch” software package for 3D printed PCBs https://www.3ders.org/articles/20160705-nano-dimension-has-completed-its-switch-software-package-for-3d-printed-pcbs.html (accessed Mar 3, 2019).

(112) Hwang, M. S.; Kim, J.; Kim, H. T.; Yoon, Y.; Hyun, S.; Kim, J.; Lee, S. N.; Moon, J. Inkjet-Printing of Nonsintered Alumina-Resin Hybrid Films and Their Dielectric Properties. *J. Appl. Phys.* **2010**, *108* (10).

(113) Nair, I. I. J.; Varma, M. R.; Sebastian, M. T. Low Cost Room Temperature Curable Alumina Ink for Printed Electronic Applications. *J. Mater. Sci. Mater. Electron.* **2016**, *27* (9), 9891–9899.

FUNCTIONAL ASPECTS OF INKJET PRINTING TECHNOLOGY

CHAPTER 2

2.1 Introduction

Inkjet printing is a type of digital-assisted printing that recreates patterns by dispensing and precise positioning of very small volume of fluid (1-100 picoliters) on a substrate before transformation to solid. Since its invention, inkjet printing has been commonly used for graphics and marking purposes, and nowadays, the inkjet printer is an omnipresent personal printing tool at office and home desktop. However, in recent years there is considerable interest on the use of inkjet printing as a manufacturing tool for depositing functional and structural materials in a several areas of technology, including displays,[1] paper and plastic electronics,[2] solder dispensing,[3] surface mount devices connecting,[4] rapid prototyping,[5] electronic components manufacturing,[6] enzyme-based sensors,[7] and tissue engineering.[8,9] The application of inkjet printing to this dissimilar group of topics reflects the versatility of the method and its potential.

Nowadays, in contemporary inkjet printers, there are two main technologies: the continuous inkjet technology (CIJ) and the Drop-on-demand (DOD) technology.[10] The CIJ basics relays on the mechanism described by Lord Rayleigh in 1878, which explains why a liquid stream breaks up into droplets.[11] From this principle, Siemens introduced the first commercial device at 1951, the Elmqvist, a medical strip chart recorder, which was the first practical Rayleigh break up ink-jet.[12] The operating principle of CIJ is shown in *Figure 2.1*

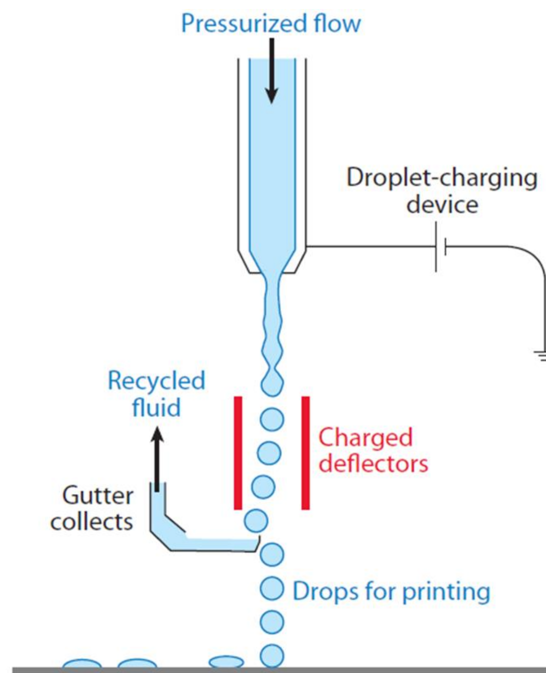

Figure 2.1 Schematic diagram of the operating principle of CIJ printer. Image from [13]

On the other hand, and concerning to DOD, there are two different technologies: the piezoelectric inkjet (PIJ) and the thermal inkjet (TIJ) also known as bubble inkjet. The inventors of the PIJ were Kyser and Sears,[14] and Zoltan[15], whose invent consists on the application of voltage pulses to a piezoelectric ceramic, which is the wall of a fluid chamber. Therefore, ink drops are ejected by a pressure wave created by the mechanical motion of that piezoelectric wall (*Figure 2.2 a*).[9,13,16] Their inventions were used in the Siemens PT-80 serial character printer (1977) and in Silonics printer (1978).[16] Following, during the same time period (1977-81), two teams of different companies develop the TIJ or bubble inkjet printer, John Vaught and Dave Donald of Hewlett Packard,[17] while Toshitami Hara and Ichiro Endo for Canon.[18] The invention consists on a resistor integrated inside the fluid chamber, which is used to heat the surrounding ink and generating a small bubble. When the current through the resistor is removed the heat transfer leads to rapid bubble collapse, thus a pressure pulse is produced, which promotes drop formation and ejection (*Figure 2.2 b*). [9,13,16]

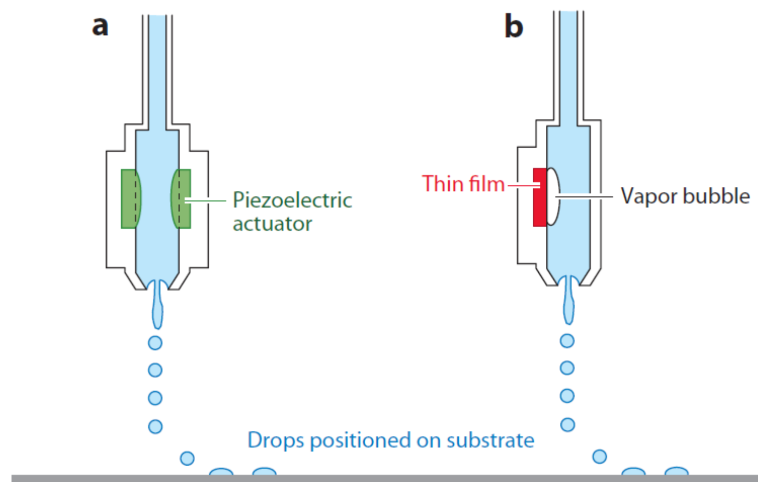

Figure 2.2 Schematic diagrams that show the operating principle of a DOD inkjet printing systems. (a) Piezoelectric inkjet (PIJ). (b) Thermal inkjet (TIJ). Image from [13]

Among the inkjet technologies available, to conduct this thesis research, the DOD systems is chosed, more economical with ink delivery than CIJ systems.[13] Moreover, the drop positioning of DOD is less complex than CIJ and the resolution is higher. Concerning to DOD, the specific technology chosen was PIJ for many reasons: with PIJ there are more available solvents that accomplish the fluid jetting requirements than for TIJ. In addition, PIJ can change the actuation pulse relatively easy, which allows higher control of drop size and velocity than TIJ. Despite of that, all the inkjet technologies

share a number of physical operations that define and constrain inkjet printing at digital image transfer process. These are:

1. Generation of droplets.
2. Positioning and interaction of droplets on a substrate and with previous deposited materials.
3. Drying and sintering mechanisms to produce a functional deposit.
4. Adhesion to receptor substrate.

This chapter pursues two objectives. The first one is to analyse the specific features of PIJ and the common ones of inkjet printing technology. The second one is to determine the most appropriated inks to conduct the rest of the thesis research.

2.2 Generation of droplets with PIJ printers.

As commented above, drops in DOD printers are formed by means of a pressure pulse inside a fluid chamber, which is practically dissipated at droplet formation. The pressure pulse must have enough energy to overcome the viscous losses and to break the surface tension of the liquid.[19] In the *Figure 2.3,* a PIJ printhead and the piezoelectric structure needed for the generation of pressure pulse are shown.

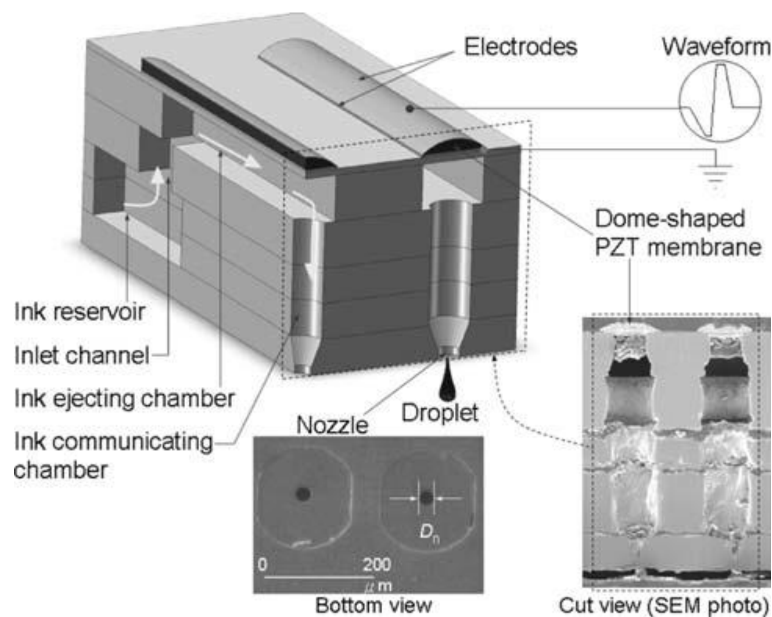

Figure 2.3 Structural, bottom view and cross section of PIJ printhead. Image from [20]

Different pressure pulses generated by voltage waveforms allow drops ejection for a specific ink,[21] but the best waveform is the one that dispenses perfectly formed drops at a high speed. This thesis has been performed practically with a Dimatix 2831 inkjet printer from Fujifilm (equipped with 10 µl or 1 µl printhead), but also some specific test were carried out on a Xennia Carnelian 4000 (80 µl Xaar printhead) (*Figure 2.4*).

Figure 2.4 (a) Picture of Dimatix 2831 inkjet printer from Fujifilm. (b) Picture of Carnelian 4000 inkjet printer from Xennia.

The voltage waveform structure proposed by printer manufacturer (Dimatix, Fujifilm) is usually used, which functionality has been checked as found on literature.[20] The waveform proposed by Dimatix is an electric pulse comprising six time intervals: filling (T1), first holding (T2), extruding (T3), second holding (T4), breakup of extruded liquid (T5-T6) and damping of residual vibrations (T6). These time intervals can be grouped on three segments: filling (T1 and T2), extrusion (T3 and T4) and breakup (T5 and T6) (*Figure 2.5*).

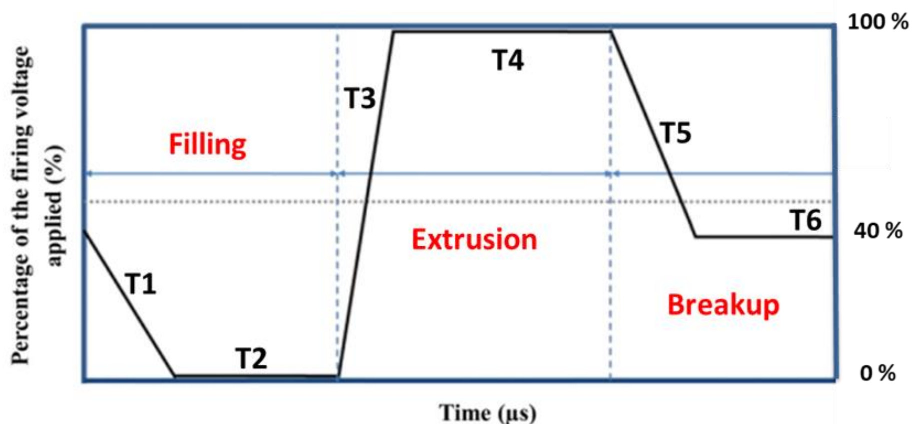

Figure 2.5 The current waveform used for drops forming, where the six time intervals are identified

After breakup occurs, the system relaxes the residual vibrations, and next, a new drop forming cycle starts. In a drop ejection cycle, the piezoelectric voltage starts as finished at previous drop ejection (T6), at this point the fluid chamber is slightly compressed (*Figure 2.6 (a)*). Following, at T1 the piezoelectric voltage is reduced with specific rate and the fluid chamber is enlarged, thus promoting the ink suction and pulling the meniscus ink/air into the nozzle. The ink suction process also comprises the T2 in which the piezoelectric remains at cero voltage. Therefore, both segments T1 and T2 are represented by *Figure 2.6 (b)*. Following, at T3 the piezoelectric voltage is increased sharply and the fluid chamber is comprised, extruding the ink from the nozzle. The fluid extrusion follows with the T4 when the piezoelectric voltage remains constant at maximum voltage applied (T3 and T4 are illustrated on *Figure 2.6 (c)*). During T5, piezoelectric voltage drops from 100% to 40%, which expands the piezoelectric membrane, and hence the fluid chamber enlarge again and the liquid suction promotes the breakup of the extruded ink forming a drop (*Figure 2.6 (d)*). During T6, piezoelectric membrane starts to oscillate at its inherent natural frequency. The oscillations after the applied electric pulse are so-called residual vibrations and are properly dampened by the discharging operation performed during T5. At the end of T6, the fluid chamber is stabilized and new drop ejection cycle is started. In addition, non-jetting waveform may be used to keep the meniscus moving in each nozzle even when not actively firing. This can help to prevent the nozzles from "skinning over" due to solvent evaporation and can improve print quality.[22]

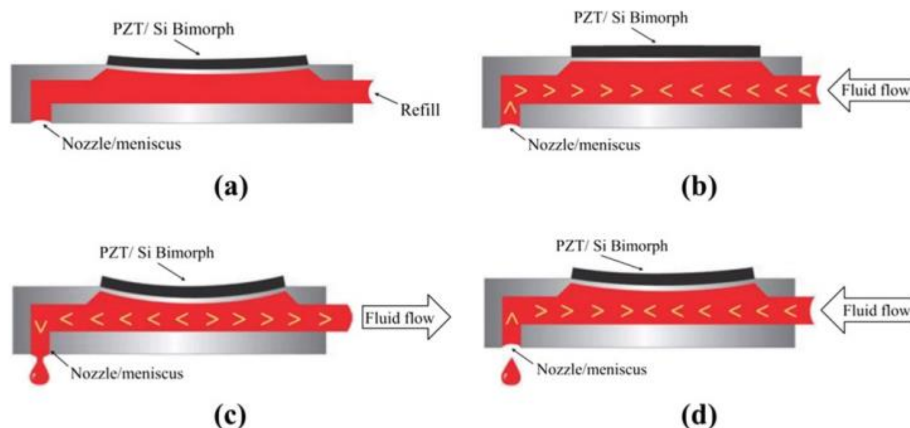

Figure 2.6 Diagram of fluid response to chamber deformation. (a) Fluid response at initial position, which correspond to final time interval of the previous drop ejection T6. (b) Corresponds to time intervals T1 and T2, where the ink is filled on the fluid chamber. (c) Corresponds to time intervals T3 and T4, where the ink column is extruded from the nozzle. (d) Corresponds to time intervals T5 and T6, where breakup and damping of the residual vibrations is produced. Image from [23]

The waveforms used for drop ejection are currently generated at acoustic frequencies (typically 1–20 kHz). As oscillation system, the chamber presents intrinsic resonances, which have strongly influence on the proper drop generation and printing stability.[20] Regarding to the drop size, the diameter of an in-flight drop is approximately equal to the nozzle diameter, although it can be tuned by means of pressure pulse waveform.[13] Concerning to the ejected drop, at extrusion process T5, a tale is generated, which is tied to fluid held on nozzle since this ligament breaks up. After breakup, if tale is too long to recoil into the main body of the drop, this can lead to satellite drops formation (*Figure 2.7*) (At next section satellite drops formation is explained with more detail). Often these drops catch up and merge to the leading large drop in flight, prior to impact, in which cases there are no defects on printing resolution. However, if there are satellite drops at impact, the noncircular footprint endangers the final deposit resolution, precision and accuracy. These satellite drops can be avoided by means a proper waveform and ink rheology, but also a stand-off distance from substrate facilitates the drop merging in flight. However, the stand-off distance has to be the minimum to avoid air currents, which can deviate drops from their desired trajectory.

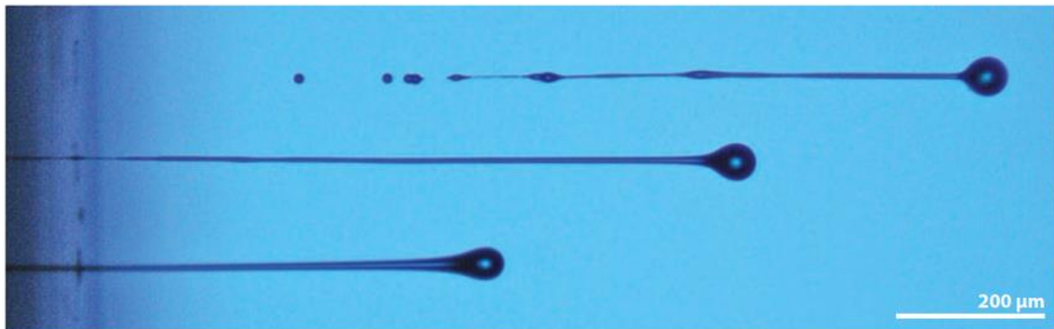

Figure 2.7 Picture showing a drop formation process by means three drops at different stages of formation. At the end the tail break up into trail of satellite droplets behind the primary drop. Image from [13]

As commented above, driving waveform parameters such as voltage value, waveform shape, and interval time duration are relevant parameters to proper drop ejection. However, at inkjet printing technique, the fluid parameters are the most restrictive on fluid jettability. These parameters are commented more deeply in this chapter.

2.3 Jettable fluids

A fluid accomplishes the inkjet requirements depending on its jettability, which can be understood as the capability of proper drop formation, as well the jetting of the drop through the nozzle of a printhead. Concerning that, chemical compatibility with cartridge and nozzles, stable droplet formation, appropriated drop shape reached, at each singular drop ejected, prior to impact and correct jetting frequency are some of the principles that define ink jettability. Many of this commented principles are fulfilled by means of the extremely relevant parameters as particle size, volatility, viscosity, surface energy and density.[24] In addition, the last three parameters are currently grouped on dimensionless numbers, which are used to classify the fluids jettability. Some of this parameters, dimensionless numbers and the performance of different inks are deeply commented later.

2.3.1 Particle size

Regarding to the inks based on nanoparticles, the jettability of a specific dispersion depends on a correlation between the particle size and the nozzle diameter. Due to the aggregation particles tendency, the nozzle takes the risk to be obstructed. To prevent the ejection standstill while printing due to the nozzle collapse, particles of 100 times smaller than the nozzle diameter should be used for ink formulation.[25,26,27] In this work, cartridges of 10 pl and 1 pl are used, which correspond to 21,5 μm and 9 μm of diameter, respectively.[28] Therefore, being conservative, any particle, polymer, or aggregate should be less than 200 nm and 90 nm for 10 pl and 1 pl, respectively. In practice, double-sized particles than recommended can be jetted easily after treating them with a disaggregation method and filtering before printing.

2.3.2 Volatility

Another parameter, which defines the fluid jettability, is the ink solvents volatility. A solvent with a high evaporation rate can lead to a rapid formation of a solid agglomeration in the nozzle due to the ink-air exposition, causing cartridge clogging and thus jetting failure. This problem is known as “the first-drop problem”.[29] In addition, ink with high volatility that remains some time at the cartridge, can increase the viscosity at nozzle, thus preventing a drop formation. Therefore, the ink solvents must have low evaporation rate at jetting temperature, but enough volatility to sinter at proper temperatures for the substrate used. In addition, solvents volatility is also

important on the drying process of the printed pattern, which defines thickness homogeneity and resolution.

2.3.3 Viscosity

Regarding to the cartridges used of 10 pl and 1 pl (DMC-11610 and DMC-11601), the recommended share viscosity (η) to assure the fluid jettability should be around 10-12 cPs ($1.0x10^{-2}$ - $1.2x10^{-2}$ Pa·s) at jetting regime, although fluids until 30 cPs can be printed in not so ideal conditions. The viscosity can be adjusted by solvent mix composition and jetting temperature. In the case of Newtonian fluids, the viscosity keeps constant across the shear rate range, while non-Newtonian fluids varies significantly.[30] This second fluid behaviour is usual in polymer solutions or concentrated dispersions of particles, on which rheological properties of such fluids can be highly nonlinear. Concerning to polymer solutions, the elongational polymer deformations leads to pressure pulse energy dissipation, which could be increased at current jetting share rates, hindering ink flow and filament break up. Jettability of polymer inks are tuned by polymer weight, concentration, and solvent media, thus allowing the appropriated share viscosity at printing regime.[23,31]

About concentrated dispersions of particles, the viscosity behaviour at different share rates is explained by the microstructure order. The jettability of these fluids is allowed by means of the particles order accomplished inside the fluid at jetting share rates, which reduce significantly the particles friction and the share viscosity at printing regime (*Figure 2.8*). When concentrated dispersion is in equilibrium, the random collisions among the particles contribute to the flow resistance and hence to increase the fluid viscosity. As the shear stress increases, the particles become organized in the flow, which reduce the friction and collision. However, at yet higher shear rates, the hydrodynamic particles interactions spawn hydroclusters (red dots in (*Figure 2.8*)), which produce difficulties at surrounding particles to flow around of these higher concentrated local regions. Therefore, this behaviour leads to a higher rate of energy dissipation, which is fitting for an increase of the viscosity.[32]

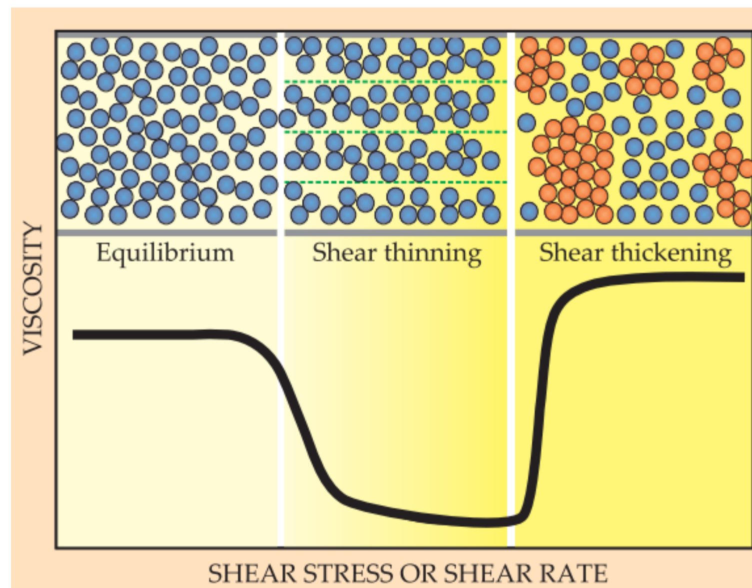

Figure 2.8 The illustration shows the microstructure dependence on shear stress applied, and how the colloidal dispersion transits between shear thinning and shear thickening at shear stress treshold. Image from [32]

2.3.4 Surface energy

Jettability of fluids is directly correlated with the application of enough energy to overcome the viscous dissipation and the energy associated to forming a new surface corresponding to ejected drop. The second energy barrier depends on the surface energy (γ) of the ink, which is a property of the liquid interface with another medium, being ink-air interface at drop forming process. The surface energy has to be high enough to avoid dripping of the nozzle, but low enough to allow the jetting. In addition, surface energy parameter is also relevant in substrate ink wettability, pattern definition and deposit adhesion, which are deeply commented later. Concerning on the cartridge used, the recommended values of ink surface energy are in the range of 28-33 dynes/cm.[27] As well as viscosity, the surface energy can be adjusted by solvent mix composition and jetting temperature.

2.3.5 Z dimensionless number

For a proper high-resolution pattern transfer, the physical parameters of jettable fluids have to be inside of a specific parameters range. There are several works that introduce some characteristic dimensionless grouping numbers, which are integrated by physical constants.[33,19] The dimensionless numbers are: the Reynols number (*Re*), which is the ratio of inertial to viscous forces; the Weber number (*We*), which is the balance between

inertial and capillary forces; and the Ohnesorge number (*Oh*), which is defined as the ratio between the Reynolds number and a square root of the Weber number, and it is independent of the fluid velocity[34]:

$$Re = \frac{va\rho}{\eta} \tag{2.1}$$

$$We = \frac{v^2 a\rho}{\gamma} \tag{2.2}$$

$$Oh = \frac{\sqrt{We}}{Re} = \frac{\eta}{(\gamma\rho a)^{1/2}} \tag{2.3}$$

where ρ, η, and γ are the density, dynamic viscosity, and surface tension of the fluid respectively, v is the velocity, and a is a characteristic length. Z number (inverse of Ohnesorge number) is the appropriate grouping of physical constants to characterise drop formation. In the earliest significant work, Fromm predicted a stable drop formation when $Z > 2$.[24] This analysis was further redefined by Reis & Derby, who propose the following range $1 < Z < 10$, on which the fluids with Z values lower than 1 cannot be ejected due to the pressure pulse viscosity dissipation, whereas at higher values than 10 satellite droplets are formed (*Figure 2.9*).[35] Jang *et al* redefined the printable range as $4 \leq Z \leq 14$ by considering characteristics of printing such as single droplet formability, the minimum stand-off distance, positional accuracy, and maximum allowable jetting frequency.[36] Fluids with low Z values, in the range of 2-4, correspond to a drop formation with large tales and droplet satellite formation, which catch up and merge the leading large drop in flight, thus large stand-off distance to assure proper drop formation before substrate impact is required. Therefore, large stand-off distance compromises the accuracy of drop positioning and thus the printing resolution. In addition, large viscosity increases the drop-time formation and hence reduces the jetting frequency. In contrast, the fluids with Z values higher than 14 are easily ejected without significant viscous dissipation. Therefore, a primary drop is generated with large kinetic energy and the separated tail cannot catch up with primary drop. [36]

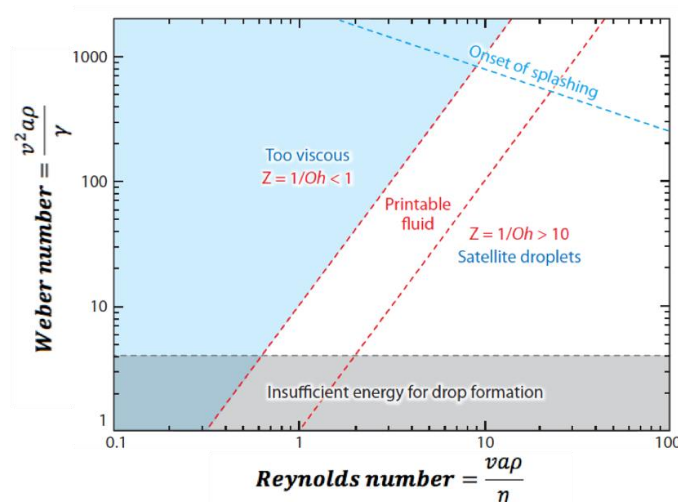

Figure 2.9 Range of Z = 1/Oh plotted in a coordinate system defined by the Reynolds and Weber numbers, at which fluid allows a stable printing on DOD inkjet printing technique. Image from [13]

2.3.6 Jettability characterization of tested inks.

In this thesis, several inkjet inks have been tested, aiming to choose the most appropriated to conduct the thesis work. The conductive inks are chosen for conductive wires, connections and electrodes applications, the resistive inks are chosen for fabricate resistors and the polymeric-inks are chosen for insulating purposes. Some of the tested inks are commercial as DGP 40LT-15C (ANP, Corea), EMD5714 (Sunchemical, USA), CI-002 (IntrinsiqMaterials, United Kingdom), XP PriElex SU-8 (MicroChem Corp., USA) and xdi-cds (Xerox, USA). The other inks were developed in collaboration with a private company. *Table 2.1* shows the most relevant ink parameters as solid content, density, viscosity, surface energy and Z number of the tested inks.

Table 2.1 Table with the rheological parameters of the tested inkjet inks at room temperature.

Ref. inks	Manufacturer	Material	Solid (%)	ρ (g/cm^3)	η (cPs)	γ (Dyne/cm)	# Z
CI-200	Intrinsiq Materials	Cu	12	-	12	30	
DGP 40LT-15C	ANP	Ag	30	3.86	10	35	5.33
EMD5714	Sunchemical	Ag	40		11	27	
8-VA12-3	-	Ag	40	1.20	13	29	2.08
79VA12-3	-	Ag	30	1.19	13	33	2.21
77-VA12-8	-	Graphite	20	0.90	14	33	1.78
92-VA12-2	-	Graphite	20	0.90	12	32	2.05
23-VA12-1	-	Al_2O_3	45	0.90	11	23	1.90
24-VA12-2	-	SiO_2		1.10	12	24	1.96
xdi-cds	Xerox	PVP	9	0,86	8.5	24.5	2.48
PriElex SU-8	MicroChem	SU-8	32	1,04	9.33	30	2.74

As shown in *Table 2.1*, the tested inks can be ejected (1 < Z < 10) by means of the Dimatix 2831 and the Xennia Carnelian 4000 inkjet printers, although most of the inks tested do not fall in the Z range defined by Jang et al. (4 ≤ Z ≤ 14),[36] which compromises on most cases the droplet positioning and thus the printing resolution. Despite of that, the ink rheology at firing time can be adjusted by the nozzle temperature,[19,37] and by extension, the Z value, which contribute significantly to proper ink jettability (*Figure 2.10*).

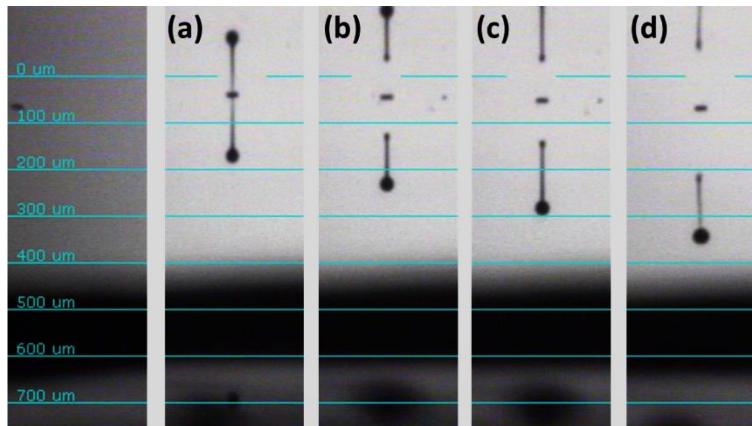

Figure 2.10 Images performed by means Dimatix printer, which show four different drops ejected with the same waveform at 40 µs after the ejection. The drop shape and the reached distance differences depend on nozzle temperature. (a) Nozzle at 30 ˚C. (b) Nozzle at 40 ˚C. (c) Nozzle at 50 ˚C. (d) Nozzle at 60 ˚C.

Among the difficulties encountered at fluids ejection, it should be pointed out the corresponding to the puddle formation phenomena, where the ink flows out from the nozzle and wets its surrounding (*Figure 2.11 (a)*). Some of the inks formulated with hydrocarbon solvents, at Dimatix "non-wetting" printheads, spreads over the nozzle platen (*Figure 2.11 (a)*), thus thick ink layer is fixed on front of the nozzle opening, which leads to drop formation and large printing instability.[20] However, at Xaar "wetting" printheads, the ink remains on the nozzle plate with very low contact angle, and hence forming a thin uniform layer, which does not obstruct the drop formation.[20]. Therefore, hydrocarbon-based inks tested shown higher compatibility with this kind of "wetting" printheads, and large printing stability is performed, as shown on *Figure 2.11 (b)*, where alumina insulating layer is printed on touch screen.

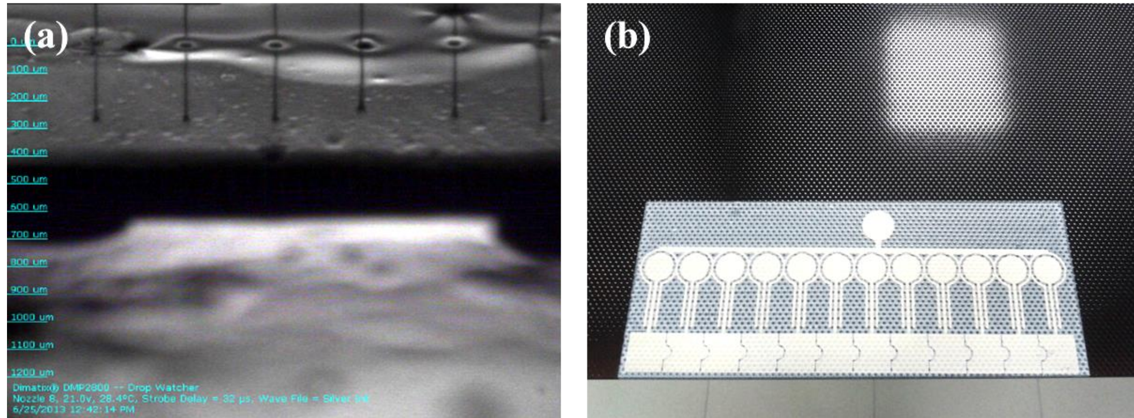

Figure 2.11 (a) Dimatix's DMC-11610 printhead, where 23VA12-1 ink (alumina-ink) is being printed and ink spreads (puddle) over nozzle platen. (b) Printed insulating (23VA12-1 ink) layer (140 mm x 55 mm) by means Xaar XJ128 printhead over a silver printed touch control, as example of large printing stability.

Regarding the polymer-based inks, the elongation of the polymer leads to dissipation of pressure pulse energy, thus hindering proper inkjet printing of large-area patterns. To perform the ejection of these inks, the most used waveform consists of two segments: a large ejecting segment and chamber recovery segment. First one allows fluid column extrusion and the second one assures filament break up (*Figure 2.12*). To avoid instabilities due to oscillations low firing frequency, about 2 kHz, was used. The corresponding waveform outcome is a high volume drop forming.

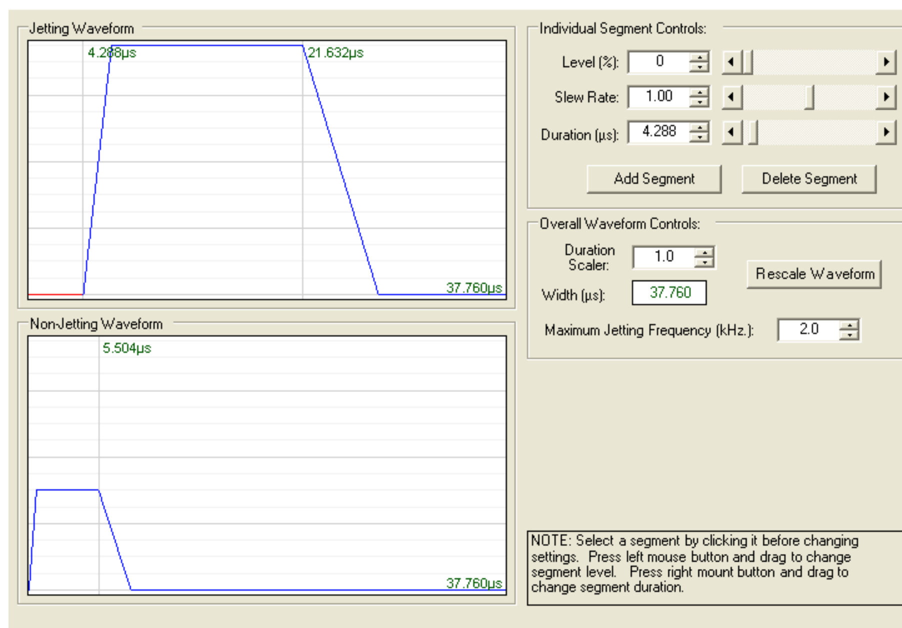

Figure 2.12 Waveform used for polymer-based ink ejection.

Following, after proper ink jettability, the next crucial parameters consist in the physico-chemical liquid-solid interaction. At the following section, the parameters that take place at liquid-solid interaction and the performances of the tested inks over different substrates are presented.

2.4 Drop-substrate interaction

Once fluid is correctly ejected, the parameters that define the drop-substrate interaction, also known as footprint, should be considered. The solidification of the printed fluid occurs after liquid-solid interaction. To achieve a well-defined pattern with homogeneous structure, the printed pattern must retain some stability in the liquid phase before solidification. In the next subsections, the different interactions that occur between substrate and liquid drops prior to solidification are identified.

2.4.1 Drop impact and spreading

The impact of drops on solid substrates is a process controlled by some physical parameters, which can be grouped on inertial forces, capillary forces and gravitational forces. Regarding to gravitational forces, the dimensionless Bond number must be considered, Bo = ρga2/γ, where ρ is the fluid density, g is the acceleration of gravity, a is the drop diameter and γ is the surface tension. However, in common fluids used for inkjet printing and drop-size ejected, the $Bo \ll 1$, hence gravitational forces can be neglected.[13] Thus, the dominant forces will be inertial and capillary. Schiaffino and Sonin divided the drop impact into two regimes: the impact driven and the capillarity driven.[38] At the impact driven regime, the inertial forces dominate the initial drop behaviour just drop-substrate impact, while at capillarity driven regime, the initial drop behaviour just drop-substrate impact is not drop velocity-dependent and capillarity forces are predominant. The transition in behaviour/regimes occurs at a critical value of the Weber number. In addition, these authors characterized the resistance to spreading in terms of the Ohnesorge number, defining two regimes: the almost inviscid and the highly viscous.[38] These both correlations are represented in *Figure 2.13* (superimposed on the regime of stable DOD drop formation taken from *Figure 2.9*). Therefore, it should be noticed that inkjet-printed drop-substrate first interaction is impact driven in a region of relatively inviscid behaviour.[13]

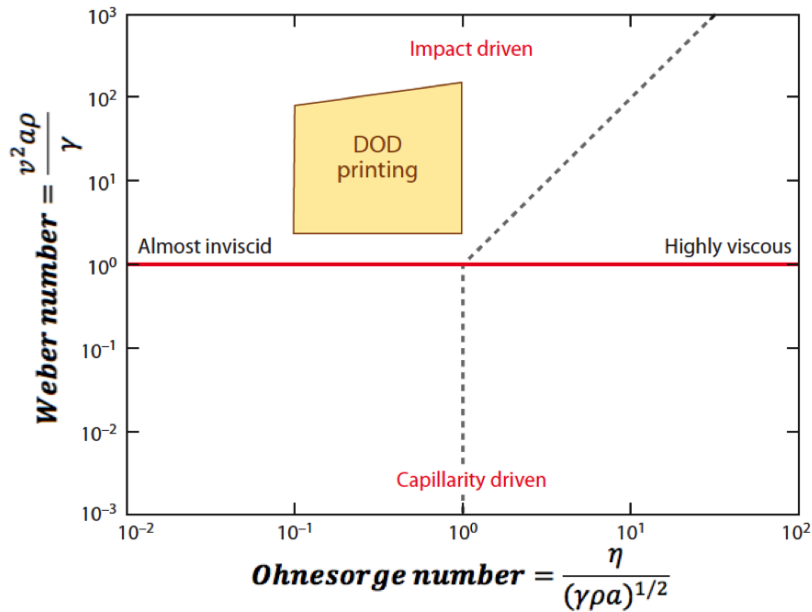

Figure 2.13 Parameter space that shows the driving force associated to drop spreading after just impact, where Ohnesorge and Wever numbers are the axes. The ejecting conditions plotted at *Figure 2.9* are shaded, which indicate that initial drop behaviour is conducted by inertial forces.[38] Image from [13]

The drop impact evolution of typical fluids used for inkjet printing is conducted by a sequence of different physical phenomenon, where each one befalls at a specific/particular timescale. R. Rioboo *et al.* distinct, on dry surfaces, four phases of the drop spreading diameter after the instant of impact: the kinematic phase, the spreading phase, the relaxation phase and the wetting/equilibrium phase.[39] The sequence of these processes is illustrated in *Figure 2.14***.**

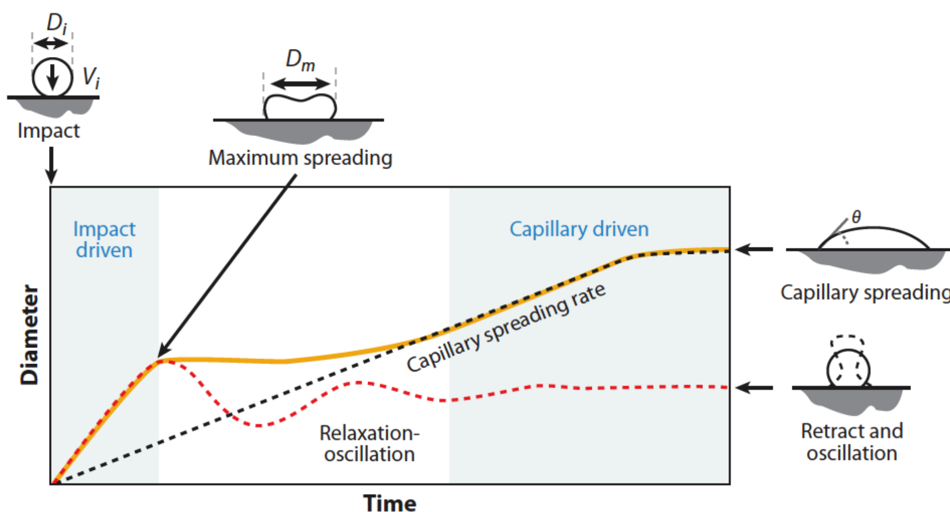

Figure 2.14 Scheme of the events sequence that occurs after droplet impact on a substrate. θ is the contact angle, D_i is the initial droplet diameter, D_m is the maximum radius reached by a drop during impact driven regime, and V_i is the droplet velocity at impact. Image from [13]

The kinematic phase comprises the initial impact stage where drop exhibits the shape of cut sphere and moves only vertically. Next, in accordance with Schiaffino & Sonin work,[38] the initial impact stage is followed by impact driven spreading, which corresponds to spreading phase.

After that, it takes place the relaxation phase, where recoil and oscillations are the following phenomenon. At this step, viscous forces turn to dampen the spreading and the oscillations, and surface tension becomes more important in controlling drop shape behaviour. At the end, at the wetting/equilibrium phase, the spreading is fully controlled by capillarity until drop-substrate reaches the equilibrium, and hence a final contact diameter or footprint, d_{con}, is determined. The footprint, d_{con}, depends on the drop volume and the equilibrium or static contact angle, θ_{eqm}. In addition, at drop impact sequence and previous to reach the equilibrium, the spreading of the drops shows two angles, the advancing angle θ_{adv} and the receding angle θ_{rec}, which are shown in *Figure 2.15*. The difference between the advancing and receding angles at zero velocity of the drop-substrate contact line is known as the hysteresis. The classical static/equilibrium contact angle defined by Young's equation lies between θ_{adv} and θ_{rec}.[39]

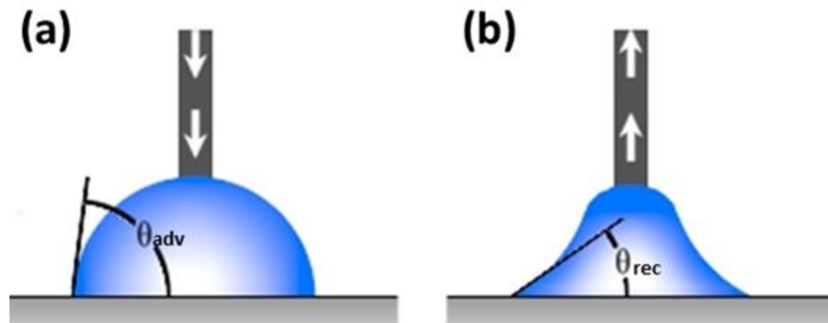

Figure 2.15 (a) Advancing angle of impacting drop on substrate. (b) Receding angle of impacting drop on a substrate. Adapted from [40]

Once drop reaches the equilibrium and for drop sizes typical of inkjet printing, the Bond number is sufficiently small that the spread drop shape can be taken as a segment of a sphere, with

$$d_{con} = d_0 \sqrt[3]{\frac{8}{\tan\frac{\theta_{eqm}}{2}\left(3 + tan^2\frac{\theta_{eqm}}{2}\right)}} \tag{2.4}$$

Where d_{con} is the footprint diameter, d_0 is the diameter of drop in flight and θ_{eqm} the equilibrium contact angle. Regarding to the equilibrium contact angle, θ_{eqm}, this parameter is defined by the equilibrium of the three interface tensions existing at that system and described by Young's equation *(2.5)*. This equilibrium is illustrated on *Figure 2.16 (a)*, and the footprint shape/wettability dependence on ink and substrate surface energy is illustrated on *Figure 2.16 (b)*.

$$\gamma^{sv} = \gamma^{sl} + \gamma^{lv} \cos\theta \tag{2.5}$$

Where γ^{sv}, γ^{sl} and γ^{lv} are the tension at solid-air, solid-liquid and liquid-air interfaces, respectively, and θ is the contact angle.

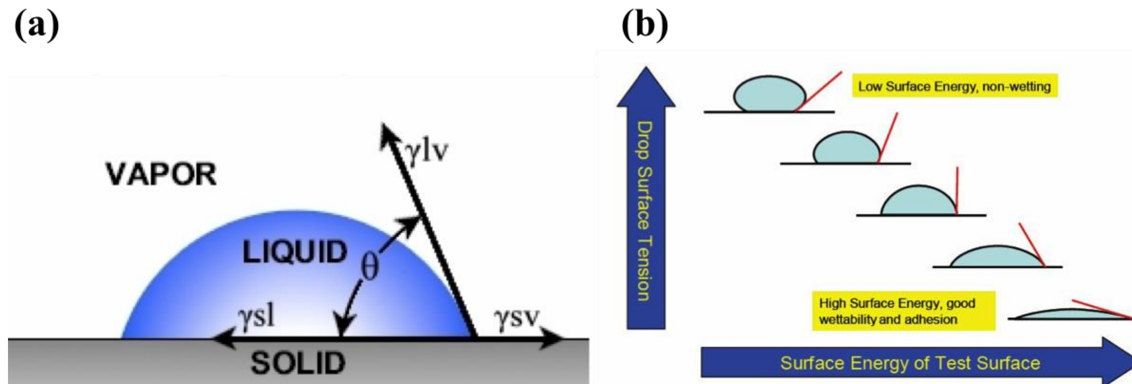

Figure 2.16 (a) Scheme of the interface tensions that define the contact angle. (b) Diagram where the footprint shape/wettability is represented depending on the ink and substrate surface energy. Adapted from [41,42]

The drop-substrate interaction can be modified and hence the contact angle by two main strategies: modifying either the surface tension of the ink or the free energy of the substrate surface. The first strategy covers the co-solvent control with the addition of a low- or high- surface tension solvents such an alcohol or water, respectively, or the addition of additives such as surfactants. Regarding the second strategy, increasing the substrate temperature during the printing can slightly help to this purpose by increasing the substrate surface energy,[43] but when a stronger modification of the contact angle is needed, the substrate surface is activated by means of plasma or chemical etching treatment.[26] In addition, the corresponding increase of available bonds at interlayer becomes an improvement of deposit-substrate adhesion, which is discussed later.[42]

To better understand the drop-substrate evolution from impact to equilibrium, Rioboo *et al.* presented a real sequences of drops impact[39] where all the sequence phases can be observed (Figure 2.17).

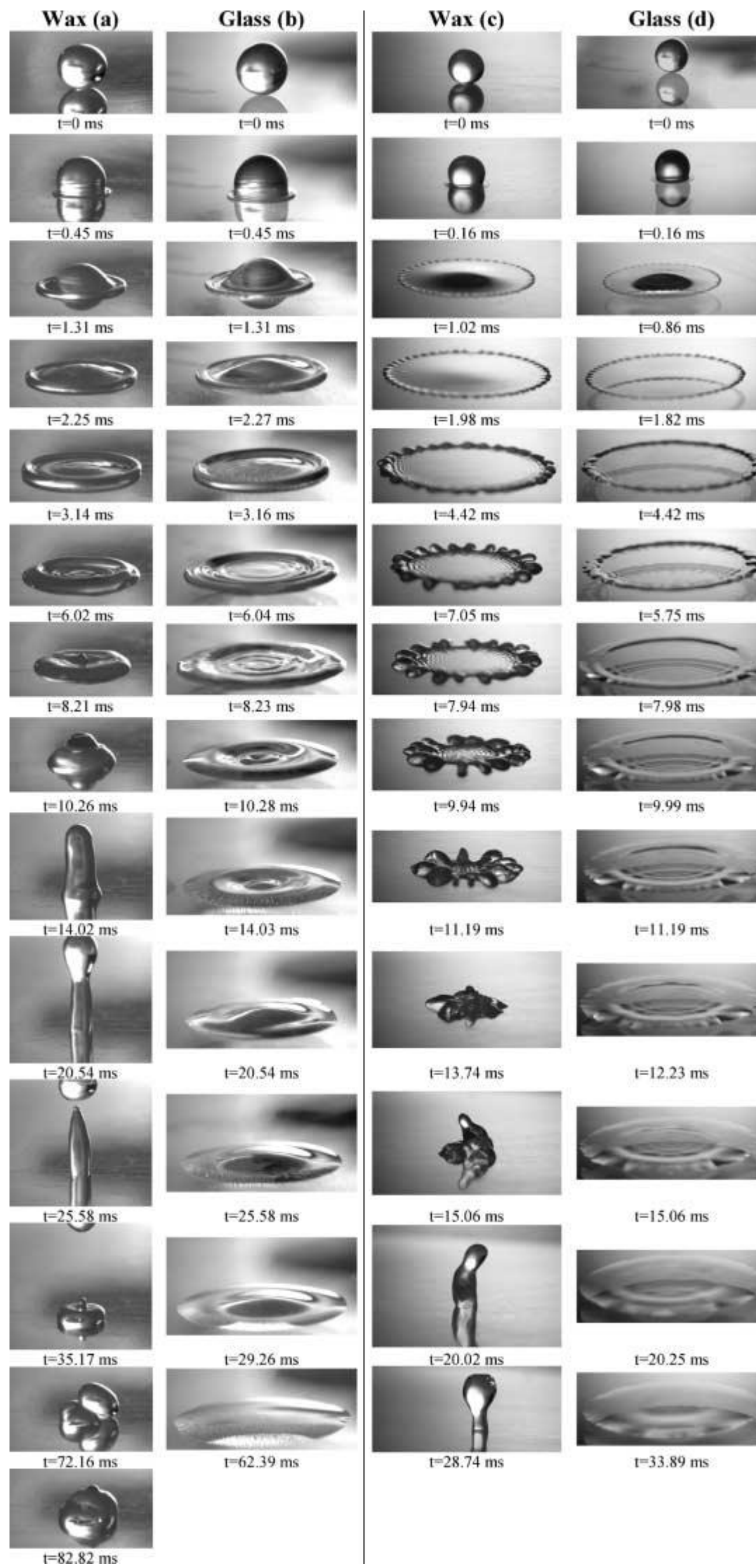

Figure 2.17 Sequences of water drop impacts on two substrates: Wax and Glass with R_a=0.4 µm and R_a=0.003 µm of roughness, respectively. (a) Impact on Wax at V_i=1.18 m/s. (b) Impact on glass at V_i=1.18 m/s. (c) Impact on Wax at V_i=3.6 m/s. (d) Impact on glass at V_i=3.6 m/s. Adapted from [39]

2.4.2 Drop-substrate interaction of tested inks.

In this section, the ink-substrate interaction was characterized and to perform this study a homemade setup was mounted. The setup was integrated by 10 µl syringe (Hamilton), a pushing system with goniometer mechanism and a digital camera (Dino-Lite). The pictures were taken 2 second after drop impact, at this time the drops have reached the equilibrium contact angle θ_{eqm}. It should be noticed that all the inks characterized show a high degree of wettability, with $\theta_{eqm} < 90°$ on both glass and polyimide substrates. *Figure 2.18* shows the equilibrium contact angle of a commercial silver ink (DGP 40LT-15C) on glass and polyimide substrate.

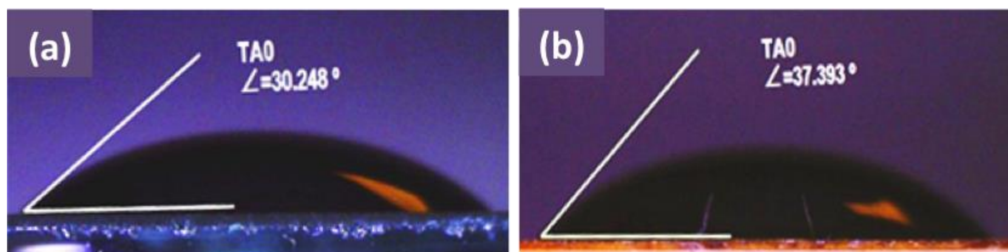

Figure 2.18 Contact angle of silver ink (DGP 40LT-15C) after 2 seconds of the drop impact. (a) On glass. (b) On polyimide.

Figure 2.19 shows the equilibrium contact angle θ_{eqm} of deionized water on glass substrate before and after surface activation (30 seconds of argon plasma treatment). The measured angle shown in *Figure 2.19* is the complementary of θ_{eqm}, thus the θ_{eqm} before and after plasma treatment are $\theta_{eqm} = 49.5°$ (*Figure 2.19a*) and $\theta_{eqm} = 26.5°$ (*Figure 2.19b*), respectively. This test was performed aiming to increase the adhesion of the deposits, which we will introduce with more detail in subsection 2.8.

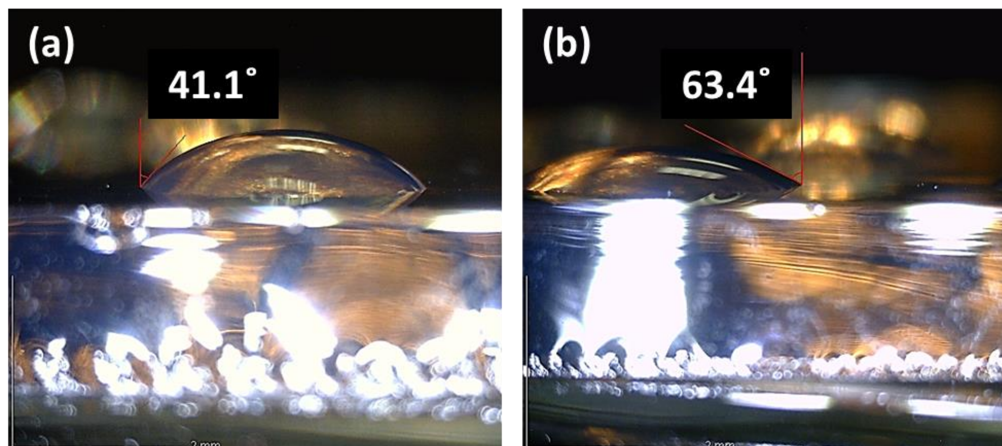

Figure 2.19 (a) Contact angle of deionized water drop on glass substrate. (b) Contact angle of deionized water drop on the same glass substrate of (a), but after argon gas plasma of 30 s.

As commented above, the footprints of the tested inks depend on the drop volume and the ink-substrate interaction. The *Table 2.2* summarizes the footprint of different inks reached on polyimide substrate.

Table 2.2 Footprint of different tested inks on polyimide.

Ref. inks	**Material**	**Solvent**	**γ (Dyne/cm)**	**d_p on polyimide (µm)**
CI-002	Cu	Alcohol	30	40
DGP 40LT-15C	Ag	Alcohol	35	30
EMD5714	Ag	Alcohol	27	40
8-VA12-3	Ag	Hydrocarbon	29	62
79VA12-3	Ag	Alcohol	33	37
77-VA12-8	Graphite	Hydrocarbon	33	107
92-VA12-2	Graphite	Alcohol	32	76
23-VA12-1	Al_2O_3	Hydrocarbon	23	81
24-VA12-2	SiO_2	Hydrocarbon	24	79
xdi-cds	PVP		24.5	90
PriElex SU-8	SU-8		30	60

The inks formulated with hydrocarbon solvents show higher footprint than inks formulated with alcohol solvents, although both groups of inks have comparable values of surface tension and are ejected at similar conditions. This behaviour could be due to different volume of ejected drop or, as hydrocarbon inks show higher evaporation rate than alcohol inks, the line pinning could happens faster, which reduces the receding process. It should be pointed out, that bigger footprint supposes lower resolution, and hence the hydrocarbon inks behave less appropriated for high resolution patterns.

Previous drop-substrate interaction was done considering dry substrate surface and isolated drops. However, an overlapping train of drops blend/bind between them, which does vary significantly the drop spreading behaviour, as introduced in the following subsection.

2.5 Drop spacing, drop coalescence and fluid bead stability

The transference of 2-D patterns to a substrate needs of the overlapping train of drops, which form a liquid bead. In the same line, 3-D structures are produced by overprinting sequential layers, but in this case drops interact with a solidified deposit. Before to pattern transfer, the printing parameters should be determined in order to assure that printed deposit matches as close as possible the digital pattern. The main length to know is the ink-substrate or ink-solid footprint, which is described previously. As a first approximation, a proper pattern profile can be attained with 50 % to 60 % of overlapped drops. This overlapping is defined by drop spacing parameter.

On the Dimatix 2831 printer, the carriage only moves in one direction ($\hat{x}$), and the drops are ejected at the same time that carriage sweeps one line-pixel of the pattern. Next, simultaneously, the carriage comeback to ($\hat{x}$) start position and the platen moves one pixel on ($\hat{y}$) direction, thus this process is repeated until pattern is completely transferred. As carriage sweep ($\hat{x}$), the cartridge supplies drops at the firing frequency defined by the waveform, thus the printer adapts the carriage sweep-velocity suppling drops at fixed drop spacing distance. In the perpendicular direction ($\hat{y}$) to carriage movement, the drops are supplied, at specific drop spacing, by tuning the orientation of the cartridge holder, as it can be seen in *Figure 2.20*.

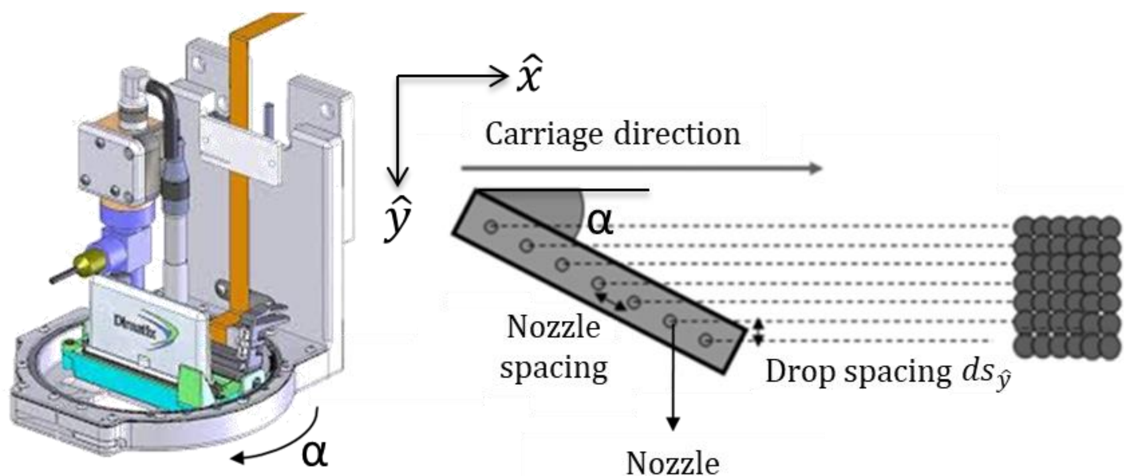

Figure 2.20 Schematic of the Dimatix's cartridge carriage and the strategy for supply drops on ($\hat{y}$) direction at specific drop spacing.

Therefore, the distance between consecutive nozzles at $(\hat{y})$ direction, which corresponds to $(\hat{y})$ drop spacing, is:

$$ds_{\hat{y}} = d \sin \alpha \tag{2.6}$$

Where $ds_{\hat{y}}$ is the drop spacing in $(\hat{y})$ direction, d = 254 μm is the nozzle spacing and α is the angle between the line of nozzles and the sweep direction. Regarding to Xennia Carnelian 4000, on $(\hat{x})$ direction it works equal than Dimatix 2800 series, but in $(\hat{y})$ direction the drop spacing is only controlled by platen movement, with about 250 nm step resolution.

As commented above, the 2-D pattern manufacturing requires the drops overlapping to form continuous features, as a fluid line. Therefore, two overlapping drops tend to coalesce, as well a train of overlapping drops tend to form a fluid line or bead, if there is significant contact line pinning. Regarding this, several authors have studied the stability of these fluid lines or liquid beads, Duineveld[44] found three scenarios of behaviour when investigated the performance of inkjet-printed liquid beads on a range of substrates. One scenario shows unstable fluid lines when the liquid has an identical or very similar advancing and receding contact angles, as predicted by Davis[45] and observed by Schiaffino & Sonin[46]. This case is fitting for the scenario where low wettability liquid-substrate is produced. Second scenario observed by Duineveld is when significant hysteresis in the contact angle is presented, thus stable liquid patterns can be printed at low values of the receding contact angle $\theta < \pi/2$. This case corresponds to scenario where high/good wettability of liquid-substrate is produced. As mentioned previously, the hysteresis is referred to the difference between the advancing contact angle and the receding contact angle when contact line is stopped. Finally, at the third scenario, although significant hysteresis (i.e. good wettability) in the contact angle is shown, it is not possible to form a parallel liquid bead, and instead of that bulges are observed, spaced regularly along the printed liquid bead (*Figure 2.21d*). The onset of this bulging instability is a function of both drop spacing and the frequency of overlapping drops (i.e., the traversing velocity of the inkjet printer relative to the substrate).

Soltman & Subramanian[43] carried out an experimental study of liquid beads formation. Their observations are consistent with those of both Duineveld and Smith *et al*.[44,47] At

large values of drop spacing, where no overlapping occurs, a train of discrete drops is observed (*Figure 2.21a*). At spacing slightly smaller than the diameter of the footprint, drop coalescence is observed, but the resulting liquid bead is “scalloped” and does not show parallel sides (*Figure 2.21b*). At the proper deposited drop spacing, a stable liquid bead with smooth parallel sides is found (*Figure 2.21c*). Finally, when the drop spacing is too small, the bulging instability occurs (*Figure 2.21d*). Therefore, Soltman & Subramanian[43] demonstrated experimentally that there are two limiting lower and upper bounds to the width of a parallel-sided liquid bead produced by inkjet printing, even in the stability regime identified by Davis[45]. Furthermore, if the drop dries before the following drop impact on the head of line, then no fluid bead is performed and stacked coins profile is presented (*Figure 2.21e*), which could be produced by several reasons, high solvent evaporation rate, substrate temperature or printing strategy.[43]

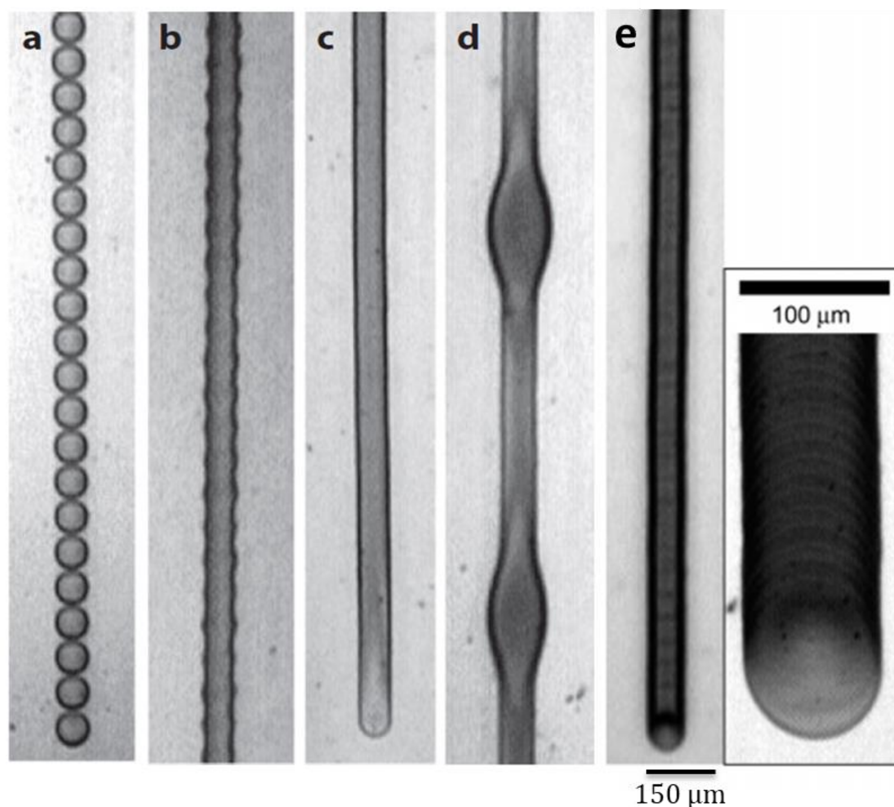

Figure 2.21 (a) Drop spacing is too large for drop coalescence. (b) Initial coalescence leads to a liquid bead with a periodic irregularity. (c) After sufficient overlap a parallel-sided bead occurs. (d) If the drop spacing is too small, a bulging instability forms. The critical spacing is a function of the printhead traverse speed relative to the substrate. (e) Drops dries before new addition, thus leads on stacked drops without coalescence (stacked coins). Adapted from [43]

2.5.1 Fluid beads characterization of tested inks

As commented above, the behaviour of liquid beads is more complex than the individual drops, and proper pattern stability is achieved at specific conditions. Among the tested inks, the scenario of free contact line moving associated to fixed contact angle line is observed, at some cases. *Figure 2.22* shows this behaviour in two different situations: Ag-ink (8VA12-2) printed on low temperature curing ceramics LTCC substrate (*Figure 2.22a*), and Ag-ink (DGP 40LT-15C) printed on a solidified deposit of 3Glycocidoxypropyltrimethoxysilane (GPTMS) (*Figure 2.22b*). This scenario leads on Rayleigh instability and instead of fluid beads, sessile drops are formed, whose size depends on sweep speed and overlapping frequency. When there is enough distance between the sessile drop formed and the new arriving drop, the coalescence between them is missed and it becomes the seed for the new sessile drop. This behaviour was predicted by Davis[45] and observed by Duineveld[44] and Schiaffino & Sonin[46].

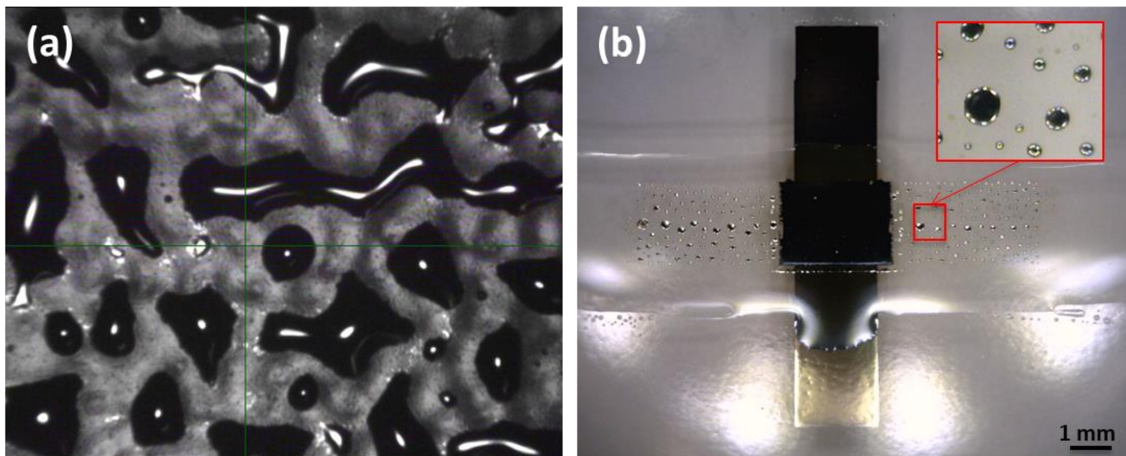

Figure 2.22 Liquid bead instability. (a) The Ag-ink (8VA12-2) printed on low temperature curing ceramics LTCC substrate presents liquid macrodrops, thus the rectangular pattern can be performed. (b) The Ag-ink (DGP 40LT-15C) printed on GPTMS solidified deposit presents sessile drops.

Concerning *Figure 2.22b,* it should be pointed out an interesting behaviour, the surface energy of the GPTMS top surface shows a considerable difference depending on the material at his underside. The GPTMS solidified deposit in contact with glass shows low wettability to Ag-ink (DGP 40LT-15C) printed on it. Instead of this, the GPTMS deposited over the previous printed conductive strip performs good wettability to silver DGP 40LT-15C. This behaviour is not deeply studied, but it should be remarked as example of the complexity of heterogeneous multilayer inkjet manufacturing.

Regarding the instability presented, the ink-substrate wettability can be adapted by tuning the surface tension of the ink or the free energy of the substrate surface. Therefore, 30 seconds of argon plasma treatment was performed over the substrate, in this case on GPTMS insulating material, before printing the top crossover conductive strip. After plasma treatment, the substrate surface energy reached has proper contact angle hysteresis and thus leads to form parallel liquid beads (*Figure 2.23*).

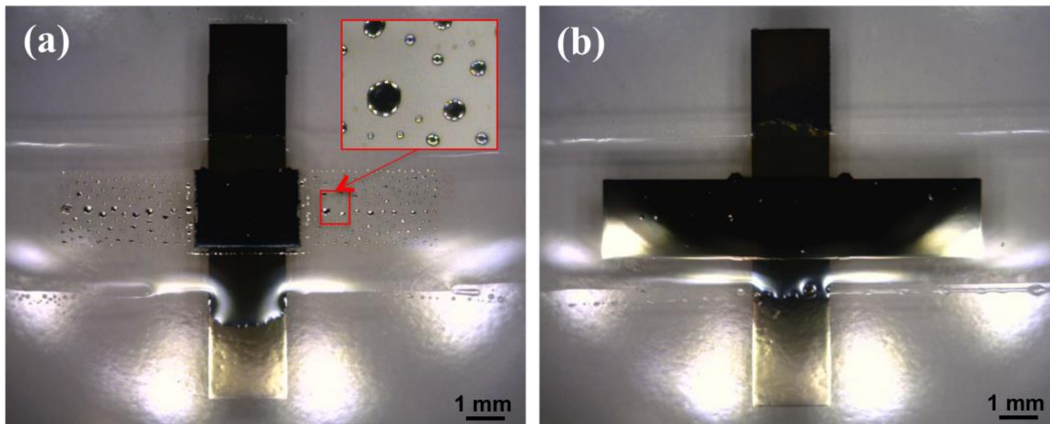

Figure 2.23 (a) The Ag-ink (DGP 40LT-15C) printed on GPTMS presents sessile drops. (b) After 30 seconds of Argon plasma treatment, the Ag-ink (DGP 40LT-15C) printed on GPTMS present proper wettability, which leads to parallel liquid beads.

As introduced above, although significant hysteresis (i.e. good wettability) in the contact angle is shown, it is not always possible to form a parallel liquid bead. In order to reach parallel liquid beads with the tested inks, a specific pattern was printed on each substrate aiming to obtain the proper printing parameters. The printed pattern consists on isolated drops and mono-pixel lines width in the carriage motion direction ($\hat{x}$) and in the perpendicular direction to it ($\hat{y}$) (*Figure 2.24*).

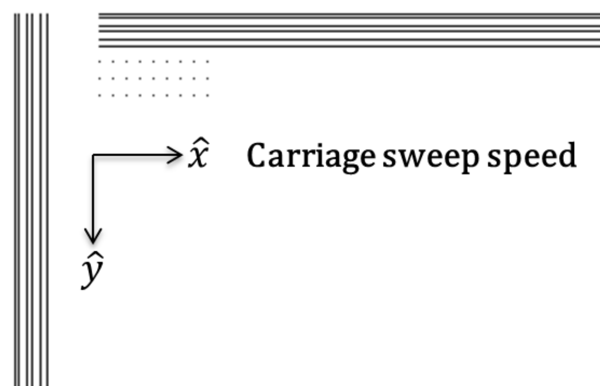

Figure 2.24 Pattern of isolated drops and mono-pixel lines width in both directions, the carriage motion direction ($\hat{x}$) and the perpendicular to it ($\hat{y}$).

From this test, performed for obtain the printing parameters for each tested ink, the observations of Dan Soltman and Vivek Subramanian commented above were also observed, as shown in the follow *Figure 2.25*, although images correspond to the dried deposits instead of the liquid ones.

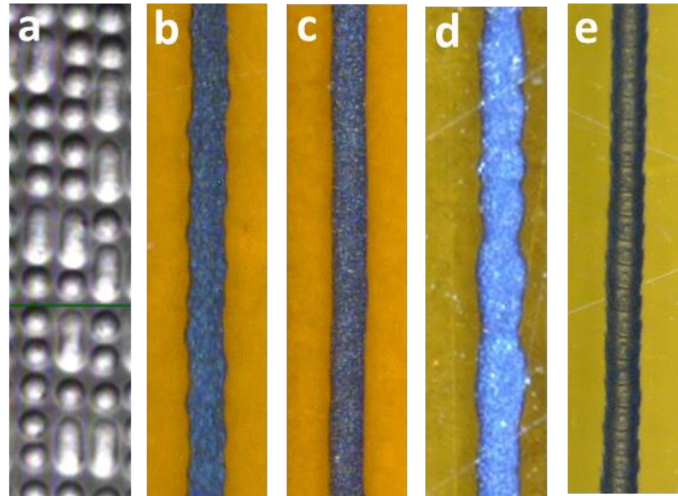

Figure 2.25 (a) Drop spacing is too large for drop coalescence. (b) Although closer to parallel-sided deposit, not enough overlapping leads to a deposit with a periodic irregularity. (c) After sufficient overlap a parallel-sided deposit occurs. (d) If the drop spacing is too small, a bulging instability forms. (e) Drops dries before new addition, thus leads on stacked drops without coalescence (stacked coins).

2.5.2 Fluid beads profile depending on the printer constrains.

From the test presented above, performed in order to find the proper printing parameters for each tested ink (*Figure 2.24*), we found significant line-width differences depending on the printing direction. It should be pointed out that these differences are produced while the following printing parameters are kept constant: the waveform, nozzle temperature, the substrate temperature, the drop spacing and the firing frequency. In order to verify the line-width differences observed, a test is performed with two different inkjet printers, which used the same printing methodology, the Xennia Carnelia 4000 (with 80 µl Xaar 128 printhead) and the Dimatix 3831 (with 10 µl printhead). The materials used are Ag-ink (79VA12-3) and polyimide, as ink and substrate, respectively.

As can be seen at *Figure 2.26* (test performed with Xennia printer) the results are significantly different since *Figure 2.26a* shows scalloped profile at line growth on ($\hat{y}$) direction, while a proper two parallel fluid bead is formed in ($\hat{x}$) direction (*Figure 2.26b*). The drop spacing used is 55 µm and the platen temperature is 40 °C. The result of vertical printed line width is 59 µm and the horizontal printed line width is 79 µm.

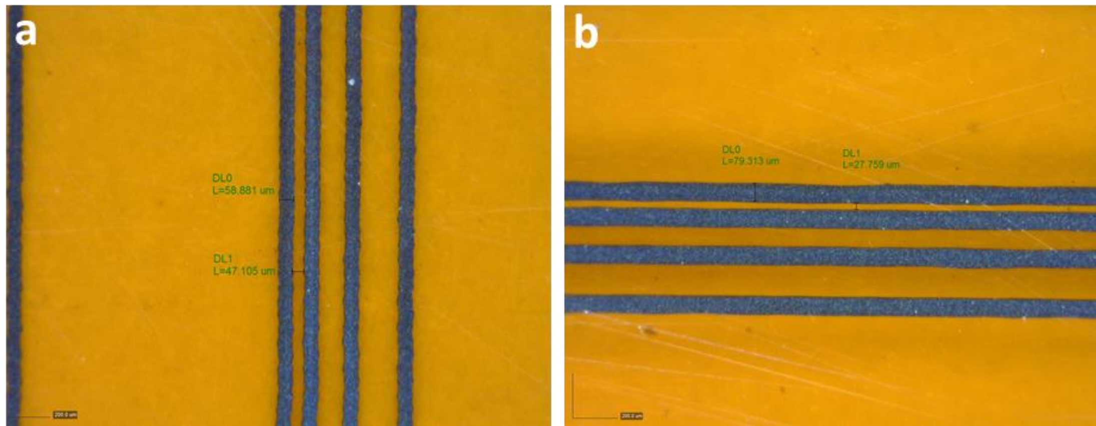

Figure 2.26 Printed and sintered pattern (*Figure 2.24*) by means Xennia Carnelian 4000 printer at 55 μm of drop spacing and 40 °C platen temperature. (a) Vertical printed lines width = 59 μm. (b) Horizontal printed lines width = 79 μm

As can be seen, at *Figure 2.27* (test performed with Dimatix printer) the results are also significantly different since lines growth in ($\hat{y}$) direction (*Figure 2.27 a and b*) are narrower than the printed lines in ($\hat{x}$) direction (*Figure 2.27 c and d*). The *Figure 2.27 a and b* corresponds to dried lines and the *Figure 2.27 c and d* to the liquid beads. The drop spacing used is 17 μm and the platen temperature is 40 °C. The result of vertical printed line width is 30 μm and the horizontal printed line width is 45 μm.

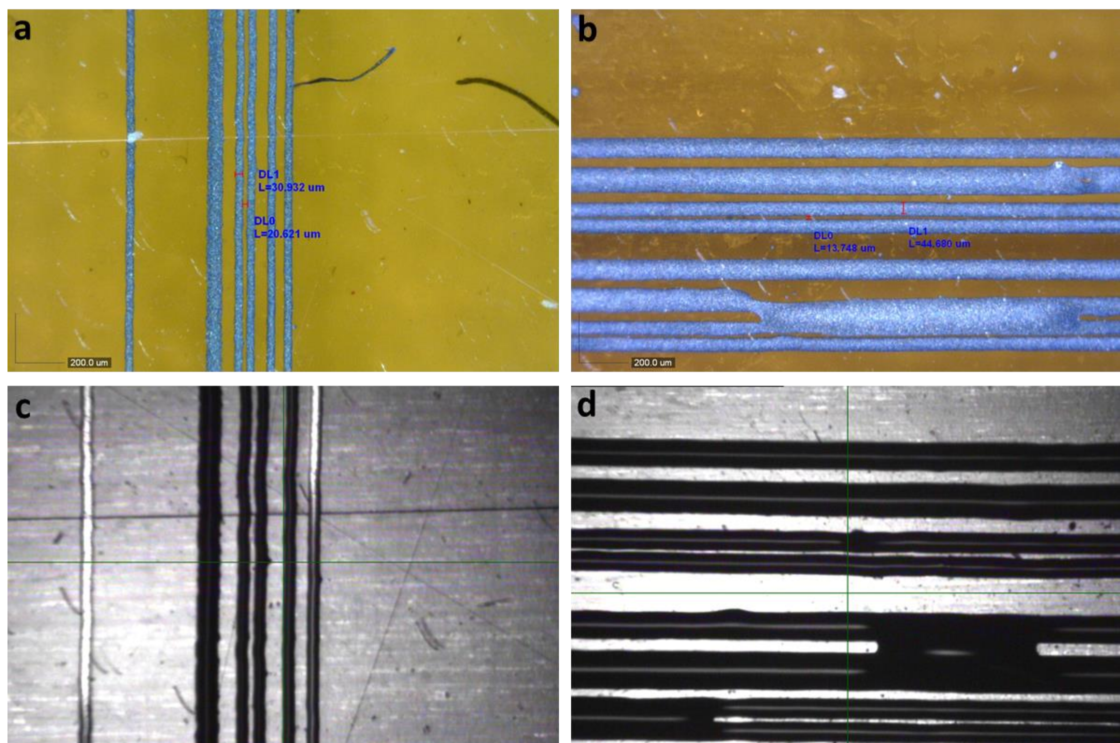

Figure 2.27 Printed pattern (*Figure 2.24*) by means Dimatix 3831 printer at 17 μm of drop spacing and 40 °C platen temperature and nozzle temperature. (a) Vertical printed lines width = 30 μm. (b) Horizontal printed lines width = 45 μm. (c) The corresponding (a) liquid bead. (d) The corresponding (b) liquid bead.

Following, the corresponding line width and spreading ratio measured with both inkjet printers are summarized in
Table 2.3.

Table 2.3. Table with the line width and spreading ratio of Ag-ink (79VA12-3) ink printed with Dimatix 3831 and Xennia Carnelian 4000 inkjet printers.

Inkjet Printer	Line width $w_{\hat{y}}$ (µm)	Line width $w_{\hat{x}}$ (µm)	Spreading ratio ($w_{\hat{x}}$ /$w_{\hat{y}}$)
Dimatix 3831	30	45	1.50
Xennia Carnelian 4000	59	79	1.34

From the results, it can be observed that all fluid lines printed on the same direction as carriage movement show wider section profile than the printed in the perpendicular direction to carriage movement, as can be seen in *Figure 2.26* and *Figure 2.27.* As the printer parameters remain unchanged at printing pattern process, this anisotropy should be explained by the difference on the liquid line growth, which could leads in a different contact line spreading and hence receding angle. Comparable phenomenon was observed by Gao & Sonin[48] when they deposited at two different fluid beads growth, while keeping constant the same dimensionless ratio defined as f(2a)/U, where a is in-flight microdrop radius, $f(2a) = 2a * f$ with f as the jetting frequency, and U is the sweep velocity. The two fluid beads were printed at two very different sweep speeds and jetting frequencies, and deposited on a substrate with significantly lower temperature than ejected drop. From Gao & Sonin (Gao and Sonin 1994, figure 18)[48] at low sweep speed the bead width is smaller than for higher sweep speed at the same dimensionless ratio f(2a)/U, which breaks down their prediction model (Gao and Sonin 1994, equation 36)[48]. To explain these differences, they conclude: "this suggest that the lateral advance of the bead's contact line has been arrested by freezing and the bead has growth upward, swelling over the arrested contact line".

In the test performed, a specific drop spacing (a) and jetting frequency (f) are chosen as printing parameters, and hence sweep speed (U) is consequently determined. However, as commented above, the inkjet printers tested only moves the cartridge carriage on the ($\hat{x}$) direction. Therefore, when a pattern line sweep is finished, either the carriage comebacks to initial ($\hat{x}$) position and platen moves one pixel on ($\hat{y}$) and hence process is repeated multiple times until pattern is completely transferred. Then, as drop spacing (ds) is equal in ($\hat{x}$) and ($\hat{y}$) direction, $\frac{f_x}{U_x} = \frac{f_y}{U_y} = \frac{1}{ds}$, is also fulfilled the same

dimensionless ratio $f_x 2a/U_x = f_y 2a/U_y$, but with very different sweep speed (U) and jetting frequency (f) between ($\hat{x}$) and ($\hat{y}$) directions, while the pattern is substrate transferring. From the test performed, the lines that grown on ($\hat{y}$) direction even show lower width than the isolated drops footprint, which suppose a higher contact line receding in comparison to isolated drops.

Regarding the differences on spreading ratio between the two different printers shown at
Table 2.3 could be related on the different sweep speed, jetting frequency and drops volume.
In summary, it is concluded that the narrower liquid beads on ($\hat{y}$) direction than ($\hat{x}$) direction could be due to lower spreading and higher receding contact line associated to the low rate of drop addition. Moreover, the lower rate of material addition could leads to earlier effect of solidification and hence the corresponding arrest of the contact lines contribute to keep the narrow width once new drop is landed, which is relatively in accordance with Gao and Sonin conclusions.

Concerning the outcome of this characterization, it should be pointed out that for specific devices where highest resolution is required, as gate electrodes on a printed transistor,[43] the device should be designed taking into account this anisotropic inkjet printer behaviour. In addition, this behaviour should be studied deeply, evaluating its dependence with the different parameters that take place, aiming to give a more precisely explanation.

2.6 Liquid/solid phase change of the functional deposit.

After the liquid pattern is deposited on the substrate, a phase change must be done, where solvents are evaporated and solid charge remains on the substrate. The liquid/solid phase change is not only performed aiming to dry and keep the shape of the printed pattern, but also aiming to extract the functionality of the deposited material. The phase change process of the deposit can occurs by a number of mechanisms, including solvent evaporation, cooling through a transition temperature, gelling of a polymer precursor, and chemical reaction. In fact, in inkjet printing manufacturing process, the mechanisms of solid formation, through evaporation from a solution, are common used for conducting and semiconducting polymers solutions and also for metal

and ceramic nanoparticle suspensions. As above commented, the solvents evaporation allows to extract the functionality of the deposited material, but in addition sintering or polymerization of the functional material or reduction of the precursor is also required. These processes can be performed by means of thermal treatment,[4] plasma,[49,50] laser sintering,[51] electrical sintering,[52,53] intense pulse light (IPL),[54] photonic and microwave exposure,[55,56] electron beam,[57] and by chemical reaction or even self-sintering while solvent evaporation.[58]

Pattern drying process is one of the main manufacturing steps and takes even more relevance at multi-material printed devices, where thickness homogeneity is critical. The inkjet inks must fulfil some requirements in order to avoid issues concerning the non-uniform drying of the printed films. The most relevant problem could be the so called coffee-stain effect, where the final solid deposit shows a characteristic ring.[59–61] When the coffee-stain effect is happening, an increment of solvent flow from fluid bead centre towards the edges is produced (caused for many reasons), which drive more solute to the edges. The coffee-stain effect can be mitigated using several methods.[62] The most used one is the incorporation at the ink formulation of a co-solvent with higher boiling point and lower surface tension. Then, due to the higher evaporation at the contact lines, the solvent compositions at the edges become mainly on the co-solvent with high boiling point. As a result, the solvent at the edges has a lower surface tension than in the centre, resulting in a surface tension gradient. This gradient promotes the Marangoni flow that carries the solute inward to the drop centre, thus reducing the coffee-stain effect (*Figure 2.28*).[63,64]

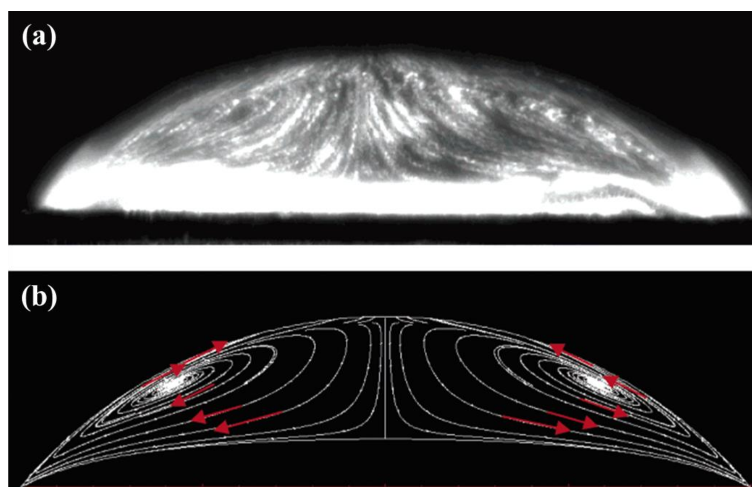

Figure 2.28 Marangoni vortex flow field in a drying octane droplet, (a) imaged experimentally and (b) predicted (Ma=45800). Image from [64]

The Marangoni effect is not the only phenomenon which generates inward flux of material. As observed by Byung Mook and co-workers, their experimental results reveals that big particles are capillary forced to move towards the centre of drop after initial coffee ring flow, while small particles keep always flowing towards the edges.[65] This phenomenon generates a profile of multiple rings. Leonid Schmuylovitch and co-workers performed another work where multiple rings profile is studied which could be related also with Byung Mook and co-workers work. A study of the contact line evolution was performed with solutions of two different particle size and, as well different drops volume. As result a stick-slip motion of the contact line is observed, where successive contact line pinning and depinning was produced. Therefore, for each pinning the segregation of particles was produced generating a ring-like deposit, while at depinning step the contact line is freely to move until the next pinning. The observations suggest that not all parts of the contact line are pinned equally. This behaviour is in accordance with some observations of the tested inks at this section and presented below.

Another flow inward reported is produced when co-solvent formulation have contribution of highly volatile solvent with a corresponding low surface tension contribution. When this liquid formulation is deposited the low temperature boiling point solvent starts considerable evaporation, hence the rest of the co-solvents whose surface tensions are much higher, reduces strongly the contact area with the substrate and the fluid motion is directed toward the pattern centre. This effect is strongly influenced by the evaporation rate; the quicker the evaporation, the faster the inward movement of the fluid. To prevent this effect, the drying should be done as low as possible.[26]

On the other hand, Dan Soltman and co-workers, using a fluid with free-Marangoni flow, have demonstrated that the natural higher rate of solvents evaporation at pinned contact line than centre can be tuned by means of the substrate temperature (*Figure 2.29).*[43]

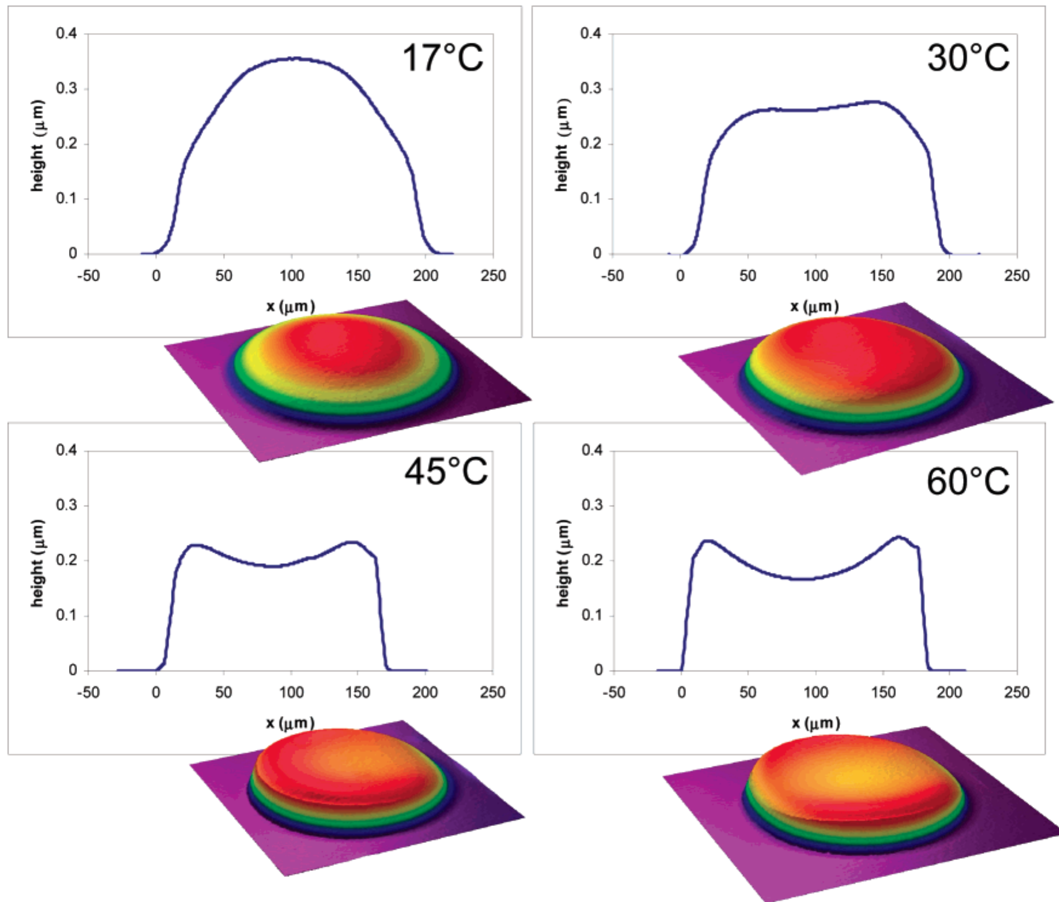

Figure 2.29 Influence of the substrate temperature in the profile of the dried deposited drops. Image from [43]

Once the solvent of deposited pattern is evaporated, the nanoparticles or polymers start the sintering and the polymerization, respectively. Regarding on the nanoparticles sintering, surface energies existing at the nanoscale allow them to coalescence with extremely low heat requirements in comparison with their bulk material.[4] However, to reach a higher degree of coalescence/sintering, heat is applied aiming to obtain the closest properties to bulk material. Concerning the polymerization, at specific temperature the polymer chain start to generate crosslinking and the polymer behaves solid. This is further explained in the next subsections.

2.6.1 Profile of the tested inks

At this subsection, the tested inks are thermal cured and the profile of the remained solid characterized. After that, the pattern profiles were evaluated in order to know if the deposits accomplish the uniformity requirements for electronic manufacturing. Depending on this, some of the inks were discharged.

The methodology used for drying the printed patterns was similar in practically all inks tested. The samples were kept on the printer platen at 40 ˚C for roughly 10 minutes, where the deposit was dried depending on the ink solvents volatility. Following, each deposit was sintered, polymerized or precursor reduced by means of thermal processes, which are reported on *Table 2.4***.**

Table 2.4 Table of drying and sintering or polymerizing processes of the tested inks.

Ref. inks	Material	Drying	Sintering or polymerizing
CI-002	Cu	40 ˚C	500 ˚C @ 30 min*
DGP 40LT-15C	Ag	40 ˚C	150 ˚C @ 30 min
EMD5714	Ag	40 ˚C	150 ˚C @ 30 min
8-VA12-3	Ag	40 ˚C	150 ˚C @ 30 min
79VA12-3	Ag	40 ˚C	200 ˚C @ 45 min
77-VA12-8	Graphite	40 ˚C	275 ˚C @ 90 min
92-VA12-2	Graphite	40 ˚C	150 ˚C @ 30 min
23-VA12-1	Al_2O_3	50 ˚C @ 2-3 h	150 ˚C @ 30 min
24-VA12-2	SiO_2	50 ˚C @ 2-3 h	150 ˚C @ 30 min
xdi-cds	PVP	80 ˚C @ 10 min	140 ˚C @ 30 min
PriElex SU-8	SU-8	40 ˚C	135 ˚C @ 30 min

*In reducing atmosphere.

To perform the profile characterization, an interferometer DCM3D (Leica) was used. At this subsection, the most dissimilar profiles observed are shown, as a representation of the possible profiles that may occur.

The first profile example corresponds to the Ag-ink (79VA12-3) printed on polyimide substrate (*Figure 2.30* and *Figure 2.31*). This patterns profiles are printed by Dimatix in the two different fluid bead growth commented above (*Figure 2.27a* and *Figure 2.27b*). This characterization also serve for validate the observations and the suggestions of Gao and Sonin[48] presented in subsection 2.5.2.

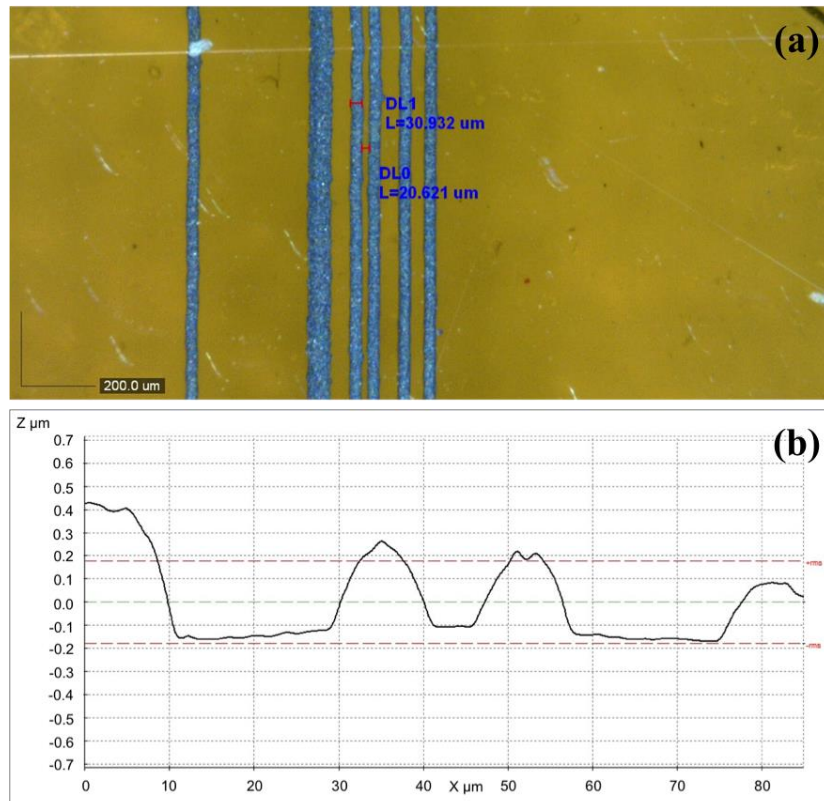

Figure 2.30 (a) Printed lines on ($\hat{y}$) direction of Ag-ink (79VA12-3) on polyimide by Dimatix. (b) 2D profile, where mono-pixel lines have a thickness about 400 nm.

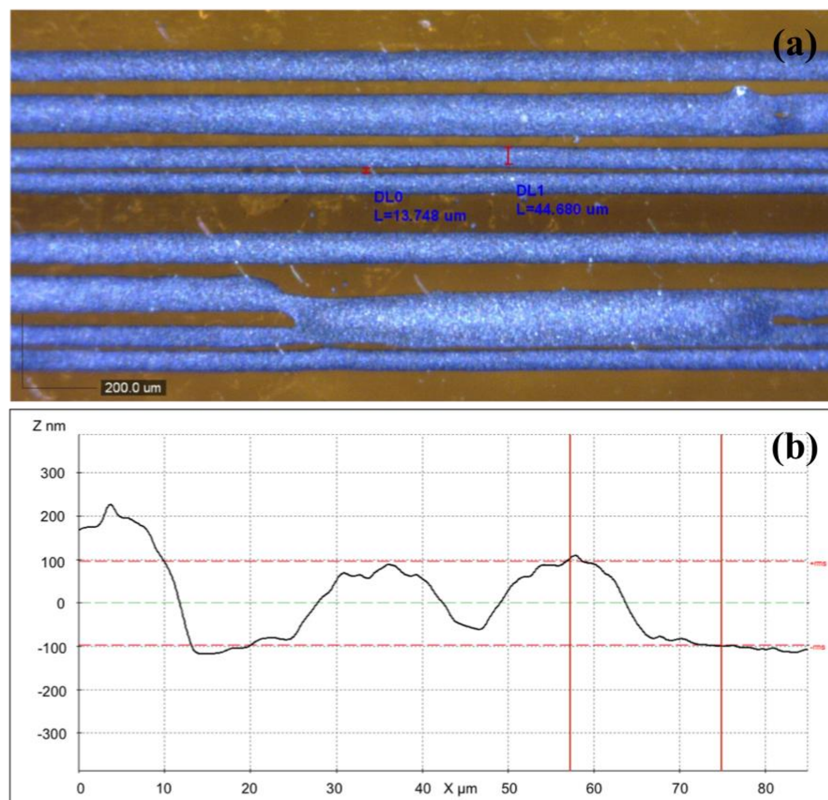

Figure 2.31 (a) Printed lines on ($\hat{x}$) direction of Ag-ink (79VA12-3) on polyimide by Dimatix. (b) 2D profile, where mono-pixel lines have a thickness about 200 nm.

As can be seen in (*Figure 2.30* and *Figure 2.31*), a smooth profile without coffee ring effect is performed. This performed profile is the outcome of a continuous receding contact line as fluid-drying process is happens and/or by exploiting the Marangoni flow circulation. All the inks tested except the graphite inks and SU-8 ink, present similar profile performance than observed with Ag-ink (79VA12-3). The performed profile accomplishes the uniformity requirements for electronic manufacturing. The thicknesses measured differs roughly two times between the mono-drop lines corresponding to *Figure 2.30* in comparison with *Figure 2.31*, which is in accordance with the conclusions presented in subsection 2.5.2 and as well with Gao and Sonin[48] suggestion.

Following, the second profile example corresponds to the graphite-ink (77VA12-8) printed on polyimide substrate (*Figure 2.32*).

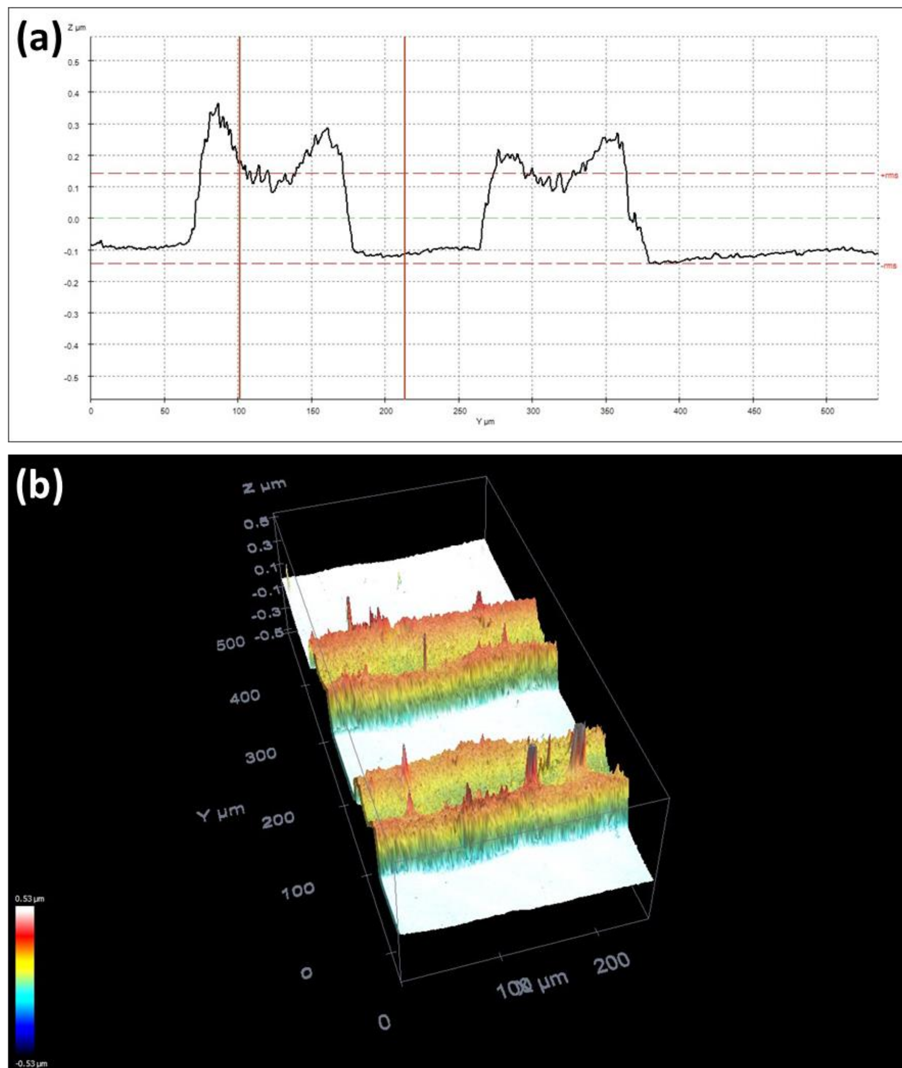

Figure 2.32 Profile characterization of graphite-ink (77VA12-8) printed lines. (a) 2D profile, where mono-pixel lines have a thickness about 300 nm. (b) 3D Interferometer profile image.

The graphite-ink (77VA12-8) shows high rate of solvents evaporation and coffee ring profile. The high rate of solvents evaporation promotes the natural solution flux from centre toward edges, summed to free-Marangoni flow inks leads to coffee-stain effect, as shown in *Figure 2.32*. This performance is also happened with graphite-ink (92VA12-2) and Ag-ink (8-VA12-3).

When graphite-inks (77VA12-8 and 92VA12-2) are used to print higher dimension patterns, a characteristic performance is produced as shown in *Figure 2.33*.

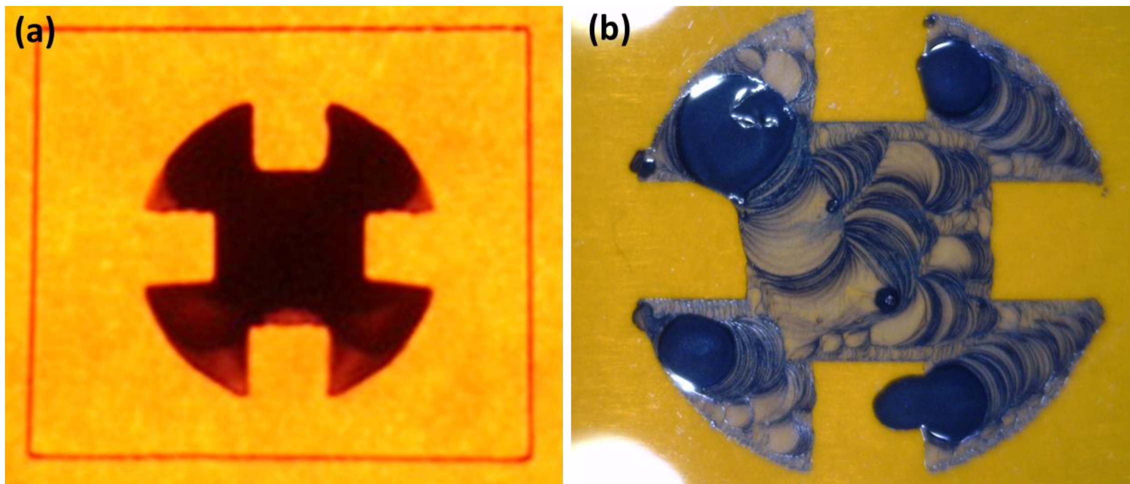

Figure 2.33. Van der Pauw pattern printed on polyimide. (a) Graphite-ink (77VA12-8) present some flux toward pattern centre when is sintered. (b) Graphite-ink (92VA12-2) present dramatically flux when is sintered showing islands of concentred material and multiple rings.[66]

In the case of the graphite-ink (77VA12-8) the dried deposit shows lower thickness at the edges (*Figure 2.33a*), instead of the profile presented for small ink volumes (*Figure 2.32*). This behaviour is slightly visible and is necessary to hold the sample to backlight to perceive the thickness inhomogeneity at the edges of the pattern (*Figure 2.33a*). This behaviour could be due to rapid evaporation of low temperature boiling solvents, thus ink changes rapidly its contact angle and hence produce a receding contact line motion.

For graphite-ink (92VA12-2) the effect of contact line pinning and depinning is strongly presented as can be seen directly in *Figure 2.33b* where receding contact line moves due to poor fixation.

The performed profile presented not accomplishes the uniformity requirements for electronic manufacturing and thus graphite-inks (77VA12-8 and 92VA12-2) and Ag-ink (8-VA12-3) are discharged.

The third profile example corresponds to the SU-8 polymer-ink (PriElex SU-8) printed over Al_2O_3 and silver deposit on paper substrate. This ink has a singular behaviour at polymerizing step, as shown in *Figure 2.34*.

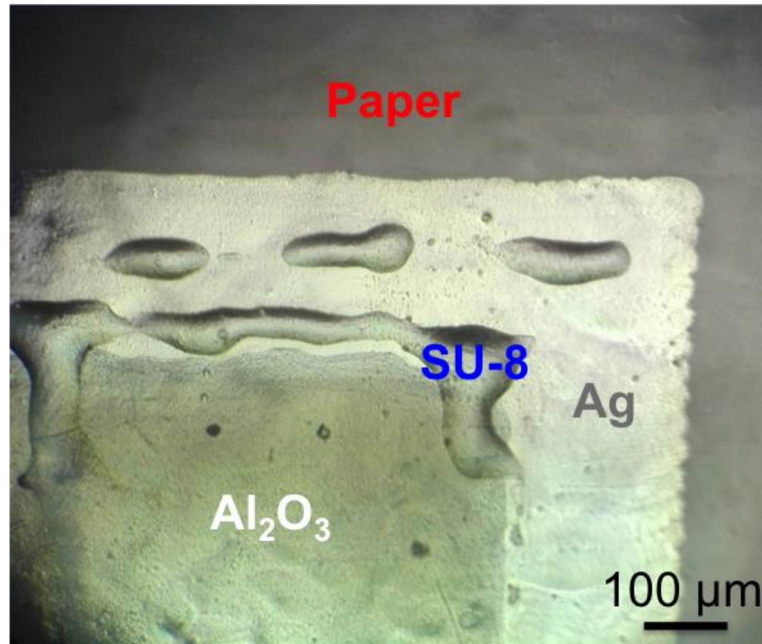

Figure 2.34 Image of the PriElex SU-8 printed on Al_2O_3 and silver, all supported by photographic paper substrate. The pattern of the SU-8 must overlap the Al_2O_3 instead of island forming.

Once SU-8 polymer-ink is printed, the ink presents good wetting on substrate and on solidified previous functional materials deposited. However, the ink bead loses the line pinning and moves forming big islands at polymerizing step, as shown in *Figure 2.34* where a multilayer structure is printed on a photographic paper substrate.

Summarizing, the 77VA12-8, 92VA12-2, 8-VA12-3 and PriElex SU-8 inks show thickness inhomogeneity or uncontrolled material movement at sintering or polymerizing treatment, thus these inks were discarded to perform the following studies in the thesis. The rest of the inks tested presented acceptable profile deposits for electronic manufacturing.

2.7 Functionality

Nowadays, inkjet printing is, in addition to colour printing, a highly attractive technique for additive manufacturing, which is used at many fields of research and development. Concerning to the present work, the inkjet printing technique was used to deposit

different functional materials, whose properties must fulfil the requirements for electronics manufacturing. All of the functional materials used on electronic components and circuits are clustered in three big families: conductors, semiconductors and insulators (large band-gap semiconductors). In this work, the materials used are conductors and insulators, and a proper characterization of the electrical properties of the sintered deposits were performed to determine the proper inks

In the case of conducting materials, the electrical resistivity is the key parameter and it depends on the functional material used, the sintering degree and the organic compounds remaining after thermal treatment. The sintering is the process where the particles or powders ink-contains coalescence, and it is promoted by both heat and pressure. This process is energetically favourable due to large particles have less surface area than smaller ones with equal total volume, and hence lower free surface energy. In addition, the smaller the particles the higher their free surface energy, thus higher degree of coalescence is produced at specific energy applied.[67] The current sintering temperatures performed at printed electronics, not allow a completely nanoparticles melting, and hence some voids persist that make the deposit less dense and with electrical resistivity about 10 times greater than the bulk material. This could be solved using other sintering strategy, as well formulating ink with a particle size distribution, which promotes higher degree of packing. The size distribution strategy is used in multi-modal silver ink NGAP NP Ag-2103 from NanoGap.[67]

As commented above, besides the solvents evaporation, additional sintering or polymerization of the functional material or reduction of the precursor is also required. These processes can be performed by means of thermal treatment, plasma,[49,50] laser sintering,[51] electrical sintering,[52,53] intense pulse light (IPL),[54] photonic and microwave exposure,[55,56] electron beam,[57] and by chemical reaction or even self-sintering while solvent evaporation.[58] *Figure 2.35* shows the degree of sintering of three Au nanoparticles with two different sintering treatments. After solidification, the functional materials should be electrically characterized to know the degree of sintering or polymerization achieved.

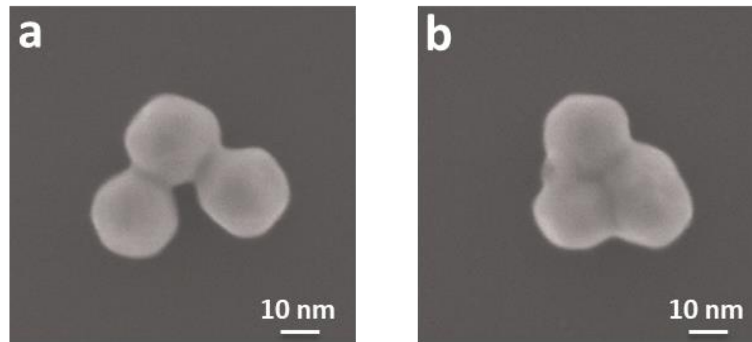

Figure 2.35 (a) SEM image of three NPs of starting mean diameter of 102.7 nm operating coalescence after 773 K 1h annealing and (b) SEM image of the same three NPs in (a) after about 30 min under the SEM electron beam. Image from[57]

2.7.1 Functional material characterization

In order to test the functional properties of the deposited functional materials, equipment for electrical characterization was mounted. This equipment consists on a Keithley 2400 source meter, 4 micro-positioners tips EB-700 (Everbeing), and a thermal wafer chuck. Labview's programs were designed to perform automatically a resistivity and resistance test at desired platen temperature, by means 4-probe method. The *Figure 2.36* shows the setup mounted to perform this electrical characterization.

Figure 2.36 Setup for electrical characterization measures.

To perform the resistivity measures of the conductive materials, it was used the Van der Pauw method for thin layers.[68] For each specific material, the sintering was performed by thermal treatment at different temperature on a range of exposure time. The curve of

resistivity depending on time exposure was performed at each temperature. The corresponding resistivity curves of different conductive materials as silver-inks, copper-ink and graphite-ink are presented. All the samples were dried previous heat treatment. In addition, all the inks were sintered in air atmosphere, instead of the copper-ink (CI-002), that was sintered at reductive atmosphere to avoid copper oxidation.

In the case of graphite-ink (77VA12-8), the maximum sintering is not achieved at the performed temperature-time exposure configurations (*Figure 2.37*). Considerable decrease of resistivity is shown at 275 °C in comparison with the curves at lower temperature, which could be related with a solvent evaporation. Higher temperatures were not tested because the polyimide substrate used to perform the study is not compatible. Regarding the resistivity found on literature, the bulk graphite is $\rho = (2.5 - 5.0) \cdot 10^{-6} (\Omega\text{m})$ when electrical conduction is parallel to basal planes and $\rho = 3.0 \cdot 10^{-3} (\Omega\text{m})$ when is perpendicular to them.[69] As printed layer consist on random oriented particles, we can consider that electrical resistivity is defined by a sort of both contributions. Then, the value of $\rho = 3.7 \cdot 10^{-3} (\Omega\text{m})$ achieved for 275 °C and 90 minutes of time exposure could be still far to the minimum resistivity available and denotes a low degree of coalescence. As commented above, this ink was discharged due to the inhomogeneity presented by the sintered deposit at the borders. In addition, this ink is also discharged because the temperatures required to proper ink sintering are forbidden for the coated paper used at this work.

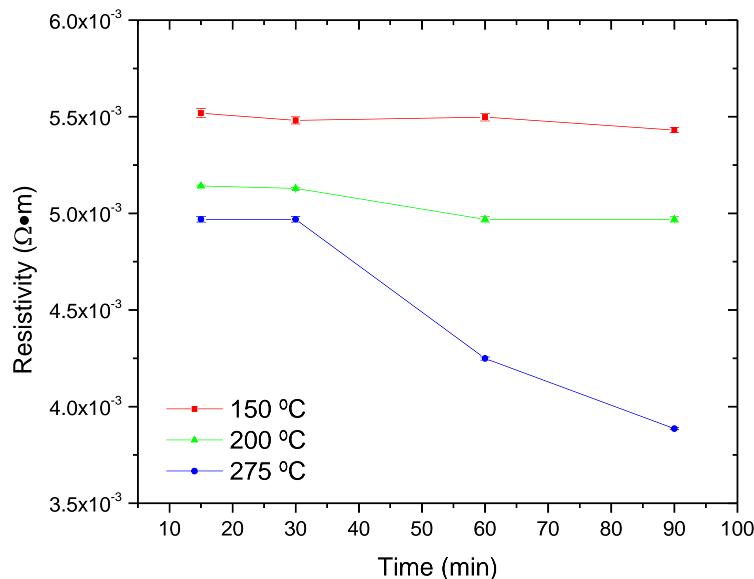

Figure 2.37 Resistivity versus curing time of graphite-ink (77VA12-8) at different temperatures.

Concerning on the copper-based ink (CI-200), it was sintered by heat treatment in N_2 inert atmosphere, and the resistivity results are shown on the *Figure 2.38*. The minimum resistivity value reached is 30 times higher than the bulk resistivity, which is $\rho = 16.78 \cdot 10^{-9}(\Omega\text{m})$.[70] Although better results of electrical resistivity could be achieved if deposits are sintered in reducing atmosphere, this ink was discharged because proper sintering of copper nanoparticles requires temperatures not compatible with coated paper used at this work.

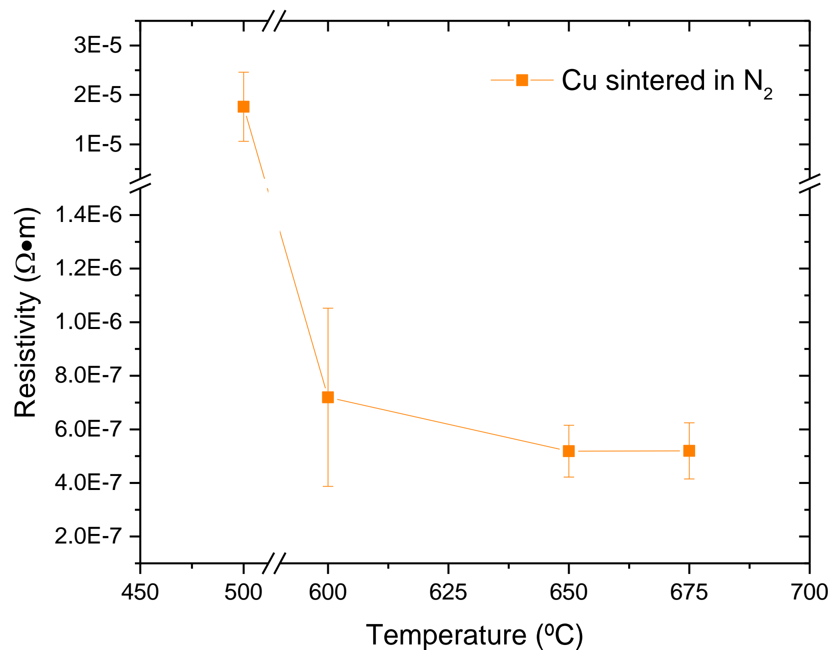

Figure 2.38 Resistivity of copper-ink (CI-200) assured at different temperatures (curing time 1 hour).

Regarding to the Ag-ink (79VA12-3) (*Figure 2.39*), the minimum resistivity is around $\rho = 3.5 \cdot 10^{-7}(\Omega\text{m})$ which is practically reached at 200 °C and 90 minutes of time exposure. Slightly lower resistivity could be achieved at 225 °C and 250 °C with less time exposure. Depending on the substrate used, the sintering curve most appropriated must be chosen. The minimum value of the resistivity reached at this characterization is 23 times higher than the bulk resistivity, which is $\rho = 15.87 \cdot 10^{-9}(\Omega\text{m})$.[70] This ink was discharged because proper sintering of Ag nanoparticles requires temperatures not compatible with coated paper used at this work.

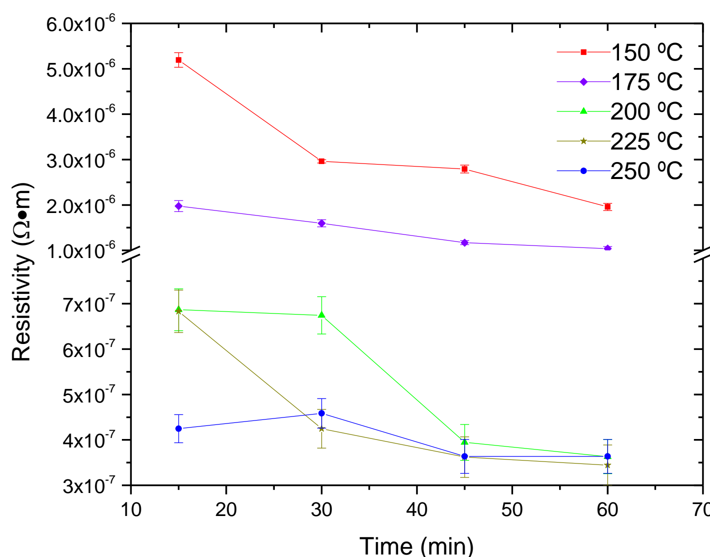

Figure 2.39 Resistivity versus curing time of Ag-ink (79VA12-3) at different temperatures.

Concerning the Ag-ink (EMD5714), the sintering at 250 °C shows a significantly change in comparison with lower sintering temperatures tested. The resistivity reaches stable value as soon as 5 minutes of exposure, thus high degree of solvent evaporation is produced at this temperature. The minimum value of resistivity is about $\rho = 1.9 \cdot 10^{-7} (\Omega\mathrm{m})$, which is 12 times higher than the bulk resistivity. Then, the EMD5714 shows promising resistivity performance regarding temperature and time exposure, which is appropriated for low temperature substrates. Although this ink fulfils the requirements for inkjet manufacturing on coated paper substrate, this ink was also discharged due to difficulties with the ink supplier.

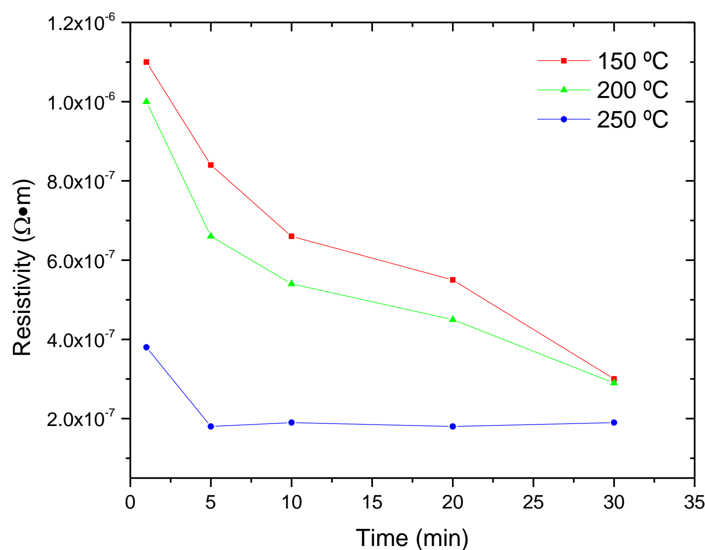

Figure 2.40 Resistivity versus curing time of Ag-ink (EMD5714) at different temperatures.

In the case of the Ag-ink (DGP 40LT-15C), the manufacturer presents a resistivity about $\rho = (1.1 - 1.2) \cdot 10^{-7}(\Omega\text{m})$ while ink is sintered at the range of 120-150 °C, where exposure time is not specified. This value of resistivity is about 7 times greater than the bulk resistivity, which is the best resistivity performance achieved among the silver ink available. The ink was tested only at one time and temperature configuration, which consist on 30 minutes at 150 °C, and the corresponding value of resistivity reached is $\rho = (1.6) \cdot 10^{-7}(\Omega\text{m})$, which is 10 times greater than the bulk resistivity and hence the value provided by the manufacturer supposes a higher exposure time. Yoon Jae Moon and co-workers also characterized this ink, on which study they sintered it by means electrical sintering, and a resistivity 1.7 times higher than bulk is reported.[47]

Summirizing, among the conductive inks tested the Ag-ink (DGP 40LT-15C) fulfils the requirements of low electrical resistivity at low curing temperatures, which is required to perform the following work of the thesis. As commented above, the rest of the conductive inks are discharged.

In addition, the insulating properties of different materials were tested deeply in the chapter 6. The inks used were Al_2O_3-ink (23-VA12-1), SiO_2-ink (24-VA12-2) and PVP-ink (xdi-cds) and the substrates used were coated paper and glass. Five different fully inkjet-printed metal-insulator-metal (MIM) structures are proposed (*Figure 2.41*). From devices employing a single dielectric material (Al_2O_3, SiO_2 and PVP) to more complex structures where two dielectrics materials are used (Al_2O_3-PVP or SiO_2-PVP). The MIM structures are reliability studied; as well are electrically evaluated by relative permittivity, loss tangent and dielectric strength parameters. The work and results achieved are detailed in chapter 6.

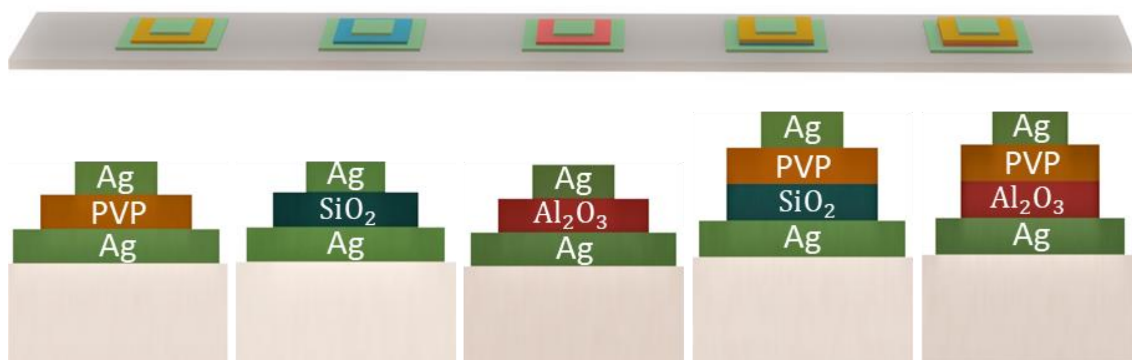

Figure 2.41 Illustration that shows printed devices used for test the dielectric structures

2.8 Adhesion

The adhesion between deposited material and substrate depends on several factors: the ink wettability, the surface roughness, the chemical bonds and the adhesion promoters. The proper adhesion of deposited materials between them as well the substrate is crucial on the additive manufacturing process. From this interaction depends the functionality and self-life of the electronic components and circuits.

2.8.1 Wettability

Wetting is, perhaps, the major limiting factor in adhesion. If a liquid does not spread over a substrate surface, the intermolecular contact between the substrate surface and liquid is poor (no proper wetting) and hence reduced contribution to adhesion is performed. The relationship between wettability and adhesion was studied extensively by Zisman.[71] A proper adhesion scenario requires that the liquid has a lower surface tension than the surface free energy of the receptor substrate. If the droplet of liquid stays as a small ball, spreading is poor and adhesion problems should be expected. If the drop spreads out to a thin, wide circle, the coating meets at least one criterion for good adhesion. As commented above, the wettability could be tuned modifying the surface tension of the ink or the free energy of the substrate surface. About the free energy of substrate surface, it could be activated by means of plasma or chemical etching treatment. These both treatments remove the dirt particles attached at the substrate (*Figure 2.42*), and thus promote an increment of the available bonds, which means a better deposit-substrate interlayer and hence adhesion.[42]

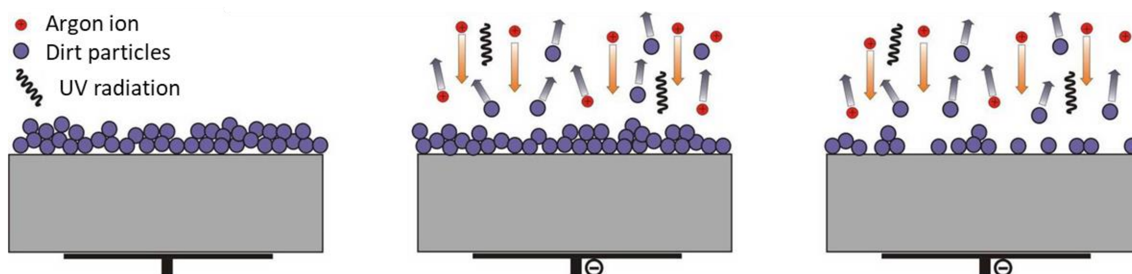

Figure 2.42 Surface activation by means argon plasma treatment. Image from[72]

2.8.2 Surface roughness and diffusive effect.

On very smooth surfaces, the interfacial attractive force per unit area is the only mechanism that intervenes to adhesion, which holds the substrate and coating together.

When surfaces have irregularities at microscopic scale, as undercuts, pores, holes, crevices or voids, the ink spreads inside these irregularities, and thus when solidifies a mechanical inter-locking (*Figure 2.43*) is formed in addition to the attractive forces. In some cases, these irregularities could be comparable as a dovetail joint (or anchoring) to hold two pieces of wood together. Moreover, the rough surfaces provide a substantially larger surfaces than the geometric area, which is known as effective surface, thus the interface is increased as well the available bonds. However, the advantage of surface roughness is favourable only if the ink penetrates completely into all surface irregularities. If the ink does not completely penetrate into the microscopic pores and crevices, dovetail effects are not performed, and the actual interfacial contact area can be smaller than the geometric area of rough surface. For other hand, some surfaces allow the ink molecules diffusion through them. Therefore, an entangled network is generated, which promote a significant adhesion.

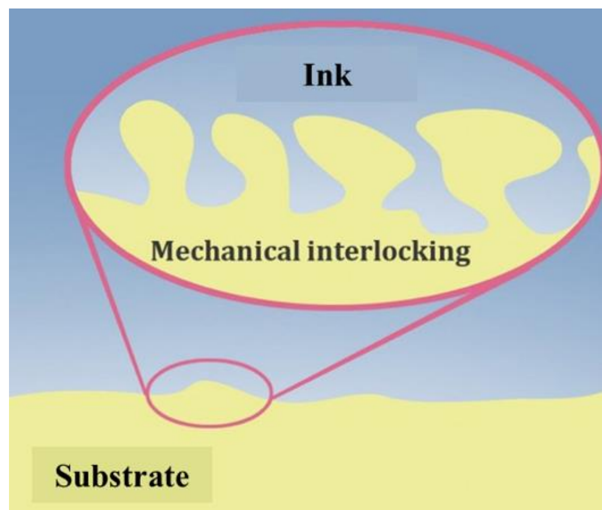

Figure 2.43 Schematic of the mechanical interlocking adhesion phenomena that happens at surfaces which present undercuts, pores, holes, crevices or voids. Image from [73]

In some cases, the printing patterns that show mechanical interlocking or diffusive effect perform considerable improvement of adhesion. In order to test the reliability of copper growth over the silver printed patterns by means of electroless, different performance was achieved depending on the substrate used. At smooth surfaces as glass, the printed pattern is removed, while keeps adhered when surface-ink show mechanical interlocking or diffusive effect. The substrates that perform good adhesion were chemical treated polyethylene terephthalate (PET) and low temperature curing

ceramics (LTCC) (*Figure 2.44*). It should be pointed out, that the generated interlocking avoid that the electroless bath contacts with these pillars fixation and hence keep hold the deposit and substrate together. However, this electroless process was discharged because was not applicable to fulfil the final requirements of this thesis, as well was not compatible with the substrates used.

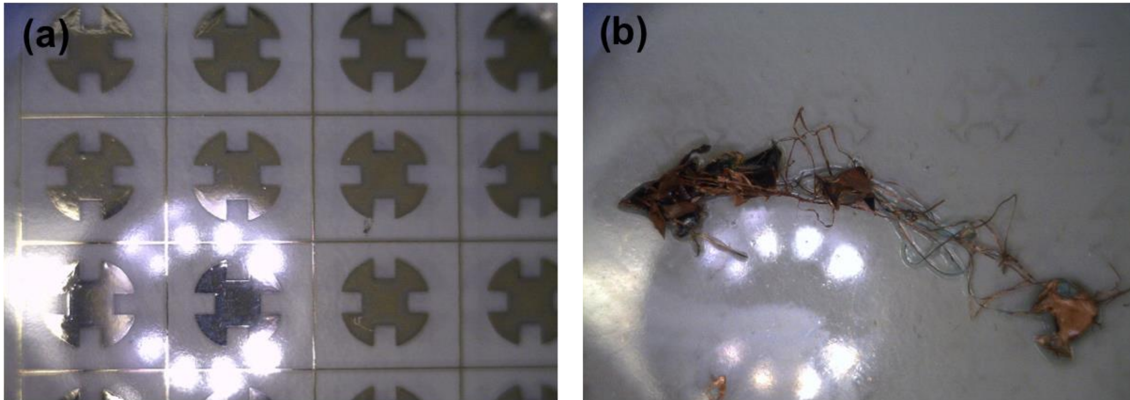

Figure 2.44 (a) Silver printed pattern on glass substrate previous to introduce in electroless bath. (b) Silver printed pattern removed of the substrate after electroless is produced.

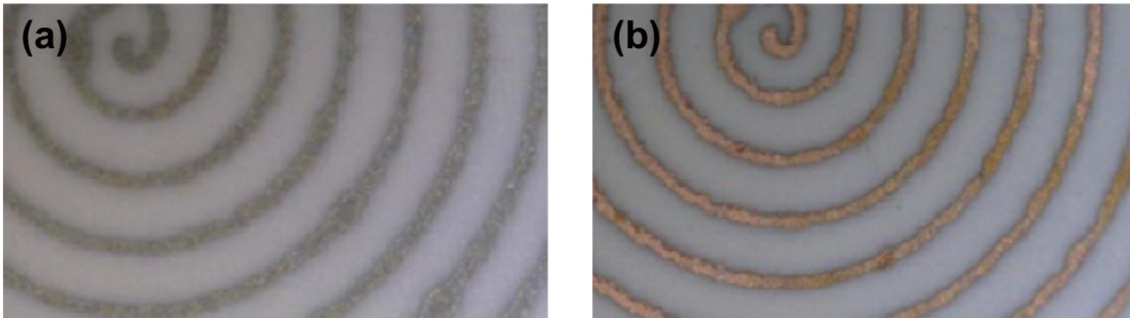

Figure 2.45 (a) Silver printed pattern on LTCC substrate previous to introduce in electroless bath. (b) Copper growth on the silver printed pattern after electroless process.[26]

2.8.3 Chemical bonds

The bonding at the interface between the deposited functional material and the substrate surface can be conducted by strong chemical bonds (chemisorption) or weaker as Van de Waals forces (physisorption). The strongest joins are where atoms of the two materials swap or share electrons (known as ionic bonding and covalent bonding, respectively). A weaker bond is formed if a hydrogen atom in one molecule is attracted to an atom of nitrogen, oxygen, or fluorine in another molecule, phenomena called hydrogen bonding. The ink-substrate compatibility enhance the bonding interface

significantly, as a polar surface and nonpolar ink or vice versa will give poor adhesion compared to polar surface and polar coating or non-polar surface and non-polar coating, which present good adhesion.

2.8.4 Adhesion promoters.

As above commented, the nature compatibility between the materials is basic to assure good adhesion. Therefore, if needed, promoter coatings can be deposited on the surface to modify the incompatibilities. Unfortunately, coating the whole surface with a promoter can lead to an alteration of the free surface energy and hence to an uncontrolled increase of the wettability.

Other option is promote the adhesion by means an increment of the cohesion. Cohesion is the property of same nature molecules to stick to each other due to mutual attraction. In some cases the ink present equal or similar substrate molecules, wich can lead to excellent results as shown on work presented by Daehwan Jang and co-workers (*Figure 2.46*).[74]

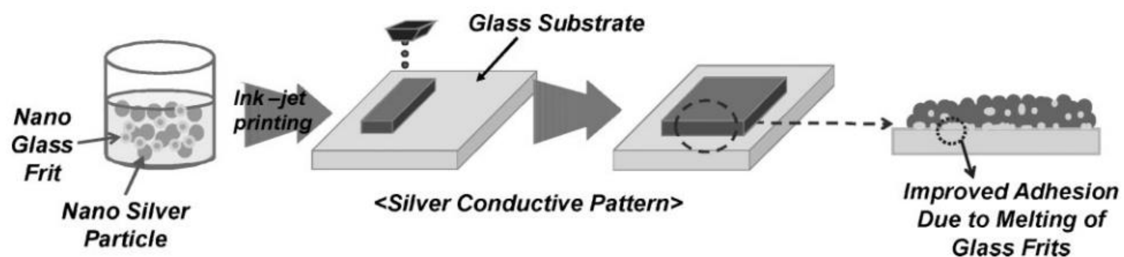

Figure 2.46 Schematic diagram shown the mechanism that improves adhesion by means cohesion. The same nature molecules of glass are mixed on the ink, which are used as adhesion promoters. Image from[74]

2.8.5 Adhesion test

There are several methods to test the deposit-substrate adhesion. Among them, there is a cross cut test which consists on cutting a grid on the printed deposit with a special blade of parallel cuts (as indicated on ISO 2409). After that, a tape is adhered over the grid and later removed. The adhesion depends on the removed grid area and is rated in accordance with the scale illustrated in *Figure 2.47*.

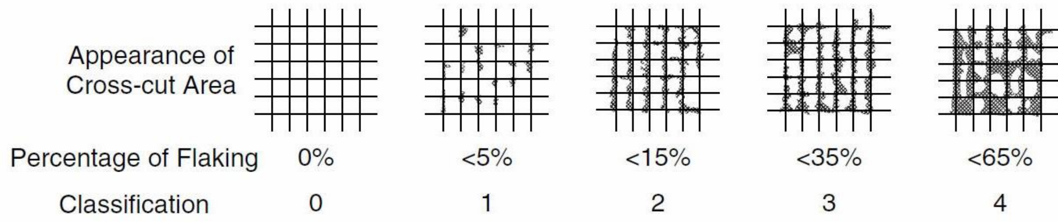

Figure 2.47 Classification of the adhesion strength according to the removal coating area after the cross-cut test. Image from[75]

This test has been performed in order to check the adhesion of the printed deposits on glass substrate. To perform this test a cross-cut kit NK2000 from Neurtek was used.[76] The results achieved are: for silver-based and polymer-based inks about 0 or 1, for carbon-based inks about 2 or 3, and for alumina-based or silica-based inks, which are not sintered at curing temperatures performed, about 3-4. In *Figure 2.48* is shown an example of the adhesion test performed with the Al_2O_3-ink (23-VA12-1).

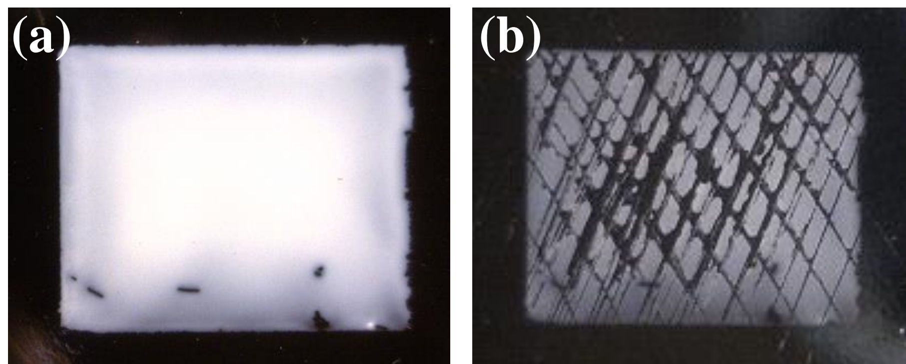

Figure 2.48 (a) Dried deposit of Al_2O_3-ink (23-VA12-1) before adhesion test. (b) After adhesion test.

2.9 Insulation and encapsulation of printed electronics

Inkjet-printed functional materials take advantage of their size scale to coalescence at significant lower temperatures instead of their bulk materials. However, after sintering process the materials deposited look like far away from the bulk structure, thus surfaces and inner parts of the printed layers show significant effective surface exposed to the surrounding chemical agents. This behaviour is not only exclusive of inkjet printing, but all of the printed electronics techniques where functional materials are deposited by means of inks or pastes formulated with micro- or nano- sized particles. In fact, the robustness is one of the main factors that limit some manufacturing techniques to supply the market with electronic devices. Regarding inkjet-printed electronic

components or circuits; several works reported deposits degradation due to surrounding environment and some works also presented insulating strategies to solve this phenomenon at first attempt. However, more efforts on printing insulating and encapsulating layers are needed to improve the self-life of the printed electronic. Among the available works where degradation to air exposure is studied, Christa M. Homenick *et al.* use PVP/PMSSQ-based dielectric ink xdi-d1.2 from Xerox as strategy for encapsulation of printed single walled carbon nanotubes-based thin transistor SWCNT TFT. They demonstrate that PVP/PMSSQ encapsulation acts as water barrier and improves the transfer characteristic performance of the insulated transistor, but the study reports only an aging test of 81 days, which is far away of the self-life for market electronic devices.[77] Dapeng Li *et al.*printed copper and nickel strips over poly(vinylidenefluoride) PVDF membrane, and demonstrate that as high is the thickness of the printed strips lower is the resistance variation with the air exposure, because surface oxidation to volume ratio is reduced. However, the aging test is only performed 20 days and 5 days for copper and nickel, respectively, which is also far away of the self-life requirements at electronic market.[78] Mathew S. Rager *et al.* presented CuO ink, which sintered by means photonic pulse thermal processing (PTP). They demonstrate that drying process previous to sintering leads to a better performance of the conductive tracks with significant lower degradation to air exposure. However, after aging test to air exposure, the best performance achieved, which is dried previous to PTP sintering, increase their resistance about 100 %.[79] B. Medina proposes a strategy to avoid the conductive strip corrosion by means of passivation of the surface with a precious metal as gold. The strategy consists on use a gold electroless as conductive strip corrosion encapsulation, aging-test was not performed.[26]

2.10 Conclusions

All the inks tested, both in the case of conductive inks and in dielectric ones have the non-dimensional Z value in the range of $1 < Z < 10$. In the case of lowest Z value, a slightly increase of the temperature of the nozzle is required for a better jetability performance. Concretely, the most used silver ink in this work has a Z value around 5.

Comparing the performance of the printheads with the hydrocarbon solvent-based inks, the wetting printheads have better jetability than non-wetting printheads. At the wetting

printheads, the ink remains on the nozzle plate with very low contact angle forming a thin uniform layer, which does not obstruct the drop formation.

There are two limiting bounds, lower and upper, to the width of a parallel-sided liquid bead produced by inkjet printing, even in the stability regime. If drop spacing is not small enough, initial coalescence leads to a liquid bead with a periodic irregularity. If drop spacing is too small a bulging instability is formed.

The liquid beads on ($\hat{y}$) direction are narrower than ($\hat{x}$) direction, and it is related with the lower spreading and higher receding contact line associated to the low rate of drop addition. The lower rate of material addition provokes earlier effect of solidification and the corresponding arrest of the contact lines. In summary, the drop ejecting frequency and sweep velocity is anisotropic at inkjet printing technology used.

In all the cases studied, proper ink-substrate wettability is assured by correct hysteresis between the receding and advancing contact angles. In addition, at proper ink-substrate wettability, the parallel-sided deposits at line or square-shape patterns depend on drops overlapping and drop ejecting frequency.

The SU-8-ink (PriElex SU-8) is discharged due to the loss of the ink bead line pinning and formation of undesirable big islands, at polymerization step.

The sintered deposits of graphite-inks (77VA12-8 and 92VA12-2) have a lack of homogeneity along the thickness, besides these deposits of graphite inks suffer coffee ring effect. In addition, the temperatures required to proper ink sintering are forbidden for the coated paper used at this work. For both reasons these inks are not suitable for the purpose of this thesis.

All the deposits of the inks, including dielectric and conductive inks except graphite ones, have free coffee ring effect at sintering process, being suitable for electronic manufacturing.

The sintering studies of conductive inks, specially silver ones, reveal that the Ag-inks DGP 40LT-15C and EMD5714 have low values of resistivity, close to bulk silver at low sintering temperatures. The rest of the conductive inks are neglected because of the temperature required for proper sintering is too high for the substrate proposed in this work.

2.11 References

(1) Mizukami, M.; Cho, S. Il; Watanabe, K.; Abiko, M.; Suzuri, Y.; Tokito, S.; Kido, J. Flexible Organic Light-Emitting Diode Displays Driven by Inkjet-Printed High-Mobility Organic Thin-Film Transistors. *IEEE Electron Device Lett.* **2018**, *39* (1), 39–42.

(2) Wang, Y.; Guo, H.; Chen, J. J.; Sowade, E.; Wang, Y.; Liang, K.; Marcus, K.; Baumann, R. R.; Feng, Z. S. Paper-Based Inkjet-Printed Flexible Electronic Circuits. *ACS Appl. Mater. Interfaces* **2016**, *8* (39), 26112–26118.

(3) Hayes, D. J.; Wallace, D. B.; Royall Cox, W. MicroJet Printing of Solder and Polymers for Multi-Chip Modules and Chip-Scale Packages. *Proceedings-SPIE Int. Soc. Opt. Eng.* **1999**, 242–247.

(4) Arrese, J.; Vescio, G.; Xuriguera, E.; Medina-Rodriguez, B.; Cornet, A.; Cirera, A. Flexible Hybrid Circuit Fully Inkjet-Printed: Surface Mount Devices Assembled by Silver Nanoparticles-Based Inkjet Ink. *J. Appl. Phys.* **2017**, *121* (10).

(5) Schnitker, J.; Adly, N.; Seyock, S.; Bachmann, B.; Yakushenko, A.; Wolfrum, B.; Offenhäusser, A. Rapid Prototyping of Ultralow-Cost, Inkjet-Printed Carbon Microelectrodes for Flexible Bioelectronic Devices. *Adv. Biosyst.* **2018**, *1700136*, 1700136.

(6) Fang, Y.; Wu, X.; Lan, S.; Zhong, J.; Sun, D.; Chen, H.; Guo, T. Inkjet-Printed Vertical Organic Field-Effect Transistor Arrays and Their Image Sensors. *ACS Appl. Mater. Interfaces* **2018**, *10*, acsami.8b06625.

(7) Li, Y.; Dahhan, O.; Filipe, C. D. M.; Brennan, J. D.; Pelton, R. H. Optimizing Piezoelectric Inkjet Printing of Silica Sols for Biosensor Production. *J. Sol-Gel Sci. Technol.* **2018**, *87* (3), 657–664.

(8) Bittner, S. M.; Guo, J. L.; Melchiorri, A.; Mikos, A. G. Three-Dimensional Printing of Multilayered Tissue Engineering Scaffolds. *Mater. Today* **2018**, *xxx* (xx).

(9) Williams, C. Ink-Jet Printers Go beyond Paper. *Phys. World* **2006**, *19* (1), 24–29.

(10) Martin, G. D.; Hoath, S. D.; Hutchings, I. M. Inkjet Printing - The Physics of Manipulating Liquid Jets and Drops. *J. Phys. Conf. Ser.* **2008**, *105* (1).

(11) Eayiieigh, B. L. Lord Bayleigh on The. *Writing* **1879**, *1873* (June 1873).

(12) Instrument, M.; The, O. F.; Type, R. Sept. 4, 1951 R. ELMQvist. **1951**, 21–23.

(13) Derby, B. Inkjet Printing of Functional and Structural Materials: Fluid Property

Requirements, Feature Stability, and Resolution. *Annu. Rev. Mater. Res.* **2010**, *40* (1), 395–414.

(14) Kyser, E. L.; Sears, S. B. Pulsed Droplet Ejecting System. US3683212A, 1976.

(15) Zoltan, S. Pulsed Droplet Ejecting System. *US Pat. 3683212* **1972**.

(16) Le, H. P. Progress and Trends in Ink-Jet Printing Technology. *J. Imaging Sci. Technol.* **1998**, *42*, 49–62.

(17) Vaught, J. L.; Cloutier, F. L.; Donald, D. K.; Meyer, J. D.; Tacklind, C. A.; Taub, H. H. THERMAL INKJET PRINTER. US4490728A, 1981.

(18) Darling, R. Micro Fabrication. *Univ. Washingt. Coll. Eng.* **2012**, 77–80.

(19) Reis, N.; Derby, B. Experiments of Droplet Formation. *Mater. Res.* **2000**, *625*, 117–122.

(20) Liou, T. M.; Chan, C. Y.; Shih, K. C. Effects of Actuating Waveform, Ink Property, and Nozzle Size on Piezoelectrically Driven Inkjet Droplets. *Microfluid. Nanofluidics* **2010**, *8* (5), 575–586.

(21) Liu, Y. F.; Tsai, M. H.; Pai, Y. F.; Hwang, W. S. Control of Droplet Formation by Operating Waveform for Inks with Various Viscosities in Piezoelectric Inkjet Printing. *Appl. Phys. A Mater. Sci. Process.* **2013**, *111* (2), 509–516.

(22) MicroChem. *XP PriElex SU-8 Process Guidelines*.

(23) Haque, R. I.; Vie, R.; Germainy, M.; Valbin, L.; Benaben, P.; Boddaert, X. Inkjet Printing of High Molecular Weight PVDF-TrFE for Flexible Electronics. *Flex. Print. Electron.* **2016**, *1* (1), 12.

(24) Fromm, J. E. Numerical Calculation of the Fluid Dynamics of Drop-on-Demand Jets. *IBM J. Res. Dev.* **1984**, *28* (3), 322–333.

(25) Vescio, G. Inkjet-Printed Flexible Electronic Devices: From High-k Capacitors to h-BN/Graphene Thin Film Transistors, Universitat de Barcelona, 2017.

(26) Medina, B. Inkjet and Screen Printing for Electronic Applications, Universitat de Barcelona, 2016.

(27) Fujifilm Dimatix. *Jettable Fluid Formulation Guidelines*; 2013.

(28) Dimatix, F. *Individual Tunable Nozzles Nozzle Plate DMP-5005 Cartridges & Printheads*; 2012.

(29) Calvert, P. Inkjet Printing for Materials and Devices. *Chem. Mater.* **2001**, *13* (10), 3299–3305.

(30) Wang, X.; Carr, W. W.; Bucknall, D. G.; Morris, J. F. High-Shear-Rate Capillary Viscometer for Inkjet Inks. *Rev. Sci. Instrum.* **2010**, *81* (6).

(31) Xu, D.; Sanchez-Romaguera, V.; Barbosa, S.; Travis, W.; De Wit, J.; Swan, P.; Yeates, S. G. Inkjet Printing of Polymer Solutions and the Role of Chain Entanglement. *J. Mater. Chem.* **2007**, *17* (46), 4902–4907.

(32) Wagner, N. J.; Brady, J. F. Shear Thickening in Colloidal Dispersions. *Phys. Today* **2009**, *62* (10), 27–32.

(33) Fromm, J. A Numerical Study of Drop-on-Demand Inks Jets. **1982**.

(34) Bergeron, V.; Bonn, D.; Martin, Y. V; Vovelle, L. Controlling Drop Deposition with Polymer Additives. *Nature* **2000**, *405* (June), 772–775.

(35) Reis, N.; Derby, B. Ink Jet Deposition of Ceramic Suspensions: Modeling and Experiments of Droplet Formation. *MRS Proc.* **2000**, *625*, 117.

(36) Jang, D.; Kim, D.; Moon, J.; Jang, D.; Kim, D.; Moon, J. Influence of Fluid Physical Properties on Ink-Jet Printability Influence of Fluid Physical Properties on Ink-Jet Printability. *Langmuir* **2009**, *25* (5), 2629–2635.

(37) Murshed, S. M. S.; Tan, S. H.; Nguyen, N. T. Temperature Dependence of Interfacial Properties and Viscosity of Nanofluids for Droplet-Based Microfluidics. *J. Phys. D. Appl. Phys.* **2008**, *41* (8).

(38) Schiaffino, S.; Sonin, A. A. Molten Droplet Deposition and Solidification at Low Weber Numbers. *Phys. Fluids* **1997**, *9* (11), 3172–3187.

(39) Rioboo, R.; Marengo, M.; Tropea, C. Time Evolution of Liquid Drop Impact onto Solid, Dry Surfaces. *Exp. Fluids* **2002**, *33* (1), 112–124.

(40) Clegg, C. Advancing and Receding Contact Angles. 2008.

(41) TOGWT. TOGWT: Is your paint coating still viable? http://togwt1980.blogspot.com/2015/06/is-your-paint-coating-still-viable.html (accessed Oct 22, 2018).

(42) Ramé-hart instruments co. Contact Angle http://www.ramehart.com/contactangle.htm (accessed Oct 22, 2018).

(43) Soltman, D.; Subramanian, V. Inkjet-Printed Line Morphologies and Temperature Control of the Coffee Ring Effect. *Langmuir* **2008**, *24* (5), 2224–2231.

(44) Duineveld, P. C. The Stability of Ink-Jet Printed Lines of Liquid with Zero Receding Contact Angle on a Homogeneous Substrate. *J. Fluid Mech.* **2003**, *477* (477), 175–200.

(45) Davis, S. H. Moving Contact Lines and Rivulet Instabilities. Part 1. The Static Rivulet. *J. Fluid Mech.* **1980**, *98* (02), 225.

(46) Schiaffino, S.; Sonin, A. A. Formation and Stability of Liquid and Molten Beads on a Solid Surface. *J. Fluid Mech.* **1997**, *343*, 95–110.

(47) Smith, P. J.; Shin, D. Y.; Stringer, J. E.; Derby, B.; Reis, N. Direct Ink-Jet Printing and Low Temperature Conversion of Conductive Silver Patterns. *J. Mater. Sci.* **2006**, *41* (13), 4153–4158.

(48) Gao, F.; Sonin, A. A. Precise Deposition of Molten Microdrops: The Physics of Digital Microfabrication. *Proc. R. Soc. A Math. Phys. Eng. Sci.* **1994**, *444* (1922), 533–554.

(49) Wolf, F. M.; Perelaer, J.; Stumpf, S.; Bollen, D.; Kriebel, F.; Schubert, U. S. Rapid Low-Pressure Plasma Sintering of Inkjet-Printed Silver Nanoparticles for RFID Antennas. *J. Mater. Res.* **2013**, *28* (9), 1254–1261.

(50) Wünscher, S.; Stumpf, S.; Teichler, A.; Pabst, O.; Perelaer, J.; Beckert, E.; Schubert, U. S. Localized Atmospheric Plasma Sintering of Inkjet Printed Silver Nanoparticles. *J. Mater. Chem.* **2012**, *22* (47), 24569.

(51) Ko, S. H.; Pan, H.; Grigoropoulos, C. P.; Luscombe, C. K.; Fréchet, J. M. J.; Poulikakos, D. All-Inkjet-Printed Flexible Electronics Fabrication on a Polymer Substrate by Low-Temperature High-Resolution Selective Laser Sintering of Metal Nanoparticles. *Nanotechnology* **2007**, *18* (34).

(52) Moon, Y. J.; Lee, S. H.; Kang, H.; Kang, K.; Kim, K. Y.; Hwang, J. Y.; Cho, Y. J. Electrical Sintering of Inkjet-Printed Silver Electrode for c-Si Solar Cells. *Conf. Rec. IEEE Photovolt. Spec. Conf.* **2011**, 001061–001065.

(53) Hummelgård, M.; Zhang, R.; Nilsson, H. E.; Olin, H. Electrical Sintering of Silver Nanoparticle Ink Studied by In-Situ TEM Probing. *PLoS One* **2011**, *6* (2), 1–6.

(54) Kang, J. S.; Ryu, J.; Kim, H. S.; Hahn, H. T. Sintering of Inkjet-Printed Silver Nanoparticles at Room Temperature Using Intense Pulsed Light. *J. Electron. Mater.* **2011**, *40* (11), 2268–2277.

(55) Perelaer, J.; Abbel, R.; Wünscher, S.; Jani, R.; Van Lammeren, T.; Schubert, U. S. Roll-to-Roll Compatible Sintering of Inkjet Printed Features by Photonic and Microwave Exposure: From Non-Conductive Ink to 40% Bulk Silver Conductivity in Less than 15 Seconds. *Adv. Mater.* **2012**, *24* (19), 2620–2625.

(56) Gaspar, C.; Passoja, S.; Olkkonen, J.; Smolander, M. IR-Sintering Efficiency on Inkjet-Printed Conductive Structures on Paper Substrates. *Microelectron. Eng.* **2016**, *149*, 135–140.

(57) Ruffino, F.; Torrisi, V.; Grimaldi, M. G. Experimental Study on the Coalescence Process of SiO 2 Supported Colloidal Au Nanoparticles. *Phys. E Low-dimensional Syst. Nanostructures* **2015**, *74*, 388–399.

(58) Grouchko, M.; Kamyshny, A.; Mihailescu, C. F.; Anghel, D. F.; Magdassi, S. Conductive Inks with a “Built-in” Mechanism That Enables Sintering at Room Temperature. *ACS Nano* **2011**, *5* (4), 3354–3359.

(59) Deegan, R. D.; Bakajin, O.; Dupont, T. F.; Huber, G.; Nagel, S. R.; Witten, T. A. Contact Line Deposits in an Evaporating Drop. *Phys. Rev. E - Stat. Physics, Plasmas, Fluids, Relat. Interdiscip. Top.* **2000**, *62* (1 B), 756–765.

(60) Deegan, R. D. Pattern Formation in Drying Drops. *Phys. Rev. E* **2000**, *61* (1), 475–485.

(61) Deegan, R. D.; Bakajin, O.; Dupont, T. F.; Huber, G.; Nagel, S. R.; Witten, T. A. Capillary Flow as the Cause of Ring Stains from Dried Liquid Drops. *Nature* **1997**, *389* (6653), 827–829.

(62) Li, Y.; Lan, L.; Xiao, P.; Sun, S.; Lin, Z.; Song, W.; Song, E.; Gao, P.; Wu, W.; Peng, J. Coffee-Ring Defined Short Channels for Inkjet-Printed Metal Oxide Thin-Film Transistors. *ACS Appl. Mater. Interfaces* **2016**, *8* (30), 19643–19648.

(63) Hu, H.; Larson, R. G. Analysis of the Effects of Marangoni Stresses on the Microflow in an Evaporating Sessile Droplet. *Langmuir* **2005**, *21* (9), 3972–3980.

(64) Hu, H.; Larson, R. G. Marangoni Effect Reverses Coffee-Ring Depositions. *J. Phys. Chem. B* **2006**, *110* (14), 7090–7094.

(65) Weon, B. M.; Je, J. H. Capillary Force Repels Coffee-Ring Effect. *Phys. Rev. E - Stat. Nonlinear, Soft Matter Phys.* **2010**, *82* (1), 1–4.

(66) Shmuylovich, L.; Shen, A. Q.; Stone, H. A. Surface Morphology of Drying Latex Films: Multiple Ring Formation. *Langmuir* **2002**, *18* (9), 3441–3445.

(67) Buffat; Borel, J.-P. Size Effect on the Melting Temperature of Gold Particles. *Phys. Rev. A* **1976**, *13* (6), 2287–2298.

(68) L. J. van der Pauw. *A Method of Measuring Specific Resistivity and Hall Effect of Discs of Arbitrary Shape*; 1958; Vol. 13.

(69) Helmenstine, A. M. Table of Electrical Resistivity and Conductivity https://www.thoughtco.com/table-of-electrical-resistivity-conductivity-608499 (accessed Nov 2, 2018).

(70) Matula, R. A. Electrical Resistivity of Copper, Gold, Palladium, and Silver. *J.*

Phys. Chem. Ref. Data **1979**, *8* (4), 1147–1298.

(71) Zismann, W. A. *Contact Angle, Wettability, and Adhesion*; Fowkes, F. M., Ed.; Advances in Chemistry; AMERICAN CHEMICAL SOCIETY: WASHINGTON, D.C., 1964; Vol. 43.

(72) Electronic diener. Plasma cleaning https://www.plasma.com/en/plasmatechnik/lexikon/plasma-cleaning/ (accessed Nov 5, 2018).

(73) Ashish. Why Doesn't Glue Stick To The Inside Of The Bottle It's Packed In? » Science ABC https://www.scienceabc.com/eyeopeners/why-doesnt-glue-stick-to-the-inside-of-the-bottle-its-packed-in.html (accessed Nov 8, 2018).

(74) Jang, D.; Kim, D.; Lee, B.; Kim, S.; Kang, M.; Min, D.; Moon, J. Nanosized Glass Frit as an Adhesion Promoter for Ink-Jet Printed Conductive Patterns on Glass Substrates Annealed at High Temperatures. *Adv. Funct. Mater.* **2008**, *18* (19), 2862–2868.

(75) Durgesh Kumar Soni; P.K. Kamani. Adhesion A key property of paints and coatings https://www.chemarc.com/content/chemarc-article/58913b6ede2afc2052ddd7ee?to=%2Farticle%2F58913b6ede2afc2052ddd7ee (accessed Nov 6, 2018).

(76) Neurtek instruments. Cross Hatch Adhesion Tester.

(77) Homenick, C. M.; James, R.; Lopinski, G. P.; Dunford, J.; Sun, J.; Park, H.; Jung, Y.; Cho, G.; Malenfant, P. R. L. Fully Printed and Encapsulated SWCNT-Based Thin Film Transistors via a Combination of R2R Gravure and Inkjet Printing. *ACS Appl. Mater. Interfaces* **2016**, *8* (41), 27900–27910.

(78) Li, D.; Sutton, D.; Burgess, A.; Graham, D.; Calvert, P. D. Conductive Copper and Nickel Lines via Reactive Inkjet Printing. *J. Mater. Chem.* **2009**, *19* (22), 3719–3724.

(79) Rager, M. S.; Aytug, T.; Veith, G. M.; Joshi, P. Low-Thermal-Budget Photonic Processing of Highly Conductive Cu Interconnects Based on CuO Nanoinks: Potential for Flexible Printed Electronics. *ACS Appl. Mater. Interfaces* **2016**, *8* (3), 2441–2448.

DEVELOPMENT OF A NOVEL SMD ASSEMBLING METHOD CAPILLARITY-ASSISTED

CHAPTER 3

3.1 Motivation

PCB technology has evolved constantly due to the emergence of new manufacturing techniques and the increase of functional materials and substrates. As an example, printed electronic circuits can be manufactured by means of inkjet printer or laser induced forward transfer (LIFT) on flexible substrates as polyethylene terephthalate (PET), polyethylene-naphthalate (PEN), polyimide (PI), coated foil, and paper.[1–3,4,5]

In the same line, the electrical connection between components and conductive strip has evolved, long time ago, from through hole technology to surface mount technology (SMT). Nowadays, the most usual PCBs manufacturing process for mass production is composed by photoengraving as copper patterning technique (large volumes and fine features could be achieved),[6,7] by screen printing or a dispensator jet as solder paste depositing systems,[8] and by a pick and place system for locate the SMDs on the corresponding mounting sites on the PCB.

Regarding the novel PCBs, and among the existing manufacturing techniques, inkjet printing technique is growing on interest because of the fast prototyping at low-cost. In fact, there are many works on direct printing of electronic components, which reported advances in the fabrication of transistors,[9,10,11] MIMs,[12] OLEDs,[13] and diodes[14] These works go ahead towards the consecution of fully inkjet-printed electronic circuits.[15,16]

However, most of the inkjet-printed electronic components have still to overcome severe drawbacks: poor performances[16,17] and self-life[18,19] due to parasitic capacities, poor isolation and resolution. In addition, the present electronics devices require a high degree of reliability and quality. In order to accomplish these requirements, hybrid electronics fulfils them by combining the advantages of the printing technologies with the surface-mount technology.[20–24,25] The main issue related to this procedure is the surface mount device (SMD) attachment onto the inkjet patterned substrate. The usual material employed at SMT is reflow paste,[26] a sticky mixture of flux and solder particles which shows high incompatibility with inkjet-printed pads. Solder particles on reflow process provoke leaching effect by removing and damaging printed pads and generate undesired functional errors,[22] as well the elevated processing-temperature are not compatible with some of the substrates used in the incoming applications. Recently, Niittynen et al. implemented SMDs on inkjet-printed substrates by using an screen-printed isotropically conductive adhesive (ICA).[22] Moreover, Andersson et al. assembled SMDs onto ink-jet printed paper with ICA, solder and conductive adhesive

tapes.[23,24] Nonetheless, none of these works used the inkjet for deposit the electrical connecting materials. In this chapter, a novel technique for assembling SMDs by inkjet printer with a low temperature process is proposed.[3,27]

3.2 Novel procedure for hybrid circuit manufacturing by inkjet printer

The use of silver nanoparticle-based inkjet ink (AgNP ink) as a new approach for assembling SMDs by means of ink capillarity and high-resolution inkjet printing technology is presented in this section. ES-2564760_A1.[27,3] The new proposed method is compared with usual commercial benchmark materials employed for standard assembling. Therefore, AgNP ink, ICA and solder are tested on inkjet-printed flexible (paper, Kapton®) and rigid substrate (glass). Assembling methods performance and their reliability are evaluated by means of electrical contact resistance and shear strength of the SMDs onto the inkjet-printed pads.

3.2.1 Materials

All the experimental tests were carried out by means of a inkjet printer machine Dimatix 2831 model series (Fujifilm USA). A cartridge with an ink droplet volume fixed at 10 pl was used. For the printed pads and wires, Silverjet DGP HR (ANP, South Korea) 40 % of silver weigh concentration with a viscosity around ~16 cP was used. The experimental set-up during printing processes was maintained stable at room temperature (22 °C), and meantime nozzles firing drops and the inkjet platen substrate were fixed at 40 °C. Equal temperature nozzle-platen was chosen to promote volatile solvents evaporation that ensures the best drop size on the surface after impacting the substrate.

Paper substrate Powercoat 230 (Arjowiggins, USA) with a thickness of 222 µm and single side adhesive plastic polyimide Kapton® (ISOAD TAPE 7004, DuPont, USA) with a thickness of 25 µm were used as flexible substrates. The paper substrate presents an organic coating around 15 µm that prevents the paper in terms of ink penetration. Microscope slide glass was employed as rigid substrate.

Three materials were tested to assemble the SMDs onto the inkjet-printed pads, Silverjet ink compound, the same used for pattern manufacturing, ICA (CircuitWorks Conductive Epoxy CW2400, Chemtronix), and the solder (Sn 97 % Cu 3 %, Qualitek)

after a previous flux (Omnifix) application on the pads. The resistivity values are summarized in *Table 3.1*. SMDs resistors of 0 Ω and model size 1206 (3.2 mm x 1.6 mm) (CR1206 resistors, Bourns®) were selected for the assembling characterization.

Table 3.1 Nominal electrical resistivity of the assembling materials used once cured

Product reference	**Assembling material**	**Resistivity (nΩ·m)**
ANP, Silverjet DGP	AgNP ink	≈16
Chemtronics,W2400	Conductive silver epoxy glue (ICA)	$>10^4$
Qualitek Sn97/Cu3	Solder alloy Sn97/Cu3	>115

3.2.2 Procedure

Prior to the printing process, standard cleaning of the surface substrates was carried out. The glass and polyimide (kapton®) substrates were cleaned with a sequence of ultrasonication baths: 5 minutes acetone, following 5 minutes in isopropyl alcohol and finally 2 minutes in deionized water. Once finished the susbstrates were dried at oven for 10 minutes at 100 °C. The paper substrates were cleaned through a thermal process keeping the samples in an oven at 160 °C / 45 min. The paper has a surface coating and at printing or sintering process this coating diffuses through conductive layer, thus the conductive strips show considerable electrical resistivity. When thermal treatment is performed before printing, the outcome strips shows considerable improved electrical resistivity.

A pattern of AgNP ink was printed and thermally cured in a convection oven at 150 °C for 30 minutes, in order to evaporate the organic ink solvents, sinter the silver nanoparticles and reach a resistivity around 16 μΩ·cm, which is among the best values found in the literature with thermal sintering.[31,32,33] The sintering process was checked by Thermogravimetric Analysis (TGA). First of all, an ink sample was analysed by TGA from 30 °C to 600 °C with 10 °C/min rate (*Figure 3.1*). From 230 °C, all surfactants and solvents were evaporated.

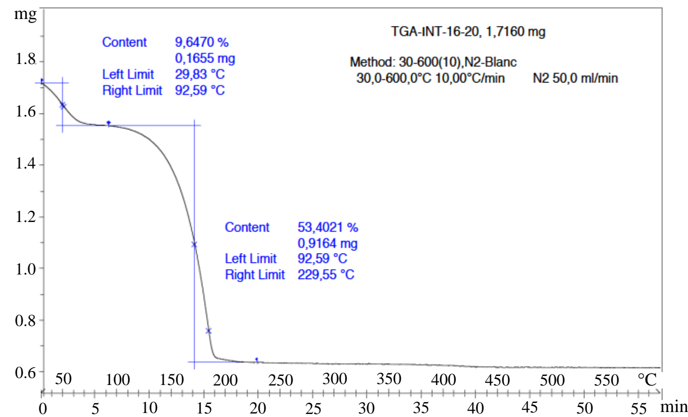

Figure 3.1 Termogravimetric analysis of Silverjet DGP HR ink. Analysis performed from 30 °C to 600 °C with 10 °C/min rate.

In *Figure 3.1*, the initial mass consists on a dispersion of solvents, additives and silver nanoparticles. Once temperature is increased, the solvents and additives are evaporated. Two different processes appear indicating two main solvents. Finally, the non-removed mass corresponds to the silver nanoparticles, which is roughly 36.95 % (w/w). This value matched with manufacturer technical data sheet.

Due to the incompatibility of the paper substrate with temperatures higher than 180 °C, a thermal treatment for silver ink sintering process of 10 °C/min rate from 30 °C to 150 °C, followed by 30 minutes at 150 °C was performed. As commented on chapter 2, the value of the electrical resistivity reached after this thermal treatment is $\rho = (1.6) \cdot 10^{-7} (\Omega\text{m})$, which is 10 times greater than the bulk resistivity. This thermal process was extended to all the substrates used at this work. Then, aiming to check the degree of solvents ink evaporation, another thermogravimetric analysis of the silver ink was performed where once 150 °C was reached the TGA was kept on this isotherm, (*Figure 3.2*).

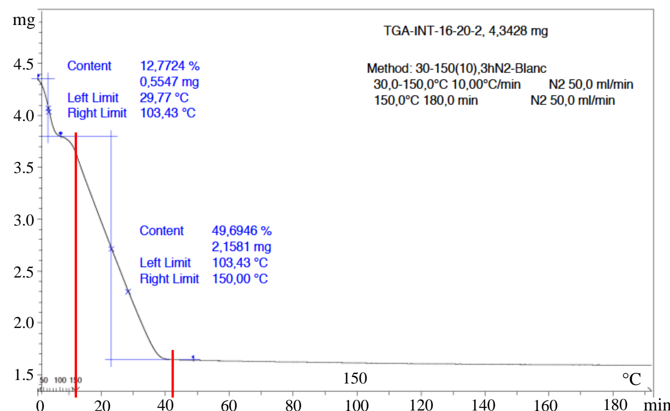

Figure 3.2 Termogravimetric analysis of Silverjet DGP HR ink. Analysis performed from 30 °C to 150 °C with 10 °C/min rate and kept the 150 °C isotherm until 180 minutes.

In the case of a curing process compatible with the paper substrate and taking into account that silver nanoparticles are the 36.95% (w/w) of the initial dispersion, all the remaining mass that exceeds after to specific time duration at 150 °C is solvents and additives not evaporated. From *Figure 3.2* the initial mass is $m_i = 4.3428$ mg, and the actual silver content can be computed as:

$$m_{silver} = m_i * 0.3695 = 1.6047 \text{ mg} \quad (3.1)$$

As shown on TGA, after 30 minutes at 150 °C the remaining mass is

$$m_{remainning} = m_i - x_1 - x_2 = 1.63 \text{ mg} \quad (3.2)$$

Where the first solvent evaporated is $x_1 = 0.5547$ mg and the second solvent evaporated is $x_2 = 2.1581$ mg. The difference between $m_{remaining}$ and m_{silver} is the non-evaporated material after the sintering process considered. Therefore, the remaining deposit after thermal sintering contains ≈ 98 % (w/w) of sintered silver nanoparticles, which is achieved by means a thermal curing process of 10 °C/min rate until 150 °C and 30 minutes at 150 °C. This curing process is compatible with the paper substrate used, and hence this sintering process is assumed as the silver ink (Silverjet DGP) sintering process for all the substrates used.

Following, a pattern based on tracks and pads with average thickness of ~250 nm was printed. Inkjet-printed pads of two strips 7 mm × 1.6 mm with 1 mm pitch were printed to carry out the electrical contact resistance study for each assembling test. Similarly, a pattern consisting of two 5 mm × 3 mm strips with 1 mm pitch was printed to estimate the strength stress tests. In both cases, the study was performed with 30 samples for each assembling method.

In order to join the SMD electrodes with the printed pads, by means of the AgNP ink, the SMDs were manually located onto the printed pads, and an adapted pattern was printed afterwards with the high resolution drop jetting printer. *Figure 3.3* shows all the hybrid manufacturing process conducted by means of inkjet, from conductive strips printing to SMD assembling.

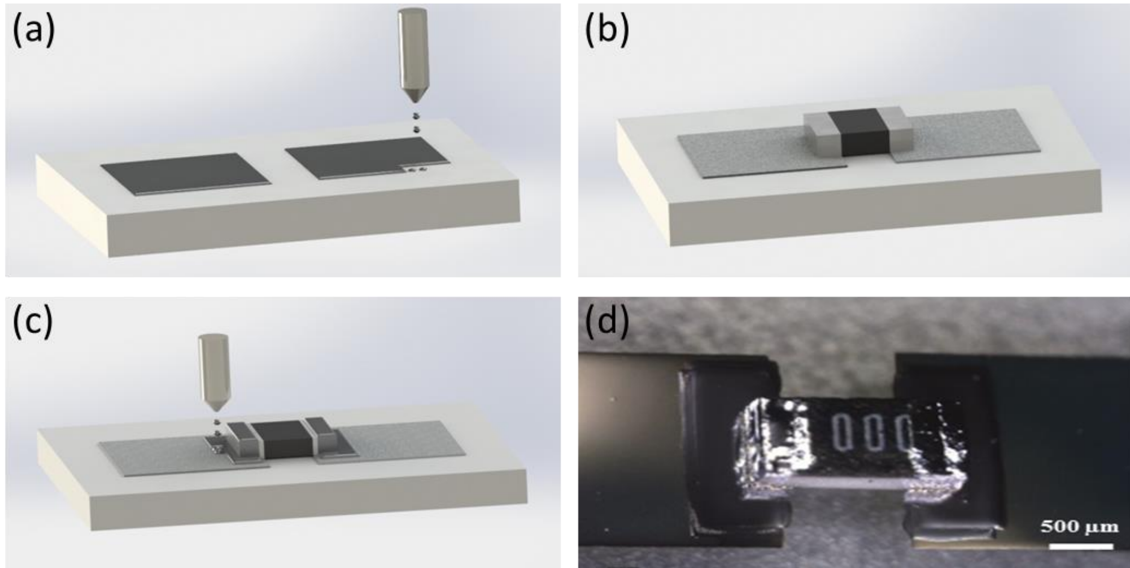

Figure 3.3 Hybrid manufacturing (a) Illustration of conductive strips printing process. (b) Illustration of conductive strips sintered and SMD located. (c) Illustration of SMD AgNP ink assembling method. (d) Picture of SMD 0402 package of 0 Ω AgNP ink-assembled.

In the case of ICA and solder, the processing steps were manually operated. Previous to soldering, adopting the iron at 200 °C, a proper plating of component pads was applied. Afterwards, SMDs were soldered onto AgNP ink-printed pads. The three different mounting techniques onto the three chosen substrates are shown in *Figure 3.4*.

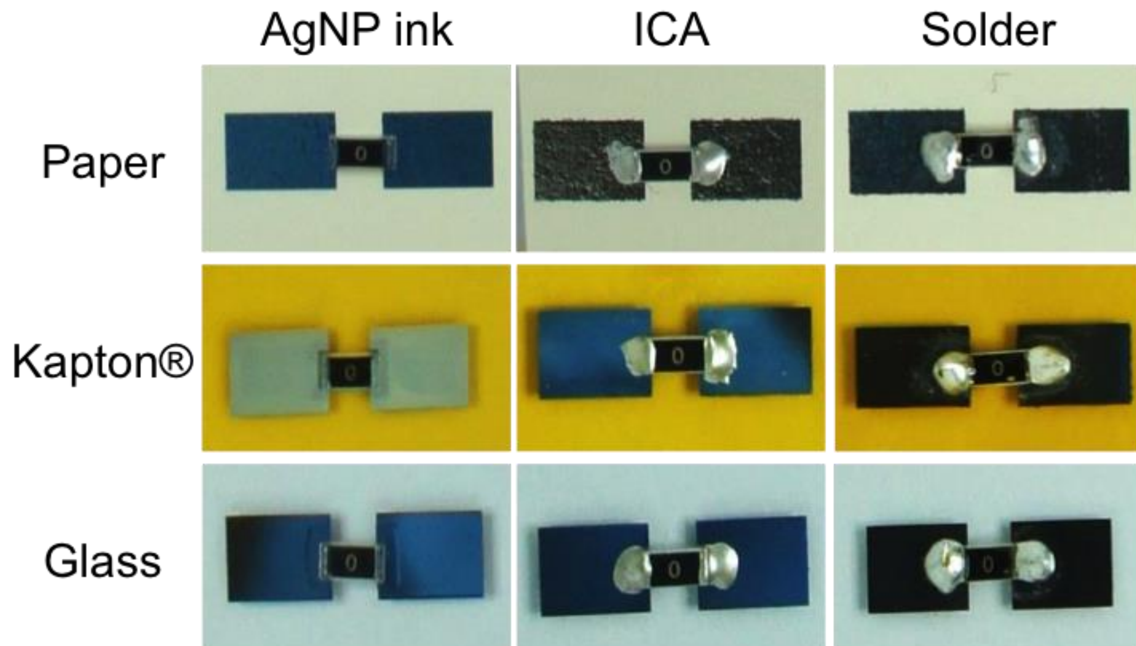

Figure 3.4 Assembling SMDs on the substrates paper, Kapton® and glass, trough three different connecting methods: AgNP ink, ICA and solder. SMDs devices are (3.2 mm x 1.6 mm).

3.2.3 Characterization

Resistance measurements were performed by means of a Keithley 2400 source meter with 4-probe method. In order to obtain an accurate value of the contact resistance, SMDs resistors of nominally 0 Ω were previously measured to subtract its contribution from the contacts-SMD system. Each value was divided by the two contact junctions. For each assembling method and substrate used, an average contact resistance was determined.

The shear strength analysis was conducted by means of a Zwich/Roell ZMART.PRO with a load cell with nominal force of 200 N. The evaluation test was done following the Japanese industrial standard for mechanical tensile test (JIS Z 3198-7).[34] The values of strength resistance, in MPa, were obtained from the breaking force and the joined surfaces in parallel to the applied force direction. The *Figure 3.5* presents the scheme of the mechanical test performed according Japanese industrial standard JIS Z 3198-7.

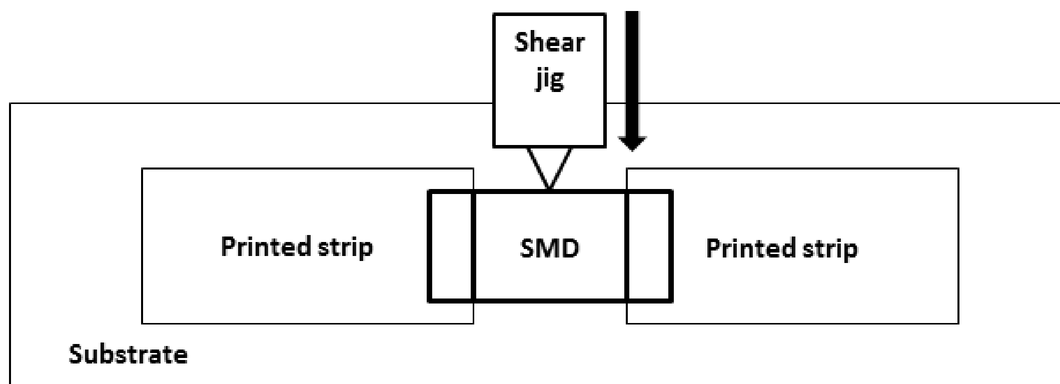

Figure 3.5 Scheme of the tensile probe conducted according Japanese industrial standard JIS Z 3198-7.

The morphology of the different junctions related to each assembling technique was inspected by Field Emission-Scanning Electron Microscopy (FEI Nova 200). In order to observe the interface of junctions, samples were embedded in resin and subsequently polished.

3.3 Results and discussion.

The assembling performances were compared in terms of electrical, mechanical and morphological properties in order to evaluate the reliability and feasibility of the different techniques by an in-depth junction characterization.

Roughness and porosity of paper surface plays an important role impeding the interaction of the picoliter drops ink with the printed pad substrate and the SMD electrode. The ink could be adsorbed and not fill totally the interface between inkjet-printed pad and the SMD electrode, which would induces a weak junction. In order to solve this issue, the paper substrate selected is provided with a $CaCO_3$ precoating. Ohlund *et al.* [35,36] demonstrated that AgNP ink sintering could be impaired by the coating pore size, but greatly enhanced by using a porous $CaCO_3$ precoating. They proved that small concentrations of Cl and Ca are present at the surface of the papers with $CaCO_3$ precoating, and due to the presence of Cl also into the AgNP ink, low temperature sintering with high conductivity values of printed pads can be facilitated by the presence of chloride.[35,36]

The precoatings surface roughness and pore size, around 16-39 nm from company datasheet, are small enough compared to the thickness of the printed junction (~ 1µm). Therefore, in order to ensure the SMDs assembling by AgNP ink, thick contacts were printed.

Regarding the smooth substrates as glass and kapton, high resolution drop size is ensured by small value of contact-angle (using flash volatile solvents that evaporate during drop in-flight) but consequently the system droplet would be more inclined to generate coffee rings [37] due to the non-uniform drying that lead to an excess of solute at the drop edges. The coffee ring effect was solved by the company exploiting the Marangoni flow circulation in a drying drop, where, adding a proper co-solvent (triethylene glycol monoethyl ether) with high boiling-point, a surface tension gradients is generated in order to reverse coffee-ring deposits.[38,39]

3.3.1 Electrical contact resistance

Electrical contact resistance measurements were performed aiming to demonstrate that similar performance to benchmark materials can be achieved by the novel assembling technique proposed. From the electrical contact resistance study and for each assembling method, all the deficiently attached components were considered as failures and rejected. Then, considering only the properly soldered components, a contact resistance average value was estimated as shown on the following example.

Example of contact resistance value estimation of SMDs assembled by means AgNP ink on glass substrate.

At first step, the components on short-circuit or open-circuit are considered as failures in a first qualitative assessment. Following, the electrical contact resistance average value is calculated discarding the components considered as failure, which is 0.55 Ω. At second step, the "Rcontact" of each component is divided by the average value previously calculated. When the "Rcontact" is higher than two times the "Average Rcontact", the component is also considered as failure. At the end, an electrical contact resistance average value is recalculated discarding the failed components, which is 0.37 Ω. The results are summarized in *Table 3.2*.

Table 3.2 Electrical contact resistances (Rcontact) of components assembled on glass by means AgNP ink. The samples on short-circuit or open-circuit are considered as failure (in red) in a first qualitative assessment. In a second qualitative assessment, when "Rcontact" is higher than two times the first "Average Rcontact", the component is also considered as failure (in yellow).

Sample	Rcontact (Ω)	1st Qualitative Assessment	Rcontact/Average Rcontact	2nd Qualitative Assessment
1	0.31	Correct	0.57	Correct
2	0.41	Correct	0.75	Correct
3	0.75	Correct	1.37	Correct
4	0.28	Correct	0.51	Correct
5	0.30	Correct	0.55	Correct
6	0.41	Correct	0.75	Correct
7	0.33	Correct	0.61	Correct
8	0.18	Correct	0.33	Correct
9	1.85	Correct	3.37	Failure
10	0.35	Correct	0.63	Correct
11	Open circuit	Failure	-	-
12	Short circuit	Failure	-	-
13	0.40	Correct	0.73	Correct
14	0.31	Correct	0.57	Correct
15	0.35	Correct	0.64	Correct
16	0.40	Correct	0.73	Correct
17	0.35	Correct	0.64	Correct
18	Short circuit	Failure	-	-
19	0.38	Correct	0.69	Correct
20	0.45	Correct	0.82	Correct
21	0.37	Correct	0.67	Correct
22	1.77	Correct	2.86	Failure
23	0.36	Correct	0.66	Correct
24	0.31	Correct	0.57	Correct
25	0.42	Correct	0.77	Correct
26	1.95	Correct	4.38	Failure
27	Open circuit	Failure	-	-

28	0.29	Correct	0.53	Correct
29	0.39	Correct	0.71	Correct
30	0.33	Correct	0.60	Correct

The outcome of the different assembling methods tested over different substrates are summarized on *Table 3.3* and *Figure 3.6.*

Table 3.3 Electrical contact resistance of assembled SMDs onto inkjet-printed pads depending on attaching material and substrate.

Mounting method	Substrate	Contact resistance (Ω)	Failure (%)
AgNP ink	Paper[a]	0.27 ± 0.09	17
	Kapton®	0.39 ± 0.15	17
	Glass	0.37 ± 0.10	23
ICA	Paper	0.56 ± 0.07	10
	Kapton®	0.39 ± 0.06	13
	Glass	0.39 ± 0.10	10
Solder	Paper	0.40 ± 0.11	3
	Kapton®	0.12 ± 0.05	40
	Glass	0.47 ± 0.09	13

a SMDs assembled by double AgNP ink layers than in the case of Kapton® and glass.

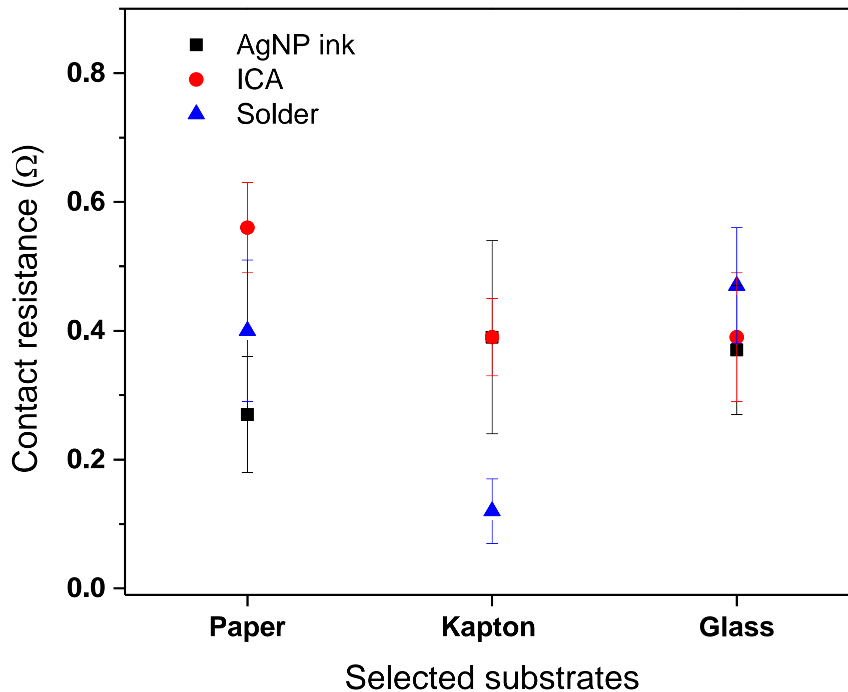

Figure 3.6 Electrical contact resistance of assembled SMDs onto inkjet-printed pads depending on attaching material and substrate.

Regarding the use of AgNP ink as connecting material, the best result for the electrical contact resistance was obtained with paper substrate with a value of 0.27 ± 0.09 Ω. This value was achieved by adding double silver ink layers than in the case of kapton® and glass. This is due to paper substrate has higher surface roughness than the other substrates used and is needed thicker connecting material to achieve similar performance. The measured high conductive contacts can be due to silver nanoparticles generate an interlayer with high conductive performance after new sintering process for successive printed layers forming well defined conductive paths.[40] The other interlayer is promoted by the well-studied interaction between Ag nanoparticles and SMD Sn-plated.[41]

In the case of ICA assembling material, the best results were achieved on Kapton® and glass substrates. The electrical contact resistance exhibited by ICA are equivalent and comparable to AgNP ink.

Concerning solder material, the best result was obtained on Kapton®, however the high number of failures showed lack of reliability. During the soldering process it was observed a degradation and displacement of the inkjet-printed pads due to the leaching effect.[22] Similar phenomena appeared slightly on glass and paper substrate. Solder achieved, on paper substrates, the best process reliability and a suitable value for electrical contact resistance.

In summary, all the three different tested assembling techniques showed an equivalent electrical resistance value, which allows stating the feasibility of the proposed AgNP ink as alternative straight forward and cost-efficient interconnecting material.

Andersson *et al.* determined the lowest electrical contact resistance of 0.4 ± 0.15 Ω using ICA material to connect SMDs on inkjet-printed pads onto paper substrate.[24] This value is equivalent and comparable to proposed AgNP ink on all the different selected substrates. In addition, due to the high resolution drop jetting control, the proposed novel attaching technique is also cost-effective, avoiding wasted material during the assembling process.

3.3.2 Shear strength

Shear strength measurements were performed with the aim to investigate the performance of the proposed assembling technique in comparison with benchmark materials.

A shear load is a force that tends to produce a sliding failure on a material along a plane that is parallel to the direction of the applied force. Therefore, given total force at failure (F) and the force-resisting area parallel to force direction ($A_{parallel}$), ultimate shear strength (τ) is:

$$\tau = \frac{F}{A_{parallel}} \qquad (3.3)$$

Two different force-resisting areas can be considered taking into account the SMD size and the material deposited. The first one consists on the bottom area of the SMD electrodes and the second one consists on the lateral and upper areas of the SMD electrodes plus the substrate area covered by the connecting material. SMD sizes are shown on *Figure 3.7* and the nominal force-resisting areas considered are summarized in *Table 3.4.*

Dimension	Model CR1206
L	3.20±0.25 (0.126±0.010)
W	1.60±0.15 (0.063±0.006)
H	0.60±0.15 (0.024±0.006)
I1	0.50±0.25 (0.020±0.010)
I2	0.50±0.20 (0.020±0.010)

DIMENSIONS: MM / (INCHES)

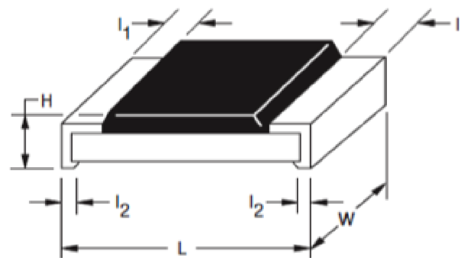

Figure 3.7 Size dimensions of SMD model 1206.

Table 3.4 Theoretical force-resisting areas.

Area	Theoretical force-resisting area (mm^2)
A. Under electrode	2·I1·W = 1.60
B. Lateral and upper electrode plus substrate covered	2·W·(I1+H) + 2.40*= 5.92

* Average value of the substrate area covered by the connecting material extracted from 30 samples.

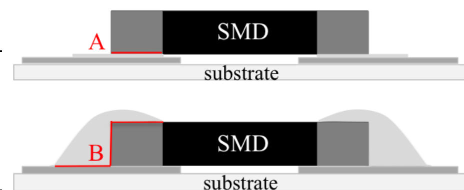

The shear strength value for each mounting method was estimated by applying a similar procedure as done for the electrical measurements. At shear strength study and for each assembling method, all the deficiently attached components are considered as failures and rejected. Then, considering the components properly attached, a shear strength average value is estimated as shown on the following example.

Example of the shear strength value estimation of SMDs assembled by means AgNP ink on paper substrate.

The components removed with extremely low shear force are considered as failures. Concerning the AgNP ink assembling method, the shear strength is calculated considering the contacting area from the first scenario of *Table 3.4*. Following, the shear strength average value is calculated taking into account only the properly attached components, which is 1.45 MPa. Then, the shear strength value of each component is divided by the average value previously calculated. When the shear strength is higher or lower than two times the "average shear strength", the component is also considered as failures. At the end, the shear strength average value is recalculated discarding failure components, which is 1.27 MPa. The results are summarized in the *Table 3.5*.

Table 3.5 Shear strength values measured from 30 samples assembled on paper substrate by means AgNP ink. The samples with extremely low shear force are considered as failure (in red) in a first qualitative assessment. In a second qualitative assessment, when shear strength is higher or lower than two times the first "average shear strength", the component is also considered as failure (in yellow).

Sample	Shear strength (MPa)	1st Qualitative Assessment	Shear strength/ Average shear strength	2nd Qualitative Assessment
1	0.79	Correct	0,54	Correct
2	2.35	Correct	1,62	Correct
3	1.26	Correct	0,87	Correct
4	0.03	Failure	-	-
5	1.11	Correct	0,77	Correct
6	1.28	Correct	0,88	Correct
7	1.03	Correct	0,71	Correct
8	1.94	Correct	1,33	Correct
9	1.36	Correct	0,94	Correct
10	1.08	Correct	0,74	Correct
11	1.46	Correct	1,01	Correct
12	0.81	Correct	0,56	Correct
13	1.29	Correct	0,89	Correct
14	1.00	Correct	0,69	Correct

15	4.43	Correct	3,05	Failure
16	0.23	Correct	0,16	Failure
17	0.89	Correct	0,62	Correct
18	1.03	Correct	0,71	Correct
19	1.45	Correct	1,00	Correct
20	0.86	Correct	0,59	Correct
21	1.18	Correct	0,81	Correct
22	4.39	Correct	3,02	Failure
23	0.93	Correct	0,64	Correct
24	1.53	Correct	1,05	Correct
25	1.23	Correct	0,85	Correct
26	1.03	Correct	0,71	Correct
27	0.94	Correct	0,65	Correct
28	2.68	Correct	1,85	Correct
29	1.24	Correct	0,86	Correct
30	1.32	Correct	0,91	Correct

The calculated shear strength values for the assembled SMD using AgNP ink, ICA and solder, as well failures are summarized in *Table 3.6* and *Figure 3.8*. The force-resisting area considered for AgNP ink connecting material is the bottom side electrode. It is important to realize that the area considered is overestimated, because the AgNP ink not wets always the full bottom side electrode. The force-resisting area considered for ICA and solder material is the sum of the upper and lateral side electrode plus the substrate area covered by the connecting material.

Table 3.6 Shear strength resistance of the SMD assembled onto inkjet-printed pads depending on the attaching material and substrate.

Mounting method	Substrate	Shear strength (MPa)	Failure (%)
AgNP ink	Paper	1.27 ± 0.47	7
	Kapton®	1.77 ± 0.92	10
	Glass	0.73 ± 0.24	13
ICA	Paper	3.01 ± 0.62	3
	Kapton®	1.87 ± 0.37	3
	Glass	3.52 ± 0.90	3
Solder	Paper	2.30 ± 0.61	3
	Kapton®	1.03 ± 0.50	20
	Glass	0.55 ± 0.44	50

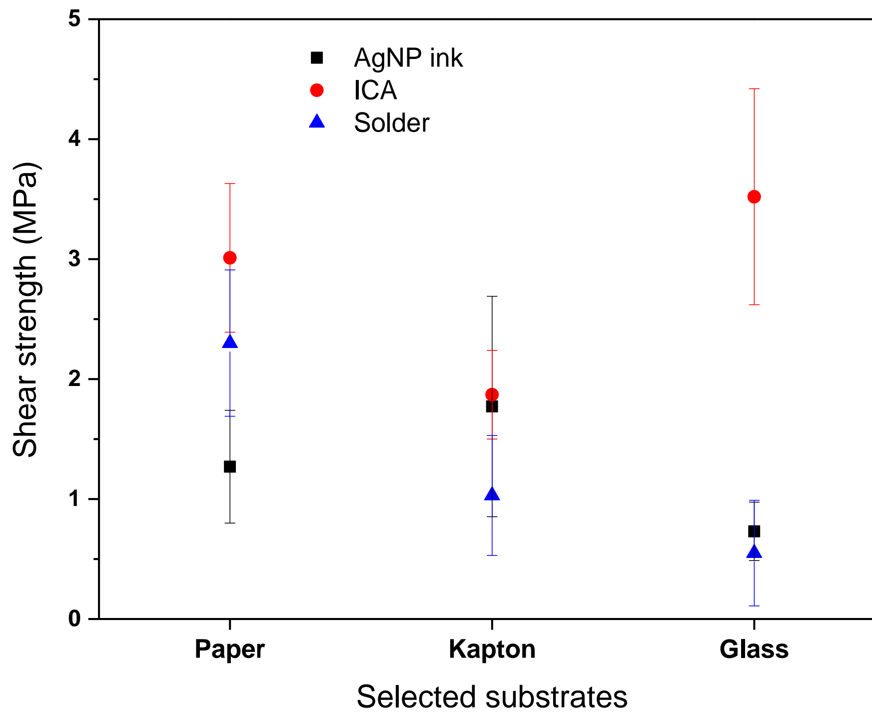

Figure 3.8 Shear strength resistance of the SMD assembled onto inkjet-printed pads depending on the attaching material and substrate.

With regards to AgNP ink connecting material, polyimide Kapton® substrate showed the maximum shear strength value, followed by paper and glass substrates. The images in *Figure 3.9* show evidences that the shear strength value is the result of two contributions: the interaction of the assembling material with SMD electrode and the adhesion strength of the printed pads onto the selected substrate. Indeed, the latter contribution is directly correlated with the roughness and porosity of the substrate.

In the case of ICA assembling material, the strongest adhesion was obtained on glass substrate, and a comparable value was observed on the paper substrate.

The lowest shear strength, achieved with ICA, was obtained with Kapton® substrate. The mechanical tests show greater ICA material remains on glass than on Kapton®, demonstrating a better fixation between ICA and printed pad on glass, and justifying the higher shear strength reached (*Figure 3.10 (b)* and *Figure 3.10 (d)*). The adhesion results could be explained by the different ICA wettability onto each printed substrate. In the case of solder connecting material, a general tendency to weaker shear strength as substrate roughness decreases was observed. The strongest solder adhesion value was obtained on paper substrate due to its considerable porosity and roughness that ensure a larger surface-area than in the other substrates.

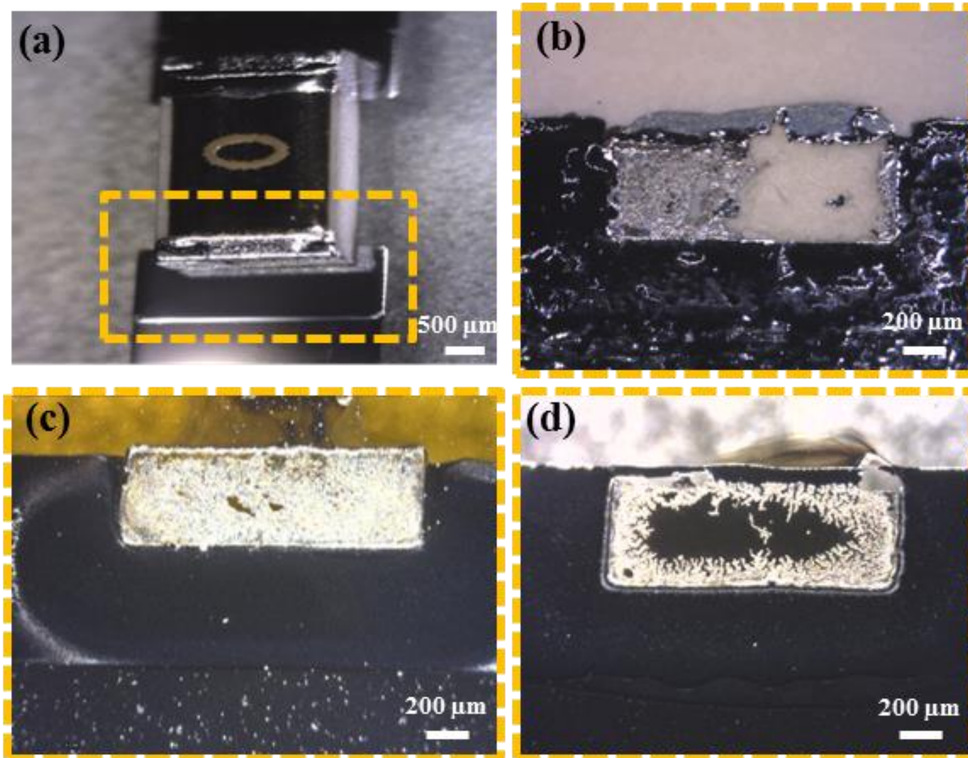

Figure 3.9 (a) Image of SMD AgNP ink-connected on glass substrate. (b), (c), and (d) images corresponding to substrate pad after removing SMD, AgNP ink-attached, from paper, Kapton® and glass, respectively. All the cases show partially-removed inkjet-printed pad.

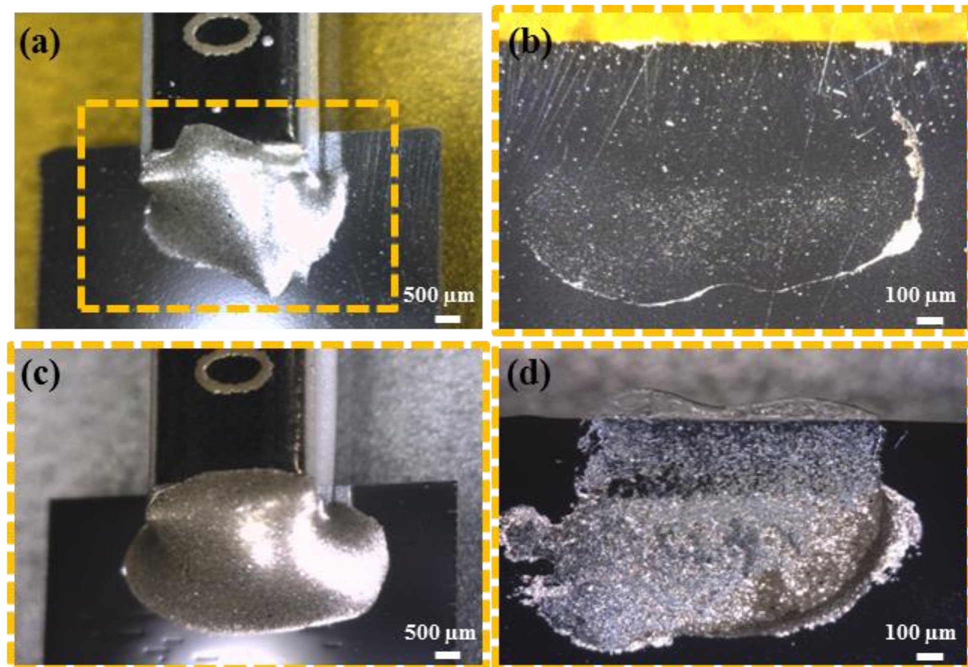

Figure 3.10 (a,c) Images of the epoxy assembling before the shear strength test onto Kapton® and glass, respectively. (b,d) Optical images of the epoxy assembling after the shear strength test onto Kapton® and glass, respectively.

The mechanical test results show that AgNP ink, exploiting the capillarity action in order to assemble the SMDs (*Figure 3.11 (b)*), is performing weaker adhesion than ICA on paper and glass substrate, but comparable adhesion on Kapton® substrate. However, comparable adhesion to solder material is performed on all substrate used. The image *Figure 3.11 (b)* shows how an isolated underlying contact point between the SMD electrode and the inkjet-printed pad is produced by inkjet-printed AgNP ink. Although mechanical performance must be improved, the electrical and mechanical study highlighted the AgNP ink as a promising alternative assembling material for SMDs.

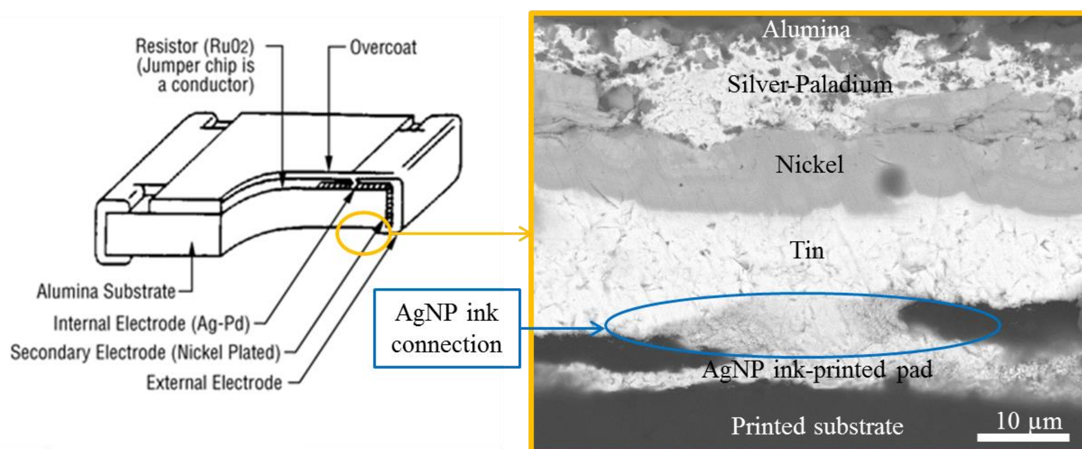

Figure 3.11 (a) Schematic of the SMDs. (b) FE-SEM cross-section image of an isolated underlying contact area by AgNP ink between SMD tin-plated extremities and inkjet-printed solder pad. Furthermore, presented description of the different layers, proved by EDX analysis

3.3.3 Morphology characterization

Microscopic analyses of device cross-sections were performed by FE-SEM technique. The cross-section image of tin-plated SMD electrodes displays the junction area between surface component and inkjet-printed pad. Employing AgNP ink, the capillarity action moves the printed ink up to the underlying tin-plated SMD electrode. *Figure 3.12 (b,c and d)* highlights the excellent junction between printed connection and printed pad, which is proved by the indistinguishable bottom contact thickness contrast. The ink distributes almost uniformly down the edges of the SMD electrodes contributing to the high quality validated electrical contact properties. In a different way, devices connected by ICA are not assisted by capillarity. ICA, manually applied, embeds the whole SMD electrode area. However, the contact resistance measured is worse than with the AgNP ink. This is due to the existent adhesive filler mixed (≈50:50) with the silver flakes, as shown in *Figure 3.13* by the dark zones between the bright silver particles.

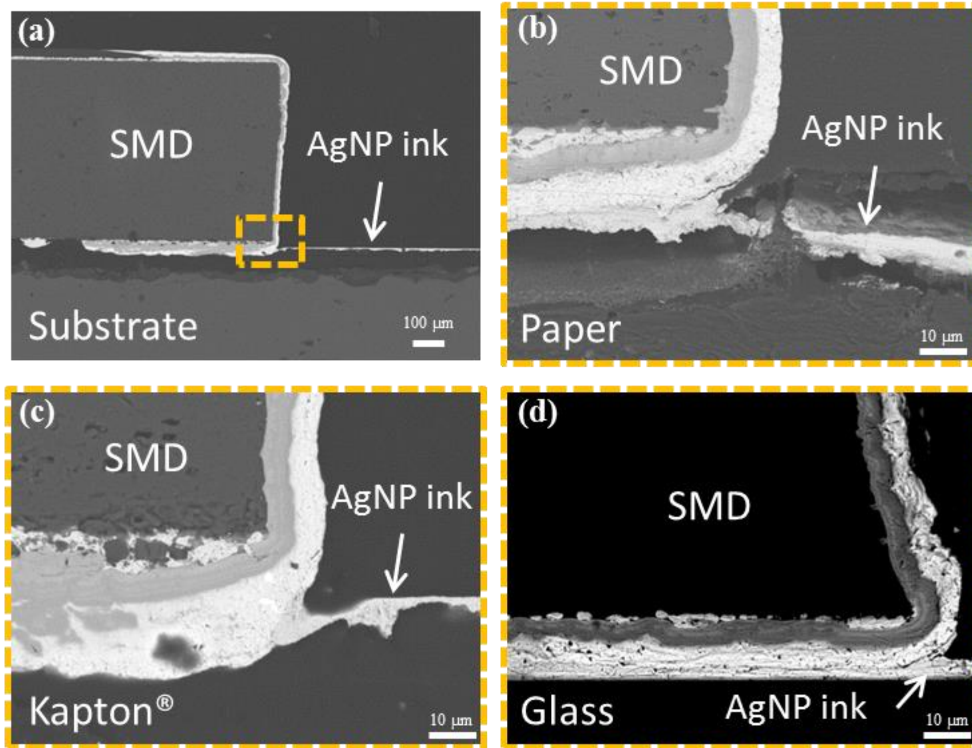

Figure 3.12 (a) FESEM image of a cross-sectional view of one SMD electrode AgNP ink-assembled on printed pad. (b), (c), and (d) FE-SEM images correspond to the details of the junction zone of SMD Sn-plated pad, AgNP ink connector inkjet-printed and AgNP ink inkjet-printed pad on paper, Kapton® and glass substrates, respectively.

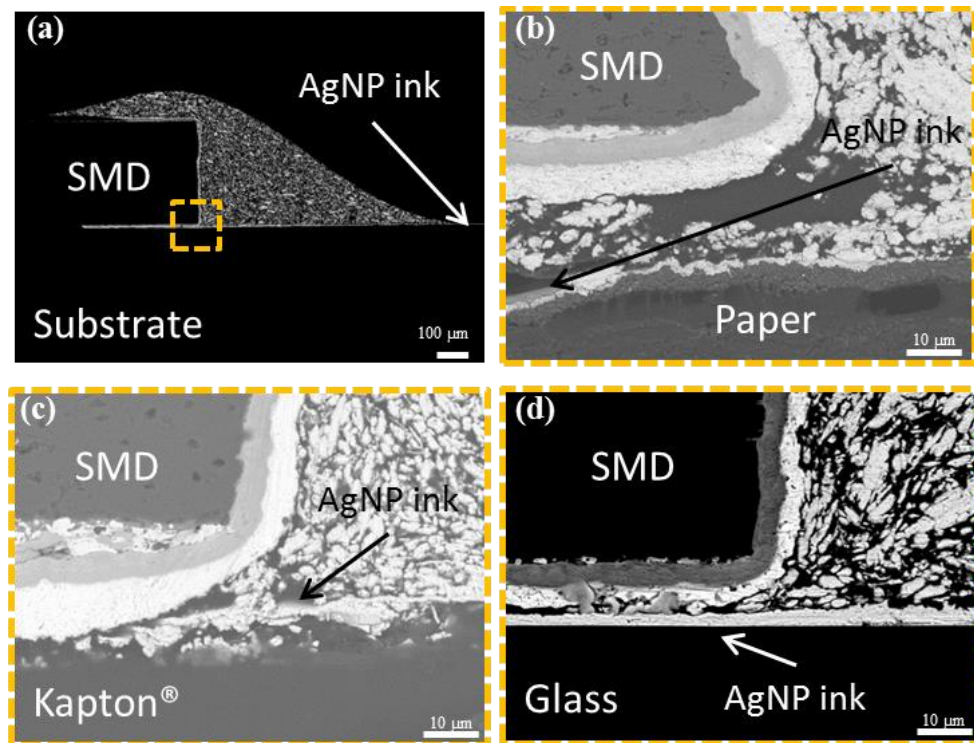

Figure 3.13 (a) FE-SEM image of a cross-sectional view of an SMD electrode ICA-assembled on inkjet-printed pad. (b), (c), and (d) FE-SEM images correspond to the details of the junction zone of SMD Sn-plated pad, ICA connector and AgNP inkjet-printed pad on paper, Kapton® and glass substrates, respectively.

The solder was manually deposited in order to assemble the SMD. The *Figure 3.14* point out a continuous junction interface between the soldering material and the inkjet-printed pad onto the different selected substrates. As observed in the case of ICA, and due to lower conductivity than AgNP ink, an outwardly covered SMD electrode does not ensure a better contact resistance.

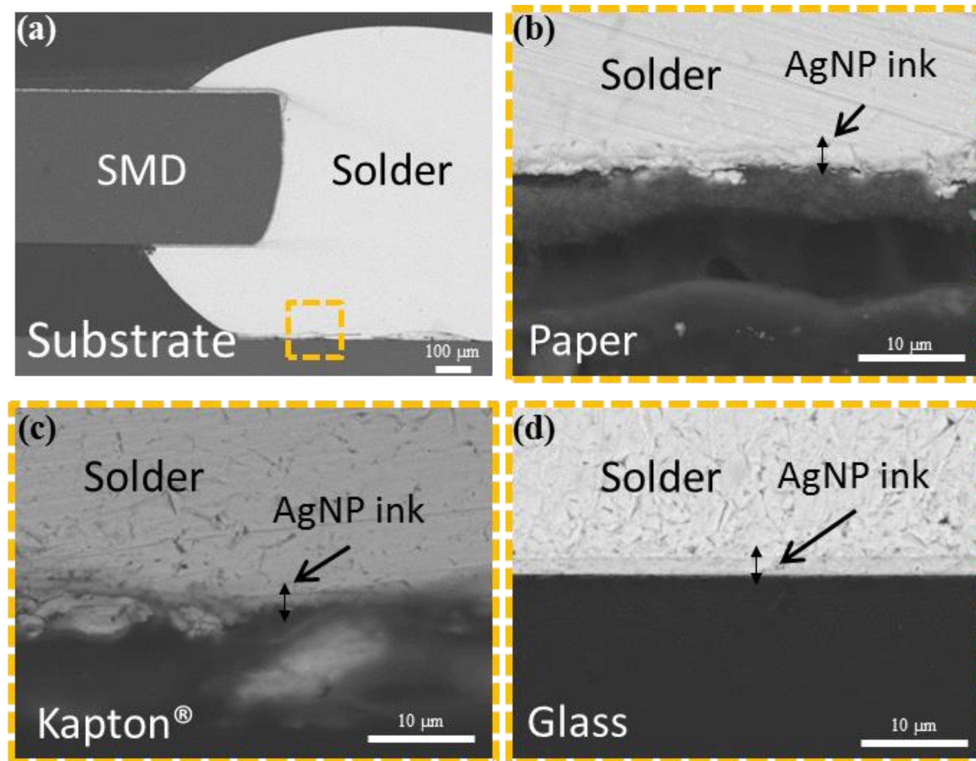

Figure 3.14 (a) FESEM image of a cross-sectional view of one SMD electrode Sn-assembled. (b), (c), and (d) FE-SEM images correspond to the details of the junction zone of solder connector and AgNP inkjet-printed pad on paper, Kapton® and glass substrates, respectively.

Overall, FE-SEM images demonstrate that the assembling SMD technique by AgNP ink is uniformly adapting and enveloping the Sn-plated SMD electrodes, without wasting unnecessary material surrounding the contact area as in the case of ICA and solder methods. The micro-structural characterization has shown that the morphology of the inkjet-printed silver connections evidences a solid and stable structure without detrimental fractures or pin-holes.

3.4 Application: a multi-sensor circuit on paper

As practical demonstration, a fully inkjet-printed hybrid electronic circuit has been successfully manufactured onto paper substrate in order to show the feasibility of the new proposed method (*Figure 3.15*).[3] The hybrid circuit tracks and pads were inkjet-printed on paper substrate and sintered, as can be observed in *Figure 3.15 (a)*. Following, the SMDs were manually located onto the printed pads, and a well-adapted pattern was printed afterwards to connecting them by inkjet (*Figure 3.15 (b)*).

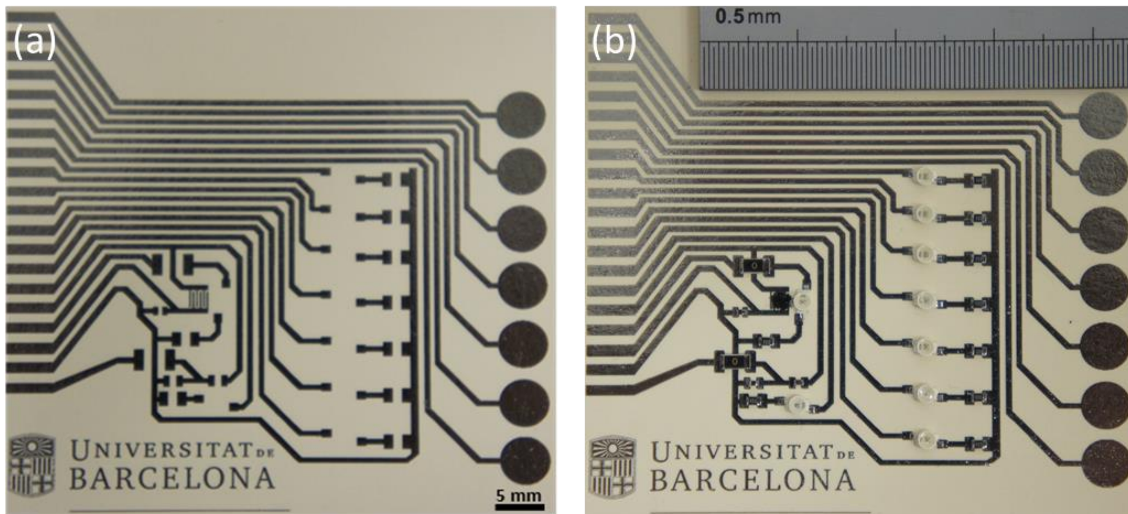

Figure 3.15 (a) Circuit pattern printed with AgNP ink on paper substrate. (b) Circuit (a) with SMDs AgNP ink-connected.

The fully inkjet-printed hybrid electronics circuit was controlled by an Arduino One board, which was programmed to monitor three different functional modes: capacitive touch control, temperature sensor and humidity sensor. Each mode had a specific LED that indicates if the mode is running. Concerning the humidity sensor, carbon nanofibers (dispersed on isopropanol 70% w/w) were deposited by drop coating onto an interdigitated electrodes as active layer for the humidity gas sensor, taking advantage of previous works of our group.[42,43,44] A SMD NTC thermistor, case size 0402 (1 mm x 0.5 mm) was used as temperature sensor. SMDs resistors, case size 0603 (1.55 mm x 0.85 mm) and 0402, of different resistance values, properly estimated for the circuit requirements, were selected. Finally, SMD LEDs bar (LW P473 from OSRAM) were employed to obtain light-response information from the signal sensors changes. A zoom image on the assembled components and the circuit on running state is shown (*Figure*

3.16). In addition, a video of the hybrid printed circuit on running state can be seen at the supplementary information of the published paper.[3]

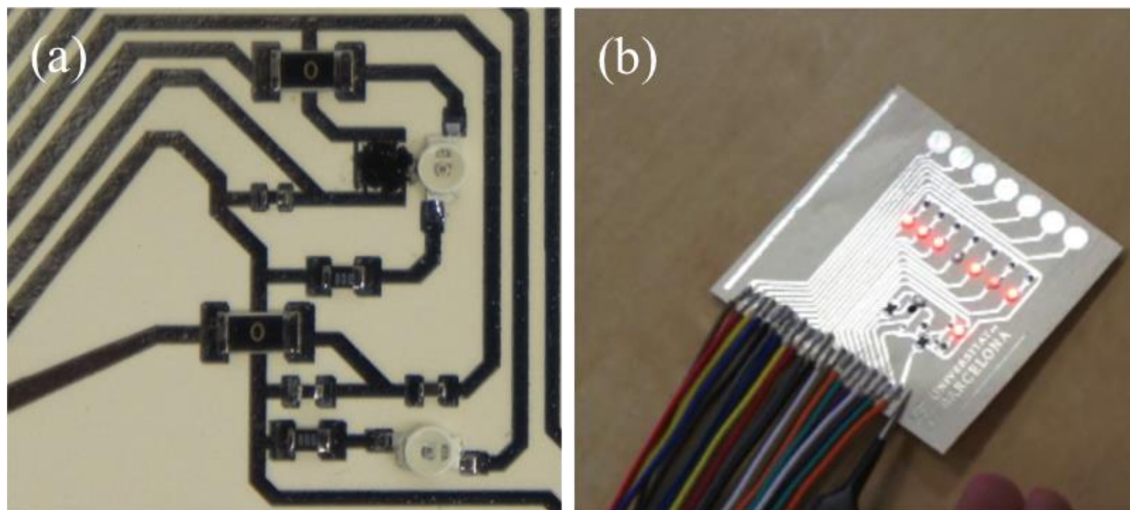

Figure 3.16 (a) Zoom image on the assembled components by means AgNP ink. (b) Hybrid circuit in temperature mode running.

3.5 Conclusions

Taking advantage of surface energies existing at the nanoscale, AgNP ink ensures high electrical conductivity and a high electrical conducting interconnection after thermal process at very low temperatures (150 °C).

Electrical contact resistance and shear strength measurements performed by AgNP ink are comparable to benchmark connecting materials. In conclusion, drop-on-demand inkjet printing technology is a valid technique to incorporate on SMT.

In other words, the proposed high resolution drop jetting technique sheds light on how, employing few picoliter drops, AgNP ink reveals comparable electrical performance to benchmark assembling materials onto several inkjet-printed substrates.

In summary, all the SMDs assembled by AgNP ink, ICA and solder have similar electrical resistance value around 0.3 Ω in all the substrates proposed, paper, Kapton® and glass. The low electrical contact resistance achieved by the low quantity of deposited material at AgNP ink assembling method allows stating the feasibility of the proposed AgNP ink as alternative straight forward and cost-efficient interconnecting method.

The AgNP ink, exploiting the capillarity action in order to assemble the SMDs, has weaker adhesion than ICA in paper and glass substrate, and similar adhesion in Kapton® substrate. However, AgNP ink and solder material have analogous adhesion in all substrate used.

The assembling SMD technique by AgNP ink is uniformly adapting and enveloping the Sn-plated SMD electrodes, without wasting unnecessary material surrounding the contact area as in the case of ICA and solder methods. The micro-structural characterization of the inkjet-printed silver connections evidences a solid and stable structure without detrimental fractures or pin-holes.

In sum up, flexible hybrid circuit is successfully manufactured by AgNP ink on paper, where different SMDs size-shaped are assembled demonstrating the reliability and feasibility of the proposed method.

3.6 References

(1) Vanfleteren, J.; Gonzalez, M.; Bossuyt, F.; Hsu, Y. Y.; Vervust, T.; De Wolf, I.; Jablonski, M. Printed Circuit Board Technology Inspired Stretchable Circuits. *MRS Bull.* **2012**, *37* (3), 254–260.

(2) Eshkeiti, A.; Reddy, A. S. G.; Emamian, S.; Narakathu, B. B.; Joyce, M.; Joyce, M.; Fleming, P. D.; Bazuin, B. J.; Atashbar, M. Z. Screen Printing of Multilayered Hybrid Printed Circuit Boards on Different Substrates. *IEEE Trans. Components, Packag. Manuf. Technol.* **2015**, *5* (3), 415–421.

(3) Arrese, J.; Vescio, G.; Xuriguera, E.; Medina-Rodriguez, B.; Cornet, A.; Cirera, A. Flexible Hybrid Circuit Fully Inkjet-Printed: Surface Mount Devices Assembled by Silver Nanoparticles-Based Inkjet Ink. *J. Appl. Phys.* **2017**, *121* (10).

(4) Fernández-Pradas, J. M.; Sopeña, P.; González-Torres, S.; Arrese, J.; Cirera, A.; Serra, P. Laser-Induced Forward Transfer for Printed Electronics Applications. *Appl. Phys. A* **2018**, *124* (2), 214.

(5) Sopeña, P.; Arrese, J.; González-Torres, S.; Fernández-Pradas, J. M.; Cirera, A.; Serra, P. Low-Cost Fabrication of Printed Electronics Devices through Continuous Wave Laser-Induced Forward Transfer. *ACS Appl. Mater. Interfaces* **2017**, *9* (35), 29412–29417.

(6) Barbucha, R.; Kocik, M.; Mizeraczyk, J.; Kozioł, G.; Borecki, J. Laser Direct Imaging of Tracks on PCB Covered with Laser Photoresist. *Bull. Polish Acad. Sci. - Tech. Sci.* **2008**, *56* (1), 17–20.

(7) Khandpur, R. S. *Printed Circuit Boards : Design, Fabrication, Assembly and Testing*; McGraw-Hill, 2006.

(8) Jianping, L.; Guiling, D. Technology Development and Basic Theory Study of Fluid Dispensing - a Review. *High Density Microsyst. Des. Packag. Compon. Fail. Anal. 2004. HDP '04. Proceeding Sixth IEEE CPMT Conf.* **2004**, 198–205.

(9) Ko, S. H.; Pan, H.; Grigoropoulos, C. P.; Luscombe, C. K.; Fréchet, J. M. J.; Poulikakos, D. All-Inkjet-Printed Flexible Electronics Fabrication on a Polymer Substrate by Low-Temperature High-Resolution Selective Laser Sintering of Metal Nanoparticles. *Nanotechnology* **2007**, *18* (34).

(10) Huang, L.; Huang, Y.; Liang, J.; Wan, X.; Chen, Y. Graphene-Based Conducting Inks for Direct Inkjet Printing of Flexible Conductive Patterns and Their Applications in Electric Circuits and Chemical Sensors. *Nano Res.* **2011**, *4* (7), 675–684.

(11) Torrisi, F.; Hasan, T.; Wu, W.; Sun, Z.; Lombardo, A.; Kulmala, T. S.; Hsieh, G.-W.; Jung, S.; Bonaccorso, F.; Paul, P. J.; et al. Inkjet-Printed Graphene Electronics. *ACS Nano* **2012**, *6* (4), 2992–3006.

(12) Vescio, G.; López-Vidrier, J.; Leghrib, R.; Cornet, A.; Cirera, A. Flexible Inkjet Printed High-k HfO 2 -Based MIM Capacitors. *J. Mater. Chem. C* **2016**, *4* (9), 1804–1812.

(13) Chang, S.-C.; Liu, J.; Bharathan, J.; Yang, Y.; Onohara, J.; Kido, J. Multicolor Organic Light-Emitting Diodes Processed by Hybrid Inkjet Printing. *Adv. Mater.* **1999**, *11* (9), 734–737.

(14) Krebs, F. C. Fabrication and Processing of Polymer Solar Cells: A Review of Printing and Coating Techniques. *Sol. Energy Mater. Sol. Cells* **2009**, *93* (4), 394–412.

(15) Correia, V.; Mitra, K. Y.; Castro, H.; Rocha, J. G.; Sowade, E.; Baumann, R. R.; Lanceros-Mendez, S. Design and Fabrication of Multilayer Inkjet-Printed Passive Components for Printed Electronics Circuit Development. *J. Manuf. Process.* **2018**, *31*, 364–371.

(16) Tseng, H. Y.; Subramanian, V. All Inkjet-Printed, Fully Self-Aligned Transistors for Low-Cost Circuit Applications. *Org. Electron. physics, Mater. Appl.* **2011**, *12* (2), 249–256.

(17) Li, J.; Zhao, Y.; Tan, H. S.; Guo, Y.; Di, C. A.; Yu, G.; Liu, Y.; Lin, M.; Lim, S. H.; Zhou, Y.; et al. A Stable Solution-Processed Polymer Semiconductor with Record High-Mobility for Printed Transistors. *Sci. Rep.* **2012**, *2*, 1–9.

(18) Chung, S.; Kim, S. O.; Kwon, S. K.; Lee, C.; Hong, Y. All-Inkjet-Printed Organic Thin-Film Transistor Inverter on Flexible Plastic Substrate. *IEEE Electron Device Lett.* **2011**, *32* (8), 1134–1136.

(19) Faber, H.; Burkhardt, M.; Jedaa, A.; Kälblein, D.; Klauk, H.; Halik, M. Low-Temperature Solution-Processed Memory Transistors Based on Zinc Oxide Nanoparticles. *Adv. Mater.* **2009**, *21* (30), 3099–3104.

(20) Putaala, J.; Hannu, J.; Kunnari, E.; Mäntysalo, M.; Nousiainen, O.; Jantunen, H. Reliability of SMD Interconnections on Flexible Low-Temperature Substrates with Inkjet-Printed Conductors. *Microelectron. Reliab.* **2014**, *54* (1), 272–280.

(21) Pekkanen, V.; Mäntysalo, M.; Kaija, K.; Mansikkamäki, P.; Kunnari, E.; Laine, K.; Niittynen, J.; Koskinen, S.; Halonen, E.; Caglar, U. Utilizing Inkjet Printing to Fabricate Electrical Interconnections in a System-in-Package. *Microelectron. Eng.* **2010**, *87* (11), 2382–2390.

(22) Niittynen, J.; Kiilunen, J.; Putaala, J.; Pekkanen, V.; Mäntysalo, M.; Jantunen, H.; Lupo, D. Reliability of ICA Attachment of SMDs on Inkjet-Printed Substrates. *Microelectron. Reliab.* **2012**, *52* (11), 2709–2715.

(23) Andersson, H.; Sidén, J.; Skerved, V.; Li, X.; Gyllner, L. Soldering Surface Mount Components Onto Inkjet Industrial Processes. *IEEE Trans. Components Packag. Technol.* **2016**, *6* (3), 478–485.

(24) Andersson, H. a; Manuilskiy, A.; Haller, S.; Hummelgård, M.; Sidén, J.; Hummelgård, C.; Olin, H.; Nilsson, H.-E. Assembling Surface Mounted Components on Ink-Jet Printed Double Sided Paper Circuit Board. *Nanotechnology* **2014**, *25* (9), 094002.

(25) Li, X.; Andersson, H.; Sidén, J.; Schön, T. Soldering Surface Mount Components on Screen-Printed Ag Patterns on Paper and Polyimide Substrates for Hybrid Printed Electronics. *Flex. Print. Electron.* **2018**, *3* (1), 015003.

(26) Xu, S.; Pickel, A. D.; Prasitthipayong, A.; Habib, A. H.; McHenry, M. E. Modeling of Localized Reflow in Solder/Magnetic Nanocomposites for Area-Array Packaging. *J. Appl. Phys.* **2013**, *113* (17), 2011–2014.

(27) Rivera J; Peitivi A; Llorente S; Arrese X; Servera L; Cirera A. Dispositivo de Aparato Doméstico y Procedimiento Para La Fabricación de Un Dispositivo de Aparato Doméstico. *ES 2 564 760 A1* **2014**.

(28) Yan, S.; Sun, D.; Gong, Y.; Tan, Y.; Xing, X.; Mo, G.; Chen, Z.; Cai, Q.; Li, Z.; Yu, H.; et al. Temperature-Driven Directional Coalescence of Silver Nanoparticles. *J. Synchrotron Radiat.* **2016**, *23* (3), 718–728.

(29) Moon, K.-S.; Dong, H.; Maric, R.; Pothukuchi, S.; Hunt, A.; Li, Y.; Wong, C. P. Thermal Behavior of Silver Nanoparticles for Low-Temperature Interconnect Applications. *J. Electron. Mater.* **2005**, *34* (2), 168–175.

(30) Allen, M. L.; Aronniemi, M.; Mattila, T.; Alastalo, A.; Ojanperä, K.; Suhonen, M.; Seppä, H. Electrical Sintering of Nanoparticle Structures. *Nanotechnology* **2008**, *19* (17), 175201.

(31) Lee, H.-H.; Chou, K.-S.; Huang, K.-C. Inkjet Printing of Nanosized Silver Colloids. *Nanotechnology* **2005**, *16* (10), 2436–2441.

(32) Perelaer, J.; De Gans, B. J.; Schubert, U. S. Ink-Jet Printing and Microwave Sintering of Conductive Silver Tracks. *Adv. Mater.* **2006**, *18* (16), 2101–2104.

(33) Perelaer, B. J.; de Laat, A. W. M.; Hendriks, C. E.; Schubert, U. S. Inkjet-Printed Silver Tracks: Low Temperature Curing and Thermal Stability Investigation. *J. Mater. Chem.* **2008**, *18* (27), 3209.

(34) Japanese Standards Association. *Japanese Industrial Standard*.

(35) Öhlund, T.; Schuppert, A.; Andres, B.; Andersson, H.; Forsberg, S.; Schmidt, W.; Nilsson, H.-E.; Andersson, M.; Zhang, R.; Olin, H. Assisted Sintering of Silver Nanoparticle Inkjet Ink on Paper with Active Coatings. *RSC Adv.* **2015**, *5* (80), 64841–64849.

(36) Öhlund, T.; Örtegren, J.; Forsberg, S.; Nilsson, H. E. Paper Surfaces for Metal Nanoparticle Inkjet Printing. *Appl. Surf. Sci.* **2012**, *259*, 731–739.

(37) Deegan, R. D.; Bakajin, O.; Dupont, T. F.; Huber, G.; Nagel, S. R.; Witten, T. A. Capillary Flow as the Cause of Ring Stains from Dried Liquid Drops. *Nature* **1997**, *389* (6653), 827–829.

(38) Hu, H.; Larson, R. G. Analysis of the Effects of Marangoni Stresses on the Microflow in an Evaporating Sessile Droplet. *Langmuir* **2005**, *21* (9), 3972–3980.

(39) Hu, H.; Larson, R. G. Marangoni Effect Reverses Coffee-Ring Depositions. *J. Phys. Chem. B* **2006**, *110* (14), 7090–7094.

(40) Nash, C.; Spiesschaert, Y.; Amarandei, G.; Stoeva, Z.; Tomov, R. I.; Tonchev, D. A. N. A Comparative Study on the Conductive Properties of Coated and Printed Silver Layers on a Paper Substrate. **2015**, *44* (1).

(41) Dyson, B. F. Diffusion of Gold and Silver in Tin Single Crystals. *J. Appl. Phys.* **1966**, *37* (6), 2375–2377.

(42) Monereo, O.; Illera, S.; Varea, A.; Schmidt, M.; Sauerwald, T.; Schütze, A.; Cirera, A.; Prades, J. D. Localized Self-Heating in Large Arrays of 1D Nanostructures. *Nanoscale* **2016**, *8* (9), 5082–5088.

(43) Monereo, O.; Prades, J. D.; Cirera, A. Self-Heating Effects in Large Arrangements of Randomly Oriented Carbon Nanofibers: Application to Gas Sensors. *Sensors Actuators, B Chem.* **2015**, *211*, 489–497.

(44) Monereo, O.; Casals, O.; Prades, J. D.; Cirera, A. Self-Heating in Pulsed Mode for Signal Quality Improvement: Application to Carbon Nanostructures-Based Sensors. *Sensors Actuators, B Chem.* **2016**, *226*, 254–265.

MECHANICAL IMPROVEMENT OF THE SMD INKJET ASSEMBLING METHOD

CHAPTER 4

4.1 Motivation

As introduced in chapter 1 and 3, the emerging hybrid electronics requires from new assembling techniques, that must be compatible with the substrates used, which most of them have lower temperature resistance than the current used at traditional PCB manufacturing.[1,2] In order to solve this challenge, at chapter 3, a novel inkjet method for assembling SMDs was proposed and encouraging results were obtained on both mechanical and electrical properties.[3,4] In fact, the inkjet method proposed shows comparable electrical performance to benchmark materials tested. However, the mechanical performance reached is still far away of the performance shown by epoxy-based silver-filled conductive adhesive, also known as isotropic conductive adhesive (ICA), which is commonly used at the emerging hybrid PCB[5–9] and presented the best mechanical performance at chapter 3. In addition, both assembling materials, Ag-ink and ICA, show lower mechanical performance than the standard materials (solder reflow paste) used at traditional PCB manufacturing.[10] Due to that, the mechanical performance of the inkjet assembling process must be improved in order to accomplish the application requirements on reliability and quality. Therefore, in order to improve the SMDs inkjet assembling, a nonconductive polymer is studied as mechanical reinforcement.[11] On *Figure 4.1*, examples of the inkjet and the ICA assembling methods are shown, as well the current assembling method of traditional PCB.

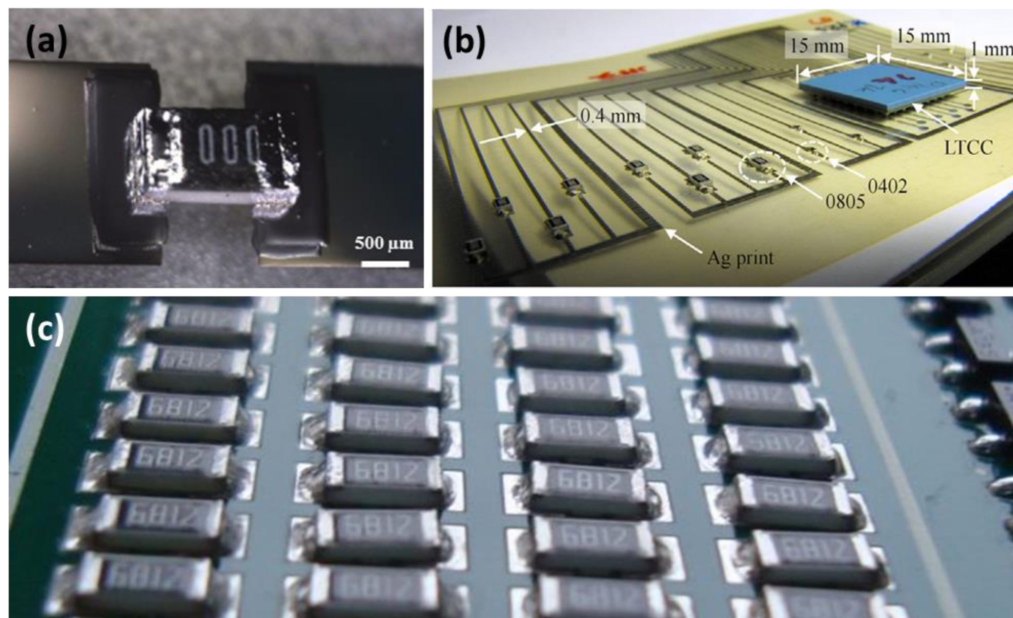

Figure 4.1 (a) Novel Ag inkjet assembling method. (b) Current ICA screen printing assembling method.[6] (c) Standard reflow paste screen printing assembling method.[12]

4.2 Inkjet-printed mechanical reinforcement for SMD assembling

As said, aiming to achieve a better shear and bending strength performance of the inkjet-printed silver junctions, a dielectric polymer ink was deposited at the junctions as a mechanical reinforcement. To perform this study, conductive strips and pads were printed above different substrates and the SMDs were connected on them by means the technique presented in chapter 3. This technique consist on connect the SMDs with Ag ink inkjet printed, where the ink wets the underlying tin-plated SMD electrodes by means capillarity. For the next step, the Laboratory of Advanced Manufacturing from the Institute of Material Science of Aragon (ICMA) printed the nonconductive polymer material as a mechanical reinforcement. At the end, the mechanical and electrical performance of the assembled SMDs were characterized.

4.2.1 Materials

The materials used to connect the SMDs by inkjet printer were the same as presented in chapter 3, which are: glass, polyimide and paper as substrates, the Ag ink and the SMDs resistors 1206 size code.

Following, the inkjet-printed reinforcement was deposited by a custom-made inkjet printer system (In-2 Printing Solution, Navarra, Spain) with Xaar-126/80 piezoelectric printheads (Xaar, Cambridge, United Kingdom). These printheads have 126 nozzles (50 μm diameter) arranged in a line with a pitch of 137 μm. The ink droplet volume was fixed roughly 80 pl and the experimental set-up during printing processes was performed at room temperature, as well platen substrate. The printhead is fixed in a frame and the substrate moves under the nozzles at a distance between the printhead and the substrate of approximately 1 mm. For print the reinforcement, a photocurable ink developed by ICMA, which based on 3Glycocidoxypropyltrimethoxysilane (GPTMS) was used, which is used as non conductive adhesive (NCA).[11] The GPTMS ink is solvent free and therefore the deposited material can be polymerized immediately after the deposition step by exposure to UV light. In addition, no baking steps are required allowing the use of thermally sensitive substrates and notably simplifying the process to one single step. Jorge Alamán *et al.* (from ICMA) perform with GPTMS ink waveguides that support optical modes with propagation losses as low as 0.5 dB cm^{-1},

demonstrating the potential of this photoacid catalysed organic–inorganic hybrid formulation and inkjet printing for the preparation of photonic devices.[11] In this work the used of the GPTMS ink is in a different application than photonic devices. The mechanical reinforcement was directly applied (ICMA, Zaragoza, Spain) on samples just received, and cleaning treatments were not applied on them previous photocurable ink deposit, thus avoiding possible degradation of the silver-printed connections.

Regarding the electrical resistance measurements over bending stress, different semi-circular pieces with different radius of curvature were printed by means BCN3D+ 3D extrusion printer (CIMS foundation, Barcelona, Spain) and polylactic acid thermoplastic was the material used.

4.2.2 Procedure

The conductive strips and the SMD electrode-conductive strip electrical connection were conducted exactly as presented in chapter 3. Prior to the printing process, standard cleaning of the surface substrates was carried out. Following, inkjet-printed pads of two strips 7 mm × 1.6 mm with 1 mm pitch were printed as a fixed pattern. In order to perform the SMD electrode-conductive strip electrical connection, the SMDs were manually located onto the printed strips, and a well-adapted pattern was printed afterwards with the high-resolution drop-jetting printer.

Regarding the application of reinforcement, an inkjet-printed pattern of two 3 mm × 5 mm separately by 2 mm pitch were printed as a fixed pattern. The NCA ink was deposited on the junction with enough area to keep away the edge of the NCA pattern to the silver contact zone, and hence focusing the bending stress at the reinforcement pattern edge instead of on the weak silver junction.

Concerning the NCA ink curing process performed by ICMA, a UV lamp OmniCure S2000 UV (Gentee, Nivelles, Belgium) was employed with a UV bandpass filter (wavelength range of 320-390 nm). The samples were cured inside a chamber provided with an optical access. A mild vacuum (100 mBa) can be attained inside the chamber by using a vacuum pump. Once desired pressure level is achieved, UV exposure is immediately carried out to minimize the evaporation of the deposited ink components. For curing the deposited pattern, a power of 10 mW cm^{-2} was applied for 5 min.

4.2.3 Characterization

Aiming to verify the no interaction between NCA and Ag-connections, electrical resistance measurements of the connections were performed before and after to NCA ink deposit. Following, a shear strength test is performed and the results compared with the values achieved at chapter 3. On the other hand, aiming to characterize the printed junctions, an electrical resistance test with the samples over bending stress is performed. Finally, the NCA reinforcement was morphological inspected.

Resistance measurements were performed by means of a Keithley 2400 source meter with 4-probe method. In order to obtain an accurate value of the contact resistance, SMDs resistors of nominally 0 Ω were measured to subtract its background contribution from the total electrical resistance measured. In addition, the contact resistance measured was divided by the two contact junctions. Finally, for each assembling method and substrate used, an average contact resistance was determined.

The shear strength analysis was conducted by means of a Zwich/Roell ZMART.PRO with a load cell with nominal force of 200 N. The evaluation test was done following the Japanese industrial standard for mechanical tensile test called “Methods for shear strength of solder joints on chip components” (JIS Z 3198-7). The methodology used to perform the mechanical test was is illustrated on the scheme of *Figure 4.2*. The values of strength resistance, in MPa, were calculated from the breaking force measured divided by force-resisting area parallel to force direction. As mentioned above,

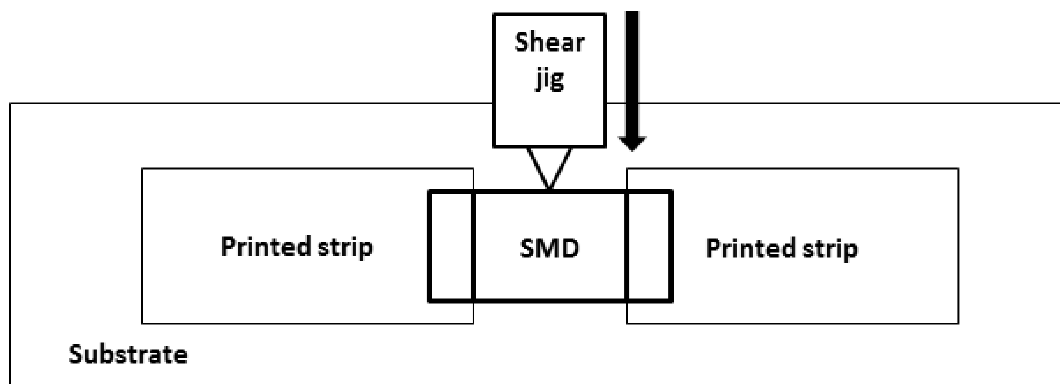

Figure 4.2 Scheme of the shear probe conducted according Japanese industrial standard JIS Z 3198-7.

Regarding the electrical resistance test over bending stress, the value of electrical resistance measured without bending was used as reference and the corresponding

results to different bend angles were normalized to that reference. About electrical resistance test over bending stress, 4 semi-circular pieces with 75 mm, 50 mm, 25 mm and 12.5 mm radius of curvature were used. The bending of the samples was applied by means the tips used on the 4-probe test and the values of contact resistance were acquired by means keithley 2400 source meter.

The NCA reinforcement was inspected by means Field Emission-Scanning Electron Microscopy FESEM JSM-7100F (JEOL, USA). In order to conduct the microscopy analyses, samples were embedded in resin and, subsequently, polished.

4.3 Results and discussion

Nowadays, the assembling of SMDs at hybrid PCB is being performed by means electrical conductive adhesives (ECA), as well solder.[9,8,5,13,6] Aiming to contribute on hybrid technology development, it has been proposed a new connecting solution as shown in chapter 3, which was compared with ICA among other assembling materials. Significant differences on mechanical properties were found, where ICA presents better performance than the inkjet method proposed. However, the electrical performance on that study is significantly better for the inkjet method proposed in comparison with ICA, achieving comparable electrical contact resistant consuming less material.[3] To the best of our knowledge, there are not works where ICA is inkjet-printed. In fact, the ICA is applied by means screen printing technique or by hand, even when is deposited over inkjet-printed PCBs, and hence combining two different printing techniques for same circuit fabrication. The assembling performance is electrically, mechanically and morphologically characterized in order to evaluate the reliability and feasibility of the reinforced inkjet-printed assembling technique.

4.3.1 Shear strength performance

Shear strength measurements were performed aiming to demonstrate that strengthen inkjet assembling can be accomplished by means applying a printed reinforcement *Figure 4.3*. The performance of the NCA ink reinforcement were compared with two of the assembling methods tested on chapter 3, the first one is the AgNP ink assembling method, and the second one is the ICA assembling, which is the most common used method for SMD assembling on part of novel PCBs (low cost, flexible and low

chemical and temperature resistance substrates). Furthermore, the performance is compared with the shear strength value of the current assembling material at traditional PCB manufacturing, which is the reflow solder paste. This value was found on literature for the same SMD model size 1206 (3.2 mm x 1.6 mm) attached to typical FR4 rigid substrates.[10]

Before the test of NCA as mechanical reinforcement, the compatibility of NCA ink with the silver connection was studied. Where was checked that electrical resistance kept invariable after NCA application.

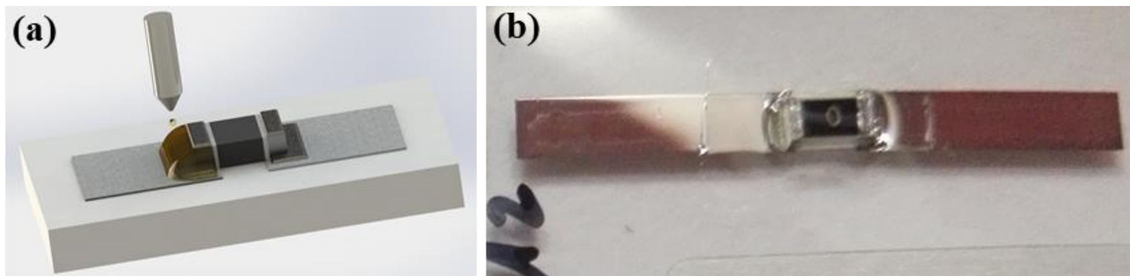

Figure 4.3 (a) Illustration of the SMD electrode-AgNP ink connection being mechanical reinforced by printed NCA. (b) A real component with printed NCA mechanical reinforcement after photocuring process.

The force-resisting area considered for AgNP ink connecting material is the bottom side electrode. The force-resisting area considered for ICA is the sum of the top and lateral side electrode plus the substrate area covered by the connecting material. Finally, the force-resisting area considered for AgNP ink plus NCA reinforcement is the sum of the bottom and lateral side electrode plus the substrate area covered by the connecting material. The nominal force-resisting areas considered are summarized in Table 4.1.

Table 4.1 Theoretical force-resisting areas.

Area	Theoretical force-resisting area (mm^2)
A. Bottom electrode	$2\cdot I1\cdot W = 1.60$
B. Lateral and top electrode plus substrate covered	$2\cdot W\cdot(I1+H) + 2.40^{*} = 5.92$
C. Lateral and bottom electrode plus substrate covered	$2\cdot W\cdot(I1+H) + 0.7^{*} = 4.24$

* Average value of the substrate area covered by the connecting material, extracted from 30 samples.

The shear strength values are shown on *Table 4.2* and *Figure 4.4*, which corresponds to the performance of AgNP ink and ICA (chapter 3), and the AgNP ink plus NCA reinforcement. The shear strength values of inkjet-printed connections are estimated by applying the same modus operandi as shown in chapter 3. It must be taken into account that the strategy with NCA reinforcement did not present any failure.

Table 4.2 Shear strength of the SMDs assembled by means different methods on paper, Kapton®, glass and FR4 substrates.

Mounting method	**Substrate**	**Shear strength (MPa)**	**Failure (%)**
AgNP ink	Paper	1.27 ± 0.47	7
	Kapton®	1.77 ± 0.92	10
	Glass	0.73 ± 0.24	13
AgNP ink + NCA	Paper	1.88 ± 0.42	0
	Kapton®	2.58 ± 0.76	0
	Glass	2.89 ± 0.46	0
ICA	Paper	3.01 ± 0.62	3
	Kapton®	1.87 ± 0.37	3
	Glass	3.52 ± 0.90	3
Sn3.0Ag0.5Cu	FR4	53.94*	-
Sn37Pb	FR4	64.53*	-

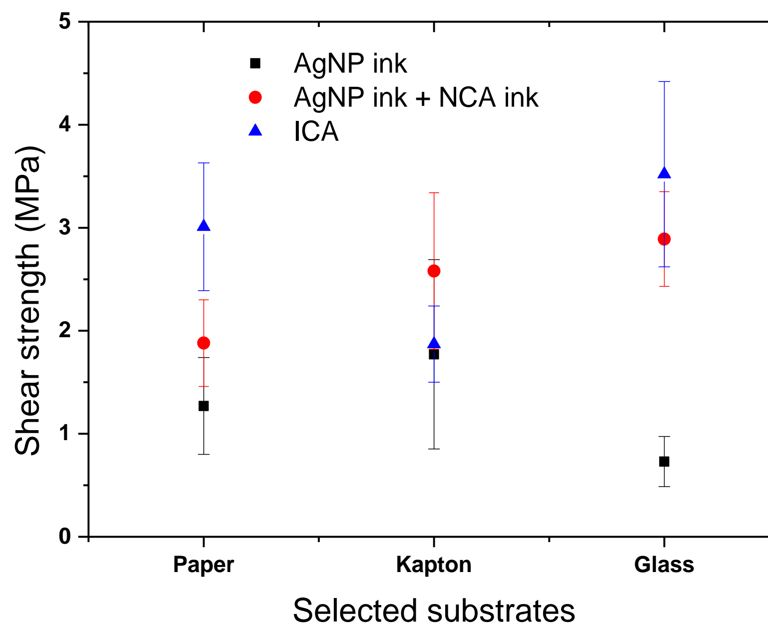

Figure 4.4 Shear strength of the SMD attached onto inkjet-printed pads depending on the connecting material and substrate.

As can be seen on *Figure 4.4*, the use of NCA ink as reinforcement generates the highest shear strength improvement on glass substrate, where is around 4 times higher. This is due to NCA ink is formulated for be applied on glass substrate.[11] On paper and Kapton® substrates, the shear strength increased roughly 1.5 times in comparison with joints made by only AgNP ink as assembling material. Although, shear strength on paper and Kapton® is lower than on glass substrate, considerable improvement of mechanical properties has been achieved with the NCA ink application. In fact, the mechanical properties are comparable to ICA performance obtained previously on chapter 3 (*Figure 4.4*) and also with values found on literature, where the shear force reported from 1206 SMDs assembled on glycol-modified polyethylene terephthalate (PET-G) substrate is about 12 N, which corresponds to 2.83 MPa taking into account similar theoretical contact area as used at this work.[9]

It is important to realize that inkjet method deposits thinner layer than screen-printed or hand-deposited ICA studies. In fact, the thickness of NCA-deposited on this study corresponds to a single pass printing, thus improved performance could be accomplished by means thicker layers, and even the SMDs could be covered if needed as embedding solution.

Summarising, the common attaching method of traditional PCB manufacturing, conducted by means of reflow solder paste on FR4 substrate (glass-reinforced epoxy laminate substrate), presents a shear strength higher than 15 times of the AgNP + NCA and the ICA performance, as shown on *Table 4.2*.[10,14,15,16] Note that the shear strength value of solder paste-FR4 extracted from literature take into account a force-resisting area of 1.6 mm^2, which is, of course, underestimated. Using a similar force-resisting area as performed at this work, the shear strength value is about 17 MPa, which is roughly 5 times greater than the values achieved by means AgNP + NCA and ICA. Despite of this, the new techniques for special PCBs manufacture on soft and flexible substrates can still improving their mechanical performance adding substrate-optimized adhesives or embedding the SMDs.

4.3.2 Electrical resistance measurements in bending stress mode

This chapter work is focused on the improvement of mechanical performance of the inkjet assembling method. In order to improve the bending strength performance, the NCA ink was deposited on the SMD junction zone covering 4 times larger area than

corresponding to junction, and hence keeping away the edge of the NCA reinforcement to the weak silver contact zone. Thereby, the bending stress is focused at the edge of printed NCA instead of on the AgNP junction.

The electrical characterization is performed by the variation of the junction electrical contact resistance at different bending radius. The results at the different bending radius are normalized with the corresponding electrical contact resistance at zero bending radius (R_0) and plotted on the following *Figure 4.5.* In addition, some pictures of the electrical test in bending stress mode are presented in *Figure 4.6*.

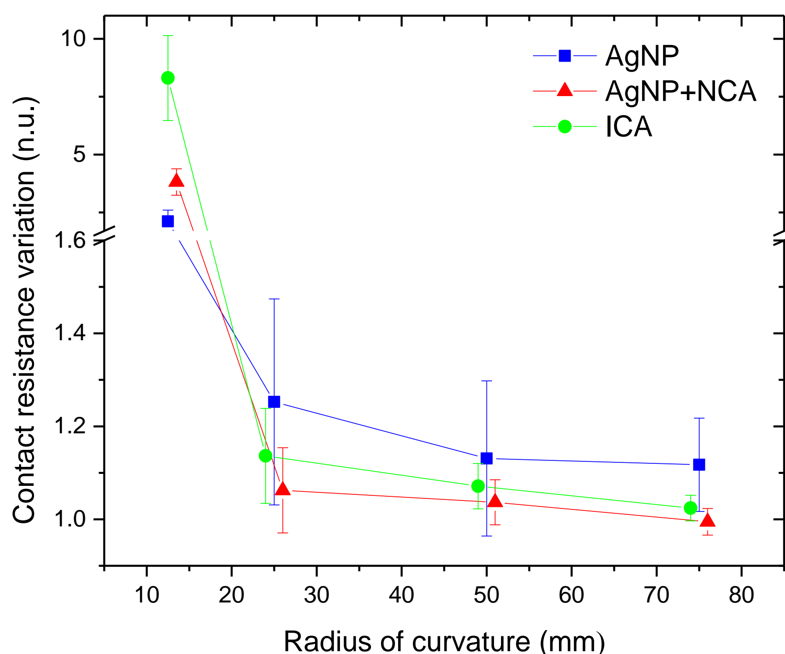

Figure 4.5 Normalized electrical contact resistance values measured at different bending radius of SMDs assembled by means AgNP, AgNP with NCA reinforcement and ICA.

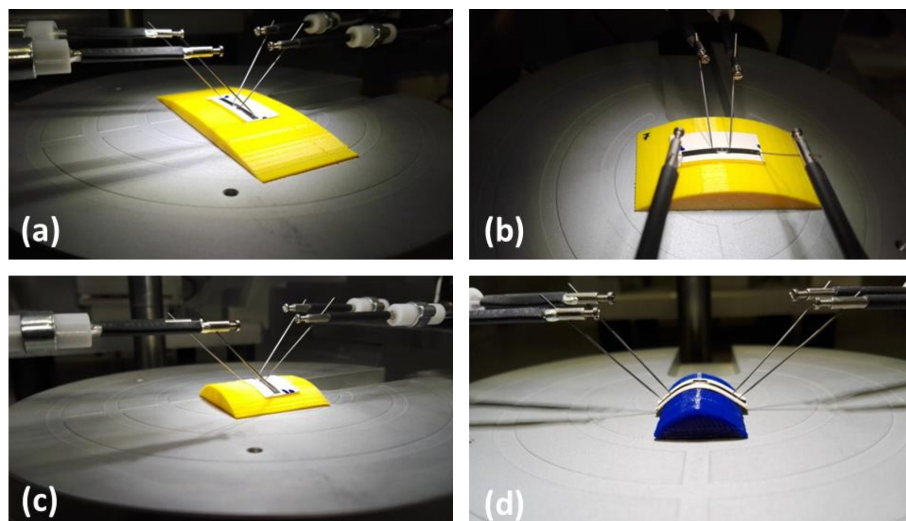

Figure 4.6 Electrical contact resistance measures at different bending angles. From (a) to (d), the radius angles are 75 mm, 50 mm, 25 mm and 12.5 mm, respectively.

The devices assembled with AgNP show a significant increase of contact resistance, even from the highest radius of curvature $R_{curvature}$ = 75 mm (roughly 1.2 times of R_0). Instead of that, devices with the NCA reinforcement or ICA show slight increment, from the radius of curvature of 75 mm until 25 mm. At a 12.5 mm of curvature radius, the joints start to be significantly damaged and the contact resistance arrives to $2R_{0,}$ $4R_0$ and $8R_0$ for AgNP, AgNP + NCA and ICA, respectively. Although all devices passed the test until curvature radius of 25 mm, at a curvature radius of 12,5 mm some junctions start to break. Regarding the AgNP-assembled, the 15% of the joints broke at 12.5 mm of curvature radius, higher amount of failures were produced with samples AgNP + NCA-assembled, where the 50% broke. For ICA-assembled, the broken junctions were the 33%.

It is important to realize that the coated paper substrate presents a considerable stiffness, with tensile modulus of E = 4.3 GPa.[17] Then, on bending process, forces are likely to separate the assembling material either from the substrate or from the component. At a curvature radius of 12.5 mm, broken joints on bending stress occur more times with NCA reinforcement and ICA than only AgNP. This could be due to the SMDs with NCA reinforcement or ICA material behave as longer device and lever forces increase over the junction surfaces. Then, for the entire radius tested, AgNP + NCA and ICA junctions are subjected to higher forces. However, except at the highest bending stress, the best performance is shown by AgNP + NCA and ICA joints.

It is important to realize that AgNP + NCA joint could present better performance with more flexible substrates as polyimide, because stresses on interconnections are smaller.[18,6]

4.4 Morphological FESEM inspection

Structural inspection of the different junctions was performed to ensure that AgNP ink + NCA assembling strategy exhibits competitive assembling performances. Microscopic analyses of device cross-sections were performed by FE-SEM technique, as shown in *Figure 4.7*. *Figure 4.7 (a)* shows how the capillarity action of AgNP ink moves the printed ink up to the underlying tin-plated SMD electrodes, then only this surface contribute to SMD adhesion. *Figure 4.7 (b)* highlights the improved junction by means NCA reinforcement, where part of the lateral SMD surface is summed to SMD

substrate-adhesion. In this study, the half of the lateral surface 0.96 mm^2 is considered, because it is the average of the covered area. In a different way than AgNP ink, devices connected by ICA are not assisted by capillarity. The ICA samples, manually applied, embed the whole SMD electrode area (*Figure 4.7 (c)*). However, in the screen printed ICA samples shown in *Figure 4.7 (d),* the covered surface is reduced in the same way that mechanical performance.

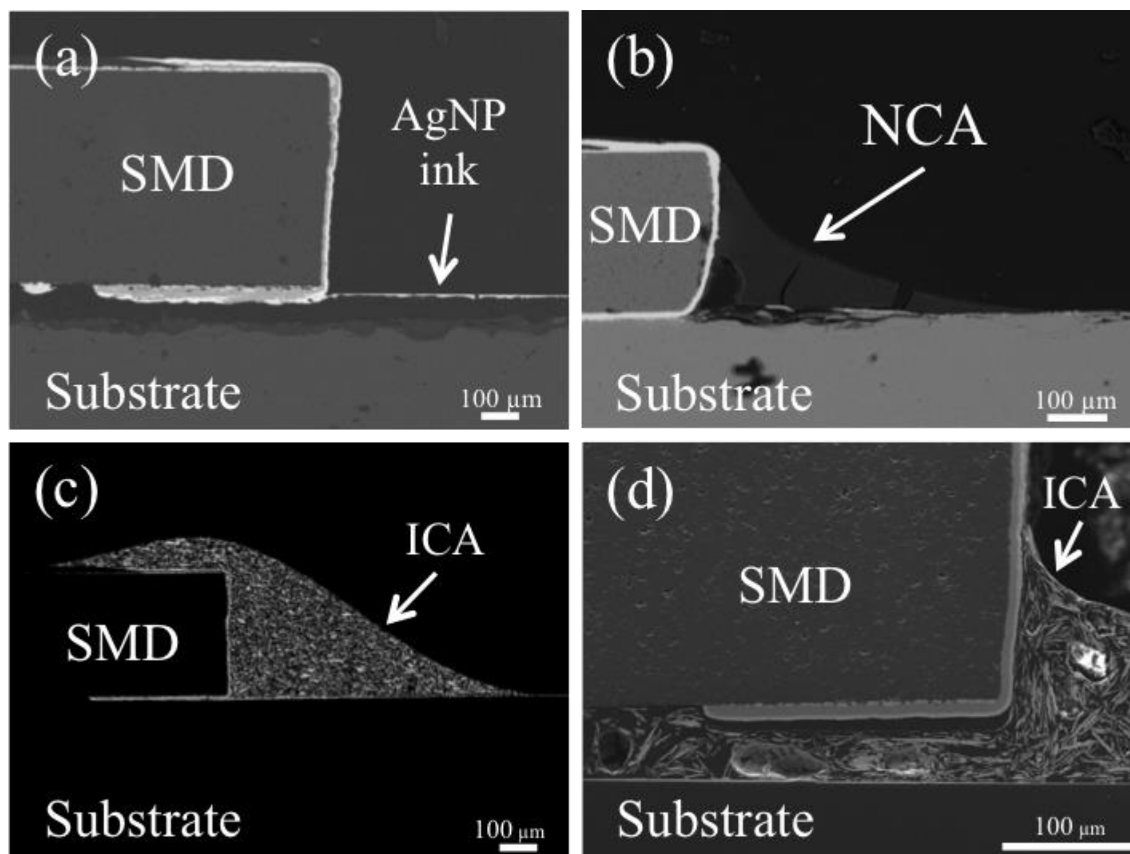

Figure 4.7 Back-scattered electron image (a) A cross-sectional view of a SMD AgNP inkjet-assembled. (b) A cross-sectional view of a SMD AgNP + NCA inkjet-assembled. (c) A cross-sectional view of a SMD ICA hand-assembled. (d) A cross-sectional view of a SMD ICA screen printing-assembled. Image (d) from [6]

4.5 Conclusions

Comparing the mechanical performance of the SMDs assembled by AgNP and the SMDs assembled by AgNP and NCA, adding the NCA reinforcement the shear strength performance is improved significantly. Concretely, the share strength increases 4 times on glass substrate and 1.5 on Kapton® and paper substrate. The higher increment of the

strength on glass substrate in comparison with the other substrates used is due to NCA ink is specially formulated for glass substrate.

The mechanical performance of the SMDs assembled by ICA hand deposited and SMD assembled by AgNP and NCA, have similar share strength in all the substrates used. In addition, the SMDs assembled by AgNP and NCA possess analogous mechanical properties to values found on literature for SMDs assembled by screen-printed ICA.

The electrical contact resistance measured in bending stress mode of the AgNP and NCA connections are similar to performance reached by ICA connections.

In the light of the results, inkjet connecting technique is a promising method, which allows selectively assembling components onto printed flexible and rigid substrates for the upcoming hybrid electronics with a non-contact process.

4.6 References

(1) Ko, S. H.; Pan, H.; Grigoropoulos, C. P.; Luscombe, C. K.; Fréchet, J. M. J.; Poulikakos, D. All-Inkjet-Printed Flexible Electronics Fabrication on a Polymer Substrate by Low-Temperature High-Resolution Selective Laser Sintering of Metal Nanoparticles. *Nanotechnology* **2007**, *18* (34), 345202.

(2) Ko, S. H.; Chung, J.; Pan, H.; Grigoropoulos, C. P.; Poulikakos, D. Fabrication of Multilayer Passive and Active Electric Components on Polymer Using Inkjet Printing and Low Temperature Laser Processing. *Sensors Actuators A Phys.* **2007**, *134* (1), 161–168.

(3) Arrese, J.; Vescio, G.; Xuriguera, E.; Medina-Rodriguez, B.; Cornet, A.; Cirera, A. Flexible Hybrid Circuit Fully Inkjet-Printed: Surface Mount Devices Assembled by Silver Nanoparticles-Based Inkjet Ink. *J. Appl. Phys.* **2017**, *121* (10).

(4) Rivera J; Peitivi A; Llorente S; Arrese X; Servera L; Cirera A. Dispositivo de Aparato Doméstico y Procedimiento Para La Fabricación de Un Dispositivo de Aparato Doméstico. *ES 2 564 760 A1* **2014**.

(5) Niittynen, J.; Kiilunen, J.; Putaala, J.; Pekkanen, V.; Mäntysalo, M.; Jantunen, H.; Lupo, D. Reliability of ICA Attachment of SMDs on Inkjet-Printed Substrates. *Microelectron. Reliab.* **2012**, *52* (11), 2709–2715.

(6) Putaala, J.; Hannu, J.; Kunnari, E.; Mäntysalo, M.; Nousiainen, O.; Jantunen, H. Reliability of SMD Interconnections on Flexible Low-Temperature Substrates with Inkjet-Printed Conductors. *Microelectron. Reliab.* **2014**, *54* (1), 272–280.

(7) Mäntysalo, M.; Mansikkamäki, P. Inkjet-Deposited Interconnections for Electronic Packaging. *NIP Digit. Fabr. ...* **2007**, 813–817.

(8) Niittynen, J.; Pekkanen, V.; Mäntysalo, M. Characterization of ICA Attachment of SMD on Inkjet-Printed Substrates. *Proc. - Electron. Components Technol. Conf.* **2010**, 990–997.

(9) Chtioui, I.; Bossuyt, F.; Bedoui, M. H.; Niittynen, J.; Pekkanen, V.; Mäntysalo, M.; Mansikkamäki, P.; Putaala, J.; Hannu, J.; Kunnari, E.; et al. Thermo-Plastically Stretchable Electronic and Sensor Circuits. *Microelectron. Reliab.* **2016**, *52* (11), 2709–2715.

(10) Pan, J.; Toleno, B. J.; Chou, T.; Dee, W. J. The Effect of Reflow Profile on SnPb and SnAgCu Solder Joint Shear Strength. *Soldering & Surface Mount Technology*. 2006, pp 48–56.

(11) Alamán, J.; López-Valdeolivas, M.; Alicante, R.; Medel, F. J.; Silva-Treviño, J.; Peña, J. I.; Sanchez Somolinos, C. Photoacid Catalyzed Organic-Inorganic Hybrid Inks for the Manufacturing of Inkjet-Printed Photonic Devices. *J. Mater. Chem. C* **2018**, 20–22.

(12) Madsen, M. Tutorial: reflow soldering http://www.maskau.dk/embedded/tutorial-reflow-soldering (accessed Jun 20, 2018).

(13) Andersson, H. a; Manuilskiy, A.; Haller, S.; Hummelgård, M.; Sidén, J.; Hummelgård, C.; Olin, H.; Nilsson, H.-E. Assembling Surface Mounted Components on Ink-Jet Printed Double Sided Paper Circuit Board. *Nanotechnology* **2014**, *25* (9), 094002.

(14) Webster, J.; Pan, J.; Toleno, B. Investigation of the Lead-Free Solder Joint Shear Performance. *J. ...* **2007**, *4* (949), 6.

(15) Engineering, M. ANALYSIS OF SURFACE MOUNT TECHNOLOGY SOLDER JOINTS Acknowledgments. **1996**.

(16) Dušek, K.; Bušek, D.; Beran, T.; Rudajevová, A. Comparison of Shear Strength of Soldered SMD Resistors for Various Solder Alloys. *Proc. Int. Spring Semin. Electron. Technol.* **2015**, *2015–Septe*, 237–240.

(17) Ranges, X. D. TECHNICAL DATA SHEET HD & XD RANGES.

(18) Dupont. DuPont ™ Kapton ®. *http://www.dupont.com/content/dam/dupont/products-and-services/membranes-and-films/polyimde-films/documents/DEC-Kapton-summary-of-properties.pdf* **2012**, *50*, 1–7.

PRINT-ON-SLOPE TECHNIQUE FOR ELECTRONIC COMPONENTS INKJET-ASSEMBLING

CHAPTER 5

5.1 Motivation

As introduced previously, the hybrid electronics requires from new assembling techniques, which must be compatible with some of the low temperature resistance substrates used at emerging electronics. In order to solve this challenge, a novel inkjet method for assembling SMDs has been proposed in chapter 3 and encouraging results were obtained on both mechanical and electrical properties in comparison with benchmark materials. Concerning the outcome achieved at chapter 3, and in order to improve the performance of the proposed inkjet assembling method, a non-conductive adhesive/polymer (NCA) is studied as mechanical reinforcement and a significant improvement is demonstrated at chapter 4. Therefore, aiming to improve even more the performance of the proposed inkjet assembling method, further work related on the electrical performance is executed. Although the tests performed at chapter 3 show that inkjet assembling method is comparable to benchmark materials tested, the SMD electrode faces oriented parallel to drops downfall direction cannot be ink covered, which reduces the connecting surface, and hence increase the failures risk. Therefore, aiming to increase the connecting surface, at this chapter, modified SMDs with ramp-shape electrodes are proposed/tested and compared with the squared-shape electrodes of current SMD.

In addition, the ramp-like shape electrodes open new possibilities of SMDs-PCBs circuit connection, where SMDs/electronic modules top face can contain part of the electronic circuit. In fact, nowadays, there are some works that present applications taking advantage of the ramp-shape connection.[1,2] Hence at this chapter, in order to go further on the potentiality of this connecting strategy, a silicon die is directly assembled to PCB and a novel setup for 2D materials characterization is manufactured.

5.2 Ramp-shaped SMD electrodes

Nowadays, the current SMDs are well adapted to standard PCB manufacturing (screen-printed reflow paste), where their squared-shape electrode is enough to accomplish the requirements on reliability and quality of the joints, (*Figure 5.1*).

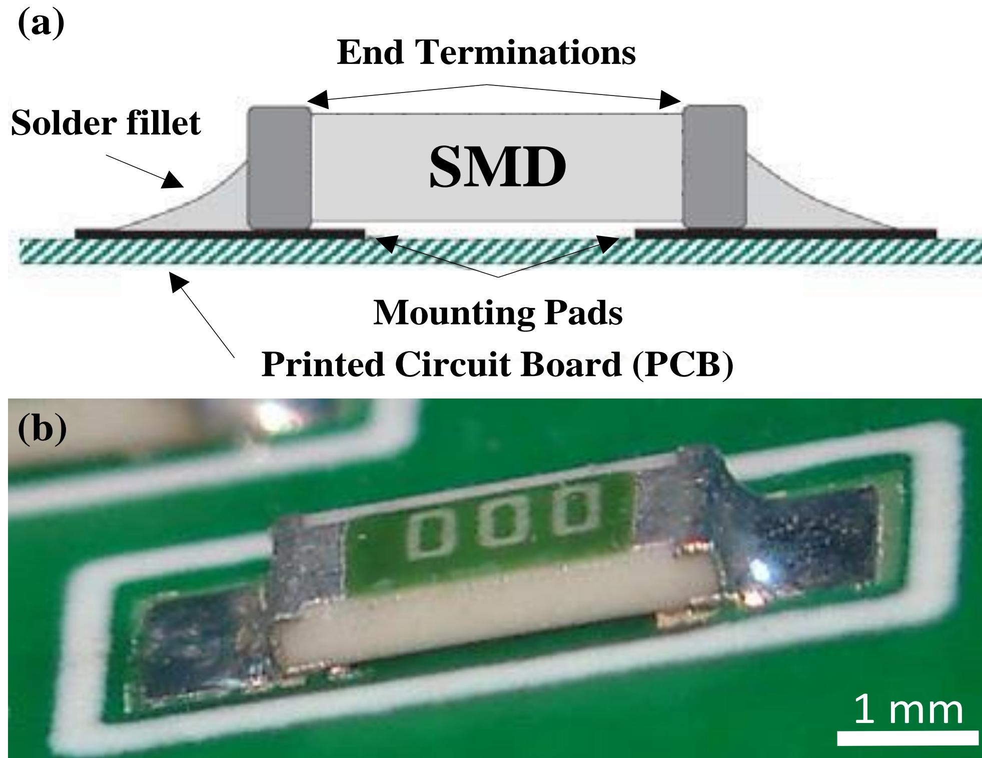

Figure 5.1 (a) Illustration of SMD soldering profile by means of reflow paste-assembling process. (b) Image of SMD assembled by means of screen-printed reflow paste. Image from [3]

However, the standard assembling process used on PCB mass production is forbidden over low temperature resistance substrates, as well when printed connecting strips are weakly adhered to substrate and suffer from leaching effect.[4] Aiming to solve this restriction, low temperature assembling processes have been reported.[4,5,6,7] Among the processes available, the inkjet assembling strategy presented on chapter 3, allows to connect this kind of components by means of conductive ink capillarity.[4,8] Although, the ink wets the underlying tin-plated surface mount technology (SMD) pads, the SMD electrode faces oriented parallel to drops downfall direction cannot be ink covered, thus connecting surface is reduced in comparison with standard SMD assembling. In addition, although the inkjet capillarity-assisted assembling has been demonstrated, the capillarity effect could be reduced depending on the substrate-SMD electrode interface, thus reducing the effective connecting area. Aiming to increase the connecting area and the reliability, modified SMDs with ramp-shape electrode (*Figure 5.2 a*) are tested and compared with the standard SMDs with square-shape electrodes (*Figure 5.2 b*). The *Figure 5.2* shows an illustration of the both geometries inkjet-assembled. It should be pointed out that the "print-on-slope" technique is not performed at current surface mount technology (SMT). In addition, there are only few works related to new additive

manufacturing techniques, where the PCBs strips are connected to the top of a silicon ICs using print-on-slope strategies.[2,1,9]

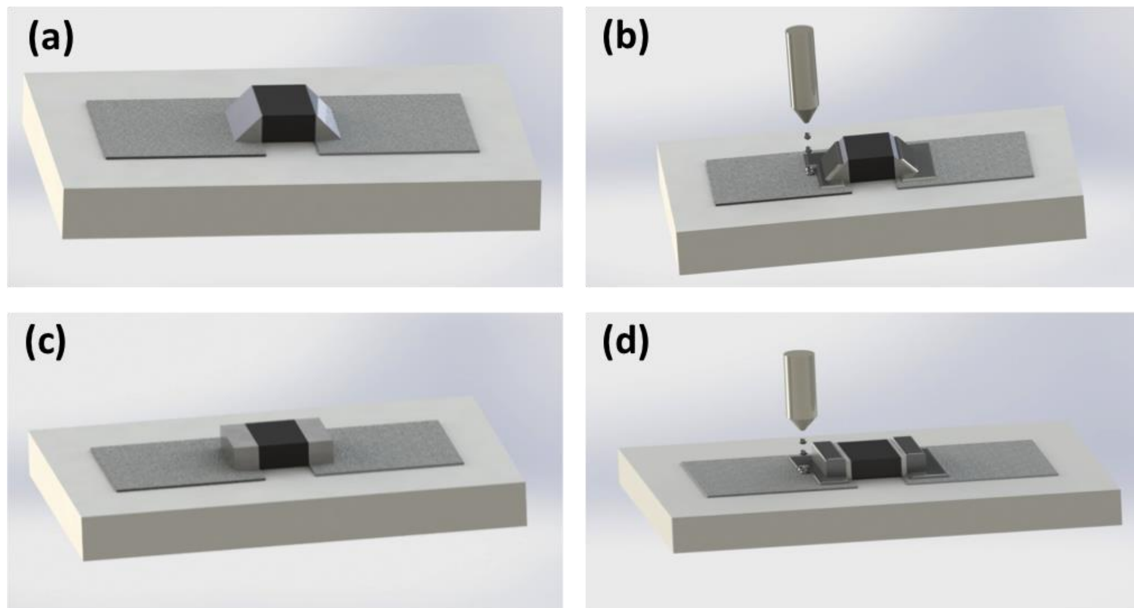

Figure 5.2 (a) SMD with ramp-like shape electrodes located over conductive strips. (b) SMD with ramp-like shape electrodes at inkjet-assembling process. (c) SMD with square-like shape electrodes located over conductive strips. (d) SMD with square-like shape electrodes at inkjet-assembling process.

5.2.1 Ramp-shape SMD electrode: materials, procedure and characterization

As said at motivation section, nowadays the SMDs available on the market have abrupt edges, and thus the inkjet junction is limited to only one face of the SMD electrode. Aiming to increase the contact surface between the SMD electrode and the printed connecting material, a modified SMD with ramp-shape electrode is proposed. From this geometry it is assumed that the biggest SMD metallized faces can be wetted by the connecting material, and hence the electrical resistance associated to the contact interface are reduced. Furthermore, by means of print-on-slope technique a new way of build/design/manufacture circuits is allowed, where IC can be connected directly on printed circuit boards by non-contact manufacturing techniques.

Materials

The modified SMD were performed with the alloy used by the SMD manufacturer, Sn96Bi4. The alloy was obtained using Bismuth powder 99,99% and Tin powder 99% (Sigma Aldrich, USA) and was melted by means of Indutherm Vacuum Pressure

Casting VC-500D machine (Indutherm, Germany). The alloy was rolled, for iron soldering. Then, the conductive alloy was attached to SMDs by a conventional iron and the ramp-shape and square-shape were mechanized with a polish machine Dremel 3000 (Dremel, USA).

The inkjet ink used to SMDs-connecting was the same as used at chapter 3, the Silverjet DGP, and the test with ramp-like and square-like shape SMD electrodes was performed only on glass substrate, taking advantage of its flatness and surface homogeneity.

Procedure

Regarding the SMD modification, the alloy was produced melting 24 g of Tin and 1 g of Bismuth in a ceramic crucible and carrying it to 600 °C for 30 min under reducing atmosphere by means of inductive heating process, (*Figure 5.3*). A post heat treatment of homogenization was performed to assure homogeneous composition of the alloy. Following, the alloy piece was sliced and rolled until thickness about 100 µm and strip-shape cut with about 2mm width.

Concerning the SMD modification, the alloy was deposited with an iron at 300 °C. The ramp-like and square-like electrode shapes were manufactured by polishing. In addition, aiming to assure comparable roughness and smoothness of the bottom face electrode, the SMDs were embedded in a wax, and grinded until achieve the desired roughness and smoothness. The wax embedding material was chosen because can be removed at low temperatures. Finally, the SMDs were cleaned in boiling water to remove remaining wax. Regarding the inkjet-assembling process, it was performed equally as described at chapter 3.

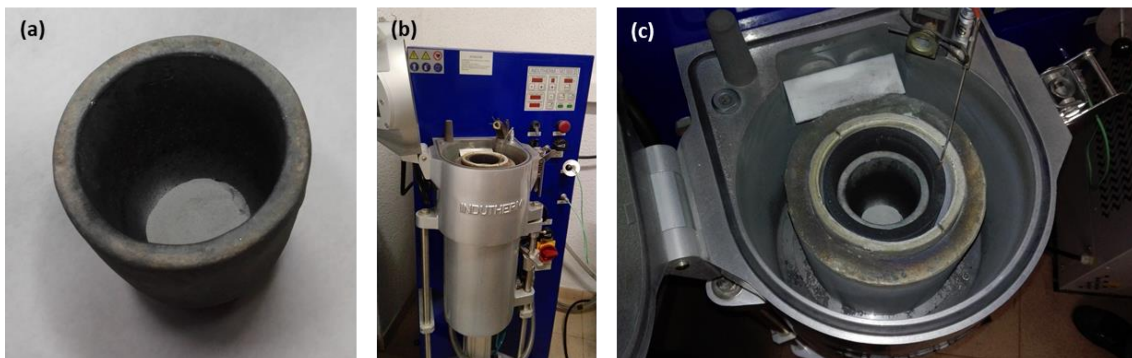

Figure 5.3 (a) Crucible with Sn and Bi powder. (b) and (d) Inductive oven used to fabricate the alloy.

Characterization

The electrical contact resistance measurements were performed by means of a SMU (Keithley 2400) with 4-probe method following the same procedure used at chapter 3.
The morphology of the junctions was inspected by Field Emission-Scanning Electron Microscopy FESEM JSM-7100F (JEOL, USA). In order to characterise the junctions, the samples were embedded in resin and subsequently polished.

5.2.2 Results and discussion

The reflow process for SMDs-assembling at current PCB fabrication is not adapted for all the substrates used at emerging electronics. Therefore, among the strategies presented to solve this challenge, the inkjet assembling is one of the most promising (chapter 3 and 4), which allows connecting this kind of components taking advantage of fluids capillarity phenomena. Despite of the inkjet SMD-assembling has been demonstrated, the SMDs pad faces oriented parallel to drops downfall direction cannot be covered by ink (*Figure 5.4*), thus connecting area is reduced in comparison with the current SMD-assembling at surface mount technology (SMT). Therefore, aiming to expose as much as possible the metallic pad faces to connecting ink, modified SMDs with ramp-shape electrode are proposed.

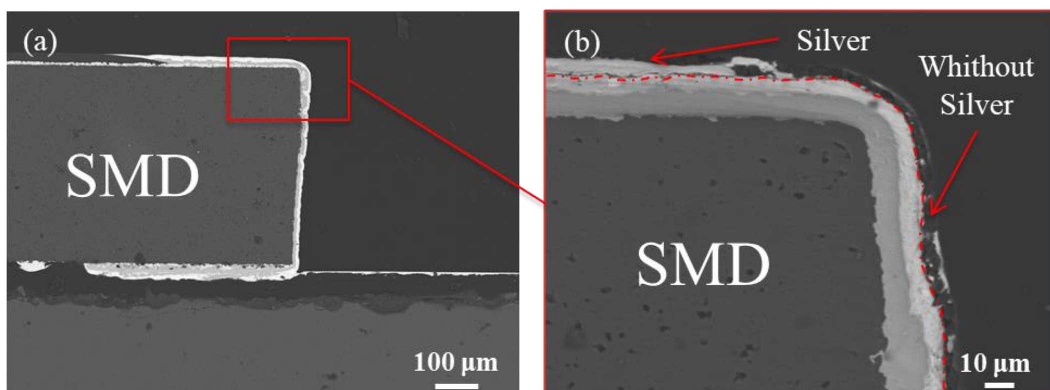

Figure 5.4. Backscattered electron scanning images. (a) No modified SMD inkjet-assembled. (b) Detail of SMD top corner, which shows silver deposit only on SMD top face.

In order to compare the connecting performance between ramp-like and square-like shape SMD electrodes, two samples of both shape electrodes are manufactured from the SMDs with added alloy (*Figure 5.5 (a)*) keeping similar bottom electrode area (*Figure 5.5 (b) and (c)*). In addition, comparable roughness and smoothness of the bottom electrode surface for all samples is performed as mentioned above. At the end, to assure

the same test conditions for all SMDs, the strips pattern contains squared points where measure tips are located, and hence keeping the drop voltage distance constant. The electrical contact resistance results are summarized in the following *Table 5.1*.

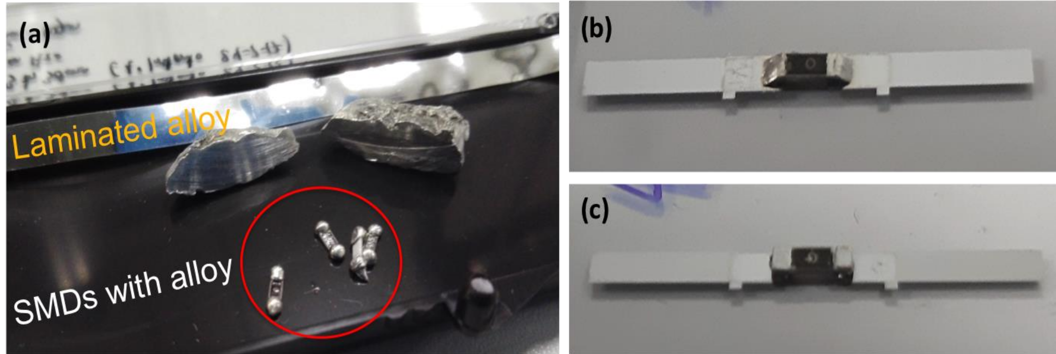

Figure 5.5 (a) Picture that shows two alloy-pieces, a laminated alloy strip and SMDs with attached alloy. (b) SMD with ramp-shape electrode inkjet-assembled. (c) SMD with squared-shape electrodes inkjet-assembled.

Table 5.1 Table of electrical contact resistance measured of the different SMDs pads termination tested.

Electrode shape	**Contact resistance (Ω)**	**Failure (%)**
As received[a]	0.37 ± 0.10	23
Ramp	0.64 ± 0.47	37
Square	3.72 ± 3.43	50

[a] Result presented in chapter 3

Modified SMDs show a considerable increment of the electrical contact resistance and failures, in comparison with no modified SMDs. The differences on electrical performance between modified and no modified SMDs are due to the manual process, which cannot assure the smoothness and reliability of automated process (*Figure 5.6*).

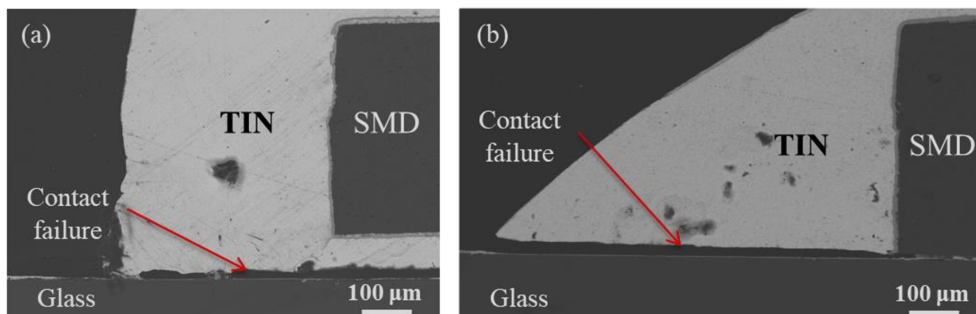

Figure 5.6 Backscattered electron scanning images. (a) Square-like SMD electrode that shows failure at electrical contact. (b) Ramp-like SMD electrode that shows failure at electrical contact.

From this study, the ramp ended SMDs shows better performance in both electrical contact resistance and failures. However, the worst performance achieved by squared-shape SMDs could be due to the lack of flatness at lateral face, which could move away the printed ink from the interface between SMD and printed strip, and hence hindering the ink capillarity. The larger length of this lateral-face increases significantly the probability of this phenomenon. Regarding the ink-wetted surface, the SMDs with ramp-shape electrode show a silver deposit on the ramp surface while it is not allowed at squared-shape electrodes (*Figure 5.7*).

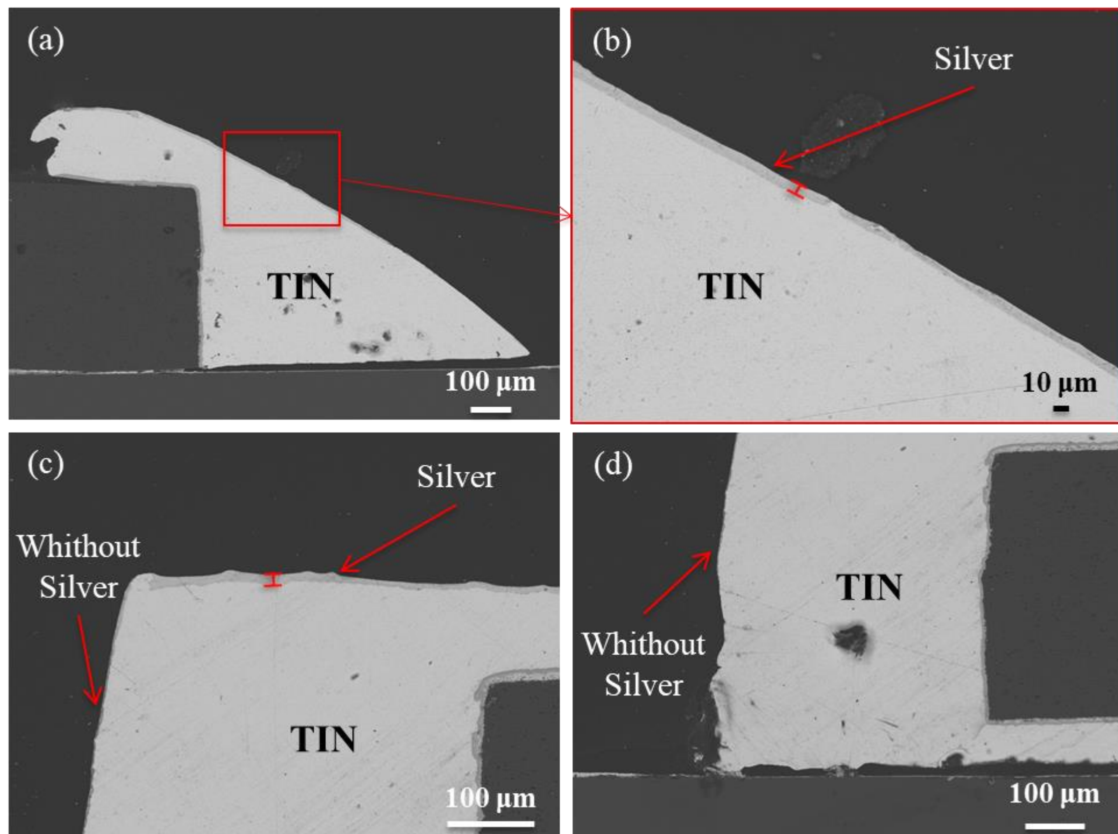

Figure 5.7 Backscattered electron scanning images. (a) Ramp-like SMD electrode inkjet-assembled. (b) Silver deposit on ramp surface. (c) Squared-shape SMD electrode inkjet-assembled, which shows silver deposit only on top face. (d) Lateral face of squared electrode without silver deposit.

In conclusion, the significant deviation achieved at electrical contact resistance measured as well the increment on failures denotes that a lack of smoothness and reliability is occurred at this test. However, the ramp-shape electrodes show better performance on ink-wetting than square-shape electrodes, which means that with ramp-shape electrodes higher electrical contact surface can be assured.

For all the above mentioned, as future work, this test should be repeated with ramp-shape and squared-shape SMDs manufactured with standard manufacturing machines.

5.2.3 Conclusions

Comparing the electrical contact resistance performed by the modified SMDs and the no modified ones, the electrical connections of modified SMDs have higher electrical contact resistance and higher failure occurrence takes place. The differences on the electrical contact resistance and failures occurrence between modified and no modified SMDs are due to non-automated electrode modification, which cannot assure the smoothness and reliability.

The SMDs with ramp-shape electrodes have both electrical contact resistance and failures lower than the SMDs with square-shape electrode. The worst performance achieved by squared-shape SMDs is because of the lack of flatness at lateral face, which moves away the ink from the interface between SMD electrode and the conductive strip, hindering the ink capillarity.

The SMDs with ramp-shape electrode retain silver deposit on the ramp surface while it is not occurred at squared-shape electrodes, which means that ramp-shape electrodes assure higher electrical contact surface.

5.3 Inkjet strategies for integrated circuits assembling

On the last decade, huge efforts are being performed, aiming to find new integrated circuits (ICs) connecting strategies to PCBs.[2,1,10,11,12] In addition, the electronic circuits are moving increasingly towards more densified structures, which need solutions that allow to overcome the space and wiring constrains.[10,11,12] Concerning the ICs components currently assembled on PCB by means of standard silicon SMD packages, the current manufacturing process used is shown at *Figure 5.8* and consist on complex steps (die cutting, mounting, wire bonding). This technology is also known as system on package (SoP). The current technologies, as wire bonding and flip-chip, used to connect the silicon die with the packaging terminations have some drawbacks. The wire bonding has high parasitic inductance and often requires of passive components for compensation at mm-wave frequencies. The flip-chip technique reduces interconnection length and parasitic, but suffer from high sensitivity to coefficient of thermal expansion (CTE) mismatch.[2] In addition, the standard silicon SMD packages size difficult the

bending and flexibility of the hybrid printed circuits.[13] Once finished, this component is located on the PCB and connected through their extremities to the corresponding pads on PCB.

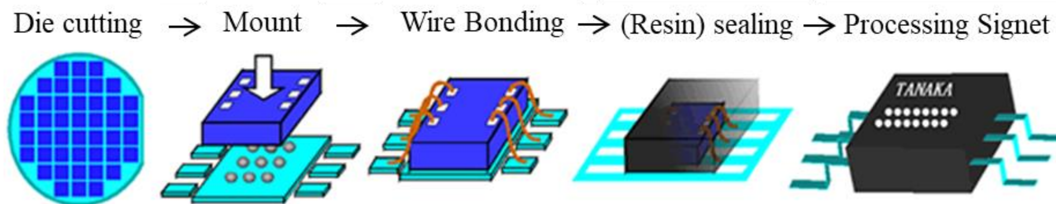

Figure 5.8 Scheme of SoP manufacturing process.

In the last decade, some authors have proposed innovative ideas to assemble directly the integrated circuits on the PCB. Thus, reducing the manufacturing steps, the manufacturing wastage and promoting the low cost electronics and the flexible hybrid electronics. These proposed ideas are clustered in two blocks. The first one consists on locate the IC dies directly on the PCB and connect them by means of inkjet, which is considered as SoP.[2,1] The second one consists on integrate the IC dies and the passive electronic components in a liquid resin matrix, and once hardened the circuit components are connected between them by means of conductive ink, which is known as system in package (SiP).[10,11,12] Regarding the innovative SoP, Bijan K. Tehrani *et al.* presented a mm-wave antenna where the IC die is attached and connected to glass substrate by the print-on-slope technique. In addition, the coplanar waveguide (CPW) transmission lines are silver-based, thus all device is inkjet-printed (*Figure 5.9*).[2]

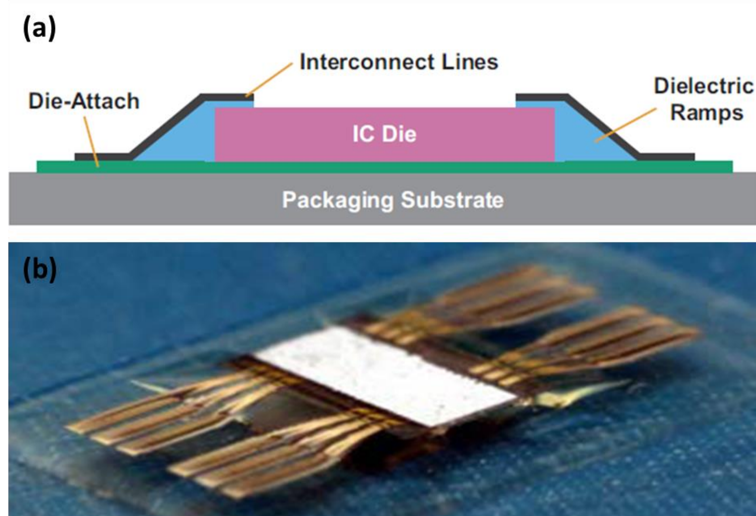

Figure 5.9 (a) Scheme of the print-on-slope technique for direct substrate IC die integration and connection. (b) mm-wave antenna on glass substrate with IC die connected by means of a SU8-based ramp using the print-on-slope technique. Image adapted from [2]

Jussi Putaala *et al.* presents radio-frequency identification (RFID), where IC die is adhesive attached to flexible substrate, and the connections are performed by inkjet print-on-slope technique (*Figure 5.10*).[1]

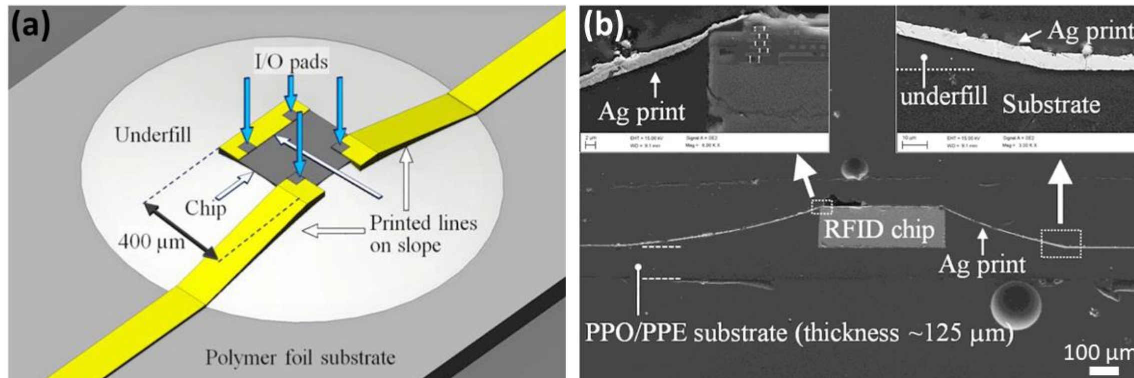

Figure 5.10 (a) Scheme of the print-on-slope technique for direct substrate IC die integration and connection. (b) Flexible radio-frequency identification (RFID), where IC die is connected by means of inkjet print-on-slope technique. Image adapted from [1]

Regarding the SiP, Matti Mäntysalo *et al.* presents a highly-integrated radio-frequency RF module where IC and discrete components are integrated together by conventional wiring board technology and partly by inkjet printing (*Figure 5.11*).[10]

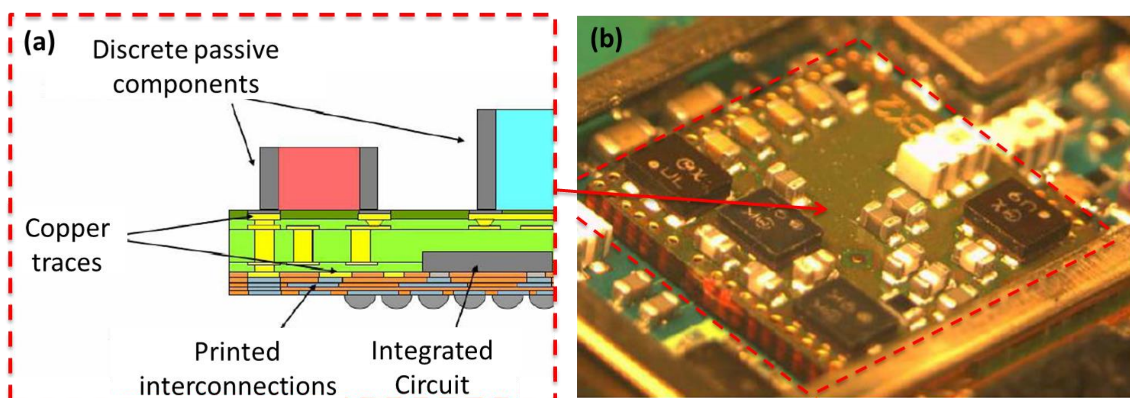

Figure 5.11 Schematic of the highly-integrated RF module architecture, where IC and discrete passive components integrated are connected by means of conventional printed wiring board technology and partly by inkjet printer. (b) The finalized SiP attached on the main board. Image adapted from [10]

Jani Miettinen *et al.* presents an electronic module where the IC and the discrete components are embedded inside a molding material that works as a substrate for inkjet printing. A multilayer circuit of six conductive layers interspersed with the respective insulating layers is inkjet-printed on the module-substrate, and hence connecting the electronic module (*Figure 5.12*).[11]

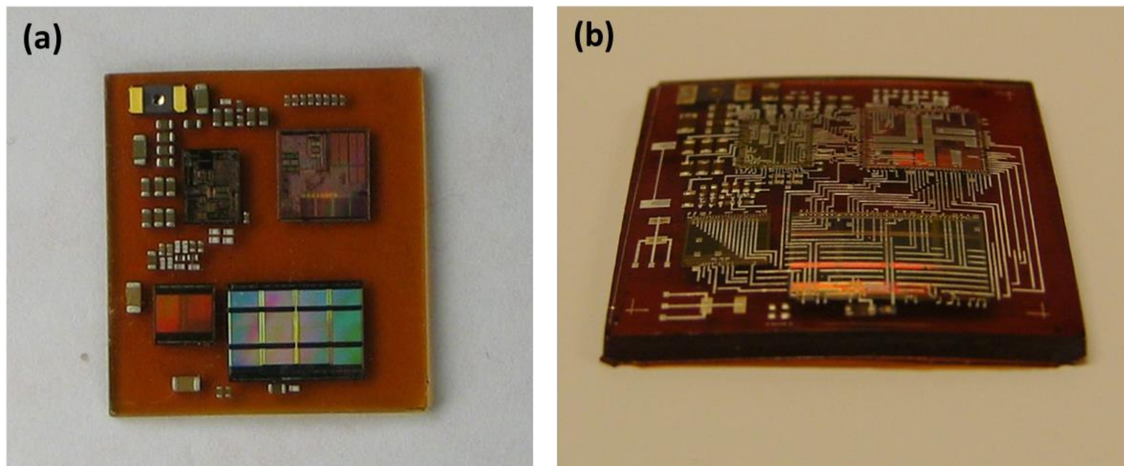

Figure 5.12 (a) Picture of the ICs and the discrete passive components embedded inside molding material. (b) After first inkjet-printed conductive layer. Image adapted from [11]

At this chapter, aiming to take advantage of the planar inkjet connections between two different circuit height levels, a novel experimental setup for 2D materials nanoscale characterization is designed in collaboration with the Reliability of Electronic Devices and Circuits (REDEC) group at the Electronic Engineering Department of the Universitat Autònoma de Barcelona (UAB). The 2D materials nanoscale characterization setup allows change between electrical and morphological measurements in a short switching time lapse.

Nowadays, it is known that there are approximately 2,000 compounds that can be synthetized or exfoliated in a 2D structure.[14,15] This richness of materials opens a wide range of possible applications in the fields of composite materials,[16] biomedicine[17] or nanoelectronics.[18] However, because its small thickness (at its limit 1 atom thickness), the 2D materials are heavily affected by its surrounding, substrate and its own structure. These local-based phenomena cannot be studied using only whole device electrical measurements techniques, but local characterization techniques as atomic force microscopy (AFM) are needed in order to have a complete picture of the overall phenomena. Moreover, various degradation phenomena are time dependent, as the bias temperature instability (BTI) degradation of 2D based transistor, which recovers over time.[19] Concerning this, the material degradation can be characterized by means of conductive atomic force microscopy (CAFM), only if the time lapse of switching between the electrical current source, which degrades the 2D material and the AFM system is performed. Because of this, the setup that takes advantage of the versatility of

inkjet printing technique is manufactured in order to connect several graphene-based field effect transistors (GFETs) to either a source measure unit (SMU) and a CAFM avoiding wire-bonding technique. Consequently, by means of planar connections the AFM tip can move freely over the characterization sample, which allows to overcome the drawback occurred when this setup was manufactured using the current wire bonding technique at the first trial. Moreover, all the measurements are performed inside a commercial AFM in order to minimize the time elapsed between the device level stress and the nanoscale electrical measurement. From this work, the experimental setup was designed and manufactured in collaboration with REDEC group, while the GFETs were fabricated and material characterized by the REDEC group.

5.3.1 System on package (SoP): materials, procedure and characterization

Materials

The characterization setup manufacturing, the SoP was carried out by the Dimatix 2831 model series (Fujifilm, USA). The circuit conductive pads and strips, were performed by means of a 10 pl cartridge and silver ink, Silverjet DGP HR (ANP, South Korea). The transistors interconnections on silicon die were performed with 1 pl cartridge and the same ink used to print pads and strips. The circuit was printed on adhesive polyimide PPI-SP-793-6 (PPI, Ireland) with 50 μm polyimide thicknesses. Following, the material used to fix the die on the PCB was isotropically conductive adhesive ICA silver epoxy (CircuitWorks Conductive Epoxy CW2400, Chemtronix).

Procedure

The novel setup for Conductive Atomic Force Microscopy (CAFM) characterization was performed using a similar SoP inkjet-printed strategy as mentioned.[2,1] Regarding the setup manufacturing, the first step was to print, by means of 10 pl cartridge, the layout designed on 50 μm thick adhesive polyimide. Once circuit was printed and sintered, the adhesive polyimide liner was released and the PCB polyimide-based was assembled to an AFM holder. Following, the silicon die was electrically connected to the PCB. To perform that, a squared grid of silver ink was printed on the PCB gate electrode, and while the ink was still on liquid state, the silicon die was manually located over the gate electrode. After that the ink was thermally sintered, thus Ag ink is

used as conductive glue to connect the silicon die to the PCB gate electrode. The ICA was used for manufacture the ramp-like connections between the different height level circuits, and also as mechanical fixation of the silicon die to PCB. Once the silicon die was attached to PCB, 1 pl cartridge was used to print the connections between the GFETs and the bottom printed circuit board. The connections were electrically checked by 4 point test, and the conductive strips thickness was increased until to achieve the desired electrical resistance. At the end, the REDEC group finished the setup integrating the SoP fabricated on the AFM holder to the AFM microscope and connecting it to SMU and AFM. Both apparatus, AFM and SMU, were connected to an external switch control unit, that allows choose the GFET under test and the type of performing measures.

Characterization

The electrical connections of SoP, the electrical continuity and the proper interconnections resistance were checked by means of Keithley 2400 SMU and visual inspection was performed by the optical microscope integrated on Dimatix printer. The GFETs were characterized at device level by the REDEC group, using an HP4145B semiconductor parameter analyser and at nanoscale level using an Agilent 5500 AFM. The setup allowed to change between these two measurements modes in-situ, this means, inside the AFM, and thus performing nanoscale measurements right after the device was stressed.

5.3.2 Results and discussion

As said, the study consists on the manufacturing of a novel setup for the electrical characterization of GFETs taking advantage of print-on-slope technique. In addition, the GFETs characterization is presented to demonstrate the capability of inkjet technology to hybrid electronic circuit manufacturing.

5.3.2.1 Setup design and manufacturing

The novel setup wire bonding-free is designed to perform CAFM 2D-material characterization. Concerning the characterization that takes place, the novel setup is used to test the graphene material of GFETs fabricated on a silicon die. As above commented, the PCB layout was designed in collaboration with REDEC group.

Following, the layout was adapted to printing condition, i.e. to ink-drop size (10 pl cartridge) and ink-substrate wettability (Silverjet DGP HR on polyimide), by means of specific drop spacing. The PCB layout is designed to test three different GFETs channel length and consists of six connecting strips. The square-shaped electrode located at the layout centre, as shown in (*Figure 5.13 (a)*), is the common bottom Gate electrode of the GFETs. On the left part, there are the source electrode strip, which is common to the three transistors, and two more connecting strips, which correspond to AFM and SMU electrical connections, that will be connected to the common Source strip by means of a external switch. Finally, the final three strips located at the upper-right corner of the PCB layout correspond to three Drain electrodes of three different GFETs. After sintered, the printed circuit is assembled on AFM holder, as shown on *Figure 5.13 (b)*.

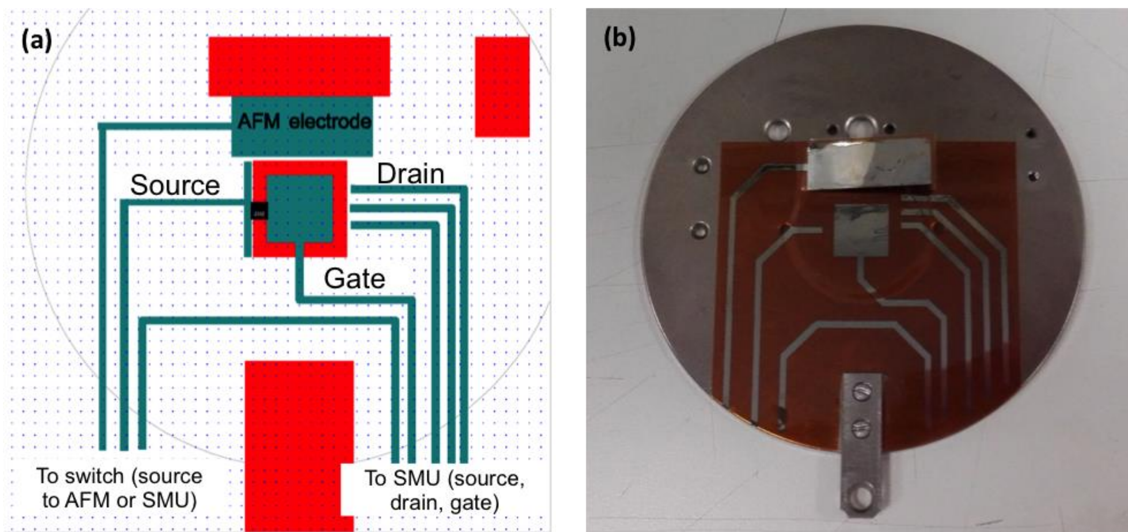

Figure 5.13 (a) Circuit layout. (b) Circuit layout printed on adhesive polyimide and assembled to AFM holder.

Following, as the GFETs must be bottom polarized, the silicon die is silver ink-attached to Gate electrode. Then, the ICA material is manually deposited, forming ramp-shaped terminations, which soften the abrupt staircase between the different height levels circuits (*Figure 5.14 (a,b)*), as well act as mechanical fixations of the silicon die to PCB. The SoP is completed by printing the GFETs connecting circuit and the connections between top and bottom circuit, as shown in *Figure 5.14 (b,c)*. This manufacturing step presented the highest complexity due to the resolution requirements; where GFETs Drain and Source pads are square-shaped with 100 µm side, and the gap between consecutive GFETs are roughly 225 µm. As the PCB layout, the GFETs

interconnections circuit is adapted to printing condition too, i.e. to ink-drop size (1 pl cartridge) and ink-substrate wettability (Silverjet DGP HR on SiO_2), by means of specific drop spacing. Concerning the conductive strips, three prints are required to reduce as much as possible the electrical resistance and hence assure that interconnections resistance is considerable lower than GFETs resistance, which are in the range of units of kΩ. In addition, the electrical conductivity of the ICA assures even more a proper electrical connection between the both different height level circuits.

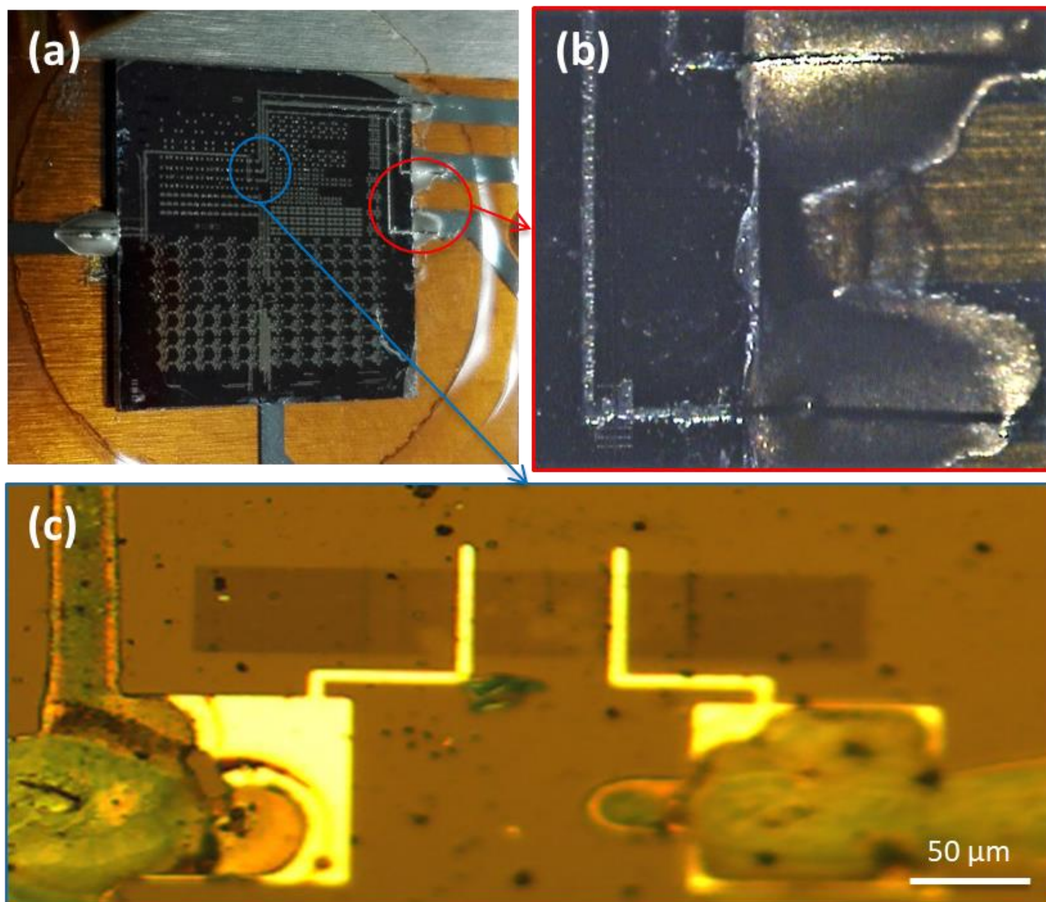

Figure 5.14 (a) Silicon die silver ink-assembled on PCB, ramp-shape ICA fabricated and inkjet-printed silicon die interconnections circuit. (b) Interconnection of a specific GFET of the silicon die inkjet-printed.

Once the inkjet-printed SoP is completely finished the removable parts of the AFM holder are assembled again as shown in *Figure 5.15(a)*. The setup is finished, integrating and connecting the SoP fabricated on the AFM holder to AFM microscope and to SMU. As shown in *Figure 5.15(a),* different colour wires are connected to printed strips by means of ICA and the other wire terminations are assembled in a RJ45 connector. The AFM holder with the SoP integrated is assembled to AFM microscope

as shown in *Figure 5.15(b)* and RJ45-connected to an external switch control unit (*Figure 5.16*), which allows choosing the GFET under test and the type of performing measures (AFM or SMU).

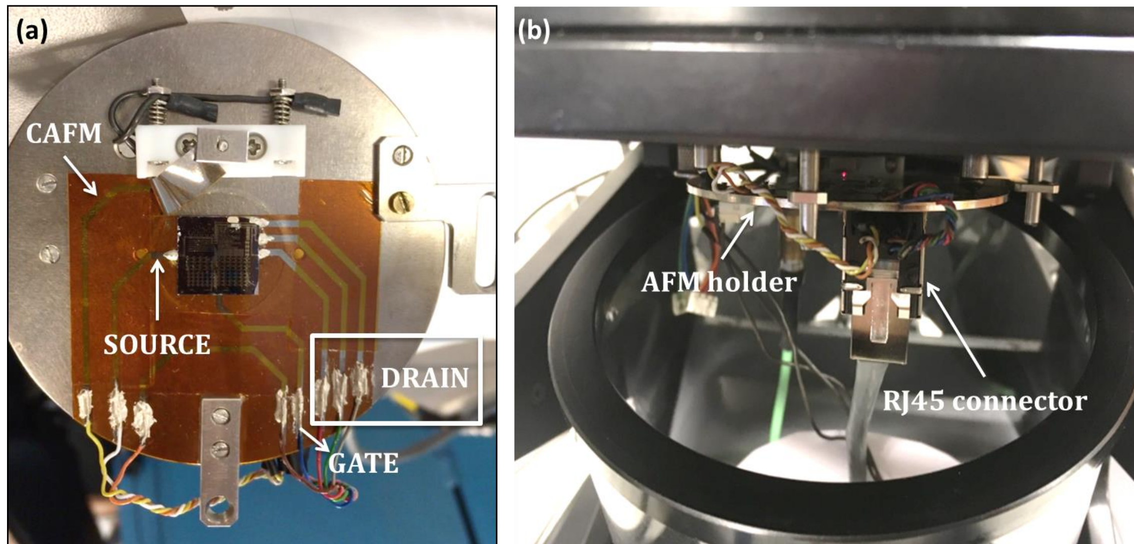

Figure 5.15 (a) SoP inkjet-printed mounted over the AFM holder. (b) Lateral view of the holder inside the AFM with the RJ45 connector.

Figure 5.16 Picture of the external switch control unit where the RJ45 cable is connected. It can be seen a control switch for AFM or SMU measurements, the selector of the three transistors (bottom-left) that selects one of the three drain connections visible on the unit.

Finally, the novel setup is used to perform electrical stress of the graphene transistors and characterize the generated degradation, which is explained in detail at the following section.

5.3.2.2 Material characterization

Now, a brief explanation of the electrical stress applied over the graphene and the characterization of the corresponding effects on it is presented. Concerning the graphene degradation, the stress is performed applying 0.5 V to the Drain electrode and keeping the Source and Gate to 0 V. On the other hand, the material characterization is conducted by AFM, obtaining simultaneously friction and current images. The current image corresponds to the local current outcome of applying -0.05 V to the Gate electrode while the tip (bulk platinum tip of 20 nm of diameter) is ground-connected. Regarding the morphological characterization, the friction channel is the method used instead of the topography channel due its higher contrast in flat materials as graphene. The friction channel consists on analysis of the cantilever torsion and depends on the material present underneath the tip. The *Figure 5.17* and *Figure 5.18* show the electrical current images and the friction images of the drain zone before and after to an electric stress of 16 h.

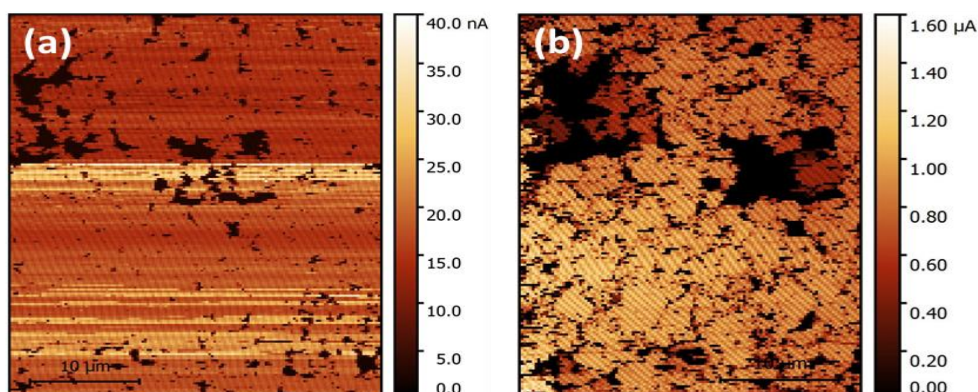

Figure 5.17 (a) Sweep electrical current image of the sample before the stress. (b) The same sample after 16 h of stress. Although the device signal level does not change considerably the graphene layer become heavily damaged during the process.

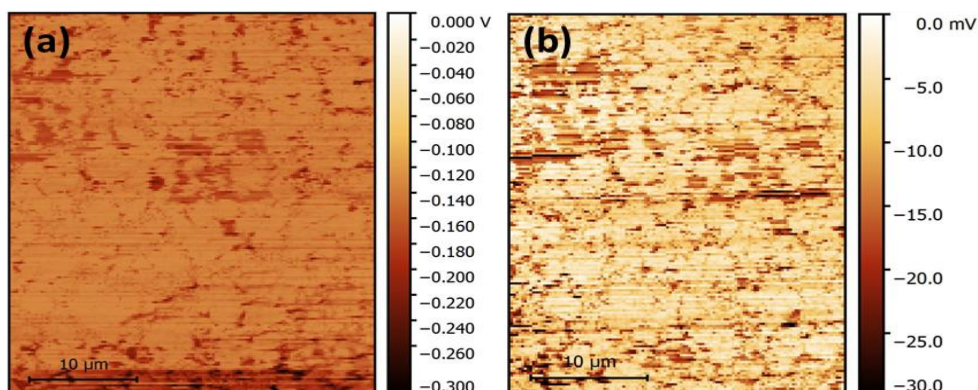

Figure 5.18 (a) Sweep friction image of the sample before the stress. (b) The same sample after 16 h of stress.

Before to apply stress on graphene, the current image shows homogeneous performance at graphene layer, except by some holes (which have the same current level as substrate) and grain boundaries (which could be clearly seen on friction image *Figure 5.18 (a)*). After 16h of stress, the current image shows significant changes at graphene layer, the holes growth significantly (*Figure 5.17 (b))*, as well the grain boundaries are accentuated. The grain boundaries accentuation can be checked at friction image (*Figure 5.18 (b)*), where graphene seems fractured due to grain boundaries growth. The corresponding morphology changes are due to graphene-air exposition, where the carbon sp3 at grain boundaries reacts with O_2 when current is forced through the graphene layer.[20] In addition, different current levels can be seen after degradation (*Figure 5.17 (b)*) in comparison to the homogeneous current level shown before degradation (*Figure 5.17 (a)*). This is known as "disconnection" of these areas after the uncontrolled growth of grain boundaries and holes, which break and weak the graphene layer.

It should be pointed out that the electrical stress is only performed over graphene layer i.e. lateral degradation study. The perpendicular measurements, i.e. the leakage of the insulating layer, SiO_2, at GFET under test cannot be characterized due to the noise contribution of leakage current through the SiO_2 between silver connecting strips and gate electrode. At future works, previous to print the GFETs connecting circuit, an insulating pattern must be inkjet-printed to allow a precise stress over the GFET gate dielectric layer and the corresponding characterization.

In order to perform perpendicular stress, and hence characterise the leakage of the insulating layer, the following GFETs under test should be inkjet-connected with an insulating layer previous to conductive strips.

5.3.3 Conclusions

The silicon die is silver ink-attached to PCB gate electrode by means of inkjet printer and have good adhesion as conductive glue. In addition, the ramp-shape terminations ICA-based are a complementary strategy for soften the abrupt staircase in the different height levels between the silicon die and the PCB. The printed silver ink over the ramp-shape electrodes by print-on-slope technique has good wettability and electrical interconnections.

The 2D connection on ramp-shape terminations gives a better functionality of SoP fabricated for CAFM material characterization than current wire bonding connections. The AFM tip moves over the silicon die without physical obstruction, giving a unique solution at this novel method to characterize degradation.

5.4 References

(1) Putaala, J.; Niittynen, J.; Hannu, J.; Myllymäki, S.; Kunnari, E.; Mäntysalo, M.; Hagberg, J.; Jantunen, H. Capability Assessment of Inkjet Printing for Reliable RFID Applications. *IEEE Trans. Device Mater. Reliab.* **2017**, *17* (2), 281–290.

(2) Tehrani, B. K.; Cook, B. S.; Tentzeris, M. M. Inkjet-Printed 3D Interconnects for Millimeter-Wave System-on-Package Solutions. *IEEE MTT-S Int. Microw. Symp. Dig.* **2016**, *2016–Augus*.

(3) Curious inventors. SMD Soldering Practice Kit - Top Sellers http://store.curiousinventor.com/top-sellers/smd-soldering-practice-kit.html (accessed Feb 13, 2019).

(4) Arrese, J.; Vescio, G.; Xuriguera, E.; Medina-Rodriguez, B.; Cornet, A.; Cirera, A. Flexible Hybrid Circuit Fully Inkjet-Printed: Surface Mount Devices Assembled by Silver Nanoparticles-Based Inkjet Ink. *J. Appl. Phys.* **2017**, *121* (10).

(5) Andersson, H. a; Manuilskiy, A.; Haller, S.; Hummelgård, M.; Sidén, J.; Hummelgård, C.; Olin, H.; Nilsson, H.-E. Assembling Surface Mounted Components on Ink-Jet Printed Double Sided Paper Circuit Board. *Nanotechnology* **2014**, *25* (9), 094002.

(6) Putaala, J.; Hannu, J.; Kunnari, E.; Mäntysalo, M.; Nousiainen, O.; Jantunen, H. Reliability of SMD Interconnections on Flexible Low-Temperature Substrates with Inkjet-Printed Conductors. *Microelectron. Reliab.* **2014**, *54* (1), 272–280.

(7) Niittynen, J.; Kiilunen, J.; Putaala, J.; Pekkanen, V.; Mäntysalo, M.; Jantunen, H.; Lupo, D. Reliability of ICA Attachment of SMDs on Inkjet-Printed Substrates. *Microelectron. Reliab.* **2012**, *52* (11), 2709–2715.

(8) Rivera J; Peitivi A; Llorente S; Arrese X; Servera L; Cirera A. Dispositivo de Aparato Doméstico y Procedimiento Para La Fabricación de Un Dispositivo de Aparato Doméstico. *ES 2 564 760 A1* **2014**.

(9) Beer, G. D2_US2006197220A1.Pdf, 2006.

(10) Mäntysalo, M.; Mansikkamäki, P.; Miettinen, J.; Kaija, K. Evaluation of Inkjet Technology for Electronic Packaging and System Integration. In *Electronic components and technology conference*; 2007; Vol. c, pp 89–94.

(11) Miettinen, J.; Pekkanen, V.; Kaija, K.; Mansikkamäki, P.; Mäntysalo, J.; Mäntysalo, M.; Niittynen, J.; Pekkanen, J.; Saviauk, T.; Rönkkä, R. Inkjet Printed System-in-Package Design and Manufacturing. *Microelectronics J.* **2008**, *39* (12), 1740–1750.

(12) Pekkanen, V.; Mäntysalo, M.; Kaija, K.; Mansikkamäki, P.; Kunnari, E.; Laine, K.; Niittynen, J.; Koskinen, S.; Halonen, E.; Caglar, U. Utilizing Inkjet Printing to Fabricate Electrical Interconnections in a System-in-Package. *Microelectron. Eng.* **2010**, *87* (11), 2382–2390.

(13) Tong, G.; Jia, Z.; Chang, J. Flexible Hybrid Electronics: Review and Challenges. *Proc. - IEEE Int. Symp. Circuits Syst.* **2018**, *2018–May*, 1–5.

(14) Novoselov, K. S.; Geim, A. K.; Morozov, S. V; Jiang, D.; Zhang, Y.; Dubonos, S. V; Grigorieva, I. V; Firsov, A. A. Electric Field Effect in Atomically Thin Carbon Films. *Science* **2004**, *306* (5696), 666–669.

(15) Mounet, N.; Gibertini, M.; Schwaller, P.; Campi, D.; Merkys, A.; Marrazzo, A.; Sohier, T.; Castelli, I. E.; Cepellotti, A.; Pizzi, G.; et al. Two-Dimensional Materials from High-Throughput Computational Exfoliation of Experimentally Known Compounds. *Nat. Nanotechnol.* **2018**, *13* (3), 246–252.

(16) Stankovich, S.; Dikin, D. A.; Dommett, G. H. B.; Kohlhaas, K. M.; Zimney, E. J.; Stach, E. A.; Piner, R. D.; Nguyen, S. B. T.; Ruoff, R. S. Graphene-Based Composite Materials. *Nature* **2006**, *442* (7100), 282–286.

(17) Yang, K.; Zhang, S.; Zhang, G.; Sun, X.; Lee, S. T.; Liu, Z. Graphene in Mice: Ultrahigh in Vivo Tumor Uptake and Efficient Photothermal Therapy. *Nano Lett.* **2010**, *10* (9), 3318–3323.

(18) Schwierz, F.; Pezoldt, J.; Granzner, R. Two-Dimensional Materials and Their Prospects in Transistor Electronics. *Nanoscale* **2015**, *7* (18), 8261–8283.

(19) Illarionov, Y. Y.; Smith, A. D.; Vaziri, S.; Ostling, M.; Mueller, T.; Lemme, M. C.; Grasser, T. Bias-Temperature Instability in Single-Layer Graphene Field-Effect Transistors. *Appl. Phys. Lett.* **2014**, *105* (14), 143507.

(20) Zhang, H.; Lee, G.; Gong, C.; Colombo, L.; Cho, K. Grain Boundary Effect on Electrical Transport Properties of Graphene. *J. Phys. Chem. C* **2014**, *118* (5), 2338–2343.

TEST AND CHARACTERIZATION OF INSULATING MATERIALS FOR HYBRID MULTILAYER INKJET-PRINTED PCB

CHAPTER 6

6.1 Motivation

At chapter 3, a novel inkjet method for assembling SMDs has been proposed and encouraging results were obtained on both, mechanical and electrical properties. In addition, at chapters 4 and 5, aiming to improve the SMDs assembling performance, different strategies have been tested in order to strengthen the joints and fulfil the application requirements on reliability and quality. These previous thesis work was performed onto monolayer circuits. However, the current printed circuits boards consist on multilayer circuits. Therefore, in order to approach as much as possible the performance of the inkjet-printed circuits to the present PCBs, much effort on multilayer inkjet manufacturing must be conducted. Additive manufacturing/rapid prototyping of multilayer PCB avoid wastage and tedious manufacturing steps of traditional PCB technology such as etching, stacking and laminating (*Figure 6.1*).[1]

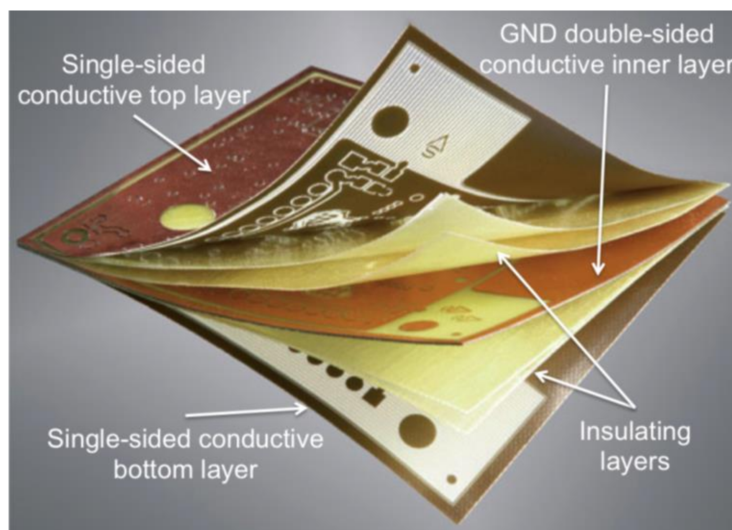

Figure 6.1 Traditional PCB technology.

The rapid prototyping feature of inkjet-printed could be an enormous benefit at electronic circuits development process and hence ensures huge benefits for the whole electronics designers. In addition, the additive manufacturing techniques added a considerable purport for the electronic designers companies, which can guard their intellectual property, avoiding the outsourcing, at least on prototypes design phase.[1] Regarding this, some companies presented pioneering solutions,[1] as Nano Dimension, which manufacture 3D PCBs by means of inkjet printer (Dragonfly) with layer by layer

sintering (*Figure 6.2*).[2] Nowadays, the prototyping market has an estimated value about $60-90 billions.[1]

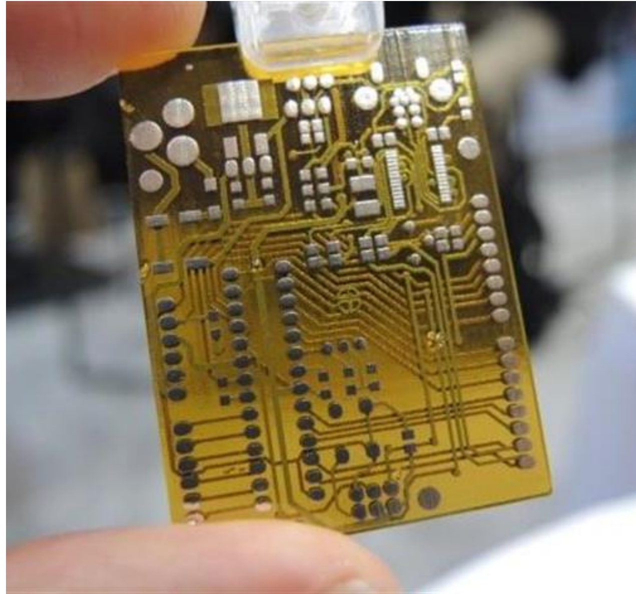

Figure 6.2 Multilayer inkjet-printed circuit board of Nano Dimension. Image from[2]

As commented in this thesis, the high demand of smart electronics integration on the daily life objects/tools, promotes a new generation of printed circuit boards that are developed on flexible, stretchable and thermoformable substrates.[3,4,5,6,7] Focusing on this new concept of PCBs, part of the currently used electronics could be replaced by flexible electronics based on paper substrate, which has attracted considerable attention as environmentally friendly, bendable, lightweight and low cost. To date, there are several works regarding paper electronics that perform electronic components such as smart pixels,[8] memory devices,[9] capacitors,[10] thin film transistors,[11] batteries,[12] photovoltaic devices[13] and touch detectors[14]. In order to contribute to this oncoming electronics, the tests with insulating materials have been performed on paper substrate.

Dielectric inks play a crucial-essential role on both, 3D multilayer PCB and single components manufacturing. The requirements for dielectric materials characteristics vary depending on the final application work conditions. Dielectric materials are used as insulators between strips and strips-ground on PCBs or into integrated circuits,[15,16,17,18,19] as well as electrical insulator on embedded devices.[20] Low relative permittivity, low dielectric loss tangent and high dielectric strength are three

fundamental parameters to be assured by the insulating material used on PCB technology. Dielectric materials are also employed in electronic components such as capacitors or transistors, [10,11,21] where high relative permittivity and low loss characteristics are required.

Several works presented the use of dielectric inks on different substrates employing additive techniques,[17,22,23] but to the best of our knowledge, to date there is not work that combines dielectric inks inkjet-printed over paper substrate. Verónica Sánchez-Romaguera *et al.* proved metal-insulator-metal crossovers with SU-8 polymer insulator onto glass substrate.[17] Myung-sung Hwang *et al.* characterised the dielectric properties of inkjet-printed alumina-resin hybrid films within copper plates.[22] Induja I. Jayapalan Nair *et al.* characterized dielectric properties of alumina films obtained by means screen printing on photographic paper and biaxially-oriented polyethylene terephthalate (BoPET) substrates.[23]

In this work, aiming to contribute on the paper PCBs manufacturing progress, a study focused on dielectric materials inkjet-printed on coated paper is presented. In addition, the tests are also performed on glass substrate, as reference. The dielectric materials tested are SiO_2, Al_2O_3, and 4-Poly(4-vinyl phenol) (PVP). The choice of the inorganic dielectric materials is related to their insulating properties and commonly use in standard electronics, while PVP is selected for its insulating properties and emerging use on printed electronics. The dielectric materials are characterized through inkjet-printed metal-dielectric-metal (MIM) multilayer structure. Therefore, the reliability of MIM structures is studied; as their relative permittivity, loss tangent and dielectric strength parameters.

6.2 Metal-Insulator-Metal structures

6.2.1 Materials

All the experimental tests were carried out by means of a printer machine Dimatix 2831 model series (Fujifilm USA). Cartridge with an ink droplet volume fixed at 10 pl was used. Silverjet DGP HR (ANP, South Korea) was applied for the conductive electrodes, xdi-cds 4-Poly(4-vinyl phenol) ink (Xerox, Canada) Al_2O_3 ink and SiO_2 ink were used as interlayer dielectric inks. To ensure a drop jetting reliability, the inks used were

chosen or prepared with viscosity range around 10-12 cPs and surface tension range between 28-33 mN/m, which are the rheological range parameters for Dimatix printheads. *Table 6.1* summarizes some of the rheological parameters of the selected inks for this work.

Table 6.1 Rheological parameters

Ink	Concentration w/w	Viscosity	Surface tension
Silverjet DGP	~40	~16	35,6
Al_2O_3	~15	~12-14	~28-30
SiO_2	~32	~12-14	~28-30
PVP (Xdi-cds)	12-13	8-9	24-25

The Al_2O_3 and SiO_2 inks were prepared dispersing the respective nanoparticles in the main vehicle based on solvents and additives that promote chemical stability (approximate concentration in *Table 6.2*)

Table 6.2 Alumina and Silica ink compounds in % (w/w).

Component	Ceramic powder	Non-polar solvent	Polar solvent	Dispersant	Additives
Al_2O_3 ink	15	60-70	5-7	6-8	0,5-2
SiO_2 ink	32	50-60	3-5	5-7	0,5-2

As commented on chapter 2, the printing parameters depend on the rheological properties of the inks (Table 6.3). Wettability, pattern resolution and adhesion of the deposited material can be promoted by tuning correctly these printing parameters. The surrounding experimental conditions during printing processes were room temperature and humidity.

Table 6.3 Printing parameters

Component	V_{nozzle} (V)	T_{nozzle} (˚C)	T_{platen} (˚C)	Drop Spacing (µm)
Ag	17-20	27-35	27-35	30
Al_2O_3	19-22	30-40	30-40	40
SiO_2	19-24	30-40	30-40	40
PVP	20-24	≈ 25*	≈ 25*	30

The substrates used to perform this work were paper substrate Powercoat 230 (Arjowiggins, USA) with a thickness of 222 µm and organic coating around ~15 µm and glass microscope slide (from Labbox Labware) substrate.

6.2.2 Procedure

Prior to the printing process, standard cleaning of the surface substrates was carried out, as mentioned on chapter 3. Ag bottom electrodes of ~1 mm^2 were Ag inkjet-printed on paper and glass substrates with an average thickness of ~1 µm and ~500 nm, respectively. The samples were thermally cured in an oven at 150 °C for 30 minutes. This thermal process facilitate, first, the evaporation of the organic ink solvents and, then, the sintering of the silver nanoparticles achieving a resistivity around 16 µΩ·cm, a value among the best values found in the literature.[24, 25, 26]

Dielectric layer of 0.6 mm^2 was printed onto the bottom silver electrodes. Five different fully inkjet-printed MIM structures are proposed, from devices employing a single dielectric material (Al_2O_3, SiO_2, PVP) to more complex structures where two dielectrics are mixed (Al_2O_3-PVP, SiO_2-PVP). The following *Figure 6.3* shows the 5 different dielectric structures tested.

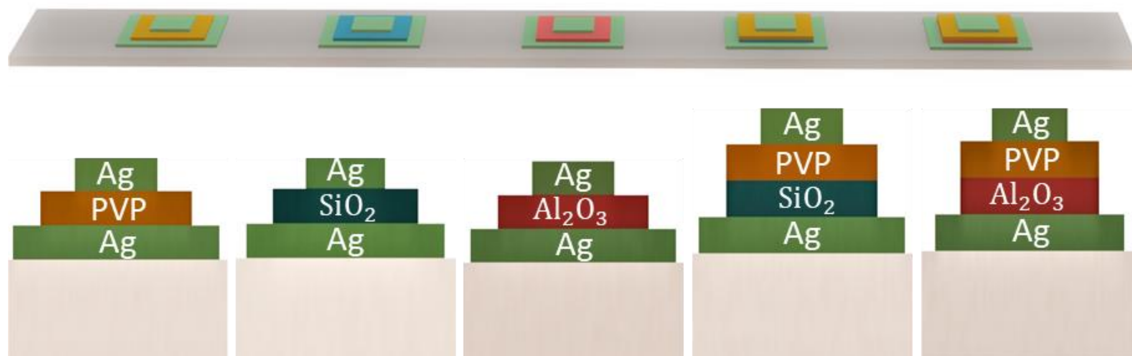

Figure 6.3 Structure of printed devices used for dielectric test.

For each structure, six different dielectric thicknesses and 10 samples for each thickness were fabricated to conduct the study. A total of 600 samples, 300 on paper and 300 on glass. Regarding the heterogeneous dielectric structures, the last inkjet-printed layer, before top electrode, is the PVP, which is ejected on top of the inorganic materials, Al_2O_3 or SiO_2. Dissimilar thermal curing/sintering processes were applied according to

the dielectric material. For the inorganic compounds, the insulator was firstly dried in an oven at 50 °C during 12 hours to avoid cracks. Following, a second thermal treatment was performed in an oven at 120 °C during 2 hours at a rate of 2 °C/min. For the polymer layer, the deposit was dried 10 minutes at 80 °C and polymerized at 140 ˚C for 30 minutes.

To complete the multi-layered structures, a 0.3 mm^2 top silver electrode was inkjet-printed and thermally cured/sintered following the same process as bottom electrode. It should be pointed that each different material deposited was sintered or polymerized previous add new one.

6.2.3 Characterization

Dielectric performance and reliability were tested by means of capacitance-voltage (*C-V*), conductance-voltage (*σ-V*) and leakage current-voltage (*J-V*). These measurements were performed by means of an Agilent Technologies B1500A Semiconductor Device Analyzer.

The capacitance-voltage and conductance-voltage were tested at frequencies from 1 kHz to 1 MHz, and DC voltage biases in the range from -2 V to +2 V. The real part of relative permittivity (hereinafter, relative permittivity) was calculated for each single MIM, and for each frequency tested by means of capacity-dielectric thickness dependence for a two parallel planar capacitor, defined by the equation *(6.1)*:

$$C = \frac{\varepsilon_0 \varepsilon_r A}{d} \quad (6.1)$$

Where C is capacitance, ε_0 is the vacuum permittivity, ε_r is the relative permittivity of the medium, A is the area of the electrode and d the distance between electrodes. Expressing the equation as *(6.2)*, we extracted the ε_r from the slope of the curve C(1/d) for each frequency tested.

$$\frac{C}{\varepsilon_0 A} = \frac{\varepsilon_r}{d} \quad (6.2)$$

Moreover, dielectric loss tangent was deduced from capacitance-voltage and conductance-voltage measurements, as shown in the equation *(6.3)*:

$$\tan\delta = \frac{G}{f2\pi C} \tag{6.3}$$

Where $\tan\delta$ is the loss tangent, G is the conductance, f is the frequency of the electric field applied and C is the capacitance.

Dielectric strength was determined by means of leakage current-voltage curves performed in the range from 0 V to 100 V, where 100 V is far away from low-power electronic applications on paper. Dielectric strength was deduced from breakdown voltage divided by the thickness of the dielectric.

From equation *(6.2)*, the thickness of the printed dielectrics must be known to extract the ε_r and the dielectric strength. Therefore, thicknesses were measured using a Focused Ion Beam (FIB)-assisted field-emission scanning electron microscopy (FE-SEM) (FEI dual beam STRATA 235). Furthermore, confocal microscope (Leica) was also used to corroborate the homogeneity of thickness.

6.3 Results and discussion

The electronic circuits and components contain dielectric materials, which, due to their different chemical and electrical properties, are used on several dissimilar applications, as insulating layers on inkjet-printed paper PCBs. To this purpose, dielectric materials with ideally low relative permittivity, low loss tangent and high dielectric strength are the best option. In order to evaluate the feasibility and the electrical properties of the proposed dielectric materials, the MIM structures were inkjet-printed on both, paper and glass substrates, respectively.

6.3.1 Feasibility

The standard paper substrates currently used for printed electronics applications, as Powercoat 230 (Arjowiggins), show low chemical and thermal durability compared to silicon technology. In this work, the selected paper substrate presents a dimensional

variation due to the thermal contraction, which is reported by the manufacturer as a substrate characteristics (shrinkage of ~ -1% at 200 ˚C / 5 min).[27] Due to that, after consecutive thermal processes, some cracks on paper coating are observed (*Figure 6.4*) and hence on deposited layers too (*Figure 6.5*). *Figure 6.6* shows two cracks, which demonstrate that they can appear along the fully inkjet-printed MIM device. Cracks are also appeared in inorganic dielectric layers printed on glass substrate, but smaller and thinner, which means that cracks are also produced by drying process. Therefore, the optimization of the thermal curing process is necessary to ensure high reliability of the inkjet-printed layers.

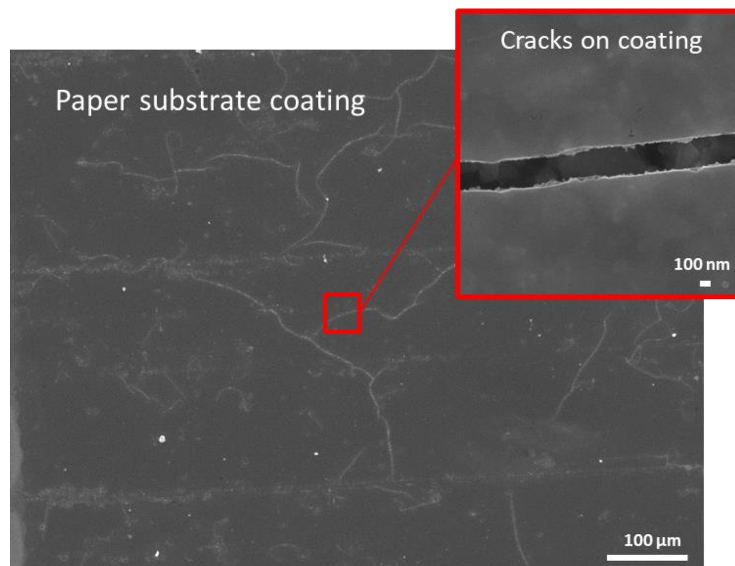

Figure 6.4 SEM image of cracks generated on paper coating after thermal treatment used to dry, sinter or polymerize the functional deposits.

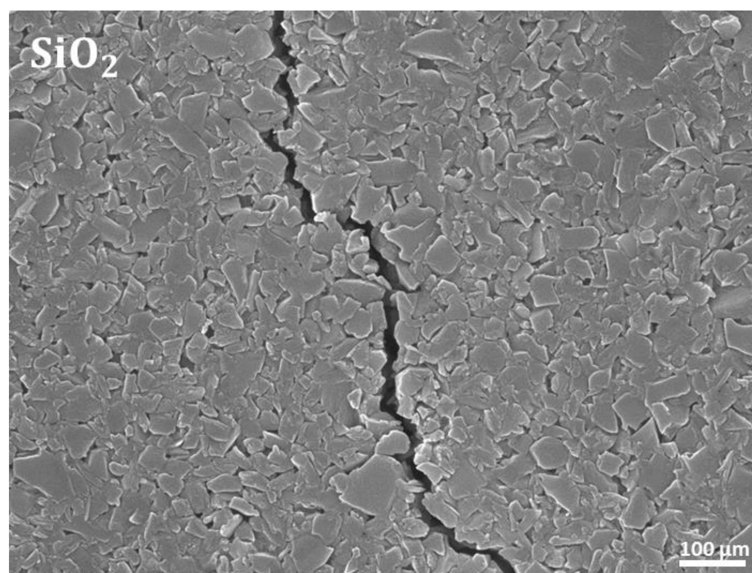

Figure 6.5 SEM image of cracks appeared on dried inorganic deposits on paper, which could be due to either substrate or deposit contraction.

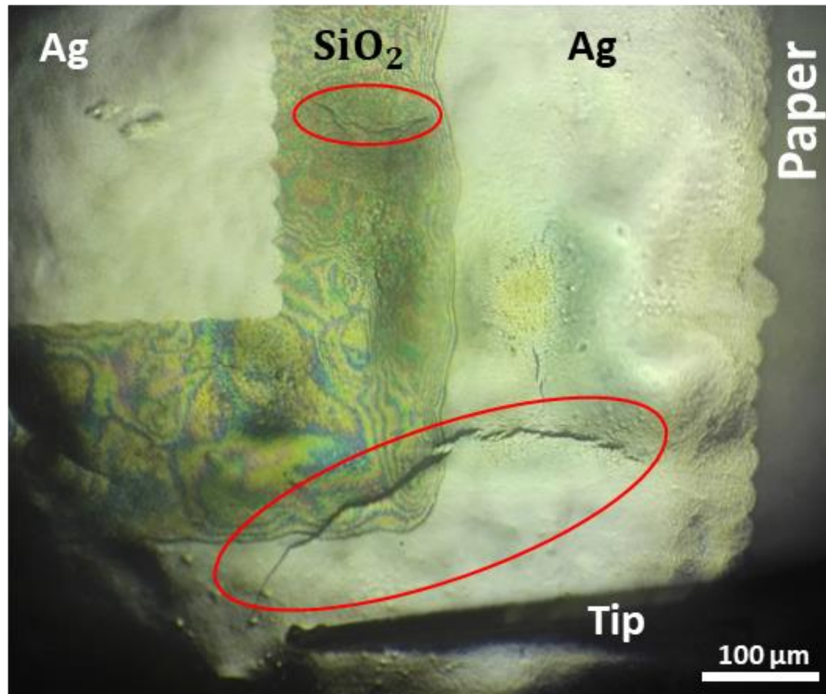

Figure 6.6 Optical image of Ag - SiO_2- Ag MIM printed on paper substrate with cracks on the electrode and the dielectric layers. The Ag - Al_2O_3 - Ag MIMs show similar performance.

On continuation, 10 MIM devices for each specific dielectric configuration are studied. The feasibility of the different insulating materials tested is determined as the percentage of the not deficient MIMs. A MIM device is considered as deficient or failure when presents short-circuit performance. The results are summarized in the following *Table 6.4* and the corresponding thicknesses to each dielectric layer are also reported.

Table 6.4 Feasibility of the printed MIM devices on paper substrate expressed as a percentage (%) of 10 samples and the corresponding thickness of the printed insulators.

	SiO_2		SiO_2+PVP		Al_2O_3		Al_2O_3+ PVP		PVP	
Layers	**F(%)**	**t (µm)**	**F(%)**	**t (µm)**	**F(%)**	**t (µm)**	**F(%)**	**t (µm)**	**F(%)**	**t (µm)**
1	0	1.00	100	1.40	0	0.30	100	1.10	0	0.70
2	50	2.00	100	2.58	0	0.60	90	1.40	100	1.40
3	70	3.03	100	3.26	0	0.90	90	1.60	100	2.18
4	70	4.13	100	4.26	60	1.20	90	2.00	100	2.95
5	80	5.12	100	5.60	80	1.50	90	2.30	100	3.60
6	100	6.20	100	6.80	90	1.80	90	2.60	100	4.30

From *Table 6.4*, it can be concluded that the tested inorganic dielectric materials show low feasibility on paper substrate. Several print-passes are needed to assure an acceptable reliability for SiO_2, while Al_2O_3 presents poor performance even after 6 print-passes. The observed short-circuit on the defective devices is due to the conductive paths generated by silver ink percolation through insulator cracks at the top electrode-printing step. As previously mentioned, cracks are promoted by paper substrate thermal contraction and by inorganic layer drying process. Among the inorganic inks tested, the SiO_2 ink shows the best reliability, which is due to thicker layer of SiO_2 than Al_2O_3 is deposited at single print (*Table 6.4*). This is in accordance with the *Table 6.1* and *Table 6.3*, where silica ink shows twice of solute concentration (w/w) than alumina ink, and the same drop spacing is used as printing parameter.

In order to avoid the devices in short-circuit originated by cracks, heterogeneous structures were tested, as considered by Myung-sung Hwang and co-workers.[22] In our work, heterogeneous multilayer of ceramics-polymer inkjet-printed is tested to approach the electrical properties of ceramics to the coated paper substrates.[22] The heterogeneous structure tested consist on a last single print of PVP, with a thickness around 700 nm, which is printed above inorganic material and previous to print the top conductive electrode. This PVP layer was proposed as short-circuit protector, and its function was to fill the dielectric layer cracks and voids. The efficiency of that barrier is demonstrated, in fact all the devices done with inorganic insulator and PVP barrier were in open circuit from the thinnest inorganic insulator, as shown on *Table 6.4*. The heterogeneous structure shows similar performance on glass substrate (*Table 6.5*).

The feasibility of PVP as insulating material shown on *Table 6.4* is in accordance with the reported in literature.[28,29] The PVP shows an excellent result considering that after double printing pass thickness, about 1.5 μm, all printed devices are working properly, which means high reliability performance. The polymerized PVP deposit top view shows continuous layer without cracks (*Figure 6.7 (a)*). However, looking at the PVP borders on paper substrate, the cracks appear surrounding the frontier between dielectric and the bottom electrode, and this could be due to dissimilar contraction between the deposited material and the substrate. Despite of that, all devices perform correctly. In comparison to paper substrate, at glass substrate the MIMs not show cracks, which is shown on *Figure 6.7 (b)*.

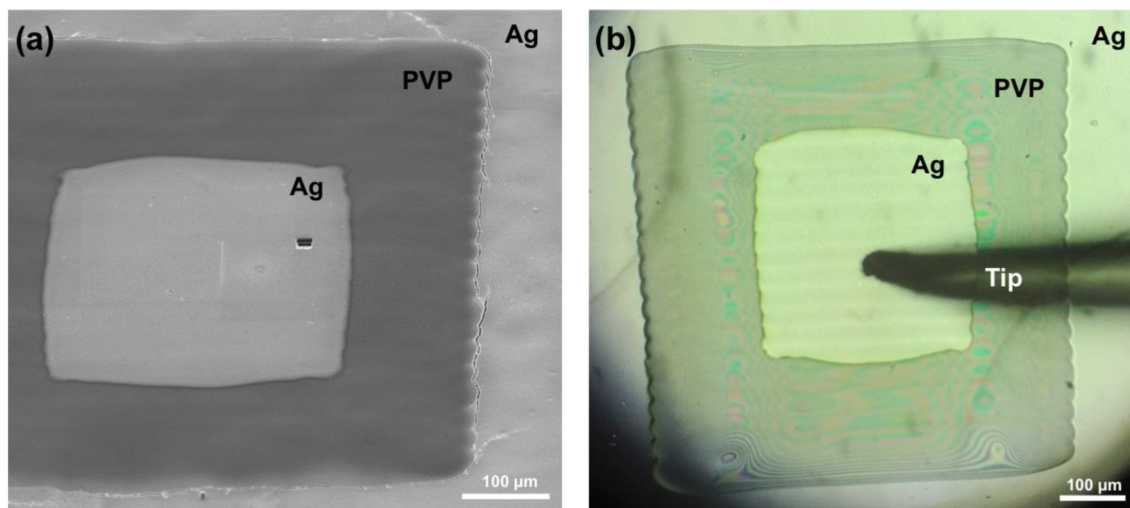

Figure 6.7 PVP insulating material. (a) SEM image of Ag-PVP-Ag MIM on paper substrate, which shows cracks at frontier between dielectric and the bottom electrode. (b) Optical image of Ag-PVP-Ag MIM on glass substrate, which shows the absence of cracks.

Following, the feasibility study is also performed on glass substrate, and the results are summarized in the following *Table 6.5* and the corresponding thicknesses to each dielectric layer are also reported.

Table 6.5. Feasibility of the printed MIM devices on glass substrate expressed as a percentage (%) of 10 samples and the corresponding thickness of the printed insulators.

	SiO_2		SiO_2+PVP		Al_2O_3		Al_2O_3+PVP		PVP	
Layers	**F(%)**	**t (µm)**	**F(%)**	**t (µm)**	**F(%)**	**t (µm)**	**F(%)**	**t (µm)**	**F(%)**	**t (µm)**
1	30	1	100	1.24	0	0.30	100	1.10	100	0.70
2	100	2	100	2.30	0	0.60	100	1.40	100	1.43
3	100	3	100	3.30	50	0.90	100	1.60	100	2.16
4	100	4	100	4.45	80	1.20	100	2.00	100	2.87
5	100	5	100	5.50	100	1.50	100	2.30	100	3.43
6	100	6	100	6.30	100	1.80	100	2.60	100	4.39

Regarding the structures printed with inorganic materials on glass substrate, the performance is significantly better (*Table 6.5*) than reached over paper substrate. Therefore, the cracks associated to paper contraction represent the main drawback of the printing on paper substrate. In addition, the PVP ink on glass substrate shows also better performance (*Table 6.5*) than reached over paper substrate. This better reliability on glass substrate is the expected, because glass substrate is rigid and stable below 170 ˚C,

thus the deposits are not subjected to substrate deformation. Furthermore, the significant reduction of roughness of glass substrates compared to paper substrate improved the homogeneity thickness of the printed dielectric layers.

Among the tested dielectric structures, the best results accomplished on paper substrate in terms of reliability are reached with heterogeneous dielectric structure and with PVP as unique dielectric material. In the same way, similar behaviour is obtained on glass substrate, which is used as reference of ideal substrate.

6.3.2 Relative permittivity and loss tangent

In this study different dielectric materials deposited by means inkjet were tested with the aim of quantify their performance as insulating materials for multilayer PCBs fabricated on paper substrate. Typical physical properties of dielectrics materials are their relative permittivity and energy losses, which are frequency-dependent to electromagnetic field applied across them. As well known, relative permittivity is expressed by means of a complex number:

$$\varepsilon_r(\omega) = \varepsilon_r'(\omega) - i\varepsilon_r''(\omega) \tag{6.4}$$

The real part ε_r' corresponds to the polarization capacity of the medium and the imaginary part ε_r'' describes the dissipation of the electrical energy due to different physical processes. Furthermore, the loss tangent ($\tan\delta$) is also a magnitude used to quantify dissipation of electromagnetic field, and is given by:

$$\tan\delta\,(\omega) = \frac{\varepsilon_r''(\omega)}{\varepsilon_r'(\omega)} \tag{6.5}$$

On this section the relative permittivity and loss tangent performance of proposed materials are discussed and the frequency-dependence of these parameters are presented. The relative permittivity is strongly dependent on porous size, shape and concentration.[30] In all cases studied, the slightly decrease of the relative permittivity over the frequency range from 1 kHz to 1 MHz, is due to the ionic polarization and the

specific dipole mobility of each dielectric material tested.[31] The dipole orientation of the tested films varies significantly with the amount of moisture trapped in the film, where the physisorbed and/or chemically bounded moisture depends on film porosity.[30] Another molecules that can contribute to dipole polarization regime are the ink organic additives, which are not completely removed at sintering or polymerizing process.[23] Conductive phenomena can also contribute to energy losses.[31,32] In fact, when the top Ag electrode is inkjet-printed, the low-viscosity (<10 cP) of the Ag-ink allow that ink penetrates through the cracks forming a leakage micro-paths.[22]

On continuation, the relative permittivity and the energy losses of the dielectric materials tested are characterized over the frequency range from 1 kHz to 1 MHz. Following, the *Figure 6.8* is the graphs of the relative permittivity and loss tangent performed by PVP MIM devices on paper and glass substrate.

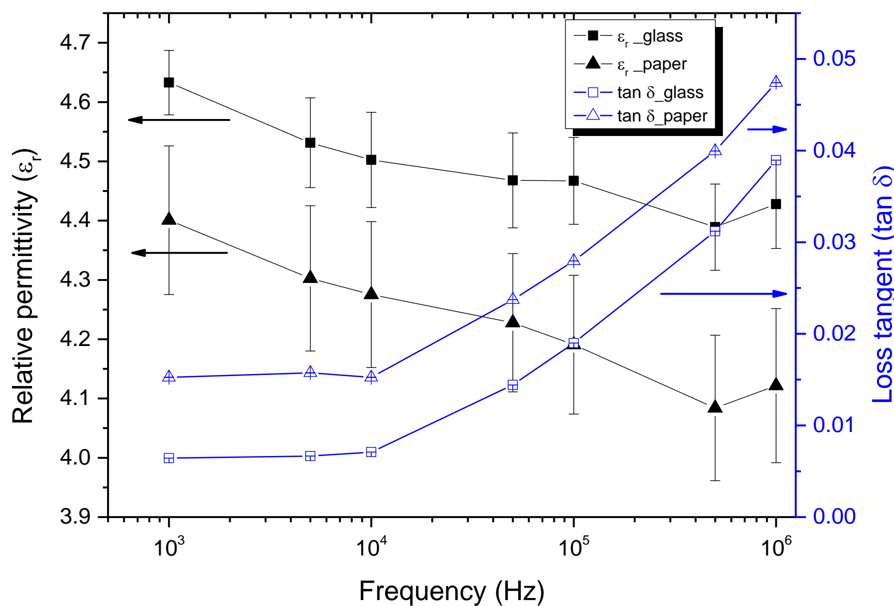

Figure 6.8 Relative permittivity and loss tangent of PVP MIM devices on paper and glass substrates

As shown on Figure 6.8, the values of ε_r are comparable with values found on literature $\varepsilon_r(\mathrm{PVP}) = 4{,}7$.[33] As commented above, the slightly difference of ε_r in comparison with the corresponding bulk material value found on the literature could be due to the presence of organic additives, which are not completely removed at polymerizing process and/or to the substrate contribution.[23] On the other hand, the outcome on paper substrate is similar to the performance shown at the reference (glass) substrate, with slightly difference on ε_r. This difference could be originated by associated error on the

insulating thickness estimation due to layer thickness inhomogeneity, by associated error estimation of the capacitor effective area due to some sort of delamination produced on paper substrate (*Figure 6.7*) and/or by the slightly lower value of capacity and higher value of conductance performed by the PVP MIMs on paper substrate. If delamination is occurred, the effective capacity area is overestimated and hence the relative permittivity underestimated. In addition, the relative permittivity could also vary depending on the substrate/electrode effect on dipole orientation. Regarding the energy losses, the slightly differences measured between the PVP MIMs printed on paper and glass is due to the lower value of capacity and higher value of conductance performed by the PVP MIMs on paper substrate. In addition, the value of the loss tangent achieved by PVP MIMs at 1 MHz, roughly 0.04, is significantly higher than the loss tangent performed (0.017-0.020)[34] by the glass-reinforced epoxy laminate material (FR4), currently used at PCB fabrication.

On continuation, the relative permittivity and the energy losses of the inorganic materials tested on paper and glass substrate are shown. The *Figure 6.9* and *Figure 6.10* correspond to the graphs of the relative permittivity and loss tangent of the SiO_2 MIM devices on paper and glass, respectively. For other hand, The *Figure 6.11* and *Figure 6.12* correspond to the graphs of the relative permittivity and loss tangent of the Al_2O_3 dielectric material on paper and glass, respectively.

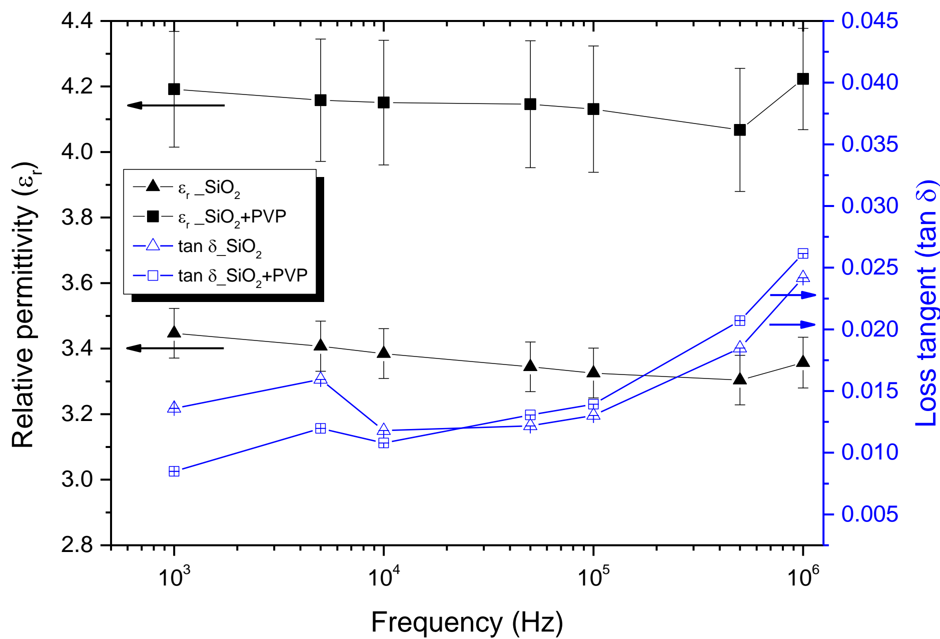

Figure 6.9 Relative permittivity and loss tangent of SiO_2 MIMs and SiO_2 + PVP MIMs on paper substrate.

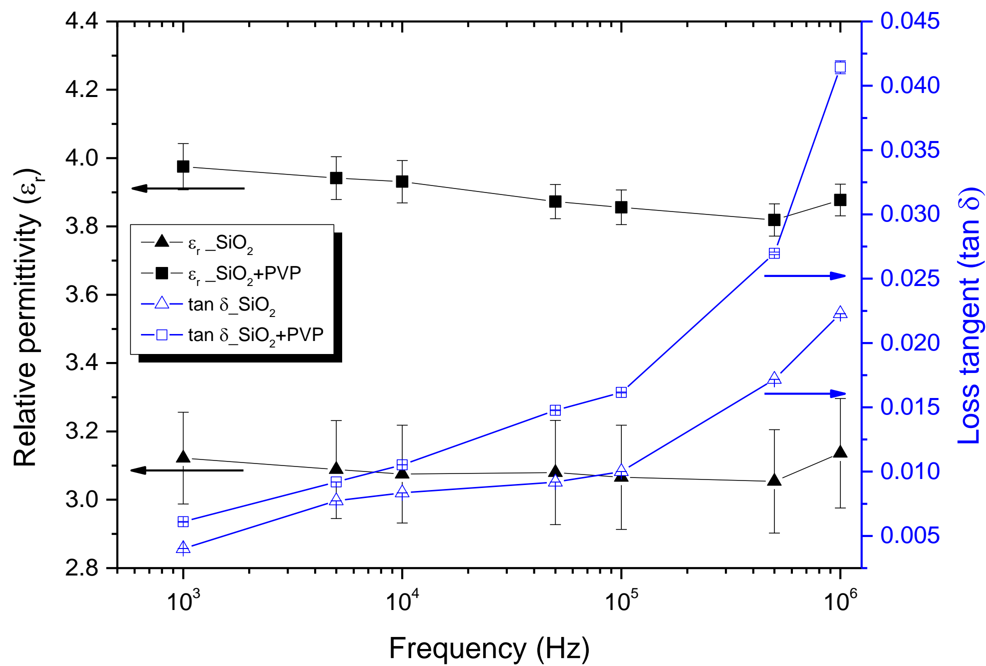

Figure 6.10 Relative permittivity and loss tangent of SiO_2 MIMs and SiO_2 + PVP MIMs on glass substrate.

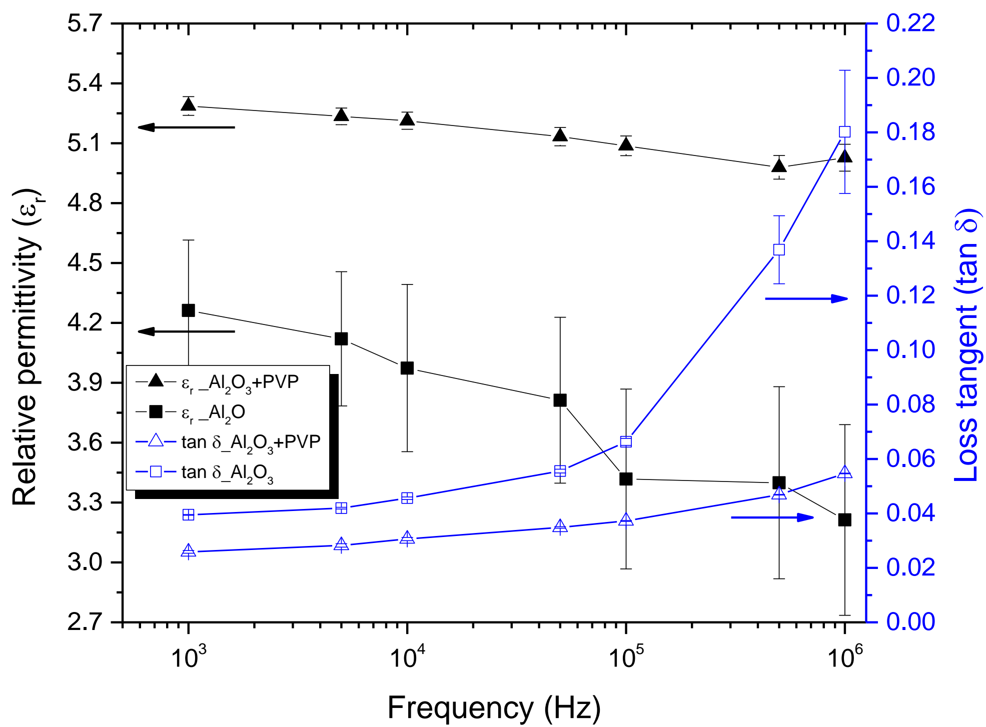

Figure 6.11 Relative permittivity and loss tangent of Al_2O_3 MIMs and Al_2O_3 + PVP MIMs on paper substrate.

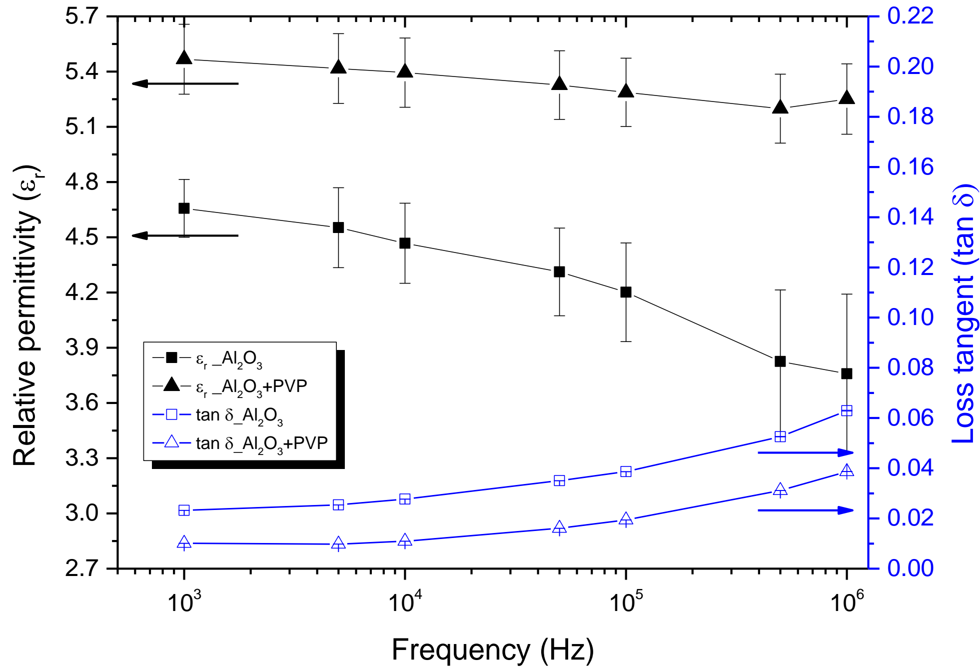

Figure 6.12 Relative permittivity and loss tangent of Al_2O_3 MIMs and Al_2O_3 + PVP MIMs on glass substrate.

The inorganic materials tested, SiO_2 and Al_2O_3, present lower relative permittivity than their bulk materials, which is explained by the nanoparticle-based of the deposited layer. As known, SiO_2 and Al_2O_3 have sintering temperatures unattainable for paper substrate. Thus, the drying process at 150 °C produces porous dielectric layers that consist on a composite of air voids, organic additives not removed and a low sintered matrix of nanoparticles, as shown below on *Figure 6.13* and *Figure 6.14*.

Regarding SiO_2 on paper substrate (*Figure 6.9*), the porous dielectric layer shows a relative permittivity around $\varepsilon_r(\mathrm{SiO_2}) = 3.4$. This outcome is the contribution of $\varepsilon_{r_{\mathrm{air}}} = 1$, organic additives and $\varepsilon_{r_{\mathrm{bulk}}}(\mathrm{SiO_2}) = 3{,}9$. Concerning the heterogeneous dielectric layer, the relative permittivity shown is around $\varepsilon_r(\mathrm{SiO_2} + \mathrm{PVP}) = 4.2$, where the PVP fills part of the SiO_2 layer porosity. The relative permittivity achieved is comparable to the performed by the current substrate used at PCB fabrication, which is about 4.2-4.6.[34] In addition, the performance of ε_r and loss tangent is comparable to the performance shown on glass substrate (*Figure 6.10*). The slightly differences observed could be originated by the insulating material thickness estimation, as well of the higher presence of cracks on paper substrate than on glass substrate, which could alter also the layer thickness. The value of the loss tangent achieved by SiO_2 MIMs at 1 MHz,

roughly 0.025, is similar to the loss tangent performed by FR4 substrate used at PCB fabrication, which is about 0.017-0.020.[34]

Regarding the Al_2O_3 on paper substrate (Figure 6.11), the porous dielectric layer shows a relative permittivity significantly lower than the bulk, $\varepsilon_{r_{bulk}}(Al_2O_3) = 9{,}6$. This considerable reduction of relative permittivity could be related on the specific porosity of this insulating layer, and/or on the error associated to effective capacity area estimation. Concerning the effective capacity area estimation, the Al_2O_3 deposits show higher presence of cracks than SiO_2, thus effective capacitive area could be overestimated and hence the relative permittivity underestimated. Moreover, the increment of cracks contributes significantly on conductive phenomena, which produces energy losses.[31,32] However, the heterogeneous dielectric layer shows a relative permittivity around $\varepsilon_r(Al_2O_3 + PVP) = 5.3$, where PVP fills part of the Al_2O_3 layer porous and cracks. At the end, the performance of ε_r and loss tangent shown on paper substrate is similar to the observed on glass substrate (Figure 6.12), being the insulating structure without PVP, which show higher differences.

Among the dielectric materials tested, for insulating applications, the best performance is shown by SiO_2 (Figure 6.9 and Figure 6.10) on both substrates used, which has the smallest value of ε_r and $\tan\delta$. Although, slightly increase of ε_r and $\tan\delta$ is shown by $SiO_2 + PVP$ in comparison with only SiO_2, the reliability presented by $SiO_2 + PVP$ makes this structure the most appropriated for insulating purposes on paper substrate Powercoat 230 (Arjowiggins, USA) PCBs. Regarding applications where higher value of ε_r and low value of $\tan\delta$ is required the most appropriated structure among the tested insulators is the $Al_2O_3 + PVP$ (Figure 6.11 and Figure 6.12).

Following, the porous dielectric layers are shown on *Figure 6.13* and *Figure 6.14*. In addition, on *Figure 6.14* it can be seen the PVP polymer printed above Al_2O_3, but the diffusion of PVP inside granular Al_2O_3 layer cannot be appreciated.

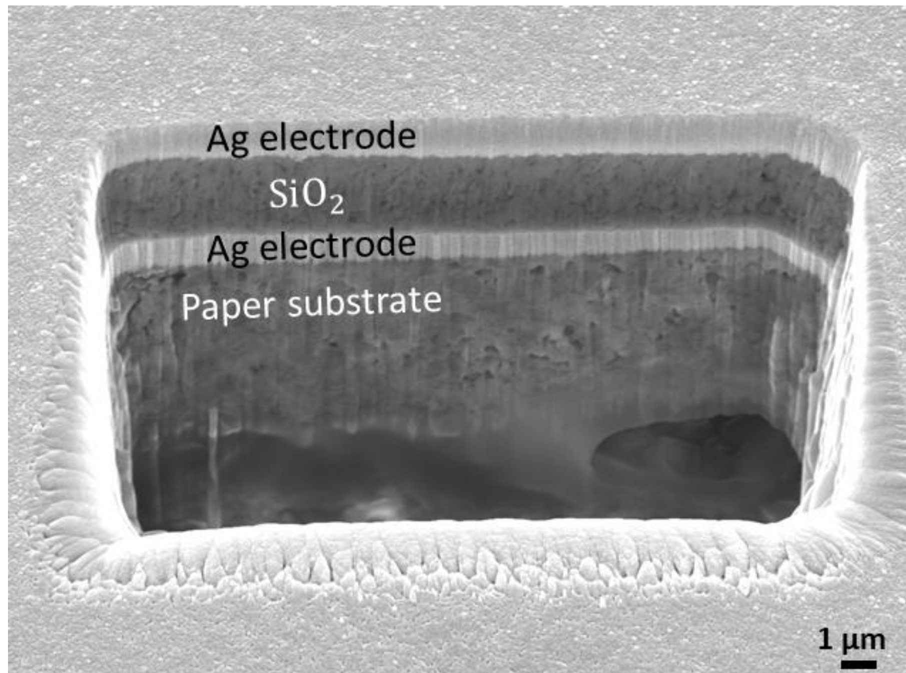

Figure 6.13 Cross sectional FESEM image of printed Ag-SiO_2-Ag MIM on paper substrate.

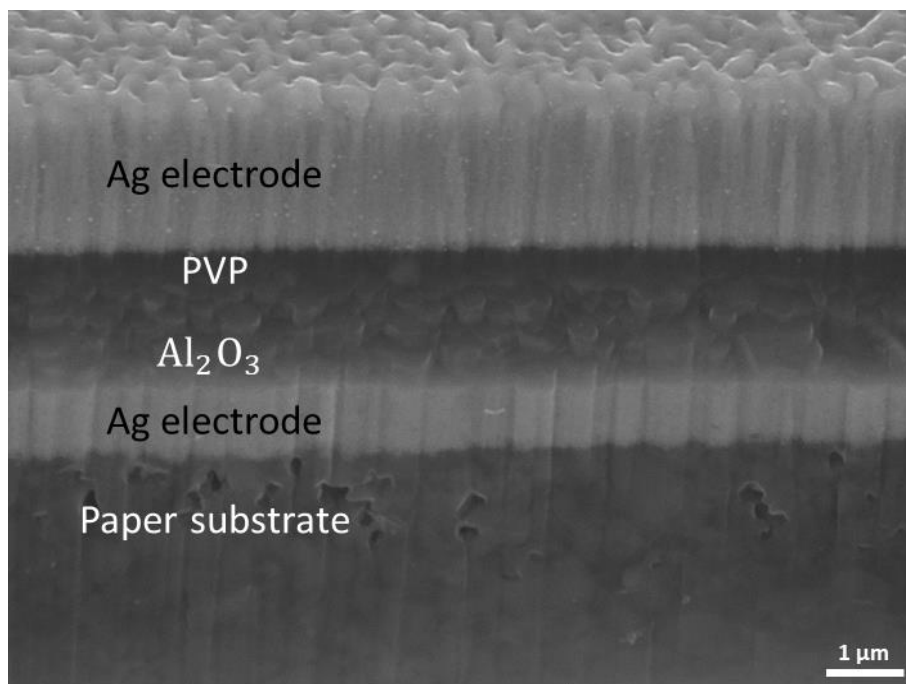

Figure 6.14 Cross sectional FESEM image of printed Ag–(Al_2O_3-PVP)-Ag MIM on paper substrate.

Regarding the current PCB manufacturing, similar relative permittivity has been achieved in comparison with standard PCB dielectric < 500 μm thick laminates, as show on *Table 6.6*.

Table 6.6 Relative permittivity values measured of the different MIMs tested, as well the corresponding to FR4 material currently used at PCB manufacturing. All the relative permittivity values correspond to 1 MHz.

Material ideal	Referenced ε_r	Measured ε_r Paper substrate	Measured ε_r Glass substrate
PVP	4.7	4	4.4
SiO_2	3.9	3.4	3.2
SiO_2+PVP	-	4.2	4
Al_2O_3	9.6	3.3	3.9
Al_2O_3 + PVP	-	5	5.4
FR4	4.2-4.6[34]	-	-

6.3.3 Dielectric strength

Other relevant physical property of a dielectric material is its dielectric strength. The dielectric strength depends on the breakdown voltage and the thickness of the dielectric. The dielectric breakdown occurs when conductive paths are generated. As voltage is increased, some conductive paths emerge but are closed immediately, however, when voltage is high enough, permanent conductive paths are induced and dielectric breakdown occurs. At *Figure 6.15* it can be seen different burned spots where dielectric is broken. The dielectric strength of the materials tested can be consulted on *Table 6.7* and *Table 6.8*, which corresponds to MIMs printed on paper and glass, respectively.

The maximum voltage applied to MIM devices was 100 V. Then, when the values of *Table 6.7* and *Table 6.8* are accompanied by “greater than” symbol, it means that the MIM devices arrive to 100 V without dielectric breakdown occurs.

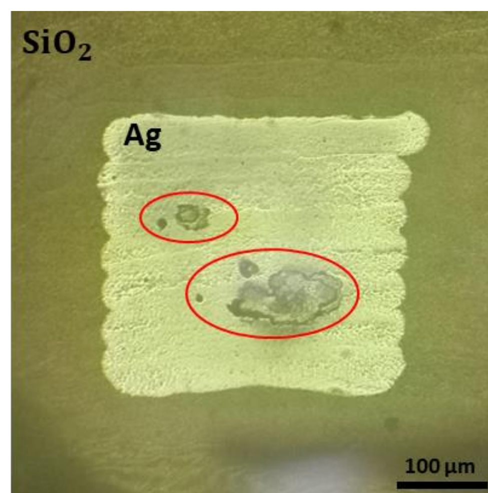

Figure 6.15 SiO_2 dielectric breakdown image

Table 6.7. Dielectric strength performed by the MIMs on paper substrate.

Thickness	E_{PVP} (MV/m)	E_{SiO_2} (MV/m)	E_{SiO_2+PVP} (MV/m)	$E_{Al_2O_3}$ (MV/m)	$E_{Al_2O_3+PVP}$ (MV/m)
1 Layer	0	0	> 66	0	> 42
2 Layers	> 59	5	> 41	0	> 59
3 Layers	> 46	9	> 27	0	> 26
4 Layers	> 34	9	> 23	30	> 49
5 Layers	> 28	5	> 18	22	> 44
6 Layers	> 23	3	> 15	> 47	> 39

Table 6.8 Dielectric strength of insulating layers on glass substrate.

Thickness	E_{PVP} (MV/m)	E_{SiO_2} (MV/m)	E_{SiO_2+PVP} (MV/m)	$E_{Al_2O_3}$ (MV/m)	$E_{Al_2O_3+PVP}$ (MV/m)
1 Layer	30	0.33	> 67	0	56
2 Layers	> 70	3	> 38	0	> 71
3 Layers	> 46	> 33	> 30	56	> 59
4 Layers	> 35	> 25	> 22	44	> 50
5 Layers	> 29	> 20	> 18	52	> 43
6 Layers	> 23	> 17	> 16	44	> 38

As can be seen on *Table 6.7* and *Table 6.8*, the dielectric strength reported decreases significantly as the thickness increase. As commented above, this is because the samples arrive to maximum voltage applied, 100 V, without dielectric breakdown. Thus, as dielectric thickness increases the dielectric strength decreases proportionally. It is important to realize that higher dielectric strength performance is expected for all insulating structures with “greater than” symbol, and the values of *Table 6.7* and *Table 6.8* have to be taken in consideration with that.

The dielectric strength performed by the current substrate used at PCB fabrication, FR4, is about 20 MV/m which is close to the values achieved.

6.4 Conclusions

The tested inorganic dielectric materials, SiO_2 and Al_2O_3, have low feasibility on paper substrate, as well on glass substrate. The failure of the devices is due to short-circuits generated by silver ink percolation through the insulator cracks at the top electrode-printing step. The insulator cracks are promoted by thermal contraction of both paper substrate and inorganic layer during the drying process.

The PVP MIMs have an excellent feasibility without short-circuits, when dielectric material has a thickness equal or higher than 1.4 µm on paper substrate and 0.7 µm on glass substrate. The relative permittivity of the PVP MIMs in paper substrate is slightly lower than in glass substrate, and the loss tangent is slightly higher in paper substrate than in glass substrate.

Heterogeneous structures combining inorganic and organic dielectric material, where PVP fills the inorganic cracks and voids, possess a similar and outstanding feasibility in both paper and glass substrate without short-circuits. The best heterogeneous structure in paper substrate is SiO_2 with PVP MIMs from a total layer thickness as low as 1.4 µm.

In paper substrate, the SiO_2 with PVP MIMs have the best performance for insulating purposes, where at 1MHz the relative permittivity is 4.2, loss tangent is 0.025 and dielectric strength is higher than 20MV/m and all of them are similar to values of the glass-reinforced epoxy laminate material, currently used at PCB fabrication.

6.5 References

(1) Muthu, V.; Chatterjee, P.; Jet, T. K. Review on Application of Additive Manufacturing for Electrical Power Converters. *Ieee Tencon* **2016**, 2327–2333.

(2) www.3ders.org. Nano Dimension has completed its "Switch" software package for 3D printed PCBs https://www.3ders.org/articles/20160705-nano-dimension-has-completed-its-switch-software-package-for-3d-printed-pcbs.html (accessed Dec 3, 2018).

(3) Wong, W. S.; Salleo, A. *Flexible Electronics : Materials and Applications*; Springer, 2009.

(4) Tong, G.; Jia, Z.; Chang, J. Flexible Hybrid Electronics : Review and Challenges.

(5) Plovie, B.; Yang, Y.; Guillaume, J.; Dunphy, S.; Dhaenens, K.; Van Put, S.; Vandecasteele, B.; Vervust, T.; Bossuyt, F.; Vanfleteren, J. Arbitrarily Shaped 2.5D Circuits Using Stretchable Interconnects Embedded in Thermoplastic Polymers. *Adv. Eng. Mater.* **2017**, *19* (8), 1–8.

(6) Wang, Y.; Guo, H.; Chen, J. J.; Sowade, E.; Wang, Y.; Liang, K.; Marcus, K.; Baumann, R. R.; Feng, Z. S. Paper-Based Inkjet-Printed Flexible Electronic Circuits. *ACS Appl. Mater. Interfaces* **2016**, *8* (39), 26112–26118.

(7) Vanfleteren, J.; Gonzalez, M.; Bossuyt, F.; Hsu, Y. Y.; Vervust, T.; De Wolf, I.; Jablonski, M. Printed Circuit Board Technology Inspired Stretchable Circuits. *MRS Bull.* **2012**, *37* (3), 254–260.

(8) Andersson, P.; Nilsson, D.; Svensson, P. O. P.-O. O. P. P.-O.; Chen, M.; Malmström, A.; Remonen, T.; Kugler, T.; Berggren, M.; Andersson, B. P. Active Matrix Displays Based on All-Organic Electrochemical Smart Pixels Printed on Paper. *Adv. Mater.* **2002**, *14* (20), 1460–1464.

(9) Nagashima, K.; Koga, H.; Celano, U.; Zhuge, F.; Kanai, M.; Rahong, S.; Meng, G.; He, Y.; De Boeck, J.; Jurczak, M.; et al. Cellulose Nanofiber Paper as an Ultra Flexible Nonvolatile Memory. *Sci. Rep.* **2015**, *4* (1), 5532.

(10) McKerricher, G.; Perez, J. G.; Shamim, A. Fully Inkjet Printed RF Inductors and Capacitors Using Polymer Dielectric and Silver Conductive Ink with through Vias. *IEEE Trans. Electron Devices* **2015**, *62* (3), 1002–1009.

(11) Fujisaki, Y.; Koga, H.; Nakajima, Y.; Nakata, M.; Tsuji, H.; Yamamoto, T.; Kurita, T.; Nogi, M.; Shimidzu, N. Transparent Nanopaper-Based Flexible Organic Thin-Film Transistor Array. *Adv. Funct. Mater.* **2014**, *24* (12), 1657–

1663.

(12) Hu, L.; Wu, H.; La Mantia, F.; Yang, Y.; Cui, Y. Thin, Flexible Secondary Li-Ion Paper Batteries. *ACS Nano* **2010**, *4* (10), 5843–5848.

(13) Nogi, M.; Karakawa, M.; Komoda, N.; Yagyu, H.; Nge, T. T. Transparent Conductive Nanofiber Paper for Foldable Solar Cells. *Sci. Rep.* **2015**, *5* (1), 17254.

(14) Arrese, J.; Vescio, G.; Xuriguera, E.; Medina-Rodriguez, B.; Cornet, A.; Cirera, A. Flexible Hybrid Circuit Fully Inkjet-Printed: Surface Mount Devices Assembled by Silver Nanoparticles-Based Inkjet Ink. *J. Appl. Phys.* **2017**, *121* (10).

(15) McKerricher, G.; Gonzalez, J.; Shamim, A. All Inkjet Printed 3D Microwave Capacitors and Inductors with Vias. *IEEE MTT-S Int. Microw. Symp. Dig.* **2013**, 9–11.

(16) Jiang, J.; Bao, B.; Li, M.; Sun, J.; Zhang, C.; Li, Y.; Li, F.; Yao, X.; Song, Y. Fabrication of Transparent Multilayer Circuits by Inkjet Printing. *Adv. Mater.* **2016**, *28* (7), 1420–1426.

(17) Sanchez-Romaguera, V.; Madec, M. B.; Yeates, S. G. Inkjet Printing of 3D Metal-Insulator-Metal Crossovers. *React. Funct. Polym.* **2008**, *68* (6), 1052–1058.

(18) Laurila, M. M.; Khorramdel, B.; Mantysalo, M. Combination of E-Jet and Inkjet Printing for Additive Fabrication of Multilayer High-Density RDL of Silicon Interposer. *IEEE Trans. Electron Devices* **2017**, *64* (3), 1217–1224.

(19) Baklanov, M. R.; Adelmann, C.; Zhao, L.; De Gendt, S. Advanced Interconnects: Materials, Processing, and Reliability. *ECS J. Solid State Sci. Technol.* **2014**, *4* (1), Y1–Y4.

(20) Boettcher, L.; Manessis, D.; Ostmann, A.; Karaszkiewicz, S.; Reichl, H. Embedding of Chips for System in Package Realization - Technology and Applications. In *2008 3rd International Microsystems, Packaging, Assembly & Circuits Technology Conference*; IEEE, 2008; pp 383–386.

(21) Vescio, G.; López-Vidrier, J.; Leghrib, R.; Cornet, A.; Cirera, A. Flexible Inkjet Printed High-k HfO 2 -Based MIM Capacitors. *J. Mater. Chem. C* **2016**, *4* (9), 1804–1812.

(22) Hwang, M. S.; Kim, J.; Kim, H. T.; Yoon, Y.; Hyun, S.; Kim, J.; Lee, S. N.; Moon, J. Inkjet-Printing of Nonsintered Alumina-Resin Hybrid Films and Their

Dielectric Properties. *J. Appl. Phys.* **2010**, *108* (10).

(23) Nair, I. I. J.; Varma, M. R.; Sebastian, M. T. Low Cost Room Temperature Curable Alumina Ink for Printed Electronic Applications. *J. Mater. Sci. Mater. Electron.* **2016**, *27* (9), 9891–9899.

(24) Lee, H.-H.; Chou, K.-S.; Huang, K.-C. Inkjet Printing of Nanosized Silver Colloids. *Nanotechnology* **2005**, *16* (10), 2436–2441.

(25) Perelaer, J.; De Gans, B. J.; Schubert, U. S. Ink-Jet Printing and Microwave Sintering of Conductive Silver Tracks. *Adv. Mater.* **2006**, *18* (16), 2101–2104.

(26) Perelaer, B. J.; de Laat, A. W. M.; Hendriks, C. E.; Schubert, U. S. Inkjet-Printed Silver Tracks: Low Temperature Curing and Thermal Stability Investigation. *J. Mater. Chem.* **2008**, *18* (27), 3209.

(27) Arjowiggins. *Technical Data Sheet of Powercoat Paper*.

(28) Cook, B. S.; Cooper, J. R.; Tentzeris, M. M. Multi-Layer RF Capacitors on Flexible Substrates Utilizing Inkjet Printed Dielectric Polymers. *IEEE Microw. Wirel. Components Lett.* **2013**, *23* (7), 353–355.

(29) Li, Y.; Torah, R.; Beeby, S.; Tudor, J. An All-Inkjet Printed Flexible Capacitor on a Textile Using a New Poly(4-Vinylphenol) Dielectric Ink for Wearable Applications. *Proc. IEEE Sensors* **2012**, 5–8.

(30) Maex, K.; Baklanov, M. R.; Shamiryan, D.; Lacopi, F.; Brongersma, S. H.; Yanovitskaya, Z. S. Low Dielectric Constant Materials for Microelectronics. *J. Appl. Phys.* **2003**, *93* (11), 8793–8841.

(31) Tang, H.; Zhou, Z.; Bowland, C. C.; Sodano, H. A. Synthesis of Calcium Copper Titanate (CaCu 3 Ti 4 O 12) Nanowires with Insulating SiO 2 Barrier for Low Loss High Dielectric Constant Nanocomposites. *Nano Energy* **2015**, *17*, 302–307.

(32) Zhu, L. Exploring Strategies for High Dielectric Constant and Low Loss Polymer Dielectrics. *Phys. Chem. Lett.* **2014**, *5*, 3677.

(33) Baeg, K. J.; Noh, Y. Y.; Ghim, J.; Lim, B.; Kim, D. Y. Polarity Effects of Polymer Gate Electrets on Non-Volatile Organic Field-Effect Transistor Memory. *Adv. Funct. Mater.* **2008**, *18* (22), 3678–3685.

(34) Würth elektronik. *Standard FR4 TG135 TDS*.

(35) Nogi, M.; Iwamoto, S.; Nakagaito, A. N.; Yano, H. Optically Transparent Nanofiber Paper. *Adv. Mater.* **2009**, *21* (16), 1595–1598.

(36) In, P. A SIMPLE MODEL FOR THE ORTHOGONAL COUPLED STRIP

LINES IN MULTILAYER PCB: (QUASI-TEM APPROACH) A. Cheldavi and A. Arshadi. **2006**, 39–50.

(37) Cauwe, M.; De Baets, J. Broadband Material Parameter Characterization for Practical High-Speed Interconnects on Printed Circuit Board. *IEEE Trans. Adv. Packag.* **2008**, *31* (3), 649–656.

GENERAL CONCLUSIONS AND FUTURE WORK

CHAPTER 7

The main conclusions of this thesis are presented in this section, exposing the overall vision of the work performed for each subject treated on the dissertation.

The greatest achievement of this work is the development and optimization of a novel capillarity-assisted SMD assembling method for the manufacturing of hybrid circuits inkjet-printed. In addition, taking advantage of print-on-slope technique, direct assembling of silicon die integrated circuits to PCB is successfully applied. Moreover, heterogeneous structures inkjet-printed open new solutions for multilayer hybrid circuits.

Functional aspects for inkjet printing technology

All the inks tested, both in the case of conductive inks and in dielectric ones have the non-dimensional Z value in the range of $1 < Z < 10$. In the case of lowest Z value, a slightly increase of the temperature of the nozzle is required for a better jetability performance. Concretely, the most used silver ink in this work has a Z value around 5.

Comparing the performance of the printheads with the hydrocarbon solvent-based inks, the wetting printheads have better jetability than non-wetting printheads. At the wetting printheads, the ink remains on the nozzle plate with very low contact angle forming a thin uniform layer, which does not obstruct the drop formation.

There are two limiting bounds, lower and upper, to the width of a parallel-sided liquid bead produced by inkjet printing, even in the stability regime. If drop spacing is not small enough, initial coalescence leads to a liquid bead with a periodic irregularity. If drop spacing is too small a bulging instability is formed.

The liquid beads on $(\hat{y})$ direction are narrower than $(\hat{x})$ direction, and it is related with the lower spreading and higher receding contact line associated to the low rate of drop addition. The lower rate of material addition provokes earlier effect of solidification and the corresponding arrest of the contact lines. In summary, the drop ejecting frequency and sweep velocity is anisotropic at inkjet printing technology used.

In all the cases studied, proper ink-substrate wettability is assured by correct hysteresis between the receding and advancing contact angles. In addition, at proper ink-substrate

wettability, the parallel-sided deposits at line or square-shape patterns depend on drops overlapping and drop ejecting frequency.

The SU-8-ink (PriElex SU-8) is discharged due to the loss of the ink bead line pinning and formation of undesirable big islands, at polymerization step.

The sintered deposits of graphite-inks (77VA12-8 and 92VA12-2) have a lack of homogeneity along the thickness, besides these deposits of graphite inks suffer coffee ring effect. In addition, the temperatures required to proper ink sintering are forbidden for the coated paper used at this work. For both reasons these inks are not suitable for the purpose of this thesis.

All the deposits of the inks, including dielectric and conductive inks except graphite ones, have free coffee ring effect at sintering process, being suitable for electronic manufacturing.

The sintering studies of conductive inks, specially silver ones, reveal that the Ag-inks DGP 40LT-15C and EMD5714 have low values of resistivity, close to bulk silver at low sintering temperatures. The rest of the conductive inks are neglected because of the temperature required for proper sintering is too high for the substrate proposed in this work.

Inkjet SMD-assembling method capillarity-assisted

Taking advantage of surface energies existing at the nanoscale, AgNP ink ensures high electrical conductivity and a high electrical conducting interconnection after thermal process at very low temperatures (150 °C).

Electrical contact resistance and shear strength measurements performed by AgNP ink are comparable to benchmark connecting materials. In conclusion, drop-on-demand inkjet printing technology is a valid technique to incorporate on SMT.

In other words, the proposed high resolution drop jetting technique sheds light on how, employing few picoliter drops, AgNP ink reveals comparable electrical performance to benchmark assembling materials onto several inkjet-printed substrates.

In summary, all the SMDs assembled by AgNP ink, ICA and solder have similar electrical resistance value around 0.3 Ω in all the substrates proposed, paper, Kapton® and glass. The low electrical contact resistance achieved by the low quantity of deposited material at AgNP ink assembling method allows stating the feasibility of the proposed AgNP ink as alternative straight forward and cost-efficient interconnecting method.

The AgNP ink, exploiting the capillarity action in order to assemble the SMDs, has weaker adhesion than ICA in paper and glass substrate, and similar adhesion in Kapton® substrate. However, AgNP ink and solder material have analogous adhesion in all substrate used.

The assembling SMD technique by AgNP ink is uniformly adapting and enveloping the Sn-plated SMD electrodes, without wasting unnecessary material surrounding the contact area as in the case of ICA and solder methods. The micro-structural characterization of the inkjet-printed silver connections evidences a solid and stable structure without detrimental fractures or pin-holes.

In sum up, flexible hybrid circuit is successfully manufactured by AgNP ink on paper, where different SMDs size-shaped are assembled demonstrating the reliability and feasibility of the proposed method.

Comparing the mechanical performance of the SMDs assembled by AgNP and the SMDs assembled by AgNP and NCA, adding the NCA reinforcement the shear strength performance is improved significantly. Concretely, the share strength increases 4 times on glass substrate and 1.5 on Kapton® and paper substrate. The higher increment of the strength on glass substrate in comparison with the other substrates used is due to NCA ink is specially formulated for glass substrate.

The mechanical performance of the SMDs assembled by ICA hand deposited and SMD assembled by AgNP and NCA, have similar share strength in all the substrates used. In addition, the SMDs assembled by AgNP and NCA possess analogous mechanical properties to values found on literature for SMDs assembled by screen-printed ICA.

The electrical contact resistance measured in bending stress mode of the AgNP and NCA connections are similar to performance reached by ICA connections.

In the light of the results, inkjet connecting technique is a promising method, which allows selectively assembling components onto printed flexible and rigid substrates for the upcoming hybrid electronics with a non-contact process.

Print-on-slope technique

Comparing the electrical contact resistance performed by the modified SMDs and the no modified ones, the electrical connections of modified SMDs have higher electrical contact resistance and higher failure occurrence takes place. The differences on the electrical contact resistance and failures occurrence between modified and no modified SMDs are due to non-automated electrode modification, which cannot assure the smoothness and reliability.

The SMDs with ramp-shape electrodes have both electrical contact resistance and failures lower than the SMDs with square-shape electrode. The worst performance achieved by squared-shape SMDs is because of the lack of flatness at lateral face, which moves away the ink from the interface between SMD electrode and the conductive strip, hindering the ink capillarity.

The SMDs with ramp-shape electrode retain silver deposit on the ramp surface while it is not occurred at squared-shape electrodes, which means that ramp-shape electrodes assure higher electrical contact surface.

The silicon die is silver ink-attached to PCB gate electrode by means of inkjet printer and have good adhesion as conductive glue. In addition, the ramp-shape terminations ICA-based are a complementary strategy for soften the abrupt staircase in the different height levels between the silicon die and the PCB. The printed silver ink over the ramp-shape electrodes by print-on-slope technique has good wettability and electrical interconnections.

The 2D connection on ramp-shape terminations gives a better functionality of SoP fabricated for CAFM material characterization than current wire bonding connections. The AFM tip moves over the silicon die without physical obstruction, giving a unique solution at this novel method to characterize degradation.

Multilayer inkjet-printed PCBs

The tested inorganic dielectric materials, SiO_2 and Al_2O_3, have low feasibility on paper substrate, as well on glass substrate. The failure of the devices is due to short-circuits generated by silver ink percolation through the insulator cracks at the top electrode-printing step. The insulator cracks are promoted by thermal contraction of both paper substrate and inorganic layer during the drying process.

The PVP MIMs have an excellent feasibility without short-circuits, when dielectric material has a thickness equal or higher than 1.4 µm on paper substrate and 0.7 µm on glass substrate. The relative permittivity of the PVP MIMs in paper substrate is slightly lower than in glass substrate, and the loss tangent is slightly higher in paper substrate than in glass substrate.

Heterogeneous structures combining inorganic and organic dielectric material, where PVP fills the inorganic cracks and voids, possess a similar and outstanding feasibility in both paper and glass substrate without short-circuits. The best heterogeneous structure in paper substrate is SiO_2 with PVP MIMs from a total layer thickness as low as 1.4 µm.

In paper substrate, the SiO_2 with PVP MIMs have the best performance for insulating purposes, where at 1MHz the relative permittivity is 4.2, loss tangent is 0.025 and dielectric strength is higher than 20MV/m and all of them are similar to values of the glass-reinforced epoxy laminate material, currently used at PCB fabrication.

Future works

Overall, in this work the assembling of electronic devices on printed circuit boards using the inkjet printer as unique manufacturing equipment is successfully performed.

Looking backward the here presented inkjet based technologies for hybrid printed circuit boards, there are several points that could be extended and studied in future works.

Concerning the multilayer hybrid printed circuit boards, the next study that could take place is the SMD connection by inkjet onto printed multilayer circuit. The electrical contact resistance and the adhesion mechanical performance of the SMD inkjet connections should be studied and compared with the performance reached at this thesis onto monolayer circuits.

The system on package here presented was manufactured by using ICA manually deposited. In order to fully inkjet SoP manufacturing, the next work that should be performed is the test of the polymeric ink (GPTMS) used at chapter 4 for printing the ramp-like connections between the silicon die to PCB, as well fix mechanically the silicon die to PCB. The electrical contact resistance and the mechanical performance of the silicone die inkjet connections should be studied.

The capillarity-assisted inkjet connecting method here presented was studied in electrical and mechanical performance. In future works, the study of the substrate wettability control to improve the feasibility and the resolution of the inkjet connecting method could be performed.

The wettability of a substrate can be tuned by increasing the substrate free bonds, as plasma/cleaning treatments. In addition, the wettability of a substrate can be also tuned increasing the effective surface by substrate treatment as laser ablation. In this way, laser ablation allows to substrate pattern transfer without masks, changing significantly the wettability of the ablated surface. Microchips in Quad Flat Packs (QFP) with leads pitch about 300 µm should be inkjet connected after tuning the substrate wettability. Two specific proposals could be performed. The first one is to print an amount of ink directly over the leads without a defined pattern and study if the ink moves dominated by the two different surface energy of the substrate, being only the ablated areas occupied by the ink. This solution is inspired by deep soldering of the trough-hole technology. The second proposal is to print the ink over the leads following a well-adapted pattern. For both, the connectivity and the short-circuiting should be checked as well functionality.